Department of Civil Engineering

J.L. Domingues Costa

Rigid-Plastic Seismic Design of Reinforced Concrete Structures

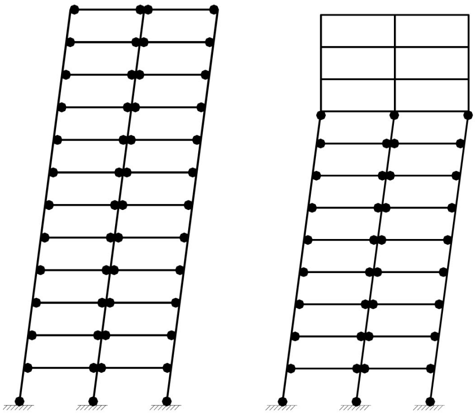

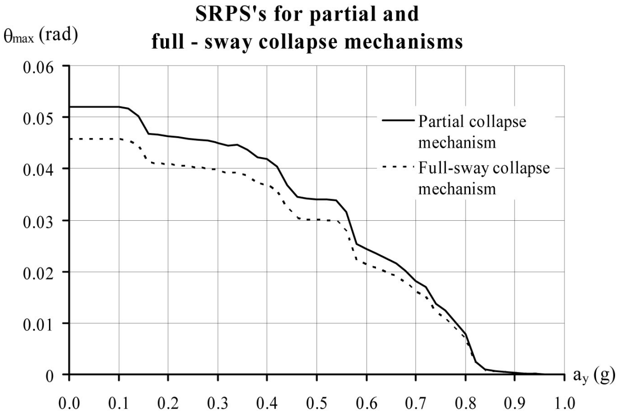

PHD THESIS

BYG • DTU

Rigid-Plastic Seismic Design of Reinforced Concrete Structures

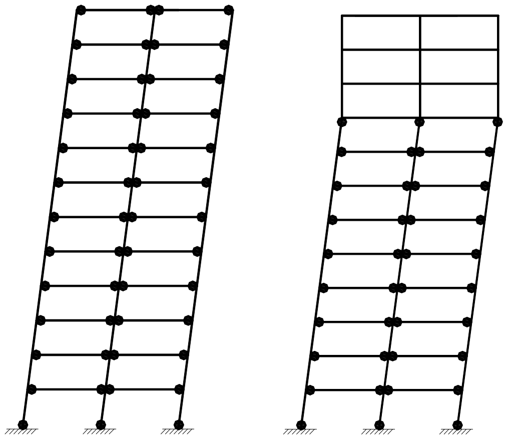

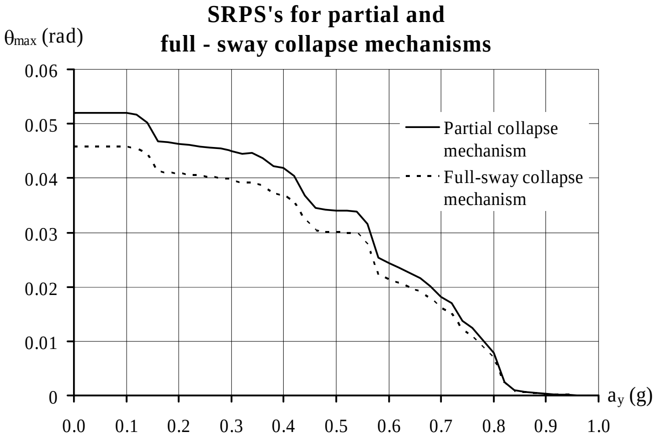

J.L. Domingues Costa

Ph.D. Thesis

BYG-DTU – Department of Civil Engineering
Technical University of Denmark

2006

Rigid-Plastic Seismic Design of Reinforced Concrete Structures

J.L. Domingues Costa

Ph.D. Thesis

BYG-DTU – Department of Civil Engineering
Technical University of Denmark

2006

Rigid-Plastic Seismic Design of Reinforced Concrete Structures

Copyright ©, J.L. Domingues Costa, 2006
Printed by DTU-Tryk
BYG-DTU – Department of Civil Engineering
Technical University of Denmark
Byg Rapport: R-149
ISSN number: 1601-2917
ISBN number: 87-7877-221-4

Preface

The present thesis is part of the requirements to attain the Ph.D. degree at the Technical University of Denmark. The work has been carried out at the Department of Civil Engineering of that university (BYG●DTU) under the supervision of Professor dr. tech. Mogens Peter Nielsen.

Firstly, I would like to thank my supervisor for all his dedication and commitment during the course of the entire Ph.D. project. Aside from providing invaluable technical guidance and inspiration (without which this thesis would never have been written), Mogens Peter was *always* available to help, advise, criticise and most memorably to share his theories about life under a warm cloud of "non-Cuban" cigar smoke during our daily coffee breaks.

Many thanks are also due to the co-supervisor, Associate Professor Rita Bento – The Technical University of Lisbon, Portugal, for her motivating kindness and prompt availability in providing precious help in the form of comments and suggestions from the very beginning of the Ph.D. project.

The generous support, criticism and motivation provided by my other co-supervisor, Professor Vsevolod Levtchitch, Frederik Institute of Technology, Cyprus, is also gratefully acknowleged.

A special word of gratitude is addressed to Ph.D. candidate Thomas Hansen for his support and above all his companionship during the last three years, and for the "healthy" smoking breaks we shared together. I would also like to thank the former Ph.D. students of my supervisor, Lars Z. Hansen, Tim Gudmand-Høyer, Karsten Findsen and Jakob Laugesen for their valuable criticism and fruitful discussions.

A special word of appreciation is due to Professor Toshikatsu Ichinose, Ichinose Lab., Nagoya Institute of Technology, Japan. I had the privilege of spending three fantastic months in Japan where I received essential input on the work presented in this thesis and engaged in many stimulating discussions with Professor Ichinose. Also, I would like to thank Associate Professors Hisashi Umemura and Atsushi Sato, and Professor Ichinose's students, Matsuo Aono, Nanako Marubashi, Yo Hibino, Nobuaki Hanai, Ito Yosuke, Takashi Tozawa, Noriyuki Takahashi, Kazuya Nitta, and Masataka Hirabayashi for their constant support, friendship and help, allowing me to gain the maximum advantage of my external stay in Nagoya.

The Ph.D. project was fully sponsored by the Portuguese governmental agency for scientific and technological research, Fundação para a Ciência e Tecnologia – FCT. The financial support is gratefully acknowledged.

A word of gratitude is due to Ida and Svend Ib Andersen that kindly helped me translating the abstract into Danish language.

My friend Arun Sharma generously undertook the difficult task of improving my English. His contribution is gratefully recognized.

Finally, I would like to thank my parents, Isabel and Floriano, and Heidi for their constant encouragement, care and love.

Lyngby, October 2006

Abstract

The present Ph.D. dissertation provides a contribution to the development of rational and simplified design procedures in order to facilitate the task of seismic design of reinforced concrete structures.

It is widely accepted that it is neither economic nor necessary to design most part of reinforced concrete structures so that they remain in the elastic domain during the course of an extreme earthquake event. Currently, seismic design for strong earthquakes comprises of selecting a suitable collapse mechanism and determining an adequate distribution of strength and stiffness so that the corresponding overall structural performance in a representative seismic action lies within desired limits, i.e. Performance based-seismic design.

Non-linear time-history analysis (NLTHA) is generally accepted as the most suitable method to determine the seismic demand on structures designed to develop non-linear behaviour when subjected to earthquake motion. However, despite its superior accuracy and rationality, its use at a practical level is limited to structural assessment. Therefore, the need for simplified design procedures is still valid. Unfortunately, most of the existing simplified methods available for seismic design still make use of the Elastic Spectrum to determine seismic demand and therefore are beset with serious inconsistencies related to the inelastic nature of the dynamic response of ductile systems.

In this thesis, a new seismic design procedure for systems expected to perform in the non-linear range during a lifetime earthquake event, the *Rigid-Plastic Seismic Design method (RPSD)*, is proposed. The procedure is founded on the theory of Plasticity (Rigid-plastic structures), follows modern seismic design philosophy and combines:

a) The rationality of NLTHA for the estimation of the seismic demand solely based on the properties of the structure, and

b) The simplicity and practical value of spectral analysis for the estimation of the required dissipation capacity.

Firstly, a collapse mechanism is chosen and the dissipation capacity of the structure is determined with respect to a pre-defined performance parameter using a *rigid-plastic response spectrum*. The latter is characteristic of the ground motion alone. Then, a safe admissible stress field is found in parts of the structure outside the yield zones in order to enforce the chosen collapse mechanism. The latter task is facilitated to a great extent by applying the *extreme loading scenarios approach*, which takes advantage of the fact that the strength demand at any point of rigid-plastic structures is solely dependent on the intensity of the ground motion.

Any artificial coefficients intended to adjust results according to empirical observations are avoided, which from a conceptual point of view is considered to be an advantage over other simplified design procedures for seismic design. Moreover, there is an effective separation between the properties of the structure and those of the ground motion, which contributes to the straightforwardness of the RPSD method.

Two examples of the application of the procedure to the design of reinforced concrete frames are given. Results are compared with refined NLTHA and found to be encouraging.

Resumé

Denne afhandling er et bidrag til udviklingen af en forenklet men rationel design procedure for armerede betonkonstruktioner der skal modstå påvirkninger fra jordskælv.

Det er generelt accepteret, at det hverken er nødvendigt eller økonomisk at dimensionere hele konstruktionen således at den forbliver i det elastiske område når den udsættes for en ekstrem jordskælvshændelse. I øjeblikket er det almindelig praksis ved dimensionering for et kraftigt jordskælv at udvælge en passende/sandsynlig deformations-mekanisme for brud og bestemme den tilhørende fordeling af styrke og stivhed således, at den overordnede strukturelle opførsel ved et repræsentativt jordskælv ligger inden for de ønskede grænser: ydelses baseret jordskælvdesign (eng. Performance based seismic design).

Det er generelt accepteret, at en ikke-lineær tids-historie analyse (eng. Non-linear time-history analysis, NLTHA) er den bedst egnede metode til at bestemme påvirkningerne i en konstruktion, der er dimensioneret til at udvikle en ikke-lineær opførsel når den udsættes for jordskælvsbelastninger. Denne metode er rationel og kan give meget nøjagtige resultater, men den er i praksis alene begrænset til eftervisning af en given konstruktions opførsel. Der er derfor fortsat behov for en forenklet konstruktions- og metode dimensionerings. De forenklede metoder til dimensionering for jordskælv der i dag er til rådighed er baseret alene på elastisk opførsel og er derfor inkonsistente for systemer og konstruktioner der ved dynamiske påvirkninger opfører sig elastisk-plastisk.

I denne afhandling foreslås en ny dimensioneringsmetode for systemer der forventes at blive deformeret i det ikke-lineære område ved et dimensionsgivende jordskælv: den *Ideal-plastiske Jordskælvsdimensionerings Metode* (eng. Rigid-Plastic Seismic Design Method, RPSD). Fremgangsmåden er baseret på plasticitetsteori og tidssvarende konstruktionsfilosofi og den kombinerer:

a) Vurdering af konstruktionens opførsel baseret alene på dennes egenskaber, samme rationelle fremgangsmåde som kendetegner NLTHA.

b) Vurderingen af konstruktionens evne til at optage/absorbere energi baseret på enkel og praktisk spektral-analyse.

Det første skridt er at udvælge en brudmekanisme, for hvilken konstruktionens kapacitet til at absorbere energi bestemmes ud fra foruddefinerede ydelsesparametre og ved at benytte et ideal-plastisk response spektrum. Dette sidste er udelukkende bestemt af jordens bevægelsesmønster (ground motion). Derefter udvælges et sikkert tilladeligt spændings felt i de dele af konstruktionen som befinder sig udenfor flydeområderne. Denne opgave lettes i vid udstrækning ved at benytte ekstrem-last metoden (extreme loading scenarios approach) , som udnytter den kendsgerning, at styrkekravet i ethvert punkt i en ideal-plastisk konstruktion alene er afhængig af intensiteten af jordens bevægelser.

Det er således ikke nødvendigt empiriske at korrigere metodens resultater ud fra erfaringsmæssige observationer. Ud fra et konceptuelt synspunkt betragtes dette som en fordel ved en sammenligning med andre forenklede seismiske dimensioneringsmetoder. Derudover udviser metoden en effektiv adskillelse mellem konstruktionens egenskaber og jordens bevægelse, hvilket bidrager til at gøre RPSD metoden let tilgængelig.

To rammekonstruktioner i armeret beton er dimensioneret vha. den nye metode og en sammenligning med resultaterne fra avanceret NLTHA er opløftende.

Contents

1 **Introduction**…………………………………………………….. **1**

1.1 Seismic design philosophy for reinforced concrete structures throughout the 20th century…………………………………………….. 1

1.2 Determination of seismic demand on structures performing in the non-linear range – Overview of existing procedures………………………… 5

1.2.1 Fundamentals of structural dynamics for systems subjected to ground motion performing in the non-linear range……………………………... 6

1.2.2 Non-linear time-history analysis……………………………………... 12

1.2.3 Elastic Spectrum analyses……………………………………………. 13

1.2.4 Capacity spectrum method – Non-linear static analysis………………... 16

1.3 The theory of rigid-plastic materials and limit analysis as a rational approach towards simplified seismic design of reinforced concrete structures……………………………………………………...... 18

1.4 Outline………………………………………………………………... 20

2 **Cyclic behaviour of reinforced concrete elements**………………………………………………………. **21**

2.1 Properties of concrete and reinforcement steel………………………… 21

2.1.1 Concrete………………………………………………………………. 21

2.1.2 Reinforcement Steel………………………………………………….. 32

2.1.3 Bond between concrete and steel…………………………………….. 33

2.2 Inelastic Response of Reinforced Concrete Elements in Cyclic Loading. 37

2.2.1 Members with flexure-dominated behaviour…………………………… 37

2.2.2 Members with shear-dominated behaviour……………………………... 54

2.2.3 Joints…………………………………………………………………..... 63

2.3 Available rotation capacity……………………………………………… 67

2.4 Implications on seismic design………………………………………….. 72

2.4.1 Principles of member design……………………………………………. 72

2.4.2 Weak beam / strong column concept for ductile frames………………... 72

2.4.3 Overstrength factors…………………………………………………….. 73

3 **The rigid-plastic seismic design method**………. **75**

3.1 General assumptions of the RPSD method……………………………... 75

3.1.1 Rigid-plastic structures………………………………………………….. 75

3.1.2 Disregard for viscous damping…………………………………………. 80

3.2 Rigid-plastic dynamics………………………………………………….. 82

3.2.1 Rigid-plastic oscillators…………………………………………………. 82

3.2.2 Basic study on the dynamic response of rigid-plastic oscillators……….. 89
3.2.3 Rigid-plastic structures……………………………………………….. 98
3.3 Seismic demand……………………………………………………. 105
3.3.1 Rigid-plastic response spectra..…………………………………….. 105
3.3.2 Strength distribution in the RPSD method……………………………… 116
3.3.3 Conclusions…………………………………………………………... 121
3.4 P-Δ effects in the RPSD method……………………………………... 123
3.4.1 The case of rigid-plastic oscillators…………………………………... 123
3.4.2 The case of rigid-plastic structures……………………………………… 125
3.4.3 Conclusions…………………………………………………………... 128
3.5 The RPSD method step-by-step……………....................................... 128
3.6 Conclusions…………………………………………………………... 130

4 Applications of the RPSD method to frame structures……………………………………………………. 131

4.1 Design of a 4-storey plane frame……………………………………….. 131
4.2 Design of a 12-storey frame…………………………………………….. 143

5 Final remarks……………………………………………….. 169

Bibliography………………………………………………… 173

List of symbols ……..……………………………………….. 179

Appendix ……………………………………………………. 183

“There are two approaches to a natural problem. They are the approach of the pure scientist and that of the engineer. The pure scientist is interested only in truth. For him there is only one answer – the right one – no matter how long it takes to get it. For the engineer, on the other hand, there are many possible answers, all of which are compromises between truth and time, for the engineer must have an answer now; his answer must be sufficient for a given purpose, even if not true. For this reason an engineer must make assumptions – assumptions which in some cases he knows to be not strictly correct – but which will enable him to arrive at an answer which is sufficiently true for the immediate purpose.”

H.Q. Golder

cited by Brinch Hansen (1953)

1. Introduction

1.1 Seismic design philosophy for reinforced concrete structures throughout the 20th century

The need for structural design against strong ground motion was first appreciated in the early decades of the 20th century after a series of catastrophic earthquake events throughout the world: San Francisco, California, 1908; Messina, Italy, 1908; Kanto, Japan, 1925; Napier, New Zealand, 1932 and Long Beach, California, 1933, to mention but a few.

Essentially, the first design codes prescribed specific detailing and construction rules as well as procedures on the application of lateral inertia forces, against which the structure should be checked. In the absence of reliable measurement of ground motion intensity and lack of knowledge on Structural Dynamics, typically the magnitude of these forces was taken as 10% of the weight of the building.

By the 1960’s, ground motion measurements during an earthquake in the form of accelerograms were becoming more generally available. At the same time the development of strength design philosophies and of computer-based analytical procedures such as the spectral-modal analysis and the time-history analysis, facilitated the examination of the dynamical response of multi-degree-of-freedom structures. According to these procedures, the action effects were found in a deterministic fashion disregarding that the seismic loading is a statistical variable and the response of the structure was assumed to remain in the elastic range.

As the records of strong ground motion and of the corresponding effects on structures increased, it became apparent that the code provisions were inadequate in providing the required structural strength of the building to withstand an intense earthquake. Two fundamental observations led to this conclusion:

1. The lateral force levels specified in codes were consistently insufficient to assign enough strength capacity for the structure to endure strong ground motion shaking.
2. Structures that had been experiencing vibration close to resonance were exposed to accelerations several times larger than the ones they were designed for, and yet some of them survived the earthquake event with limited damage. Conversely, structures that had been experiencing ground motion intensity lower than they were designed for, experienced severe damage or even collapse. Invariably, poor seismic performance was due to severe reduction in strength of members particularly those with shear dominated behaviour and joints.

The first observation revealed the inconsistency of elastic design against a type of load with the degree of uncertainty such as seismic loading. The second called the attention of engineers to the property of the materials or of structures in offering resistance in the inelastic domain of response. This property is generally known as *ductility* and includes the ability to sustain deformations in the inelastic range without significant loss of strength and the capacity to absorb energy by hysteretic behaviour. Conveniently, ductility is quantified by the ratio of inelastic deformation to the elastic deformation, the so-called ductility factor, μ.

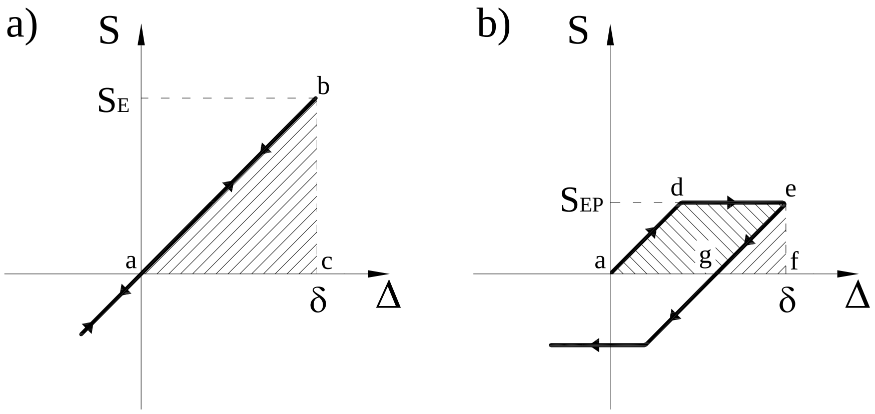

Figure 1.1 – Response S of a SDOF system to deformation Δ: a) Elastic response and b) Elastoplastic response (Park and Paulay, 1975)

Consider the simple case of a single-degree-of-freedom (SDOF) system. Assuming a fully elastic behaviour, the case of Figure 1.1a), it is necessary for the oscillator to develop strength S_E to reach a level of deformation equivalent to δ. However, provided that enough ductility is assigned, the case b) in the same figure, the system does not have to be that strong to reach the same level of deformation ($S_{EP}<S_E$).

Consider now for both cases the energy stored at deformation level δ given by the area between the load-deflection curve and the deflection axis. For the elastic response, the energy is of the elastic type and may be converted into kinetic energy (area abc). For the elastoplastic case when the mass returns to the zero load position, the elastic energy is represented by the small area efg. A significant portion of the potential energy at deformation level δ, given by the area adeg is dissipated, i.e. converted into other forms of energy such as heat.

The uncertainty of ground motion intensity, ductility and the unfeasibility of designing most structures to remain in the elastic domain during large earthquake events contributed decisively to a shift in seismic design philosophy from elastic design to plastic design in the 1970's. In this respect, the work by Park, Paulay and their co-workers carried out at the University of Canterbury, New Zealand, (Park and Paulay, 1975) was of primary importance.

Particularly in connection to the second observation discussed above, it was noted that there are modes of inelastic deformation that provide ductility and others that lead to failure. The authors mentioned above formulated that the task of seismic design should encourage the formation of modes of failure (*collapse mechanisms*) that possess ductility and prevent all the others that do not (brittle modes of failure). In this way, the structure could maintain its lateral strength and develop a mechanism that can dissipate the energy input by the ground motion. The design procedure developed accordingly was called Capacity Design Method and it may be resumed in the following main steps (Paulay and Priestley, 1992):

1. Choice of a kinematically admissible plastic mechanism according to its potential ductility capacity.
2. Identification of the regions of the structure where the energy input by the earthquake is going to be dissipated. These regions are often called yield zones or, in frames, plastic hinges.

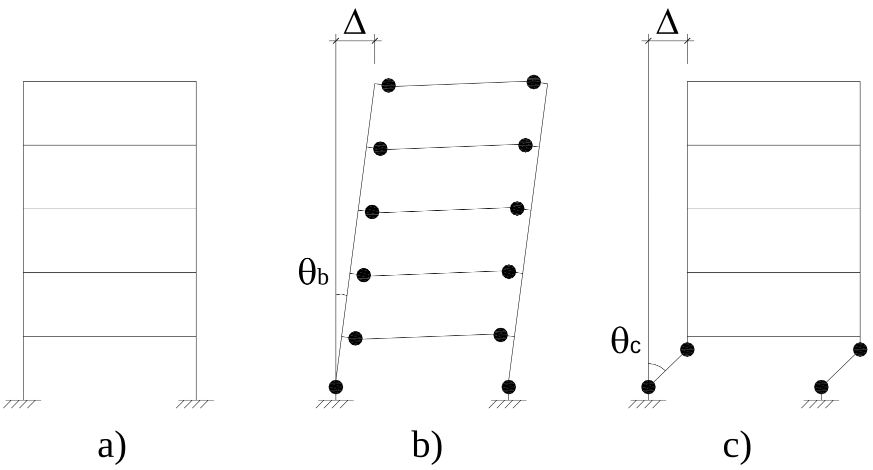

Figure 1.2 - Application of the so-called Capacity Design Method to a plane frame (Paulay and Priestley, 1992)

3. Prevention of brittle modes of failure, such as shear or anchorages failures. This is carried out ensuring that the strength capacity at the regions where brittle failure can occur is higher than the demand originating from the overstrength of the plastic hinges. In other words, all the regions outside the hinges must be designed so that they remain in the elastic domain throughout the whole seismic action.

Thus, the emphasis in design resulted in assigning ductility to structures so that large seismic forces can be evaded rather than assigning strength to resist those forces.

The application of the procedure is highlighted in the design of the plane frame of Figure 1.2a).

Typically, the most desirable mechanisms for energy dissipation for the case of building structures are the ones involving flexural behaviour at the yield zones, namely at the ends of the beams and columns. It is clear that the most suitable collapse mechanism is that shown in Figure 1.2b), which may be preferred to that shown in Figure 1.2c). In fact, the overall displacement Δ of the structure is achieved with the smallest inelastic deformation of the plastic hinges (Note in the same figure that $\theta_c >> \theta_b$). Secondly, a significant number of plastic hinges are formed before collapse, which allows an extensive distribution of plastic dissipation throughout the structure.

To prevent brittle modes of failure, a factor larger than the unity, *the overstrength factor*, is used to affect the strength demand outside the hinges corresponding to the onset of plastic behaviour in those elements. This factor accounts for the variability of the yield stress on the reinforcement and the probability of strain-hardening effects that increase the strength of the plastic hinge after yielding.

Finally, the nature and quality of detailing must be clearly distinct between the regions assigned to be plastic hinges and those that ought to remain in the elastic domain.

To the reader familiar with plastic design, the procedure described is clearly not an innovation. In fact, the very same procedure mentioned above has consistently been applied to the case of structures under static loads since the ductile properties of reinforced concrete have been acknowledged. In countries like Denmark and Switzerland (with very small seismic activity), they are the basis for the

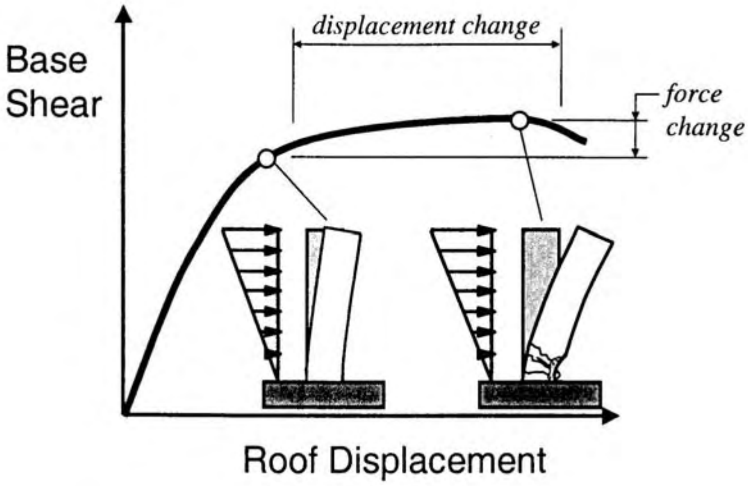

Figure 1.3 - Relation between displacement and damage (fib, 2003)

corresponding national codes for reinforced concrete design for ultimate limit states since the early 1900’s (Dansk Ingeniørforening, 1908). However, it was only after the work of Park, Paulay and their co-workers, that plastic design philosophy was fully introduced to the case of seismic loading. It has been a challenge for the author to understand this “late awakening” from the Earthquake Engineering community to the advantages of plastic design, and still this remains a riddle.

Nowadays, ductility is the single most important property sought by a structural engineer when designing in regions of significant seismicity.

The area of greatest uncertainty of response of structures designed according to the principles above is in the inelastic deformations at the plastic hinges both in terms of extension of these deformations and their maintenance throughout the seismic action. To apply the above design philosophy, it is of primary importance to understand the behaviour of reinforced concrete elements under cyclic loading in order to identify the means by which ductile behaviour may be achieved and the trends in which brittle behaviour develops and may be prevented. Only then may the engineer choose the most suitable energy dissipation mechanism and the allowable extent of plastic deformations at the yield zones.

Thus, during the 1970’s and 1980’s, much of the research effort in the field of seismic design of reinforced concrete structures was directed at the determination of available ductility capacity of structural systems by means of extensive experimental studies. It was then evident that the seismic performance of a structure may be better assessed in terms of displacement quantities rather than force quantities. To illustrate this, consider Figure 1.3 sketching the base-shear *vs.* roof displacement of a slender wall structure, designed according to the principles of plastic design discussed above and subjected to a monotonic inversed triangle shaped lateral force field.

It is clear that the extent of damage in the structure is related to the extent of plastic deformations in the yield zone, which in turn can be related with the overall displacements (in this case, the roof displacement). After the onset of plastic behaviour at the yield zone, the change of strength demand in the structure is minimal,

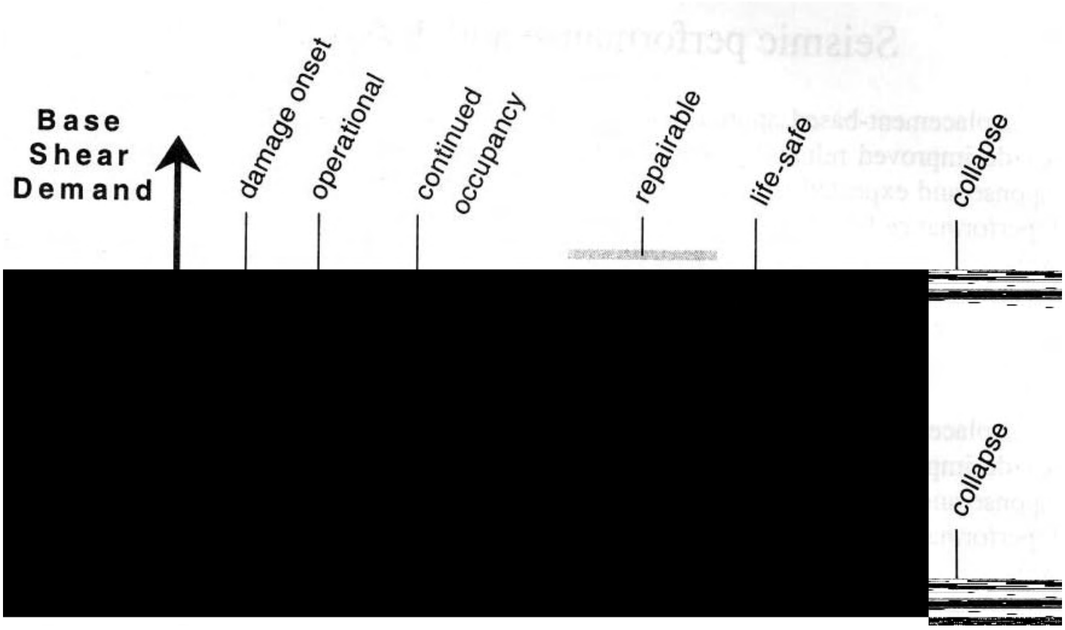

Figure 1.4 - Relation between performance levels and displacement (fib, 2003)

which indicates the poor relation between this parameter and seismic performance of the structure.

It was further acknowledged that basing seismic design on displacement capacity rather than strength capacity allows the definition of a range of performance levels easily related with displacement, see Figure 1.4. Thus performance levels may be adjusted according to the importance of the structure and the expected intensity of ground motion at the implementation site.

In the 1990's up to the present day, several seismic design procedures have been proposed based on the observations above. They have been framed by the somewhat grandiose term of Displacement-Based Seismic Design, or more generally, Performance-Based Seismic Design philosophy (fib, 2003). Currently, seismic design for strong earthquakes comprises of selecting a suitable collapse mechanism and the determination of an adequate distribution of strength and stiffness so that the corresponding overall structural performance in a representative seismic action lies within desired limits.

1.2 Determination of seismic demand on structures performing in the non-linear range – Overview of existing procedures.

In the previous section it was seen that seismic design philosophy evolved through the 20th century from an elastic-based design to a more rational plastic-based design approach. Unfortunately, this shift brought about serious difficulties for engineers, i.e. the estimation of strength and deformations demands on structures performing in the non-linear range. This is indeed a rather complicated task, due mainly to the unpredictable and dynamic nature of seismic loading, and complexity of the response of reinforced concrete elements subjected to cyclic loading.

In this chapter we intend to give a brief critical overview of the existing procedures to estimate the dynamic response of a structure governed by non-linear behaviour. The perspective taken here will firstly be from the rationality of the procedures and secondly from the degree of fulfilment of the needs of the structural engineer regarding the task of design systems able to sustain the effects induced by ground motion.

1.2.1 Fundamentals of structural dynamics for systems subjected to ground motion performing in the non-linear range

1.2.1.1 Single-degree-of-freedom systems

Figure 1.5a) depicts a SDOF system subjected to ground motion at a time, t, composed by a rolling mass, m, a spring with stiffness, k, and a damper with viscous damping constant, c. Imagine that the mass is moving with a positive relative acceleration to the ground, $a_r(t)$. The free-body diagram of the mass in the moving coordinate system at time t after d'Alembert's principle is shown in Figure 1.5b)[1].

In Figure 1.5b), $d_r(t)$ and $v_r(t)$ are the displacement and velocity of the mass relative to the ground at time t, respectively. For the sake of simplicity, in the following, these quantities will be referred to as relative displacements and velocities, since in this work we deal only with the problem of dynamic response against ground motion. $a_g(t)$ is the ground acceleration at time, t.

Dynamic equilibrium is given by the equation:

$$m \cdot a_r(t) + c \cdot v_r(t) + k \cdot d_r(t) = -m \cdot a_g(t) \tag{1.1}$$

Equation (1.1) is the general formulation of the equation of motion for SDOF systems. Three assumptions are implicit in this formulation:

1. The mass does not change;
2. The dissipation of energy is given by a viscous damping mechanism;
3. The restoring force is proportional to displacement.

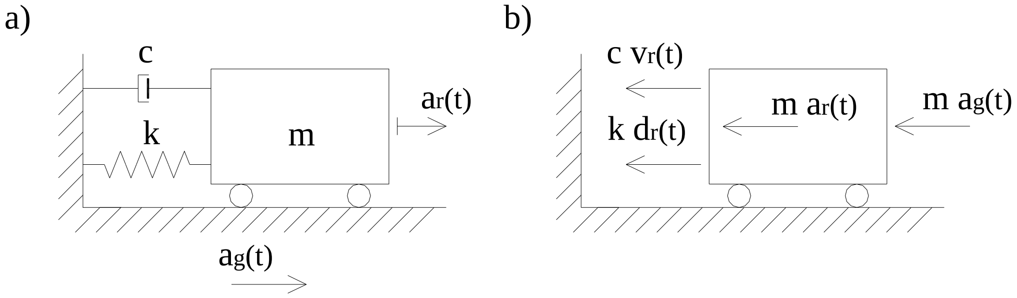

Figure 1.5 – a) Rolling mass SDOF system subjected to ground motion and b) corresponding free-body-diagram

---

[1] In this work, the sign convention regarding forces and displacements is such that positive quantities are orientated to the right-hand side of the figures. Bending moments are positive if they correspond to tension on the bottom face of horizontal elements or on the right-hand face of vertical elements.

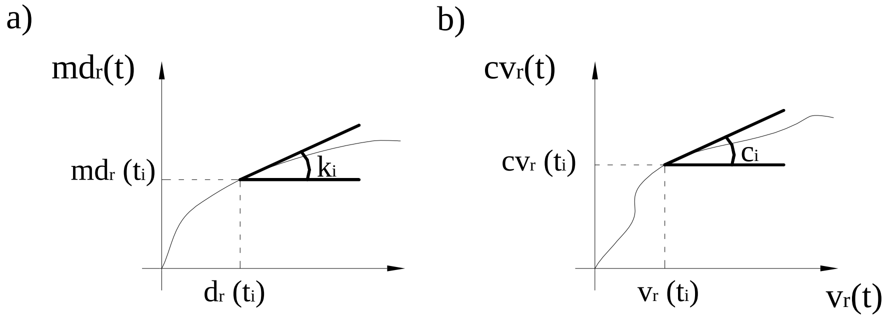

Figure 1.6 - a) Non-linear stiffness and b) Non-linear damping (Paz, 1991)

It is clear that the first assumption is applicable to the overwhelming majority of engineering problems. The second results from empirical observations. In fact, damping forces are always present in any physical system undergoing motion. These forces are part of a mechanism transforming the mechanical energy of the system to other forms of energy such as heat. The mechanism is quite complex and still not completely understood. Finally, the third assumption is only valid for systems with enough strength capacity to remain in the linear range during the whole ground motion.

If the system complies with these three assumptions, then the equation of motion in (1.1) is classified as a linear, second-order, differential equation. The general solution may be always found in the Duhamel's integral.

Clearly, the assumptions mentioned above are not fulfilled in the case of most SDOF structures designed according to modern seismic design philosophy. For these, damping is not directly proportional to relative velocity, and the restoring forces are not directly proportional to the relative displacements, see Figure 1.6.

Among the many methods available for the solution of the non-linear equation of motion, one of the most effective is the *step-by-step integration method*. In this method, the response is evaluated in successive time steps, Δt. At the beginning of each interval, i, dynamic equilibrium is established. The dynamic response for time $t_i+\Delta t$ is then approximately evaluated on the basis of constant stiffness and damping, the slopes in Figure 1.6a) and b), respectively. The relative displacement and velocities are calculated at the end of each interval and used in the next one, i+1, firstly to evaluate the corresponding slopes $k_{i+1}$and c_{i+1}, and secondly as initial conditions. Thus non-linear behaviour is approximated by successively changing linear systems. The most accurate procedure to evaluate the stiffness and damping coefficients in the time interval is to assume average values within that time interval. However, this creates much more complexity, as iteration is required. To avoid this iteration, initial tangent slopes are normally used.

Consider the equation of motion for a non-linear SDOF system as in Figure 1.5 at time instant, t_i.

$$m \cdot a_r(t_i) + c_i \cdot v_r(t_i) + k_i \cdot d_r(t_i) = -m \cdot a_g(t_i) \tag{1.2}$$

The same equation after a short time Δt is

$$m \cdot a_r(t_i+\Delta t) + c_i \cdot v_r(t_i+\Delta t) + k_i \cdot d_r(t_i+\Delta t) = -m \cdot a_g(t_i+\Delta t) \tag{1.3}$$

The subtraction of (1.2) from (1.3) is still a statement of equilibrium:

$$m \cdot \Delta a_r + c_i \cdot \Delta v_r + k_i \cdot \Delta d_r = -m \cdot \Delta a_g \tag{1.4}$$

where

$$\Delta a_r = a_r(t_i + \Delta t) - a_r(t_i) \tag{1.5}$$

$$\Delta v_r = v_r(t_i + \Delta t) - v_r(t_i) \tag{1.6}$$

$$\Delta d_r = d_r(t_i + \Delta t) - d_r(t_i) \tag{1.7}$$

$$\Delta a_g = a_g(t_i + \Delta t) - a_g(t_i) \tag{1.8}$$

We still have to make one further assumption to perform step-by-step integration of equation (1.4). One possible method is to make considerations on the development of the relative acceleration in the time interval, i. The assumption that the relative acceleration varies linearly in the time interval often produces good results. Thus, for $t \in [t_i, t_i + \Delta t[$

$$a_r(t) = a_r(t_i) + \frac{\Delta a_r}{\Delta t} \cdot (t - t_i) \tag{1.9}$$

$$v_r(t) = v_r(t_i) + a_r(t_i) \cdot (t - t_i) + \frac{\Delta a_r}{\Delta t} \cdot \frac{(t - t_i)^2}{2} \tag{1.10}$$

$$d_r(t) = d_r(t_i) + v_r(t_i) \cdot (t - t_i) + a_r(t_i) \cdot \frac{(t - t_i)^2}{2} + \frac{\Delta a_r}{\Delta t} \cdot \frac{(t - t_i)^3}{6} \tag{1.11}$$

Using (1.10) and (1.11) to determine $v_r(t_i+\Delta t)$ and $d_r(t_i+\Delta t)$, and inserting the corresponding results in (1.6) and (1.7), respectively, we have:

$$\Delta v_r = a_r(t_i) \cdot \Delta t + \frac{\Delta a_r \cdot \Delta t}{2} \tag{1.12}$$

$$\Delta d_r = v_r(t_i) \cdot \Delta t + \frac{a_r(t_i) \cdot \Delta t^2}{2} + \frac{\Delta a_r \cdot \Delta t^2}{6} \tag{1.13}$$

If Δd_r is the basic variable in the analysis, then solving (1.13) to obtain Δa_r and inserting the result on (1.12) yields:

$$\begin{cases} \Delta a_r = 6 \cdot \dfrac{\Delta d_r}{\Delta t^2} - 6 \cdot \dfrac{v_r(t_i)}{\Delta t} - 3 \cdot a_r(t_i) \\ \Delta v_r = 3 \cdot \dfrac{\Delta d_r}{\Delta t^2} - 3 \cdot v_r(t_i) - \dfrac{a_r(t_i) \cdot \Delta t}{2} \end{cases} \tag{1.14}$$

The incremental equation in (1.4) may then be re-written as in the following:

$$\begin{aligned} m \cdot \left(6 \cdot \frac{\Delta d_r}{\Delta t^2} - 6 \cdot \frac{v_r(t_i)}{\Delta t} - 3 \cdot a_r(t_i) \right) + c_i \cdot \left(3 \cdot \frac{\Delta d_r}{\Delta t^2} - 3 \cdot v_r(t_i) - \frac{a_r(t_i) \cdot \Delta t}{2} \right) \\ + k_i \cdot \Delta d_r = -m \cdot \Delta a_g \end{aligned} \tag{1.15}$$

Note that the only unknown quantity in (1.15) is the incremental displacement Δd_r, which makes:

$$\overline{k}_i \cdot \Delta d_r = \Delta F_i \tag{1.16}$$

where

$$\overline{k}_i = k_i + 6 \cdot \frac{m}{\Delta t^2} + 3 \cdot \frac{c_i}{\Delta t} \tag{1.17}$$

and

$$\Delta F_i = -m \cdot \Delta a_g + m \cdot \left(6 \cdot \frac{v_r(t_i)}{\Delta t} + 3 \cdot a_r(t_i) \right) + c_i \cdot \left(3 \cdot v_r(t_i) + \frac{a_r(t_i) \cdot \Delta t}{2} \right) \tag{1.18}$$

Then from (1.16) we can determine the incremental displacement Δd_r:

$$\Delta d_r = \frac{\Delta F_i}{\overline{k}_i} \tag{1.19}$$

Inserting (1.19) in (1.14) determines Δa_r and Δv_r, which in turn allows the evaluation of $d_r(t_i+\Delta t)$ and $v_r(t_i+\Delta t)$ applying equations (1.7) and (1.6), respectively.

The procedure described here is presented by (Paz, 1991). As the author points out, the assumptions on linear variation of relative acceleration and of constant damping and stiffness during the time step equal to the initial evaluation of c_i and k_i, introduce errors that tend to accumulate from step to step – numerical instability. Of course, the smaller the time step, the lower the magnitude of the errors introduced. As a rule of thumb, it is generally suggested that the length of the time steps should not exceed one tenth of the elastic period of the system, $T=2\pi\sqrt{m/k}$. However, we can minimize this accumulation of errors further by imposing a total dynamic equilibrium condition at the end of each time step. This is done solving directly equation (1.3) to obtain $a_r(t_i+\Delta t)$:

$$a_r(t_i + \Delta t) = -a_g(t_i + \Delta t) - \frac{c_i}{m} \cdot v_r(t_i + \Delta t) - \frac{k_i}{m} \cdot d_r(t_i + \Delta t) \tag{1.20}$$

Step-by-step integration procedures are the only completely general approach for evaluation of the dynamic response of non-linear structures. Nevertheless, these methods are equally applicable to linear systems. In fact, as (Clough and Penzien, 1993) point out, the effectiveness and simplicity of step-by-step integration procedures makes them preferable in almost every engineering application for the evaluation of the dynamic response in the time domain, irrespective of whether the behaviour of the system is linear or not.

1.2.1.2 Multi-degree-of-freedom systems

The reasoning leading to the establishment of dynamic equilibrium in multi-degree-of-freedom (MDOF) systems is exactly the same as for the case of SDOF systems. The difference now is that we have a statement of equilibrium as in (1.1) per each degree of freedom for every time, t. The procedure becomes more complex since inertia, damping and restoring forces at each degree of freedom result from the contribution of the motion at all degrees of freedom in the structure.

For instance, in a MDOF system with N degrees of freedom, the equation of motion at the i-th degree of freedom at time t is:

$$\sum_{j=1}^{N} m_{ij} \cdot a_{r,j}(t) + \sum_{j=1}^{N} c_{ij} \cdot v_{r,j}(t) + \sum_{j=1}^{N} k_{ij} \cdot d_{r,j}(t) = -m_i \cdot a_g(t) \qquad (1.21)$$

where

m_{ij}, c_{ij} and k_{ij} correspond to the forces at degree of freedom i due to unit acceleration, velocity and displacement at degree of freedom, j, respectively. These parameters are commonly called mass, damping or stiffness influence coefficients, accordingly.

$a_{r,j}(t)$, $v_{r,j}(t)$ and $d_{r,j}(t)$ are the relative acceleration, velocity and displacement at the j-th degree of freedom at time t.

m_i is the mass at degree of freedom i.

The combination of all the equations of motion for each degree of freedom yields the systems of equations of motion of the MDOF system. This is conveniently represented by matrix notation[2]:

$$\mathbf{M} \cdot \{a_r(t)\} + \mathbf{C} \cdot \{v_r(t)\} + \mathbf{K} \cdot \{d_r(t)\} = -\mathbf{M} \cdot \{a_g(t)\} \qquad (1.22)$$

where **M**, **C** and **K** represent the mass, damping and stiffness matrixes, respectively, and, $\{a_r(t)\}$, $\{v_r(t)\}$ and $\{d_r(t)\}$ the relative acceleration, velocity and displacement vectors, respectively.

The simplest method to consider the inertia properties of a structural system is to assume that the entire mass is concentrated at points at which the translational displacements are defined – lumped mass method. The mass is distributed along the structure in specified nodes. Depending on the degree of refinement, this method produces accurate results in most engineering applications. The consequence for the formulation of the equation is that the mass matrix **M** will be of the diagonal type.

In linear systems the dynamic response is expressed in terms of the normal modes of vibration by superposition of the independent modal equations (Paz, 1991). In this case, the damping matrix is conveniently expressed in terms of the modal damping ratios, ξ_n, each one addressing the damping associated with each vibration mode n[3]. The result is a diagonal matrix. However, in structures performing in the non-linear range, stiffness changes with time, and therefore so do the vibration modes. This makes it impossible to apply the principle of superposition of the uncoupled modal response. The solution is found on an explicit definition of the damping matrix. Normally this is carried out by expressing the damping matrix as proportional to the mass and stiffness matrixes.

$$\mathbf{C} = a_0 \cdot \mathbf{M} + a_1 \cdot \mathbf{K} \qquad (1.23)$$

It can be shown, (Clough and Penzien, 1993) that the damping ratio, ξ, associated with the circular frequency ω is given by:

$$\xi = \frac{a_0}{2 \cdot \omega} + \frac{a_1 \cdot \omega}{2} \qquad (1.24)$$

The relationship between damping ratio and frequency is illustrated in Figure 1.7.

---

[2] In the following, matrixes will be represented with capital boldface lettering and vectors with { }

[3] Typically, damping is expressed by the ratio, ξ, of the constant c to the critical damping value $2 \cdot m \cdot \sqrt{k/m}$, which is the largest value of damping for oscillatory motion in free vibration.

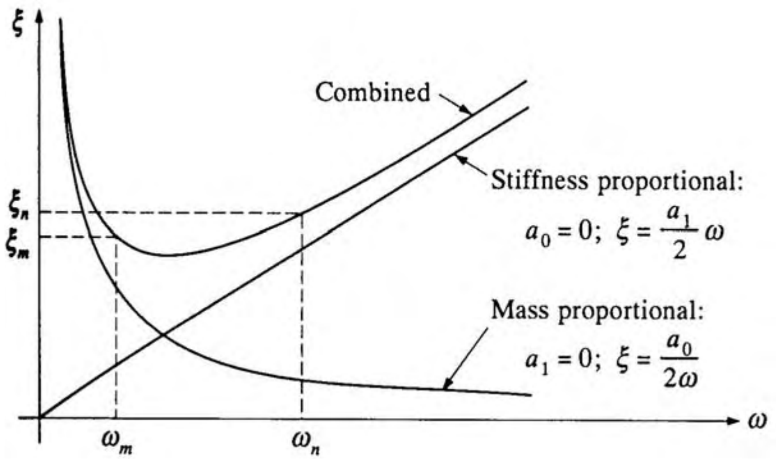

Figure 1.7 - Relationship between damping ratio and modal circular frequency (Clough and Penzien, 1993)

The convenience of this representation for damping is that we can choose a_0 and a_1 according the importance of the vibration mode for the response. Normally, the user assigns a reasonable damping ratio for the first modes of vibration, which contribute to effectively eliminate the contribution of higher modes.

Therefore, in most non-linear systems, the determination of the dynamic response is concerned with the evaluation of the stiffness influence coefficients according to the dynamical state of the system. Note that the mass at each degree of freedom is assumed to be constant for most engineering applications, and that the damping matrix is proportional to the mass and stiffness matrixes.

As in the case of the SDOF system, step-by-step integration procedures are the most adequate tool to determine the dynamic response of MDOF structures performing in the non-linear range. The concept is exactly the same as illustrated in section 1.2.1.1: non-linear response is approximated by successively changing linear response.

One of the most popular step-by-step integration procedures is that proposed by (Newmark, 1959). This is a generalisation of the linear acceleration method presented in the previous section. It uses two numerical parameters, γ and β, that replace the numerical coefficients 1/2 and 1/6 in equations (1.12) and (1.13). Thus, for the case of MDOF systems:

$$\{\Delta v_r\} = \{a_r(t_i)\} \cdot \Delta t + \gamma \cdot \{\Delta a_r\} \cdot \Delta t \tag{1.25}$$

$$\{\Delta d_r\} = \{v_r(t_i)\} \cdot \Delta t + \gamma \cdot \{a_r(t_i)\} \cdot \Delta t^2 + \beta \cdot \{\Delta a_r\} \cdot \Delta t^2 \tag{1.26}$$

According to (Paz, 1991) it has been found that the method introduces superfluous damping in the system if values of γ other than 1/2 are used. If this value is used and if β is set to 1/4, then the method is equivalent to assume constant mean acceleration in the time step. In this case the method is unconditionally stable and provides accurate results if small integration time steps are used.

1.2.2 Non-linear time-history analysis

Non-Linear Time-History Analysis (NLTHA) is generally accepted as the most suitable method to determine the seismic demand on structures designed to develop non-linear behaviour when subjected to earthquake motion. It allows the definition of the structural model on a differentiated fashion, i.e. the properties of each structural element may be explicitly defined. Moreover, the solution is determined by means of a numerical step-by-step integration procedure in the time domain, such as the ones discussed above. This enables the user to assess the entire dynamic response of the system from local to global structural performance without resorting to any type of external coefficients unrelated to the physical nature of the problem.

Two basic approaches can be pointed out regarding modelling of structural behaviour:

- Spread plasticity models
- Lumped plasticity models

The so-called fibre modelling approach is found in the first category. The sectional stress-strain state of beam-column elements is obtained through the integration of the nonlinear uniaxial stress-strain response including stress reversals of the individual fibres in which the section has been subdivided (Seismosoft, 2004). The discretisation of a typical reinforced concrete cross-section is depicted in Figure 1.8.

The advantage of this modelling approach is that non-linear behaviour can effectively be taken into account along the structural element and effects due to confinement, pinching (cf. section 2), cross-section geometry and reinforcement distribution may be realistically quantified. As a result, the variation of axial load, bending in two directions and coupling between bending and axial force can be properly taken into account with relatively limited input data, since only the non-linear uniaxial stress-strain curves of the materials are required to perform the analysis.

However, in the currently available versions, fibre modelling disregards important effects such as those related to shear deformations and buckling of the reinforcement.

Moreover, fibre modelling requires extensive calculations for the construction of the member tangent stiffness matrix in each step resulting from the integration along the section of stress and strains at each fibre. Thus, the computational effort is enormous. Furthermore, as referred to in (CEB, 1994), the large number of non-linear operations required by the computational scheme increases the possibility of numerical instability problems.

The lumped plasticity models try to capture the complex overall behaviour of structural members by means of semi-empirical hysteresis laws at the yield zones. Parts of the structure outside the yield zones remain in the elastic domain throughout the seismic action and therefore are modelled as elastic elements. They are specially suited for simple, regular structures in which the failure modes are easily identified but with an appropriate level of discretisation, more complex structures may be analysed. Spread plasticity may roughly be taken into account with a refined mesh of elements with non-linear behaviour. Computational effort is reduced regarding the requirements of the spread plasticity models.

However, significant knowledge and experience is essential to formulate and calibrate the equivalent force-deformations relationships in order to adequately represent structural behaviour. In connection with the discussion below on the cyclic behaviour of reinforced concrete elements, two of the most popular hysteresis models for cross-sections in frame structures are presented in section 2.

There is a wide range of commercial programmes available for performing NLTHA using lumped plasticity models. Typically, these are based on a finite-element (FEM) platform in which the solution is derived using the displacement method. The problem

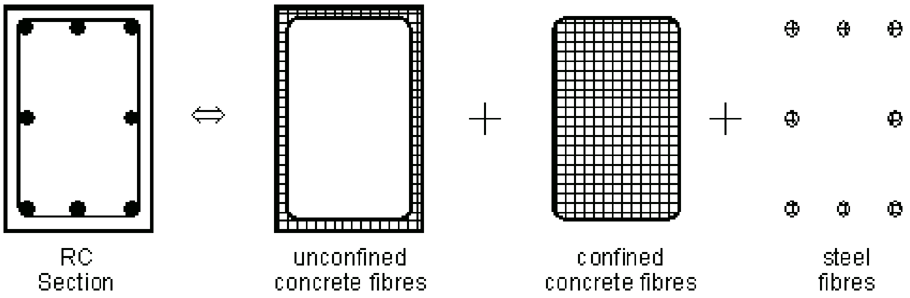

Figure 1.8 - Cross-section subdivision in fibre modelling approach (Seismosoft, 2004)

arises from the way modern structures are designed to withstand the effects of earthquakes, i.e. on the use of overstrength factors to design parts of the structure outside the yield zones. The resulting structural model in the FEM programme is characterised by discontinuities in terms of stiffness distribution at the joints between the plastic hinges and the remaining part of the linear elastic elements. This leads to discontinuities in terms of strength demand in the solution of the FEM programme and in turn violation of equilibrium. This is a drawback of the lumped plasticity models for the estimation of the strength demand in structures performing in the non-linear range.

The correct choice of the structural model depends of course on the complexity of the problem at hand as well the desired level of accuracy.

Despite its superior accuracy and rationality, there are some serious setbacks regarding the use of NLTHA as a routine design tool.

Firstly, the computational effort and time cost required to carry out NLTHA is not affordable to the majority of design offices. Also, as pointed out by (Chopra, 2004), the seismic demands estimated by this method are in general affected by modelling assumptions such as the hysteretic relationships of the plastic hinges, type of modelling approach and numerical procedure for the step-by-step integration of the equations of motion. Further, a statistical study of the dynamic response to several accelerograms is necessary, as the method cannot work directly with a spectrum. Finally and perhaps most importantly, NLTHA requires that the structure be completely defined beforehand in terms of strength and stiffness distribution as well as performance in cyclic behaviour to a level of detail hardly possible at initial stages of design. With this procedure, the design for seismic loading is a cumbersome, iterative process of data input, checking performance and changing design until satisfactory response is found. Therefore, it is unlikely that NLTHA will be implemented at a practical level. It seems that its use is destined for verification rather than design purposes.

1.2.3 Elastic Response Spectrum analyses

From the discussion above, it follows that there is a need for simplified design procedures able to provide engineers with sufficiently accurate results and maintain rationality. In recent years there have been a large number of proposals to estimate seismic demand in non-linear structural systems. Notably, many of these are fundamentally based on the concept of elastic spectrum, which was fully developed more than 60 years ago (Biot, 1942).

In its original form, elastic spectra are derived by time-history analysis of a large number of linear oscillators to a specified ground motion scenario[4]. The dynamic properties of the system, mass and stiffness are condensed in a single variable, the fundamental period of the structure, T. The latter is then related with the corresponding peak response parameter, which is the one most likely to be needed by the designer, per each value of viscous damping. The value 0.05 is normally used to define ξ in reinforced concrete structures. Figure 1.9 shows the response absolute acceleration, a, and the relative displacement, d_r, spectra[5] for the Loma Prieta, California, 1989, recorded at Corralitos station for 5% damping ratio to the critical value.

Moreover, elastic spectra have the property of being unique for each ground motion scenario, thus being a useful tool to estimate the dynamic effects associated with the seismicity of a particular region or implementation site. As long as they are available, design against ground motion typical of the implementation site may be carried out in a relatively easy to use graphical environment.

The extension to the MDOF case is based on the principle of superposition that relies on the assumption that the dynamic response of a structure results from the combination of each of the vibration modes according to the corresponding participation factor. The latter is a function of the mode shape, the mass distribution and the direction of the ground motion. In the obvious circumstance that peak response of each mode does not take place at the same time and in the same direction, further combination rules have to be included, the most popular in literature being the square root of the sum of the squares (SRSS) and the complete quadratic combination (CQC) (Paz, 1991; Clough and Penzien, 1993).

However, it is obvious that the “pure” elastic formulation of response spectra cannot be applied to the case of ductile response of structures.

Based on NLTHA of elastoplastic SDOF systems it was postulated that elastic spectra can estimate seismic demand on non-linear systems, provided that they are affected by

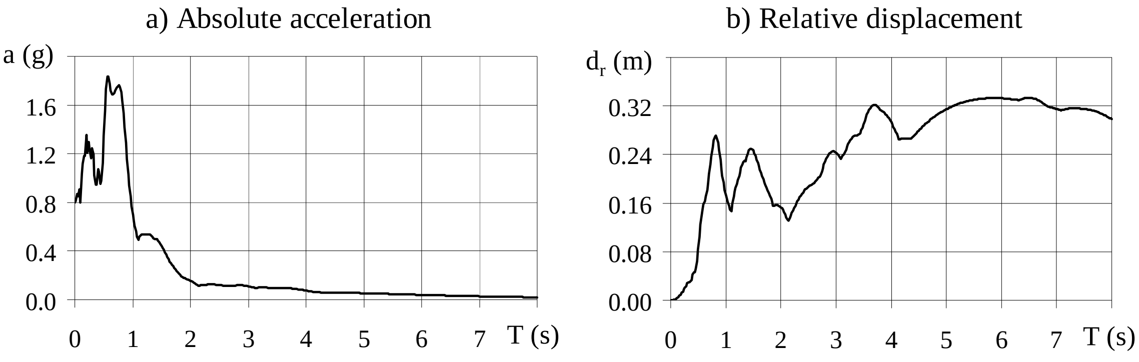

Figure 1.9 - Example of elastic spectra in terms of a) Absolute acceleration and b) Relative displacement

appropriate factors, the so-called reduction factors, R, (Newmark and Hall, 1982).

---

[4] In this work, the term *ground motion scenario* is applied to a number of records that, typically, reproduce the seismicity of a region or of a given implementation site.

[5] Normally acceleration spectra are in absolute coordinates since in this way the inertia forces in the system come out directly. Conversely, displacements and velocities are conveniently represented relative to the ground to assess the level of deformation in the system.

- In some period ranges it was observed that the peak response of elastoplastic oscillators is very close to the response of elastic oscillators with the same stiffness as the initial elastic stiffness of the elastoplastic oscillators, but with unlimited strength. As seen in Figure 1.10, this implies the reduction coefficient to be equal to the ductility factor, μ. This observation is referred as the *equal-displacement rule*.

$$R = \mu \tag{1.27}$$

- For shorter period structures, systems with typically natural period lower than the one corresponding to peak spectral acceleration value, the equal displacement rule leads to unsafe estimations, i.e. the ductility demand is larger than the force reduction factor. It seems that better agreement with NLTHA of elastoplastic SDOF systems is achieved by considering that energy consumed by an elastoplastic system with yield strength F_y to reach a certain level of deformation is the same as an equivalent elastic system developing strength $R \cdot F_y$. Thus, the relation between μ and R is taken from equalising the area below the elastoplastic curve to the area below the elastic curve in Figure 1.10. For this reason this observation is called the *equal-energy rule*.

$$R = \sqrt{2 \cdot \mu - 1} \tag{1.28}$$

However, as pointed out by (Priestley *et al.*, 1996), the basic idea of defining the seismic demand on ductile reinforced concrete structures based on observations of elastoplastic systems is weak, since this is hardly the typical force *vs.* deformation relationship defining the hysteretic behaviour of members with that material. As reported by (Miranda and Bertero, 1994), several modifications have been proposed to the formulations in (1.27) and (1.28) to account for the hysteretic behaviour of reinforced concrete. However, consensus has not yet been reached.

The most serious drawback of the use of elastic based spectra for seismic design of ductile structures deals with the principle of superposition. Modal superposition is only valid for the case of linear systems and small displacements. Response in the non-linear range is characterised by constant change of stiffness properties affecting the vibration modes, and the magnitude of deformations is large enough to invalidate the use of small displacements theory. Moreover, as (Priestley, 2003) points out, modal combination rules together with force reduction factors are of dubious validity when applied to all the modes of vibration in the same manner. For instance in the case of high-rise buildings, higher modes will translate in different axial force demands for different columns affecting not only the dissipation capacity there but also the stiffness properties. In multi-modal analysis it is impossible to allocate different stiffness to the columns according to the vibration mode, which in turn might yield estimations of forces grossly in error.

Another obvious disadvantage of using elastic based spectra for estimation of seismic demand on structures is the excessive emphasis put on the correct determination of the vibration periods. In fact, the latter quantities can only be properly estimated when stiffness distribution throughout the structure is defined. Strictly speaking, this is not the case of structures to be designed. To remedy this there are some rules yielding a crude approximation for the distribution of stiffness along the structure, but these are clearly incompatible with the sophisticated nature of the analysis techniques, such as multi-modal analysis. Even for simple structural systems where some simple rules

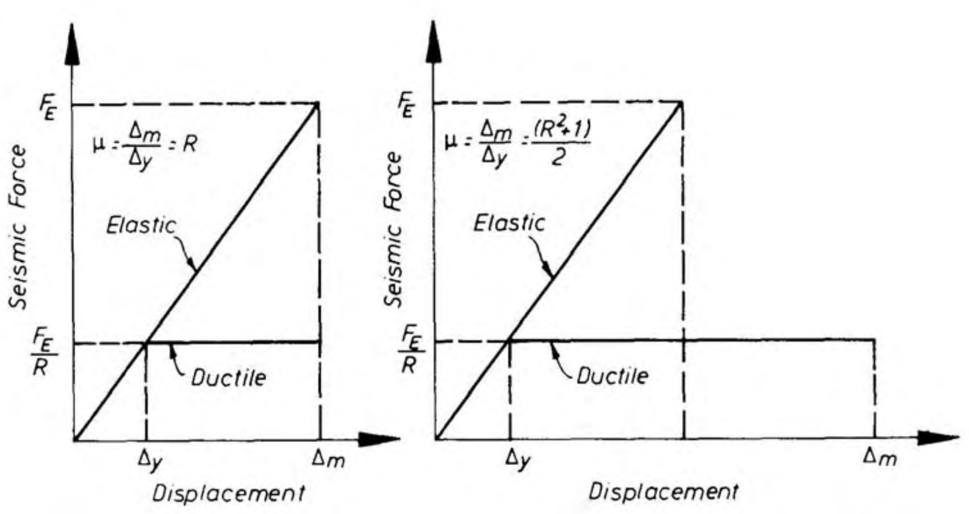

Figure 1.10 - Relationship between ductility and force reduction factors for construction of inelastic spectra(Paulay and Priestley, 1992)

might provide accurate estimations for vibration periods beforehand, duration effects including stiffness degradation cannot be taken into account by elastic based spectra.

Finally, design according to elastic based design spectra yields a system of forces that do not respect equilibrium and omit information about failure modes which, as seen in section 1.1, are crucial for structural performance evaluation.

1.2.4 Capacity spectrum method – Non-linear static analysis

A significant improvement in the development of simplified seismic design procedures for ductile structures was the so-called Capacity Spectrum Method, initially proposed by (Freeman, 1998).

In this procedure, the structure is “reduced” to an equivalent non-linear SDOF system, the seismic performance of which is derived on the basis of a highly damped elastic spectrum.

Initially, a standard static plastic analysis is carried out by imposing an incremental lateral force field “pushing” the structure well in the non-linear range. In Earthquake Engineering terminology this is often called *pushover analysis*. From this, the lateral force *vs.* global deformation relationship is obtained and plotted in an acceleration *vs.* displacement format dividing the lateral force by the weight of the structure – *the capacity curve*. The demands of a given ground motion scenario are defined by highly damped elastic spectrum also represented in an acceleration *vs.* displacement format – *demand spectrum*. The interception of the capacity curve and of the demand spectrum yields the seismic demand on the structure both in terms of acceleration and displacement demand (Figure 1.11).

The most innovative feature of the capacity spectrum method is the transformation of a MDOF structure to an equivalent SDOF structure. It has already been stated in section 1.1 that modern seismic design philosophy contemplates the choice and subsequent enforcement of a suitable collapse mechanism. This means that the mode of vibration of the structure for significant levels of plastic response is determined, which enables the treatment of the dynamic response as a generalised SDOF system

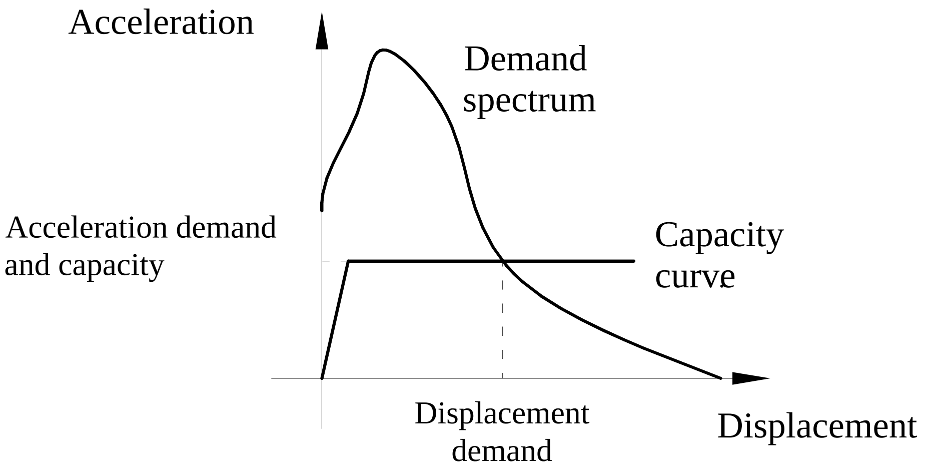

Figure 1.11 - Capacity spectrum method

(Clough and Penzien, 1993). This yields a great deal of simplicity to the process of seismic design. Moreover, from the capacity curve it is possible to verify the performance of the structure from global to local behaviour both in terms of deformations and internal forces.

However, the method is beset with some important inconsistencies, the most notorious of all being the dependence on an elastic *highly damped* spectrum to estimate seismic demand. The aim is to account for the energy dissipated by hysteretic behaviour by means of an “equivalent” artificially high viscous damping coefficient. As (Chopra and Goel, 2001) and (Krawinkler, 1994) showed, there is no physical evidence to support a relation between the hysteretic energy dissipation and an equivalent viscous damping, particularly for highly inelastic systems. Many authors (Reinhorn, 1997), (Chopra and Goel, 1999) and (Fajfar, 1999), proposed the use of inelastic spectra based on coefficients such as (1.27) and (1.28). However, as stated above, consensus on these coefficients has not yet been reached.

From a conceptual point of view, the capacity spectrum is not able to provide a solution for the limitation of the traditional elastic spectrum analyses regarding the consideration of duration effects. In fact, it is worth noting that the capacity curve is derived on the basis of a monotonic application of a lateral force field. Thus, some important aspects of dynamic response of reinforced concrete members in cyclic loading such as stiffness and strength degradation are not properly addressed.

Moreover, difficulties regarding the contribution of higher modes by pushover analysis have been reported (Krawinkler and Seneviratna, 1998). In fact, the lateral force field is usually derived based on modal combination of the most important modes of vibration. It is very difficult for the user to detect which higher mode will affect a particular member in the structure in advance, and even if this is considered, its “real effect” will be underestimated given the small participation factor. In the original versions, the final shape was kept constant but now “adaptive” pushover analyses (Antoniou and Pinho, 2004, for instance) are in order. In the latter type of analysis, the lateral load distribution is not kept constant but is continuously updated during the analysis according to the modal shapes and participation factors derived by eigenvalue analysis carried out at each analysis step. However, the problem with higher mode effects still remains.

Finally, from a practical perspective, the capacity spectrum method requires the structures to be designed to a rather detailed extent in order for the capacity curve to be properly defined. Of course, there is no need to specify the trends in which the hysteretic behaviour develops with cyclic loading as in NLTHA, but the distribution of strength and stiffness has to be well defined beforehand, which may equally compromise the straightforwardness of the design process.

1.3 The theory of rigid-plastic materials and limit analysis as a rational approach towards simplified seismic design of reinforced concrete structures

From the previous discussion, one fundamental problem with the existing analysis techniques for the estimation of the seismic demand applied to structures to be designed may be identified: the incompatibility of the growing complexity and degree of sophistication of the analysis technique and the crude definition *beforehand* of stiffness distribution throughout the structure. As (Priestley, 2003) points out, there is little point in having sophisticated analysis if it is based on very coarse and inaccurate data. Experimental and detailed analytical results on flexural behaviour reveal that yield curvature, ϕ_y, is effectively independent of strength, which means that stiffness is directly proportional to flexural strength, cf. Figure 1.12. This implies that an accurate estimation of the seismic demand cannot be carried out until the final member strengths have been defined. As Priestley suggests, at the very least, conventional seismic design based on stiffness definition is an iterative process, where this parameter is upgraded during each iteration.

Rigid-plastic theory avoids the consideration of stiffness in the definition of the properties of materials and of structural elements. In this theory, the only parameter describing the relation between demand and response is the strength capacity, in terms of yield stress in the case of materials, or yield force/ moment in the case of structural elements. The corollary of this is that seismic demand may be estimated solely on the basis of the required strength capacity assigned to the structural system. Thus a great deal of simplification may be introduced. Moreover, the only source of structural displacements is due to plastic deformations, which means that there is a direct relation between global displacement demand and the extent of damage.

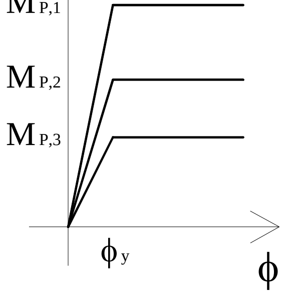

Figure 1.12 - Realistic influence of flexural strength on moment (M) vs. curvature (ϕ) relationship. Constant yield curvature approach

Of course, the assumption leading to rigid-plastic behaviour must be verified, which means that contribution of elastic deformations for the overall dynamic response must be significantly less important than plastic deformations. This is the case of structures able to develop highly ductile modes of failure under lifetime earthquake events such as reinforced concrete frames with flexure dominated behaviour.

On the other hand, one must still ensure that the chosen collapse mechanism indeed takes place. The basic tool to solve this problem is found in the application of the extremum principles of Plasticity, i.e. in the application of the limit analysis theorems (Nielsen, 1998).

Consider a given structure subjected to a specific load. The *lower bound theorem of the theory of Plasticity* states that if a safe and statically admissible stress distribution may be found in the structure, then this load is lower than or equal to the collapse load. Conversely, if the load necessary to subject the structure to a geometrically possible deformation field is calculated by the work equation, then the load is greater than, or equal to, the collapse load. This is the *upper bound theorem of the theory plasticity*. Therefore, the collapse load has been found if it is possible to assign for the same load a geometrically possible deformation field and a safe statically admissible stress field.

Structural design for a specific collapse mechanism is therefore limited to finding a stress field outside the plastic zones that respects equilibrium with the external loads. Final design is carried out assuming that the yield zones have the required strength and ductility capacity and the remaining part of the structure has enough strength not to yield.

For most structures there are of course many possible collapse mechanisms. However, only a few can assure ductile behaviour in earthquake loading, which significantly reduces the problem of choosing the most suitable one.

These are the key-principles upon which the work that will be presented in this thesis is based, namely the development of the *Rigid-Plastic Seismic Design (RPSD) method*.

This is a general, simplified, straightforward seismic design procedure that combines

a) The simplicity and practical value of spectral analysis for the estimation of the required dissipation capacity, and

b) The rationality of NLTHA for the estimation of the seismic demand solely based on the properties of the structure.

It will be shown that the seismic demand on a structure chosen to develop a collapse mechanism may be determined using an appropriate spectrum, *the rigid-plastic spectrum*, after the definition of a performance parameter able to relate dynamic performance with allowable damage. The advantage of the rigid-plastic spectrum is on the explicit relation between maximum dynamic response of the structure in a selected ground motion scenario and its dissipation capacity. Once the latter parameter is found, the dynamic response of the structure is fully determined. Final design, i.e. distribution of strength and hence of stiffness throughout the structure, proceeds with the enforcement of the chosen collapse mechanism by choosing a suitable way for the structure to withstand the stresses imposed by seismic loading. This is facilitated to a great extent by the definition of a conservative set of external lateral forces, the shape and magnitude of which are independent of the ground motion scenario – *The extreme loading scenarios*.

1.4 Outline

Although the RPSD method is quite general, in this work, special emphasis is devoted to the case of reinforced concrete frame structures with flexure dominated behaviour. This is because, if properly designed, this type of structures may develop significant levels of ductility. Moreover, they are most illustrative of the benefits of the simplification introduced by RPSD method, given the large number of degrees of freedom and extensive modelling requirements.

The discussion in the following chapter begins with an overview of cyclic behaviour of reinforced concrete elements, i.e. linear members and beam-column joints. The primary objective of this chapter is to identify the means by which ductile modes of failure are reached and brittle mechanisms are avoided. Also, a new simplified procedure to estimate the available rotation capacity of plastic hinges with flexure dominated behaviour will be discussed.

Chapter 3 deals with the formulation of the RPSD method. Firstly, we discuss the assumptions used in the design procedure and give the basis for rigid-plastic dynamics, i.e. the establishment of the equations of motion in rigid-plastic structures. Secondly, the basis for estimation of the seismic demand in the RPSD method is introduced, namely, the rigid-plastic spectrum and the extreme loading scenarios approach. Details regarding the consideration of P-Δ effects are also provided.

Finally, in chapter 4 two applications of the RPSD method for the design of reinforced concrete frames are presented.

Conclusions will be throughout the text, the most important of which are summarized in section 5.

2. Cyclic behaviour of reinforced concrete elements

It has already been mentioned that modern seismic design philosophy implies design for ductility rather than for adequate lateral strength capacity. To understand the trends in which ductile behaviour is maintained during ground motion is of fundamental importance for the structural engineer faced with the task of seismic design.

Therefore in this chapter we present a review of the cyclic behaviour of reinforced concrete elements integrated in frame systems. The discussion starts at the materials level. The bond between reinforcement steel and concrete is also discussed. It proceeds to the cyclic behaviour of linear structural members according to the type of loading rather than their structural function. Cyclic performance of joints will also be discussed.

Relevant experimental work is the basis of this chapter except in the section devoted to cyclic behaviour of joints, where the discussion is presented in a qualitative manner. This is due mainly to the scarcity of experimental work available on the subject.

The work presented was carried out during the first year of the Ph.D. study and has already been published (Domingues Costa, 2003) with the exception of sections 2.2.1.4 and 2.3.

2.1 Properties of concrete and reinforcement steel

2.1.1 Concrete

One of the most important features influencing seismic behaviour of reinforced concrete is confinement. This refers to the influence that lateral reinforcement (in the form of hoops or spirals) has on concrete, i.e. the favourable effect on ductility and strength. However, before discussing the properties of confined concrete it is important to bear in mind the main features of the behaviour of unconfined concrete.

2.1.1.1 Unconfined Concrete

Monotonic loading

Diagrams of stress (σ) versus strain (ε) for monotonic compression and for various concrete grades are depicted in Figure 2.1. These diagrams result from tests on cylinders and were carried out with deformation control after the development of the maximum strength (CEB, 1994). In Figure 2.1, f_c represents the compressive cylinder strength of the concrete.

A study of these curves leads to an important conclusion: Low grade concrete is more ductile than high-grade concrete. In fact as the concrete strength increases, the descending branch gets steeper, indicating brittle behaviour. This apparent brittleness in high-strength concrete is of great concern and it must be considered when a concrete structure is subjected to high compression strains.

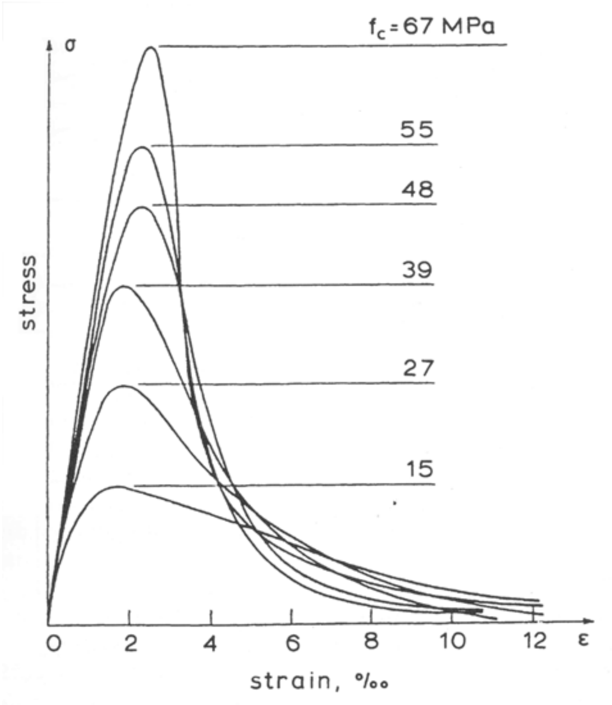

Figure 2.1 - Monotonic stress-strain relationship for compressive load (CEB, 1993)

It should be noted that these tests are of the statical type. During an earthquake, strains may vary at a rate of 1-2% per second. It is known that the concrete compressive strength under dynamical loading, $f_{c,dyn}$, exceeds up to 20% of the monotonic compressive strength for strain rates, $\dot{\varepsilon}$, of the order 1% per second in normal grade classes, this value being lower for higher classes. On the other hand, large strain rates lead to a steeper slope of the descending branch of the stress-strain diagram. This implies that high strain rates, such as those of seismic loading, have positive as well as negative effects on the response of concrete.

Three different parts can be clearly identified in the monotonic curves shown in Figure 2.1:

1. An initial part with a linear branch indicating elastic behaviour.
2. A second part for strains corresponding to stresses of 70% to 100% of the maximum strength, where a gradual reduction in stiffness is evident. In this range of stresses, bond cracks in the interface of the mortar and aggregates develop into mortar cracks mainly due to stress concentrations at the tips.
3. A third part for strains larger than the one corresponding to maximum strength. This is the above-mentioned descending branch indicating the so-called strain-softening phenomenon. In this phase the internal cracks propagate in an unstable manner and tend to become a macroscopic phenomenon.

An important parameter for strength and ductility calculations is the ultimate compressive strain, ε_{cu}. For design purposes this parameter is defined by the value at which the maximum bending capacity for a cross-section is achieved. Most of the codes range this parameter from 0.35% to 0.40%.

Because of the low value of the tensile strength compared to the compressive strength, and because the seismic action induces significant inelastic response on structural elements and pronounced tensile softening due to cyclic loading, this parameter is not

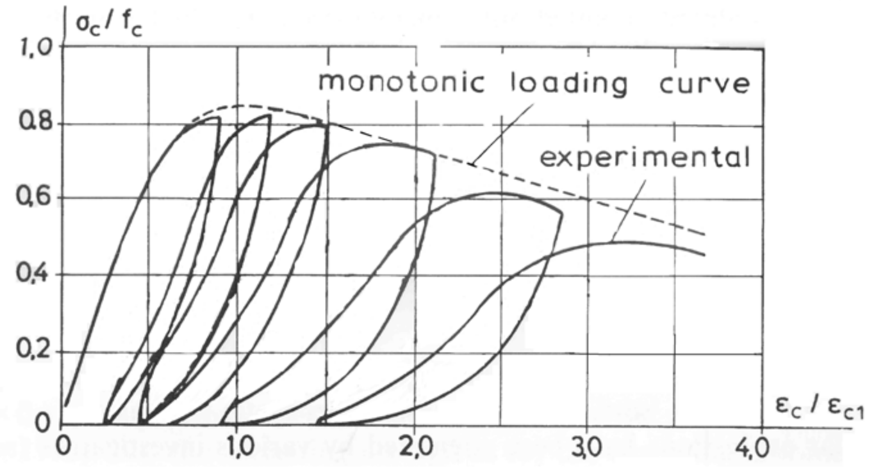

Figure 2.2 - Cyclic uniaxial compression with full unloading (Karsan and Jirsa, 1969). ε_c is the compressive strain of the specimen and ε_{c1} the compressive strain of the specimen at maximum compressive stress

usually taken into account in strength calculations for seismic design. If tensile stresses are considered, the stress-strain relation of concrete in tension may be defined as a straight line up to the tensile strength. The corresponding modulus of elasticity is considered the same as for compression.

Response to cyclic loading

With the intention to study the behaviour of unconfined concrete under alternate compression, (Karsan and Jirsa, 1969), carried out an experimental work that led to the results presented in Figure 2.2. This figure shows the stress-strain diagram of a concrete cylinder subjected to repeated uniaxial compression involving loading and unloading under deformation control.

Until the maximum strength is achieved, the loading branch coincides with the monotonic loading curve. For the unloading branches, two distinct parts can be pointed out: the one immediately after the maximum stress, which is extremely steep due to the highly compressed state of the concrete at early stage of the unloading phase, and the following with a minor stiffness as a result of the plastic deformations formed in the previous cycle. Regarding the reloading branches, as the number of cycles increases, there is a reduction in slope and maximum strength. This is due to successive degradation of the internal structure of the specimen caused by the propagation of the mortar cracks after each cycle.

An initial conclusion from the results obtained is that repeated high-intensity compressive loading produces a pronounced hysteretic effect in the compressive stress-strain relationship of concrete. This is evident when observing the slope and strength reduction of the successive unloading and reloading branches after each cycle. Thus, as the number of loading-unloading cycles increase, the compressive strength and stiffness of the concrete decreases, indicating the softening of the material with alternate loading.

It can also be seen that the envelope curve (the limiting curve below which the stress-strain curve lie) is almost identical to the monotonic loading curve. This conclusion is of particular importance when modelling the response of concrete to uniaxial compression. In fact, for this state of stress and for practical purposes, the most important aspect in modelling is the accurate description of the envelope curve rather than the detailed shape of the reloading and unloading branches.

Aoyama and Noguchi, 1979, concluded that alternate loading-unloading does not affect the behaviour of concrete as long as the imposed compressive stress, σ_c, does not exceed approximately 50% of the dynamic strength in compression, $f_{c,dyn}$. On the other hand, if $\sigma_c \geq 0.85 \cdot f_{c,dyn}$, significant reduction both in compressive strength and stiffness, as in Figure 2.2, must be expected due to the successive spreading of the mortar cracks.

For the study of the response of concrete to cyclic loading, concrete in tension has no practical significance. As soon as the tensile strength is exceeded, cracking will take place and so energy dissipation through hysteretic loops will be negligible. When a structure is subjected to an earthquake, this phenomenon might well occur at the beginning of the loading. Therefore, the effect of tensile strength is usually disregarded for seismic design purposes.

2.1.1.2 Confined Concrete

It is known that both ductility and strength of concrete significantly increase in a triaxial compression state of stress. In practise, this stress field may be approached by providing adequate lateral reinforcement as long as it prevents the element from lateral expansion when subjected to axial compression.

The effect of confinement depends on the level of the lateral expansion, which is directly related to the compressive stress by means of the *Poisson effect*. At low levels of compressive stress, the lateral reinforcement is hardly stressed and therefore the concrete is considered unconfined (first part of the monotonic curves of Figure 2.1). The concrete becomes confined for levels of compressive stress close to the uniaxial compressive strength. At this stage (second part of the monotonic compressive stress-strain relationship), the lateral expansion resulting from the spreading of the internal cracking activates the lateral reinforcement, which then leads to a confining reaction to the concrete. In this way, lateral reinforcement provides passive confinement, preventing the unstable propagation of the internal cracking.

Thus, the favourable effect of confinement is due to the fact that transverse pressure from lateral reinforcement keeps the inner structure of the concrete member preserved, delaying the failure due to sliding along the cracks.

(Scott, Park and Priestley, 1982) conducted an experimental investigation into the behaviour of short reinforced concrete columns submitted to failure in compression at different strain rates, $\dot{\varepsilon}$, ranging from $3.3\text{x}10^{-6}$/s (static loading) to $16.7\text{x}10^{-3}$/s (seismic loading). The specimens were 450 mm square by 1200 mm high and contained either 8 or 12 longitudinal reinforcement steel bars and different arrangements of square steel hoops (Table 2.1). A specimen with the same dimensions but with no reinforcement at all was also tested for comparison.

Figure 2.3 shows the stress-strain diagrams for specimens 1, 17, 18, 19 and 20.

As mentioned above, it should first be pointed out that the strain rate for the confined concrete specimens corresponded to seismic loading, $\dot{\varepsilon} = 1.67\%/\text{s}$, while the plain concrete specimen was tested under static loading. The strain rate affects the response of confined concrete in the same way as explained for the case of unconfined concrete (larger maximum strength, but steeper descending branch in the σ-ε relationships).

Table 2.1 - Details of test specimens and tests results

(Scott, Park and Priestley, 1982)

Specimen number		1	12	13	14	15	17	18	19	20
Concrete compressive strength (MPa)		25.3	24.8				24.8			
Reinforcement arrangement		-	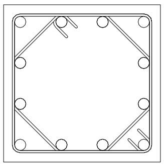				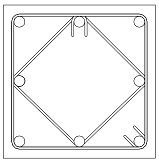			
Longitudinal reinforcement	Diameter (mm)	-	20				24			
	Yield strength (MPa)	-	434				394			
Transverse reinforcement	Diameter (mm)	-	10		12		10		12	
	Spacing (mm)	-	98	72	88	64	98	72	88	64
	Yield stength (MPa)	-	309		296		309		296	
	Volume ratio of transverse steel, ρ_w (%)	-	1.40	1.82	2.24	3.09	1.34	1.74	2.13	2.93
Strain rate, $\dot{\varepsilon}$ ($^{o}/_{oo}$/s)		$3.3x10^{-3}$	16.7				16.7			
Maximum strength (MN)		4.38	8.50	8.65	8.80	9.40	7.90	8.50	8.40	8.80
Average concrete strain at first hoop fracture ($^{o}/_{oo}$)		-	3.0	4.0	4.5	5.50	4.0	2.5	3.5	4.0

Therefore, to accomplish a direct comparison, the ordinates of the σ-ε relationships for the confined specimens should be reduced by approximately 24%.

This experimental work clearly highlights the main advantages of confined concrete over unconfined concrete:

- Confined concrete has a significantly larger compressive strength. The compressive strength of the plain concrete did not exceed 86% of the cylinder

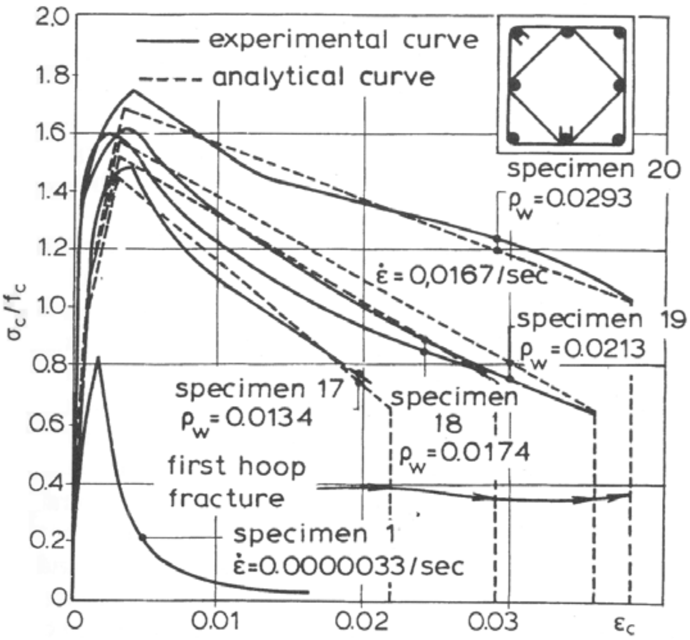

Figure 2.3 - σ_c vs. ε_c diagrams of unconfined concrete specimen and specimens with different hoop configurations (Scott, Park and Priestley, 1982)

strength, f_c. On the contrary, confined concrete compressive strengths reached values from 19% to 41% higher than f_c after the above-mentioned adjustment. It should be noted that under seismic loading (high strain rate), the concrete strength may reach values up to 80% higher than the cylinder strength.

- Confined concrete has a significantly larger reserve of ductility. In these tests the strains were measured until fracture of the first hoop. The values recorded for the ultimate strain ranged from about 25 to $40^{o}/_{oo}$, which is an order magnitude higher than the values usually obtained in unconfined concrete (3.5-$4.0^{o}/_{oo}$).

Types of Confinement

Two main types of lateral reinforcement are used to confine concrete: circular steel spirals (Figure 2.4 to the left-hand side) and square or rectangular steel hoops (Figure 2.4 to the right-hand side). Tests (Aoyama and Noguchi, 1979) show that spirals are more effective than rectangular hoops regarding the favourable effect on ductility and strength.

The reason for the considerable difference in confinement by these two types of lateral reinforcement lies in their shape (see Figure 2.4).

Circular spirals are in axial hoop tension and provide a continuous confining pressure (σ_l in Figure 2.4). When closely spaced, they provide a state of stress near triaxial compression at large transverse strains. On the other hand, square or rectangular hoops can only provide confinement in the region near the longitudinal reinforcement bars and in the centre of the cross-section, because the lateral expansion of the concrete tends to bend the sides of the hoops outwards. Thus a significant proportion of the cross-section is unconfined.

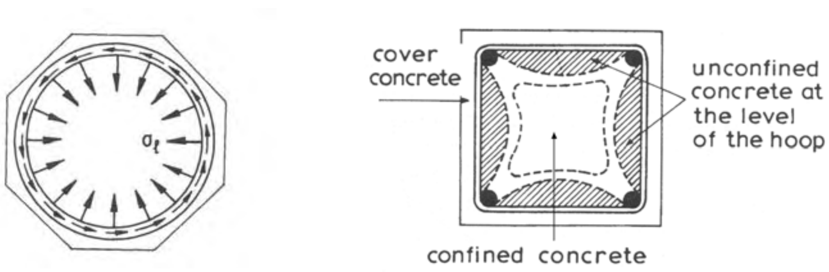

Figure 2.4 - Circular spirals and square hoops (Penelis and Kappos)

Table 2.2 - Properties of the columns (Ozcebe and Saatcioglu, 1987)

Test Specimen	Concrete Strength (MPa)	Longitudinal Steel		Transverse Steel				
		$f_{y,l}$ (MPa)	ρ_l (%)	$f_{y,t}$ (MPa)	ρ_w ($^o/_{oo}$)	s mm	Configuration	$\frac{A_w \cdot f_{y,t}}{s}$ (N / mm)
U3	34.8	438	3.27	470	16.9	75	Type A	1253
U4	32.0	438	3.27	470	25.4	50	Type A	1880
U6	37.3	437	3.27	425	19.5	65	Type B	1262

Parameters affecting confinement

With the intention of showing the influence of confinement on the cyclic behaviour of concrete, (Ozcebe and Staacioglu, 1987) tested four full-scale columns under simulated seismic loading. However, in this work only the results corresponding to three specimens (U3, U4 and U6) are discussed. The experimental program is depicted in the Figure 2.5 and in Table 2.2. In the latter, the index l refers to the longitudinal direction and the index t to the transverse direction; ρ_l is the longitudinal reinforcement ratio and ρ_w is the transverse reinforcement volume ratio; s is the hoop spacing and A_w is the nominal area of transverse reinforcement per hoop configuration.

As shown in Figure 2.5, the longitudinal reinforcement arrangement was the same for each specimen. All specimens were designed with excess shear capacities so that the failure would be governed by flexure. The differences between the specimens were in the transverse reinforcement level:

- Type A was used in both U3 and U4 specimens, but in the latter the tie spacing was 67% smaller;
- The lateral reinforcement used in specimen U6 was of the type B. This specimen was designed to have the same shear capacity as the specimen U3 (see last column of Table 2.2), while maintaining approximately the same spacing of transverse reinforcement.

The specimens were subjected to the displacement history shown in Figure 2.6. The quantity Δ_y refers to the yield displacement of the specimen. This parameter was defined as the displacement level at which the critical column section yielded as a whole and was recorded during the test in the region where the rate of strain variation

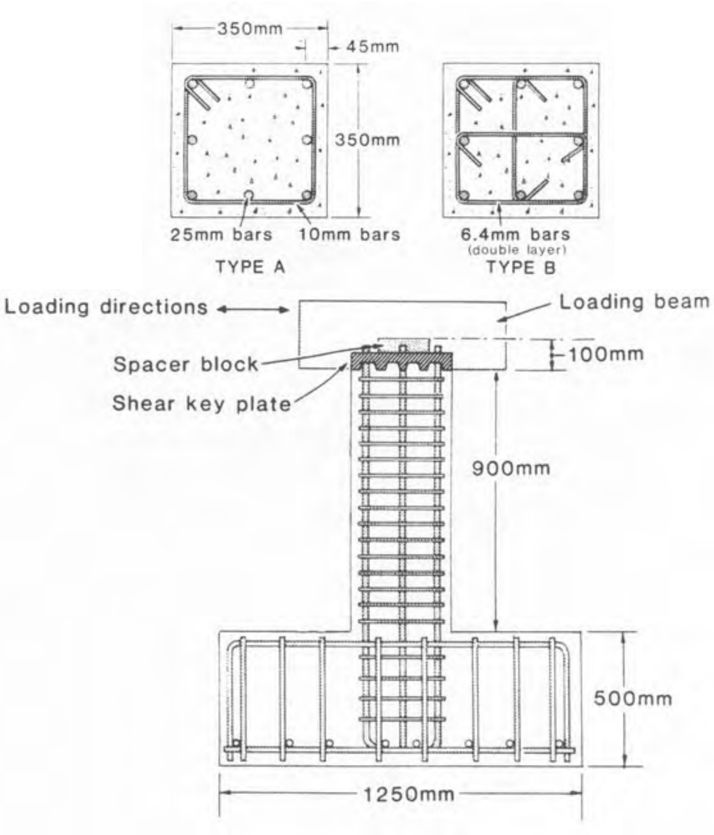
350mm
45mm
350mm
25mm bars
10mm bars
TYPE A
6.4mm bars
(double layer)
TYPE B
Loading directions
Loading beam
Spacer block
Shear key plate
100mm
900mm
500mm
1250mm

Figure 2.5 - Geometric details of the columns (Ozcebe and Saatcioglu, 1987)

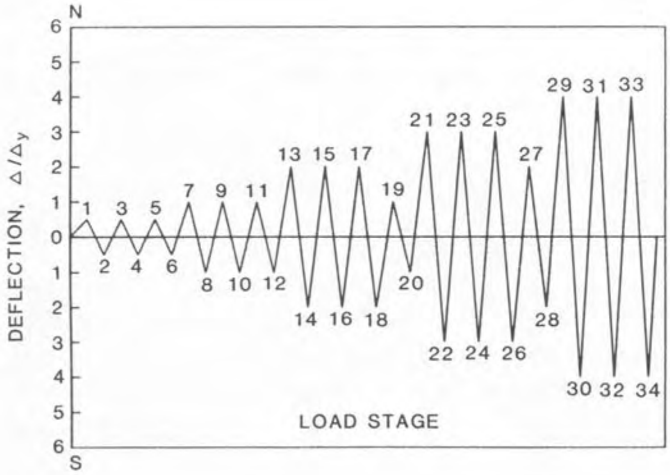

Figure 2.6 - Imposed displacement history (Ozcebe and Saatcioglu, 1987)

was very high at relatively constant load. All columns were tested under a 600 kN constant compressive axial load, which corresponded to 12% of the nominal column capacity.

The hysteretic force-deformation relationships of the three columns are shown as well as the corresponding photographs of the specimens at the end of the $3\Delta_y$ cycles (see Figure 2.7, Figure 2.8, Figure 2.9).

The main conclusions of this experimental work are:

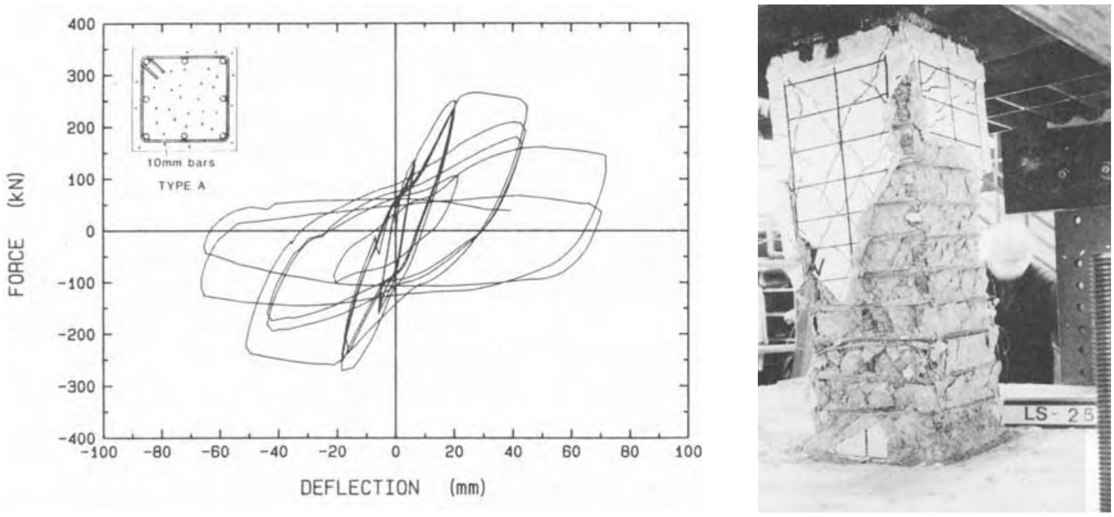

Figure 2.7 - a) Hysteretic behaviour for specimen U3 b) Specimen U3 at the end of $3\Delta_y$ cycles (Ozcebe and Saatcioglu, 1987)

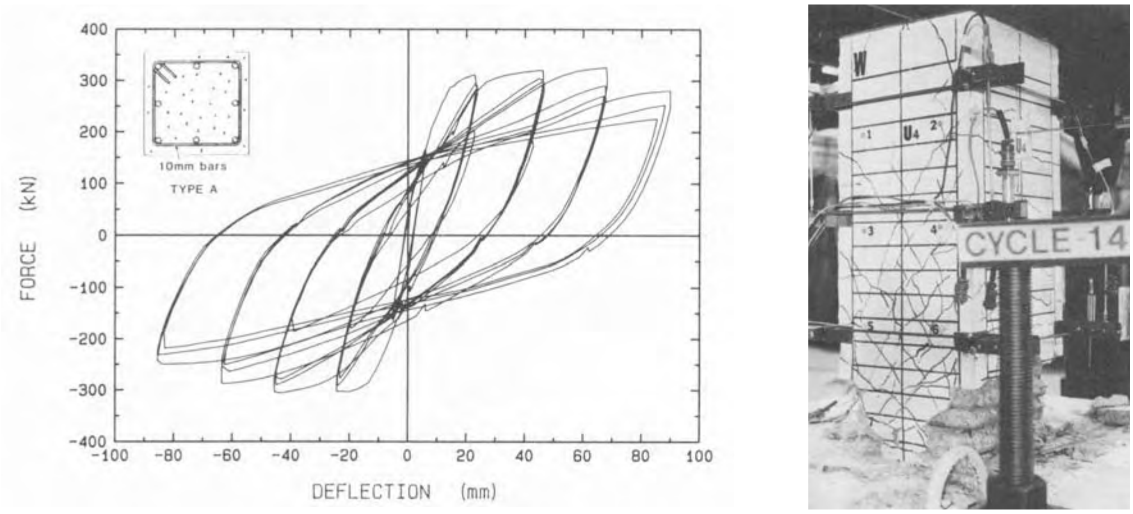

Figure 2.8 - a) Hysteretic behaviour for specimen U4 b) Specimen U4 at the end of $3\Delta_y$ cycles (Ozcebe and Saatcioglu, 1987)

- Comparing the hysteretic force-deformation relationships for specimens U3 and U6, it is evident that despite having approximately the same amount and spacing of lateral reinforcement, specimen U6 had superior behaviour with stable hysteretic loops and with negligible strength and stiffness reduction throughout the loading. On the other hand, U3 exhibited poor behaviour with rapid strength and stiffness degradation. This is confirmed when comparing the damage after stage 26 for both specimens (Figure 2.7b) and Figure 2.9b)). In fact, specimen U3 could not survive the cycles at $3\Delta_y$. This difference in behaviour is due to the difference in the types of lateral reinforcement. The superiority of Type B configuration lies in the effectiveness of longitudinal column reinforcement in confining the core concrete when supported by the crossties.
- Another parameter investigated experimentally was the influence of spacing and amount of transverse steel. Observing Figure 2.7b) and Figure 2.8b) we can

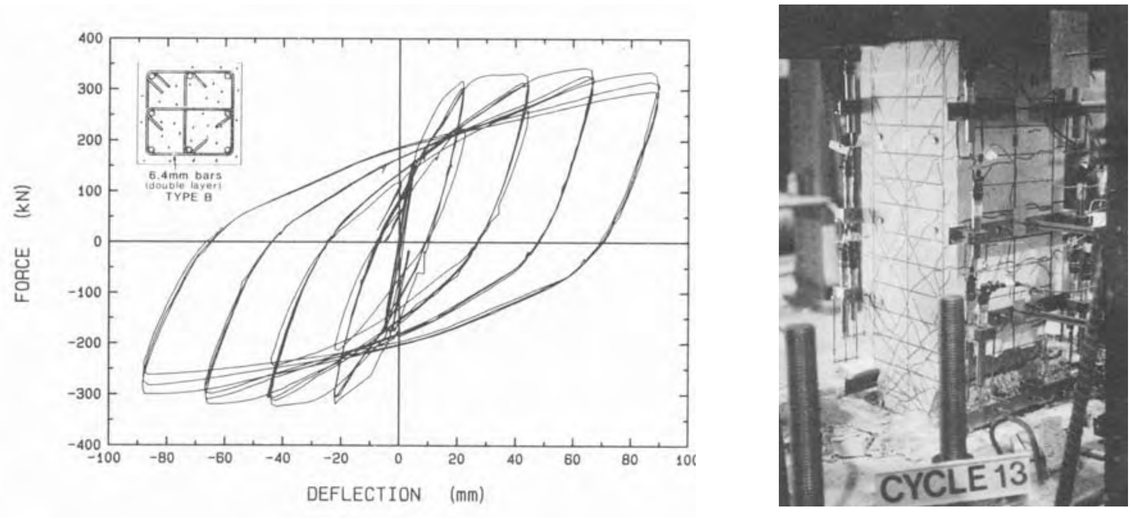

Figure 2.9 - a) Hysteretic behaviour for specimen U6 b) Specimen U6 at the end of $3\Delta_y$ cycles (Ozcebe and Saatcioglu, 1987)

conclude that specimen U3 experienced significantly larger damage than specimen U4. Referring to the corresponding hysteretic force-deformation relationships, it is evident that specimen U4 behaved in a far more ductile manner then U3. In fact, after stage 34 in the loading history, this specimen could still sustain 70% of its peak load. Therefore the behaviour of U4 showed the favourable influence of both the amount and spacing of lateral reinforcement. However, comparing the force-deformation relationship of specimen U4 with the one of specimen U6, we can see that the former, despite having a significantly larger lateral reinforcement ratio, ρ_w, had a behaviour close to, but not as favourable as the behaviour of specimen U6. This fact shows that the effect of ρ_w is outweighed by a rational hoop configuration concerning the ductile behaviour of confined concrete. This suggests that a proper choice of confinement is a more feasible solution than increasing ρ_w.

Scott, Park and Priestley, 1982, also studied the effect of spacing of transverse reinforcement on the efficiency of confinement. Their experimental work is also useful for understanding the influence of some basic parameters of confinement. Two main comments can be made:

- Firstly, as expected, both strength and ductility increase with the transverse reinforcement volume ratio, ρ_w. This is due to the fact that the transverse confining pressure increases with the content of transverse steel.
- The comparison between the behaviour of specimens 18 and 19 in Figure 2.3 can be used to assess the influence of hoop spacing. Both specimens exhibited similar behaviour as the peak stresses were almost identical and the shape of the descending branch was also (approximately) identical. However, specimen 18 had a lower transverse reinforcement ratio, but the hoops were placed closer than in specimen 19. Therefore one can conclude that similar confinements can be achieved with lower transverse ratios as long as closer spacing is used. The concrete is confined by arching in the concrete between transverse bars (Figure 2.10). If the spacing is large, it is evident that a large volume of concrete cannot be confined and may spall away.

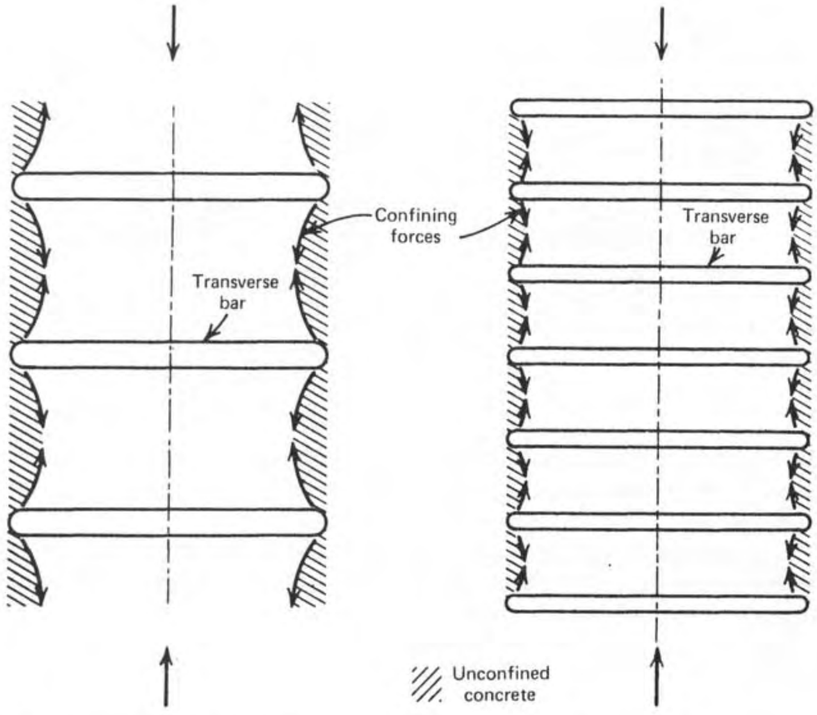

Figure 2.10 - Effect of spacing of transverse reinforcement on the efficiency of confinement (Park and Paulay, 1975)

- The maximum strength of each specimen in group 12-15 is larger than the corresponding specimen in group 17-20 (see Table 2.1). This indicates better confinement of the specimens with 12 longitudinal steel bars. In fact, the closer the reinforcement bars, the less the area of unconfined concrete, due to the bending of the sides of the hoops.

In the following the parameters affecting the efficiency of confinement are summarized:

i. The yield strength of the transverse reinforcement, as this gives an upper limit to the confining pressure;
ii. The compressive strength of concrete. As discussed previously in section 2.1.1.1, lower strength concrete is more ductile than higher strength concrete. Additionally, the lateral expansion in lower strength concrete is larger, due to the Poisson effect, for the same magnitude of axial loading. Therefore the confining pressure is activated sooner in lower strength concrete, implying that the hoops will be more stressed than for higher strength concrete;
iii. The longitudinal reinforcement as concluded from the experimental work carried out by (Scott, Park and Priestley, 1982);
iv. The ratio of the diameter of the transverse steel to the distance of lateral reinforcement between longitudinal bars. Larger diameters of the transverse steel bars lead to less bending and thus to a smaller volume of unconfined concrete along the sides of the hoops;
v. The spacing of the transverse reinforcement as shown in the experimental work carried out by (Scott, Park and Priestley, 1982);
vi. The volume ratio of reinforcement steel, ρ_w as explained in the work of (Scott, Park and Priestley, 1982) and (Ozcebe and Staaciougl u, 1987);

vii. The hoop configuration. See conclusions from the experimental work of (Ozcebe and Staaciouglu, 1987).

2.1.2 Reinforcement Steel

2.1.2.1 Monotonic loading

The typical behaviour of steel bars loaded monotonically in tension is presented in Figure 2.11.

The main conclusion taken from the results presented in Figure 2.11 is that the behaviour of low-grade steel is more ductile than that of high-grade steel. In fact, low-grade steel exhibits a wider and better-defined yield plateau. As the steel grade increases, the ratio of peak stress to yield stress increases, which clearly indicates that the influence of strain hardening is larger for high strength steel. Moreover, for high strength steel the ultimate deformation is much less than for low strength steel.

This may lead to the conclusion that the designer interested in seismic protection of the structure would prefer the use of low strength class steel, as this is more ductile. However, designing with low strength steel leads to the use of larger diameters of the reinforcement. Larger diameters have unfavourable effects regarding cracking and therefore contribute to a larger strength and stiffness degradation of structural elements (as presented in section 2.2).

Recent tests (Pipa and Vercesi, 1998) carried out at the National Laboratory of Civil Engineering (LNEC), Lisbon, Portugal, investigated the properties of the new generation of European steel type Grade B400 and B500 Tempcore. Results have shown excellent maintenance of ductile properties even at large deformations, ε_s=10%, and a strain hardening factor of 1.2.

2.1.2.2 Cyclic loading

Experimentally, curves for steel bars subjected to repeated axial loading (compression or tension) with strain rates, $\dot{\varepsilon}$, similar to earthquake loading with full unloading but

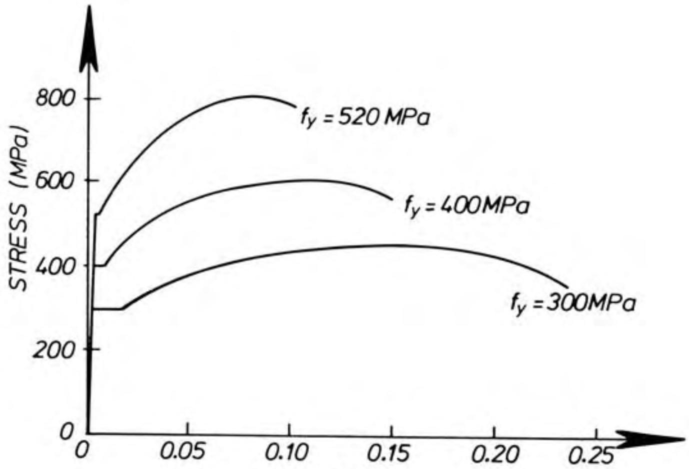

Figure 2.11 - Typical stress-strain curves for steel reinforcement (Paulay and Priestley, 1992); f_y is the yield strength of the steel reinforcement

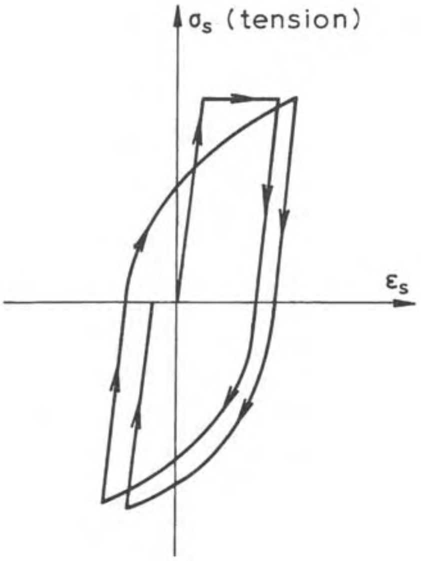

Figure 2.12 - Typical stress-strain curve for steel bar subjected to cyclic loading (Penelis and Kappos, 1997)

no stress reversal, have shown that, as in concrete, the envelope curve practically coincides with the monotonic loading curve. The unloading and consequent reloading branches on the stress-strain diagrams present a narrow hysteretic loop, indicating small energy dissipation. In most of the practical idealisations of the steel behaviour under the conditions mentioned above, this hysteretic loop is disregarded and so both unloading and reloading branches are assumed to have the same slope as the initial loading branch, corresponding to the modulus of elasticity, often taken as 200 GPa (CEN, 1991).

In the case of seismic loading, depending on the structural element, the reinforcement steel may be submitted to cyclic loading, which implies stress reversals. Figure 2.12 shows the typical stress-strain curve for a steel bar under these conditions.

This figure shows a reduction of stiffness at stresses much lower than the first yield limit after a stress reversal in the inelastic range. This feature is known as the *Bauschinger effect* and it should always be regarded when considering the cyclic behaviour of reinforced concrete. On the other hand, the first part of the unloading takes place in an almost elastic manner and therefore usually its branches are assumed to have the same slope as the first loading branch.

2.1.3 Bond between concrete and steel

It is widely known that the composite action of concrete and steel is due to bond forces between these two materials. Anchorage may take place along the bars, as in the case of plain bars, at their ends by means of hooks, anchor plates, etc. Ensuring adequate anchorage of the reinforcement steel is the most important aim when detailing reinforced structural elements. Additionally, bond plays a dominant role with respect to seismic behaviour not only because of the reasons stated above, but also because it affects stiffness and energy dissipation capacity.

Considering the equilibrium of the forces acting on an infinitesimal element of a plain steel bar, as shown in Figure 2.13, we find:

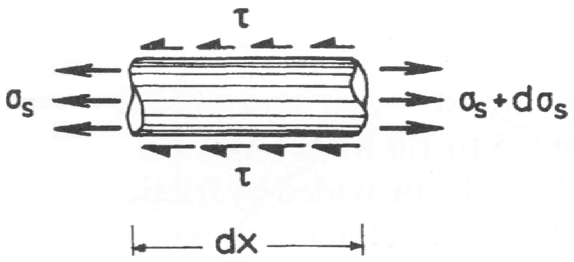

Figure 2.13 - Steel stresses in an infinitesimal element of a plain reinforcement bar (Penelis and Kappos, 1997)

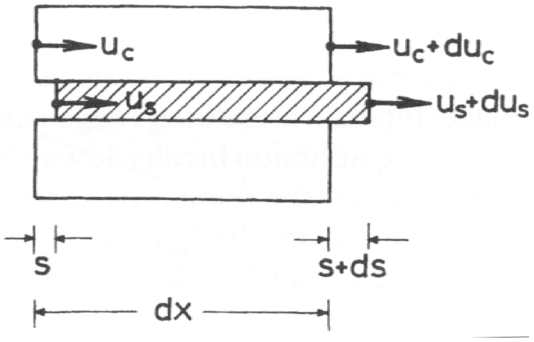

Figure 2.14 - Displacements and relative slip between concrete and plain steel bar (Penelis and Kappos, 1997)

$$A_s \cdot \left[\left(\sigma_s + d\sigma_s\right) - \sigma_s\right] = \tau \cdot u \cdot dx \Leftrightarrow$$
$$\Leftrightarrow \frac{d\sigma_s}{dx} = \frac{4}{d_b} \cdot \tau \qquad (2.1)$$

in which τ is the bond stress, u is the bar perimeter and d_b its diameter.

Examining equation (2.1), it appears that bond stresses are zero whenever the steel stress gradient is zero (constant moment areas), whereas its peak value takes place at points of steep gradients (in regions where point loads are applied, for instance).

Figure 2.14 shows the relative slip, s, between the plain bar and the surrounding concrete as a function of the corresponding displacements, u_c for concrete and u_s for steel.

According to Figure 2.14:

$$\left(s + ds\right) - s = \left[u_s + du_s - \left(u_c + du_c\right)\right] - \left(u_s - u_c\right) \Leftrightarrow$$
$$\Leftrightarrow ds = du_s - du_c \Leftrightarrow \qquad (2.2)$$
$$\Leftrightarrow \frac{ds}{dx} = \varepsilon_s - \varepsilon_c$$

As one can see, the relative slip between the plain bars and the surrounding concrete depends both on the steel strain, ε_s, and the concrete strain, ε_c. However, ε_c is usually disregarded, since its value is negligible with respect to ε_s.

Currently, the few analytical models for bond are based both on the final results of expressions (2.1) and (2.2) (constitutive equations for bond) and on experimental data. Commonly the bond stress, τ, is expressed as a function of the relative slip, s. However it should be noted that the results (2.1) and (2.2) apply only to plain bars.

2.1.3.1 Bond under monotonic loading

The behaviour of bond under monotonic loading is sketched in Figure 2.15. Figure 2.15 shows a qualitative picture of the bond stress-slip relationship. Due to the scarcity of experimental data regarding this subject, consensus has not yet been achieved in the research community regarding quantifying the behaviour of bond under monotonic loading.

Up to a certain level of bond stress, τ_0, almost no slip takes place. In this initial range of stresses, bond is mainly due to chemical adhesion of the cement paste to the surface of the bar. The value of τ_0 ranges from 0.5 to 1.0 MPa for plain bars. When adhesion breaks down, for $\tau > \tau_0$, the bond is assured mainly by friction between the cement past and the microscopic anomalies (pitting) of the bars. For deformed bars, at a bond stress level τ_1, bond cracks form, as illustrated in Figure 2.16. Bond cracking is a very complex phenomenon as it depends on several factors such as the strength of the cement paste, the rib spacing and the diameter of the reinforcement bar.

At approximately the same time as bond cracks form, separation of concrete from the reinforcement bar takes place in the region of primary (flexural) cracking. This separation causes transverse displacements leading to an increase in the circumference of the concrete surface previously in contact with the bar, and as a result, circumferential tensile stresses develop (Park and Paulay, 1975). The propagation of bond cracking up to the external face leads to splitting and therefore to the destruction of bond. This happens for levels of bond stresses around τ_2 cf. Figure 2.15. If the reinforced concrete element is not appropriately confined, this implies failure (dashed branch in Figure 2.15). Bond stresses along deformed bars are, except for low stresses, due to skew compressive stresses in the concrete. Thus, deformed bars induce transverse displacements in the concrete. This means that bond strength of deformed bars may be improved by confinement, contrary to plain bars. Confinement inhibits the propagation of the bond cracking, mainly due to the fact that transverse compression is beneficial to the anchorage of the reinforcement bar. Therefore, for confined elements, the bond resistance can reach significantly higher values (τ_{max}). Additionally, confinement leads to more ductile behaviour as it inhibits the bond failure due to splitting. After the maximum bond stress, τ_{max}, a progressive deterioration of the concrete between adjacent ribs takes place (descending branch, in Figure 2.15). The following moderate residual bond stress takes place for values of slip around s_3, due to friction at the cylindrical surface defined at the tips of the ribs.

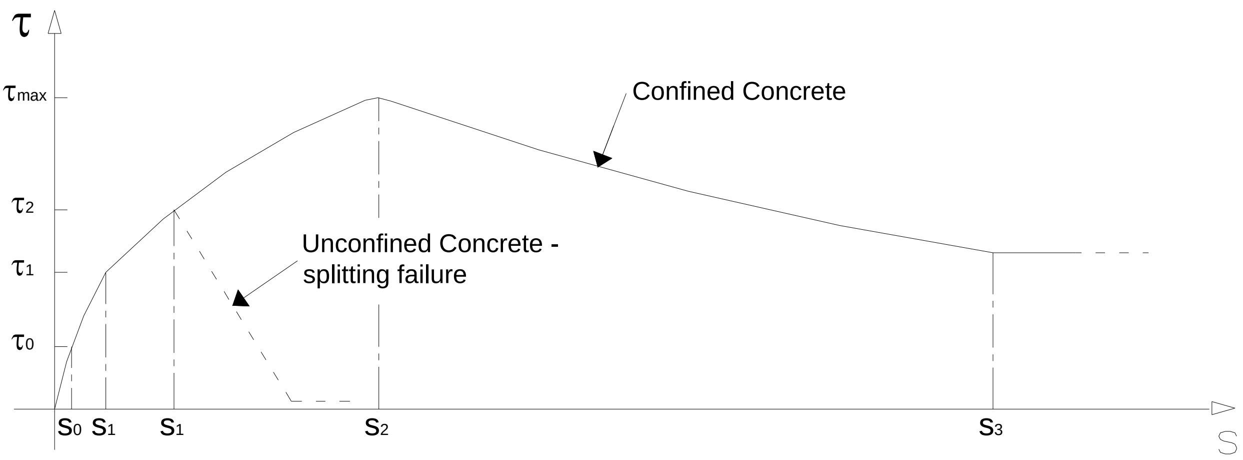

Figure 2.15 - Typical bond stress - slip relationships for unconfined and confined concrete.

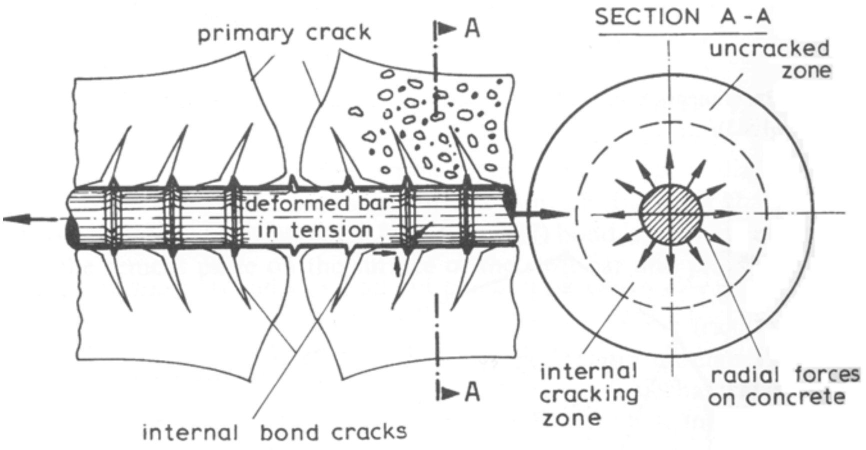
primary crack
A
SECTION A-A
uncracked zone
deformed bar in tension
A
internal cracking zone
radial forces on concrete
internal bond cracks

Figure 2.16 - Sketch of the bond cracking mechanism

2.1.3.2 Bond under cyclic loading

As for the monotonic loading, the bond resistance under cyclic loading is still only qualitatively understood. In the following, a brief description of the most important features governing the cyclic behaviour of bond will be discussed.

Observing Figure 2.17, three main features can be pointed out to describe the behaviour of bond under cyclic loading:

- The residual slip during unloading is quite large. This is mainly due to the fact that the elastic part of slip consists in the concrete deformation only, which is negligible regarding the contribution of the steel deformation. Also, microcracking in the concrete and the release of shrinkage strains result in some permanent slip. Therefore the cracks formed during the tensioning of a bar cannot close completely by removal of the load.
- One can distinguish two different parts in the reloading branches: The first part with relatively small slope up to slip values as approximately achieved in the previous cycle; The second part with a higher slope for slip values larger than in

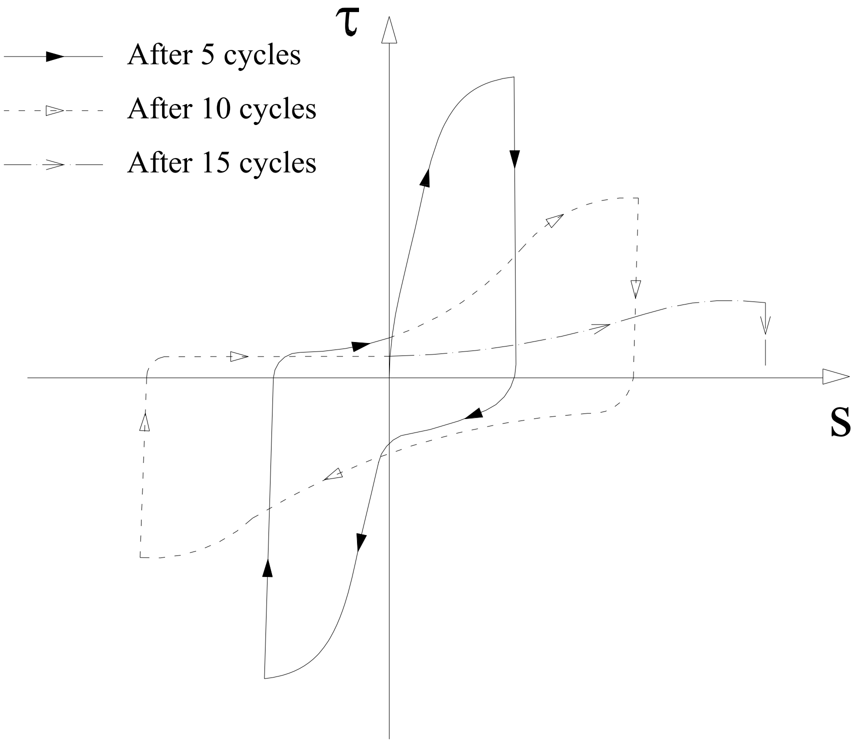

Figure 2.17 - Typical bond stress-slip relationship of a deformed bar under cyclic loading

the previous cycle. It can be easily understood that the bond resistance in the first part is merely due to friction between the bars and the surrounding concrete surface. For the second part, the reinforcement bar comes into contact with intact concrete, leading to an increase in the stiffness.

- Large softening effect and fast strength decay. Figure 2.17 shows clearly the slope reduction of the reloading branches after each cycle. This has to do with the gradual smoothening of crack interfaces, which causes a reduction of the mechanical interlock and friction forces (Penelis and Kappos, 1997).

2.2 Inelastic Response of Reinforced Concrete Elements in Cyclic Loading

2.2.1 Members with flexure-dominated behaviour

2.2.1.1 Members in uniaxial flexure

Most of the experimental work done to date regarding the cyclic behaviour of reinforced concrete members has dealt with the simplest case of uniaxial flexure under zero axial force. Although even for beams this case seldom occurs during a seismic action, its discussion is considered to be of high value to understand the cyclic behaviour of reinforced concrete members in which the flexural mode of behaviour dominates the shear mode.

Members with symmetric cross-section and reinforcement

(Brown and Jirsa, 1971) carried out a series of experiments to determine the effect of load history on the strength, ductility and mode of failure of cantilever beams. For current purposes, only the results with respect to specimens subjected to reversed loading histories are going to be discussed.

The test specimens were cantilever beams cast with an enlarged end block. The load was applied in the free end of the beam. The cross-section was rectangular (15.2x30.5 cm^2). The specimen designation (Figure 2.18) contains information about the reinforcement used, the load and the length of the shear span. Each of the values in the first pair of numbers stands for the number of longitudinal reinforcement bars used in the top and bottom face respectively. The second pair of numbers refers to the web reinforcement. The first number relates to the number of stirrups and the second one with their spacing in inches (1in=2.54cm). The designation RV5 or RV10 means that the load applied is reversed and the deflection limit is 5 or 10 times the yield deflection. The last number represents the length of the shear span, also in inches.

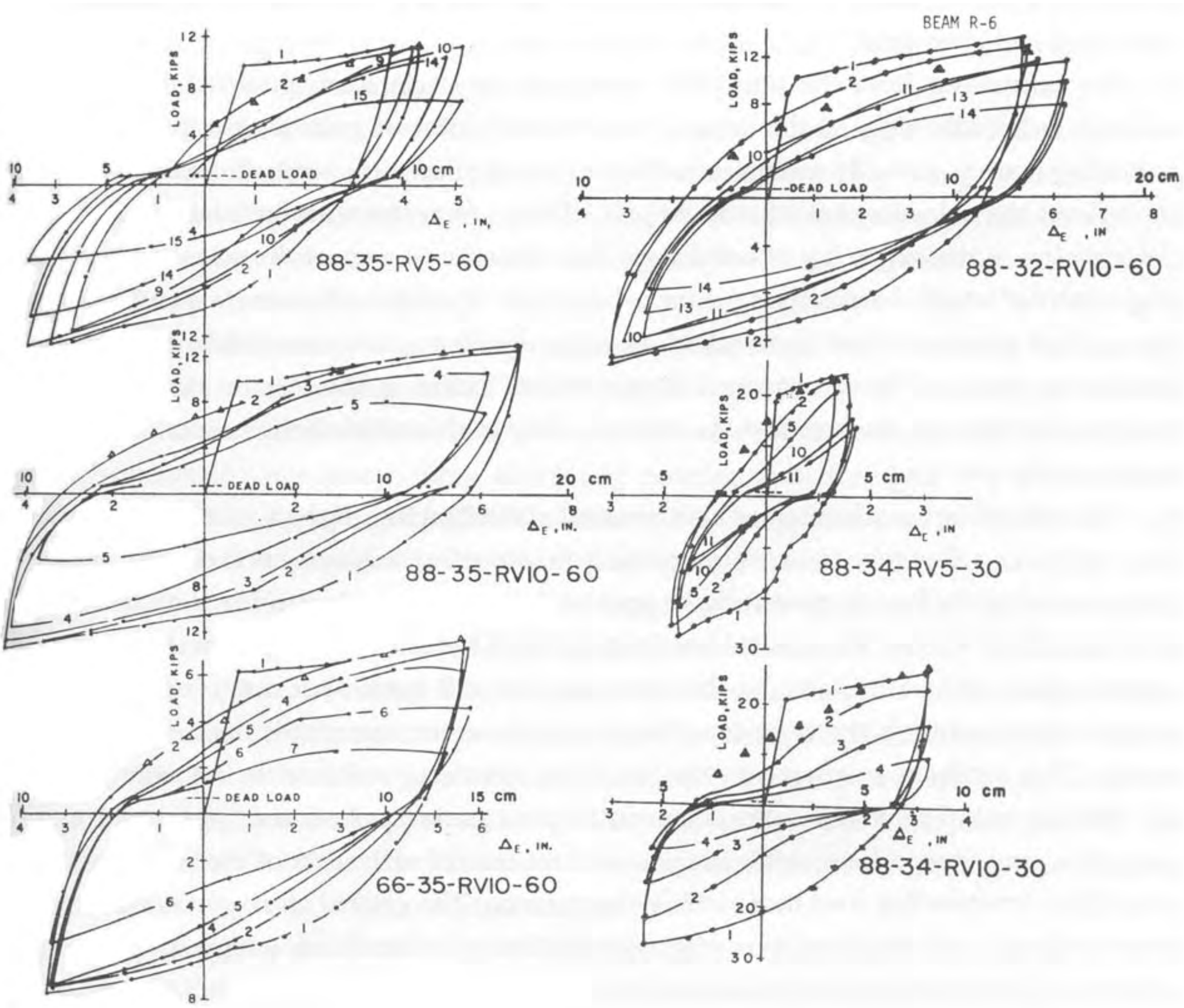

Figure 2.18 - Representative force-deflection loops of specimens with symmetric cross-section and reinforcement in cyclic uniaxial flexure with zero axial load (Brown and Jirsa, 1971) (1kip=4.45kN; 1in=2.54 cm)

The test results are illustrated in Figure 2.18 in the form of diagrams of force-displacement in terms of loads (*F*) versus deflections (δ). This type of diagram, together with those depicting moments (*M*) versus rotations (θ) are the best suited to illustrate the response of a reinforced concrete member under cyclic loading.

The main features of the curves in Figure 2.18 are:

- The stiffness gradually deteriorates in the first loading branch. This is particularly evident in specimen 88-32-RV10-60. In fact, as the load increases, flexural cracks develop in the tensile face and after a certain limit, bond slip between the reinforcement and the surrounding concrete takes place (*Zone **a)*** in Figure 2.19a)). The following abrupt softening of the response is mainly due to yielding of the tension steel at the cross-section of maximum moment (*Point **b)*** in Figure 2.19a)). After yielding, the resistance of the member keeps increasing although its stiffness is much more reduced. This relates to the reduction of the neutral axis depth due to the large post-yield extension of the tension steel, increasing the lever arm of the internal forces. Also, strain hardening of the tension steel (see section 2.1.2) contributes to a positive slope of the post yield branch for the first loading (*Branch **c)*** in Figure 2.19a)).
- The initial stiffness of the unloading branches is high, of the order of the elastic stiffness (Zone d) in Figure 2.19b)) and then gradually softens as the applied load tends to zero (Branch e) in Figure 2.19b)). When the load is removed there will be significant permanent deflections due to inelastic strains locked in the tension steel previously in the plastic domain and to the residual slip between the reinforcement and the concrete. This is the reason why the cracks remain open even at zero load (point f) in Figure 2.19b)).
- The initial part of the reloading branches on the opposite direction is rather flat, and even more so than the terminal part of the preceding unloading branch. The reason is that the cracks on the face previously in tension are still open, as explained previously, and when reloading on the opposite direction takes place, cracks will open on the new face under tension of the member. This will take

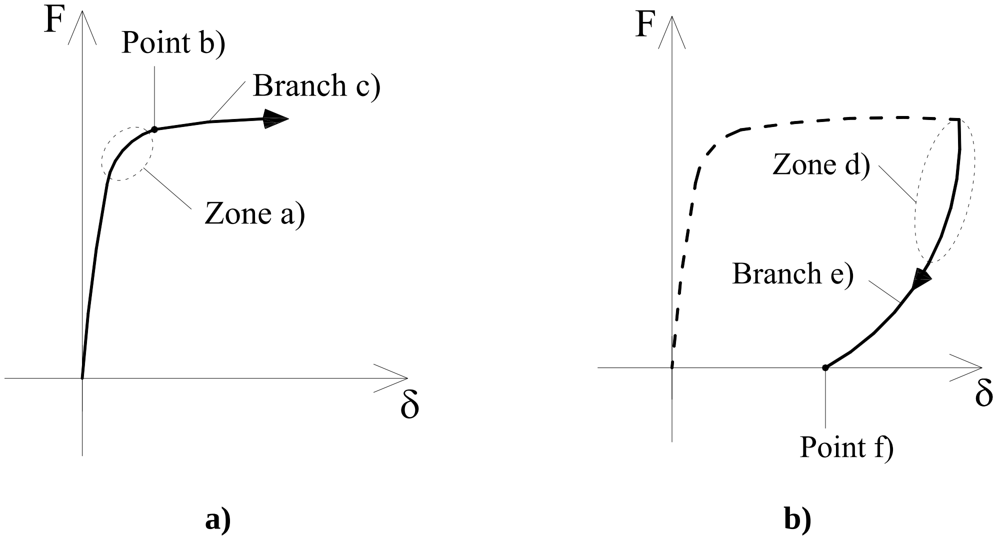

a) **b)**

Figure 2.19 - a) First loading branch and b) First unloading branch for symmetric R/C members with flexure dominated behaviour

place before full recovery of the residual bond slip and of the inelastic extension of the bars on the opposite face and therefore before the closing of the cracks there. As a result, the whole cross-section is cracked and the concrete is ineffective, which leads to the entire moment being resisted by the steel couple alone (Branch g) in Figure 2.20). As the magnitude of reloading increases, the cracks in the new face under compression gradually start to close after the corresponding steel bars yield in compression. This means the reactivation of the concrete and consequent stiffening of the reloading branch. (Zone h) in Figure 2.20). The succession of the softening-stiffening effect in the reloading branches moves the curve towards the origin, as this would be "pinched". For this reason this effect is commonly designated as pinching. This is a very important consideration when analysing the energy dissipation capacity of a structural member. The more pronounced the pinching, the less effective the member in absorbing the energy induced from cyclic loading.

- After the stiffening that concludes the pinching effect in the reloading branch, a second gradual softening can again be observed (Branch i) in Figure 2.20). This is the Bauschinger effect, mentioned in 2.1.2.2, affecting the steel bars. In fact, the steel bars now in tension have yielded in compression during the previous half cycle, and vice-versa for the bars now in compression. Therefore the steel bars start to yield earlier than for the first loading branch, meaning earlier softening in the reloading branch.
- The following unloading-reloading cycles follow the same pattern as described above. However the reloading branches seem to approach the point of extreme deformation in smoother lines as the number of cycles increase (Branch j) in Figure 2.21). This is the so-called stiffness and strength degradation process due to cyclic loading.

One of the main reasons for the degradation of the structural properties of the member is the gradual increase of the influence of shear deformations in cycling. Comparing

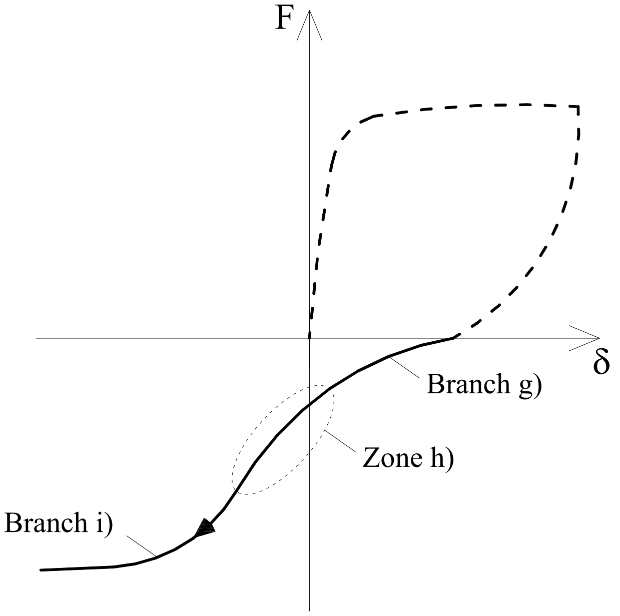

Figure 2.20 - Sketch of the first reloading branch in the opposite direction for a R/C member with symmetric cross-section and reinforcement in uniaxial flexure.

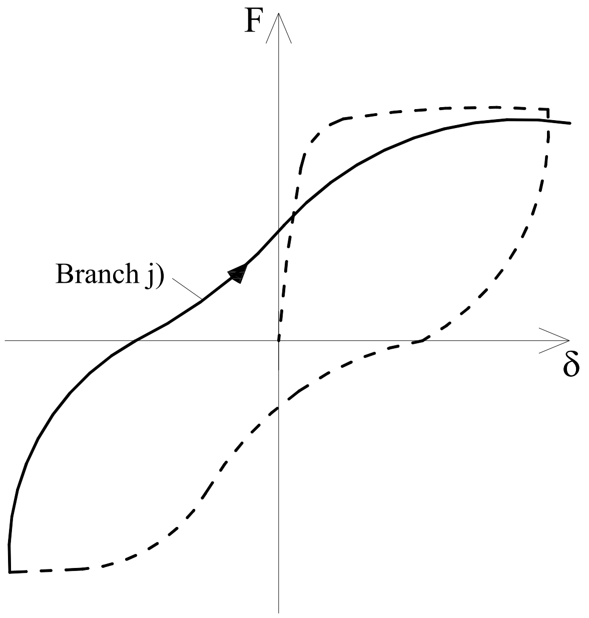

Figure 2.21 - Typical unloading-reloading cycle branch for a symmetric R/C member

Figure 2.22, which shows the end rotations of the beam for specimens 88-35-RV10-60 and 88-34-RV10-30 with the corresponding force-deflection curves (Figure 2.18), it is evident that despite the peak deflections roughly remaining constant, the end-rotations are reduced significantly, resulting in an increase in the magnitude of shear deformations. This, together with the alternate opening and closing of the cracks, causes a degradation of the concrete stiffness and strength in compression, as crack faces may not come into full contact. Another important factor contributing for the stiffness and strength degradation of the member is the bond deterioration mechanism with cycling as explained in section 2.1.3. The bond between concrete and steel gradually becomes less effective, which increases crack widths, contributing to larger *pinching* and reducing the tension-stiffening effect. Also, the combined effect of the whole cross-section when ineffective, i.e. the moment applied is resisted by the steel couple alone with shear deformations, increases the splitting of the concrete along the longitudinal bars. This leads to further bond deterioration and in certain cases may cause spalling of the concrete cover by dowel action.

The experimental work carried out by Brown and Jirsa is also useful for illustrating two important parameters influencing the cyclic response of structural members:

- As the *longitudinal steel ratio* increases, the larger the stiffness and strength degradation and also the less the energy dissipation capacity. This is evident since specimens reinforced with 8 bars failed in fewer cycles than those reinforced with 6 bars. In fact, as the load capacity increases, the greater the shear on the cross-section and so the larger the shear deformations with the consequent deterioration of the structural properties of the member. Moreover, an increase of the flexural reinforcement ratio increases the compressive stresses of the concrete, and thus increases the rate of degradation.
- Reducing the stirrup spacing significantly increased the number of cycles, as can be easily observed by comparing the force-deflection curves for specimens 88-32-RV10-60 with 88-35-RV10-60 in Figure 2.18. It is also evident that the response

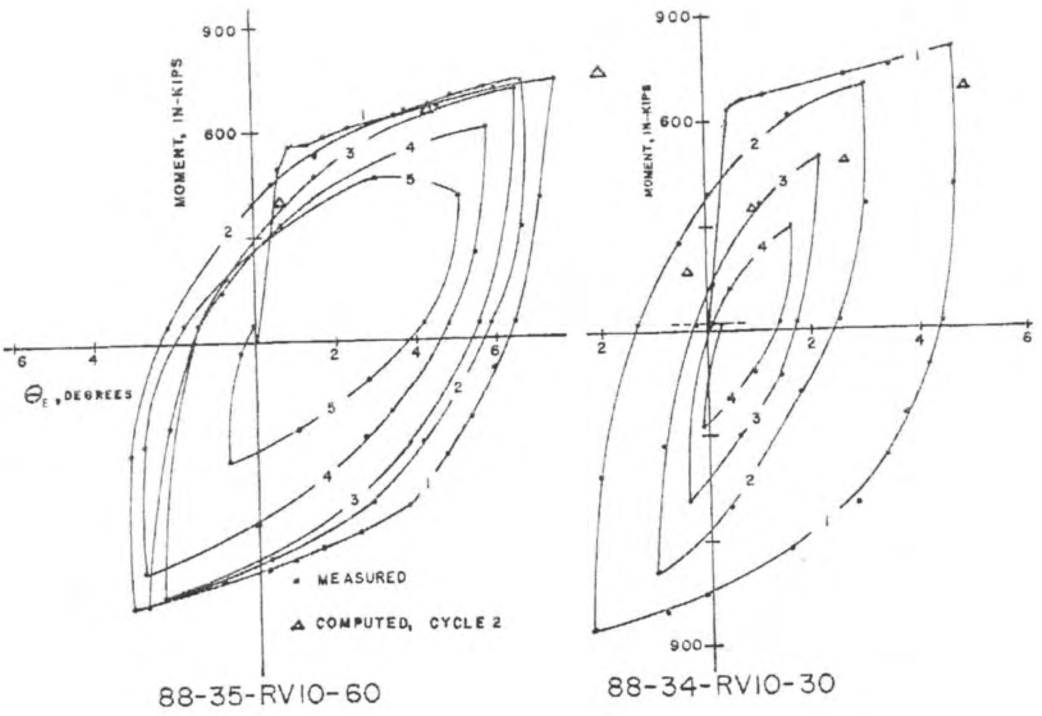

Figure 2.22 - Load-end rotation curves for specimens 88-35-RV10-60 and 88-34-RV10-30 (Brown and Jirsa, 1971) (1 kip =4.45 kN)

of the specimens with closer spacing is superior, leading to more stable hysteresis loops. This is due to the fact that better confinement of the concrete core is achieved with closer spacing of the transverse reinforcement, as explained in section 2.1.1.2. As mentioned there, adequate confinement has the favourable effect of keeping the inner structure of the concrete member preserved, diminishing the damage due to sliding along the cracks from shear deformations.

Finally, some remarks should be made regarding the *failure mode* in structural members with symmetric cross-section and reinforcement under uniaxial flexure. Generally in these cases, failure is caused by progressive deterioration of the compressive zones of the concrete combined with the growing influence of the shear deformations. If the member is submitted to strong imposed displacement history, i.e. with peak displacements several times larger than the yield displacement, damage is first observed in the uppermost or lowest fibres of cross-section with the highest flexural demand. This damage is due to successive states of high compression, leading to crushing of the cover concrete. This effect, together with the increase of bond slip between the steel bars and the surrounding concrete, leads to the separation (spalling) of the concrete cover, exposing the steel bars. At this stage, the bar may buckle due to loss of lateral support (Figure 2.23 a) and c)), which is a brittle mode of failure. In Figure 2.23 three different modes of buckling of the longitudinal reinforcement are illustrated.

Figure 2.23 shows the importance of transverse reinforcement spacing in preventing buckling of the steel bars: the closer the stirrups the better they can provide lateral support to the steel bars after spalling of the concrete cover due to reduction in the buckling length (Figure 2.23a)). Also, the yield strength of the steel used in transverse

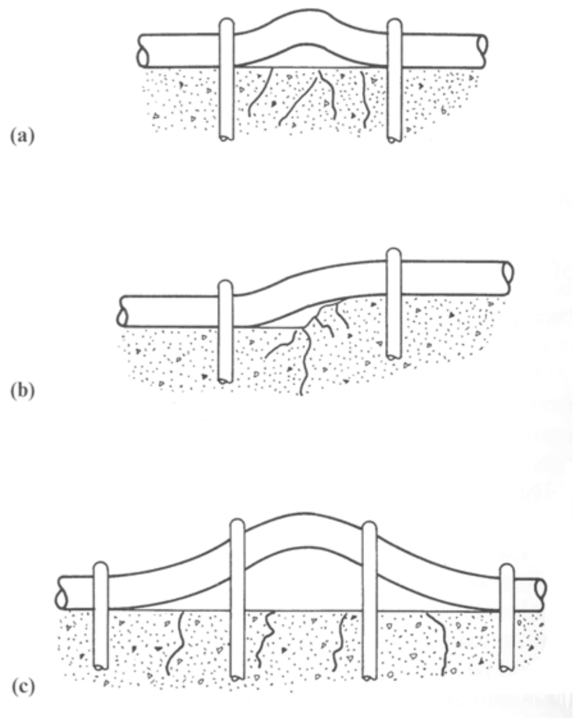

Figure 2.23 - Different modes of buckling in reinforcement bars (Penelis and Kappos, 1997)

reinforcement should not be too low in order to prevent buckling of the longitudinal bars as shown in Figure 2.23c).

Another mode of failure is that dominated by shear deformations. As the shear deformations increase with cycling, the abraded surfaces of the open flexural vertical cracks lose their shear capacity due to cyclic sliding. The propagation of the diagonal shear cracks leads to the progressive degradation of the compressive strength of the concrete core, which is evidenced by a rapid stiffness and strength decay in the force-deflection curves (see Figure 2.18, the curves referring to specimens 88-34-RV5-30 and 88-34-RV10-30). Significant shear deformations may also cause lateral buckling of the longitudinal bars as shown in Figure 2.23b). This mode of failure will be discussed in more detail in section 2.2.2.

(Wight and Sozen, 1973) undertook a test series to investigate the mode of failure for reinforced concrete columns subjected to several load reversals and deflections larger than the yield deflection. Figure 2.24 illustrates the development of the crack pattern in a cantilever specimen to a high level of damage.

It appears that the first cracks occur at the tensile face of the cross-section with maximum moment (in this case, the support cross-section). As the deflection and load continue to increase, inclined cracks emerge from the vertical cracks and splitting cracks form along the tensile reinforcement. In the figures, the development of spalling of the cover concrete in the compressed zone with the succession of cycles of deflections beyond the yield limit may be observed. The reversion of the load leads to greater damage of the concrete member as new cracks intercept the ones formed in the previous half cycle.

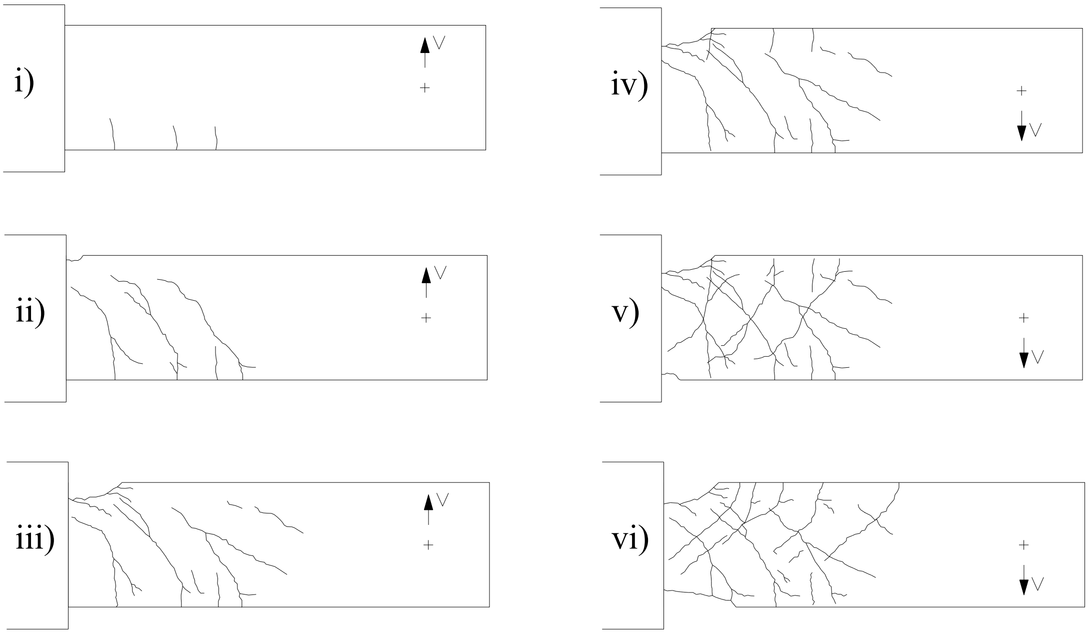

Figure 2.24 - Development of a crack pattern (Wight and Sozen, 1973)

These tests led to the following observations regarding the influence of the transverse reinforcement volume ratio, ρ_w, in the pattern of failure mode in concrete members. As this parameter increases:

- The region of inelastic behaviour (plastic hinge) extends over a smaller area
- The extension of the spalling of the cover concrete and the splitting in the tensile face diminish.

Therefore it may be concluded that transverse reinforcement can be used to control the extent of damage along a reinforced concrete member designed to undergo inelastic deformations.

2.2.1.2 Members with asymmetric cross-section and/or reinforcement

Most of the structural members used to withstand flexure are beams. Usually these members are not designed with symmetric cross-section and/or reinforcement. Further, the shape of the cross-section is not rectangular, but T or L and the amount of top steel used differs from the amount of steel used in the bottom. Also, in "symmetric" beams monolithically cast with a slab, the increase of the effective upper flange width leads to different flexural capacity for both directions. Therefore asymmetric behaviour should be considered.

(Nmai and Darwin, 1986) carried out an experimental work on lightly reinforced concrete beams under cyclic loading, in which asymmetric specimens were tested. The members had rectangular cross-section (190 x 457 mm^2). In the specimens F2 and F4, the top reinforcement consisted of 6 and 4 bars respectively, the bars being 13 mm in diameter. The same bars were used for the bottom reinforcement: 3 bars for specimen F2 and 2 bars for specimen F4. The specimens were submitted to deflection amplitudes of 5 times the yield deflection. The results of the test are depicted in Figure 2.25.

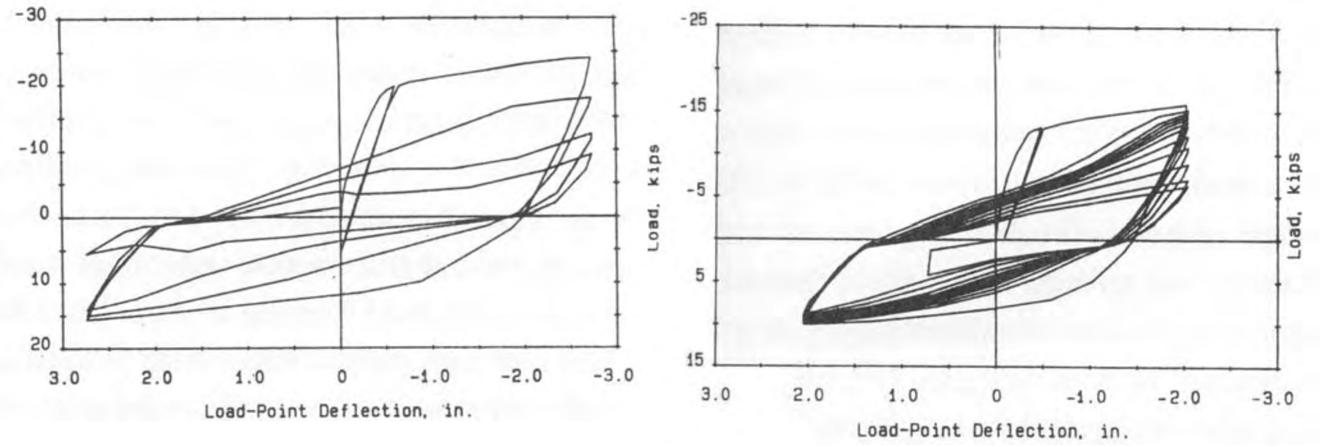

Figure 2.25 - Load-deflection curve for specimens F2 and F4 (1kip=4.45kN; 1in=2.54cm)

The main difference in the cyclic flexural behaviour between members with symmetric cross-section and reinforcement, and those with asymmetric cross-section and/or reinforcement is that the latter exhibit asymmetric hysteresis loops (CEB, 1994) – Figure 2.25. This difference is due to the fact that the stiffness and strength of the member is not identical for both loading directions. For the present case the amount of bottom reinforcement is lower than for the top reinforcement. Therefore, the strength and stiffness of both sections in the positive direction is lower than in the negative one.

It may be seen in Figure 2.25 that the specimens were first loaded in their “strong” direction. The abrupt decay in stiffness after the “elastic” branch indicates yielding of the top reinforcement due to tension. When reloading in the “weak” direction takes place, the cracks in the face previously in tension are open as for symmetric cross-section (see previous section, explanation given regarding *branch g)* in Figure 2.20). The difference now is that those cracks remain open throughout the entire reloading in the “weak” direction. This is because tensile yielding of the bottom reinforcement is not sufficient to cause yielding of the top reinforcement due to compression. So as long as yielding in the strong direction has taken place, reloading in the “weak” direction is characterised by full-depth open cracks. Therefore, the moment is resisted by the steel couple alone and the gradual stiffening caused by closing of the cracks does not take place. Thus, the reloading branch in the “weak” direction is of very low stiffness and without pinching. Pinching does take place upon reloading on the “strong” direction and is rather pronounced. This is due to the fact that only on the reloading branch in the “strong” direction does the concrete start to become effective again and the top reinforcement is still elastic, as it did not yield in compression in the previous half-cycle.

For this kind of member, failure usually develops in two ways: failure with the “strong” side in tension or failure with the “weak” side in tension. The former has a gradual development characterised by progressive disintegration and crushing of the concrete in the “weak” side. This failure mode is the most desirable one as it may reach high levels of ductility. The latter mode of failure is rather brittle as it involves the fracturing in tension of the steel bars in the “weak side” and therefore a sudden drop in strength. Often this happens after the steel bars have buckled due to compression in the previous cycles.

2.2.1.3 The effect of axial forces

In the following, the influence of axial loading on the cyclic behaviour of flexure-dominated reinforced concrete members is discussed. Most of the structural members in which the effect of axial loading in seismic performance has to be considered are columns. The way in which the degradation of the response of these members due to reversed cyclic loading develops is similar to that described in section 2.2.1. However, most of the time these elements are subjected to a biaxial state of flexure. Nevertheless, it is appropriate to discuss the uniaxial flexure case as this allows for a better understanding of the influence of the axial loading by comparison to that discussed in the previous section. Also, the way in which the axial forces influence the cyclic responses of members is similar both in uniaxial and biaxial flexure.

(Staaciouglu and Ozcebe, 1989) carried out test series with the intention of investigating the response of reinforced concrete columns to seismic loading. The experimental program is quite similar to that referred to in section 2.1.1.2. In fact, the specimens tested had the same geometry and were reinforced both longitudinally and transversely as in the 1987 tests (Figure 2.5).

The differences were in the loading program: Three different groups of specimens were tested, each one labelled according to the deformation path imposed. Specimens U were loaded uniaxially in the direction parallel to the principal axis of the column with the same loading history as shown in Figure 2.6; Specimens D were loaded as specimens U, but the load was applied along the diagonal of the section; Specimen B1 was subjected to a bi-directional deformation path as shown in Figure 2.26. This loading history was intended to simulate a major seismic action in one direction while a minor action was occurring in the orthogonal direction. The specimen was designed to have the same capacity in both directions. The properties of the different columns are shown in Table 2.1.

Members with constant compressive axial force

Depending on the intensity, compressive axial loading may have favourable as well as

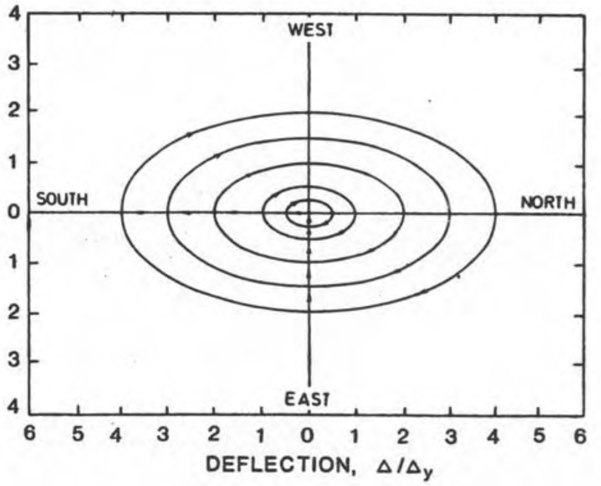

Figure 2.26 - Loading history for specimens B1 (Δ_y = yield displacement of the specimen) (Staaciouglu and Ozcebe, 1989)

Table 2.3 – Properties of the columns (Ozcebe and Staaciouglu, 1989)

Test Specimen	Concrete Strength (MPa)	Longitudinal Steel	Transverse Steel				Axial Load (kN)
		$f_{y,l}$ (MPa)	$f_{y,t}$ (MPa)	ρ_w ($^o/_{oo}$)	s (mm)	Configuration	
U1	43.6	430	470	0.85	150	Type A	0
U2	30.2	453	470	0.85	150	Type A	600
U4	32.0	438	470	2.54	50	Type A	600
U6	37.3	437	425	1.95	65	Type B	600
D1	40.3	453	470	0.85	150	Type A	0
D2	30.2	453	470	0.85	150	Type A	600
D4	43.6	430	470	2.54	50	Type A	600
B1	32.0	438	470	2.54	50	Type A	600

unfavourable effects on the strength and stiffness degradation and ductility throughout the seismic response of a structural member.

The presence of compressive axial stresses contributes to the closing of the flexural cracks. This is reflected in the final phase of unloading from a post-yield peak displacement and the first stage of reloading in the opposite direction. The additional compression state of stress due to axial loading accelerates the yielding in compression of the steel bars that have previously yielded on tension and are now going to compression. As a result, nowhere during the loading cycle are the cracks open through the full depth of the cross-section, and therefore the steel couple never resists the moment independently. This means the “suppression” of *Branch g)* (see Figure 2.20) in the first part of the reloading branch in the opposite direction. Thus the *pinching* effect, typical of the cyclic response of the structural members dominated by flexure, is not observed in a pronounced way. This means an improvement with regard to the energy dissipation capacity.

Also the stiffness of the virgin loading, unloading and reloading branches increases. This is mainly due to the increase in the depth of the compressed concrete and hence an increase in the contribution of the concrete for the overall stiffness.

In the same way as for the flexural cracks, compressive stresses contribute to the closing of the cracks perpendicular to the axis of the member, diminishing the risk of premature failure due to sliding shear.

In contrast with these favourable effects, it should be noted that after a certain level of compression, the consequences are severe regarding ductility reduction and acceleration of failure.

- The presence of compressive stresses results in a larger compression zone in the cross-section and thus in higher demands regarding concrete strains. Thus, crushing and degradation of the concrete core combined with spalling of the concrete cover take place at lower levels of displacement with subsequent drops in strength. This can be easily observed when comparing the results from specimens U1 with U2 and D1 with D2 in Figure 2.27. Members with high concrete covers due to environmental conditions are particularly exposed to this effect. As a

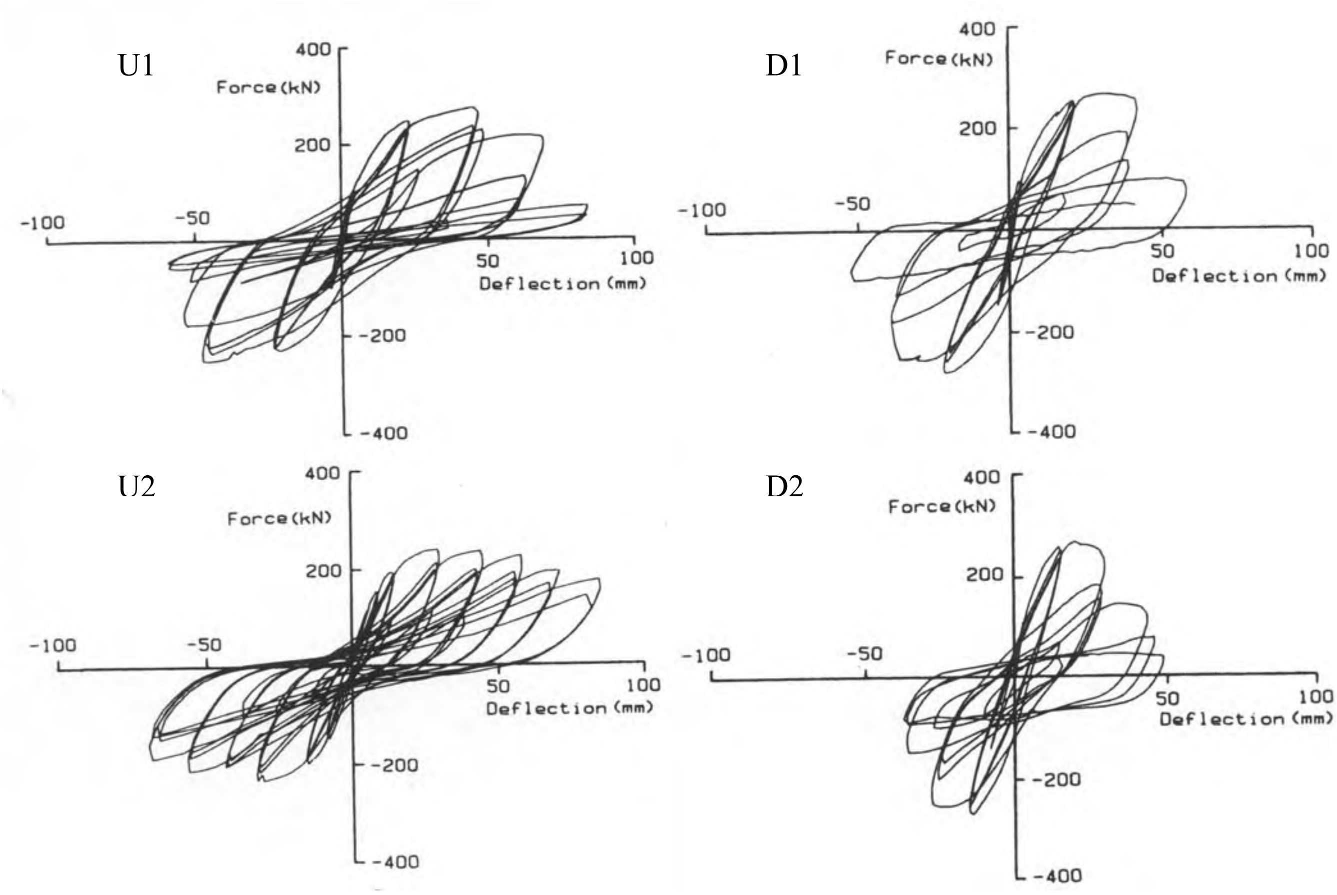

Figure 2.27 - Test results for specimens U1, U2, D1 and D2 (Staaciouglu and Ozcebe, 1989). The hysteretic relationships are in terms of lateral load – top deflection in the loading direction

consequence, the longitudinal reinforcement is exposed faster and therefore the risk of buckling due to compression is higher and may develop sooner. This last effect is actually the cause of the most common type of failure in columns subjected to high levels of axial load. This is the reason why most of the modern code provisions clearly emphasise the importance of adequate transverse reinforcement as explained in connection with Figure 2.23 in section 2.2.1. Moreover, proper transverse reinforcement (with adequate detailing and close spacing of the stirrups) improves confinement of the core concrete and therefore reduces the strength and stiffness degradation as explained in section 2.1. The improvement on the cyclic response due to confinement can easily be observed by comparing the hysteretic loops of specimen U6, with transverse reinforcement of Type B, with the hysteretic loops of specimen U2, with transverse reinforcement of Type A.

- Another negative effect of axial loading is the development of the well known second-order moments (*P-Δ effects* as it is generally known). It is obvious that as the level of axial loading rises, the more important are these effects and therefore the larger the strength requirements. The designer should avoid high levels of ductility demand in members subjected to high axial loading in order to minimise the risk of failure due to large second order moments. Underestimating the *P-Δ effects* is a frequent cause of failure as it leads to structural collapse due to lateral

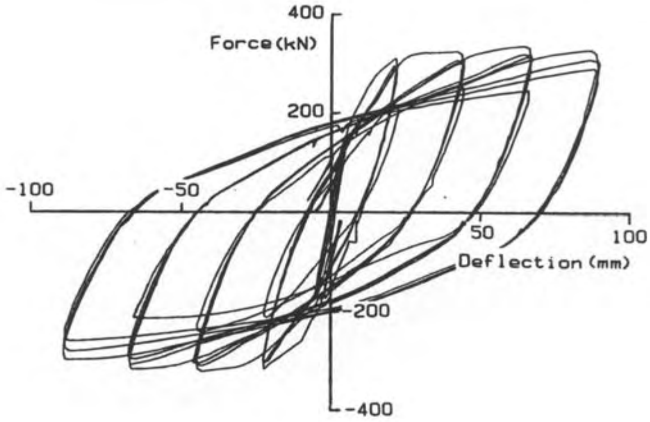

Figure 2.28 - Test results for specimen U6 (Staaciouglu and Ozcebe, 1989)

instability, particularly in buildings in which sideway mechanisms are supposed to form.

Members with varying axial force

It is well know that overturning moments are present when a structure such as a two-dimensional frame is subjected to cyclic lateral loading. These give rise to axial forces in columns, compressive on one side of the frame and tensile on the opposite side. These forces increase from the interior to the exterior of the frame. For the columns in the interior of the frame, this might not be critical, but for the external columns these forces cannot be neglected as they may drastically reduce the compressive forces or even induce tensile forces when combined with the effect of the vertical component of the seismic motion.

(Abrams, 1987) conducted a test series on the influence of axial force variations on flexural behaviour of reinforced concrete columns. In the following, the results in terms of moment-rotation relationship for two of the specimens tested are shown. Both specimens had the same geometry and reinforcement arrangements. Specimen C1 is a control specimen in which the compressive axial load was kept constant at 310 kN (normalized axial load, ν=-0.1), whereas for specimen C4 the load varied linearly with the bending moment between 55 (ν = -0.02) to 588 kN (ν=-0.25).

Low compressive forces and/or tensile forces have a rather unfavourable effect on the cyclic behaviour of structural members, regarding the energy dissipation capacity and in the stiffness development. This is due to the fact that these conditions impose restraints on the closure of cracks due to flexure and shear (extension of *branch g)*; see Figure 2.20) in the course of cyclic loading. Therefore the pinching of the loops is more pronounced, meaning loss of hysteretic energy dissipation capacity (See Figure 2.29, specimen C4). Also, the concrete in the cracked cross-section is less effective for a longer period, which directly affects the stiffness of the member. It should also be noted that further in the course of cyclic loading, shear deformations become more important, as explained in section 2.2.1.1 – Figure 2.22. Low compression forces, or tensile forces, reduce the strength significantly along the shear cracks and therefore increase the risk of failure due to sliding shear.

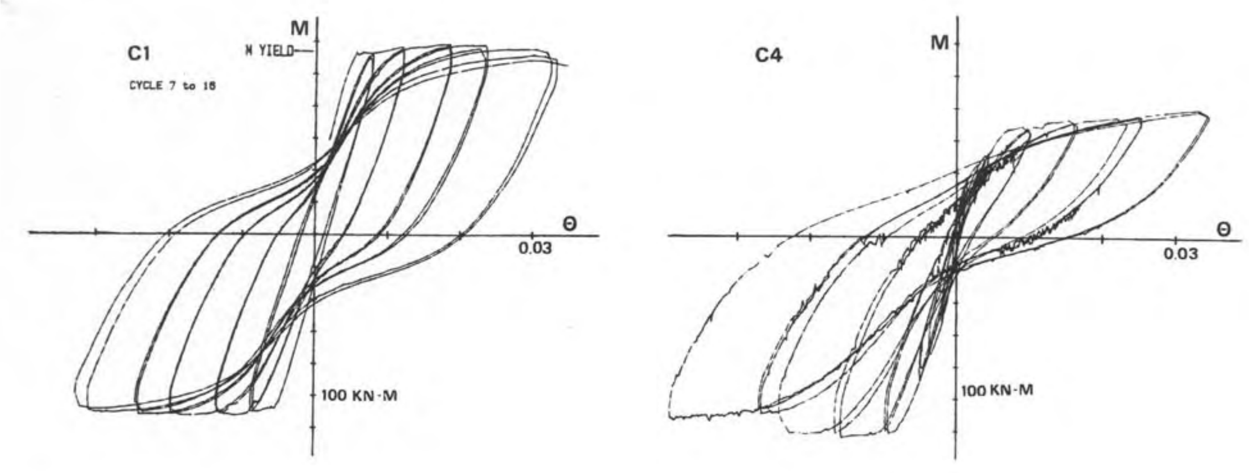

Figure 2.29 - Moment-rotation relationships for specimens C1 and C4 (Abrams, 1987)

Moreover, from the axial load – bending moment interaction diagrams, it may be concluded that a significant loss of flexural strength takes place for low compression forces and/or tensile forces regarding that reached for moderate levels of compression forces. This explains the reduction in the ordinates of the envelope curve of the upper half–cycle of the moment-rotation relationship for specimen C4.

The reverse of these tendencies was observed in the tests of (Abrams, 1987), when the axial compression was increasing. As apparent from Figure 2.27, the branches of the lower half-cycles are more inclined, and achieve greater strength values (Specimens U2 and D2). The reasons for this behaviour were given when discussing the favourable effects of moderate axial compression in the previous paragraph. This explains the asymmetric pattern of the moment-rotation curve for specimen C4. It was concluded that the shape of the hysteretic loop is influenced by the range of axial force variation and also by the rate of change of axial force with lateral deflection (Abrams, 1987).

2.2.1.4 Hysteretic relationships for plastic hinges with flexural dominated behaviour

To date, the most widely used hysteresis law for flexural behaviour is the so-called Takeda Model. Initially proposed in 1970 (Takeda *et.* al, 1970), the model was based on a trilinear skeleton curve and accounted for 16 rules covering all possible load sequences. Later, a simpler version, the Modified Takeda model, was proposed by (Otani, 1974), with “only” 11 rules, since the influence of uncracked stiffness was neglected. Thus, the skeleton curve became bilinear, cf. Figure 2.30. Currently, a wide range of hysteresis relationships based on the Takeda model are available.

Takeda relationships are characterised by softened unloading stiffness branches, and therefore may effectively account for accumulation of damage in cyclic loading. Basically there are 3 factors affecting the shape of the hysteresis loops:

- Post yield stiffness, r
- Unloading stiffness, α
- Reloading stiffness, β

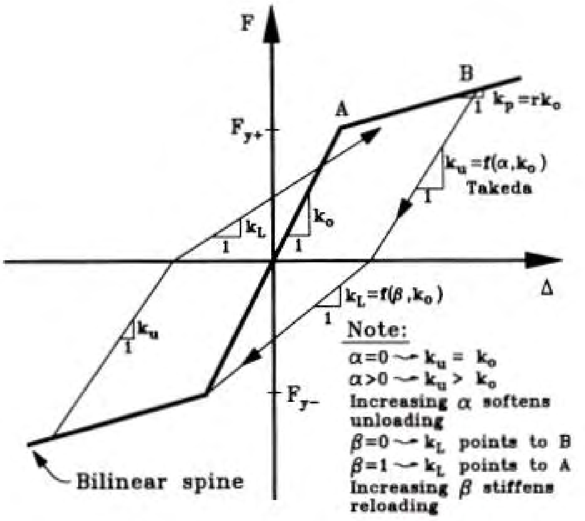
F
B
A
F_{y+}
$k_p = rk_o$
1
$k_u = f(\alpha, k_o)$
Takeda
1
k_L
1
k_o
1
Δ
$k_L = f(\beta, k_o)$
1
k_u
1
Note:
$\alpha = 0 \rightsquigarrow k_u = k_o$
$\alpha > 0 \rightsquigarrow k_u > k_o$
Increasing α softens unloading
$\beta = 0 \rightsquigarrow k_L$ points to B
$\beta = 1 \rightsquigarrow k_L$ points to A
Increasing β stiffens reloading
F_{y-}
Bilinear spine

Figure 2.30 -Modified Takeda model (Priestley et. al, 1992)

Evidently, significant experience is required to calibrate the curve according to the expected hysteretic behaviour of the structural element, which as already mentioned in section 1.2.2 limits the use of the Takeda model as a routine design tool. Furthermore, the model does not take into account the effect of varying axial load or of asymmetric cross-sections (in terms of flexural capacity). Many improvements have been proposed with regard to these limitations, but the degree of sophistication at the calculation level brings higher costs in terms of computational effort required.

A much simpler hysteresis relationship has been recently proposed as an alternative to the Takeda model. Asymmetric strength capacities and varying axial load are effectively taken into account in this model. This is the so-called Pivot Hysteresis model proposed by (Dowel et al. 1998), and the quality of results provided makes it increasingly accepted.

In this model only three rules are necessary to capture the hysteretic behaviour of the plastic hinge with flexure dominated behaviour. The model is based on two main observations from experimental results, see Figure 2.31:

1. Unloading stiffness decreases as deformation ductility increases
2. Load reversal after a non-linear excursion in one direction crosses the initial loading branch before reaching the idealised strength.

For each loading direction two factors have to be specified to calibrate the pivot hysteresis model:

- α, by which the idealised yield strength in one direction is multiplied to define the position of the corresponding primary pivot point
- β, by which the idealised yield strength in one direction is multiplied to define the position of the pinching pivot point

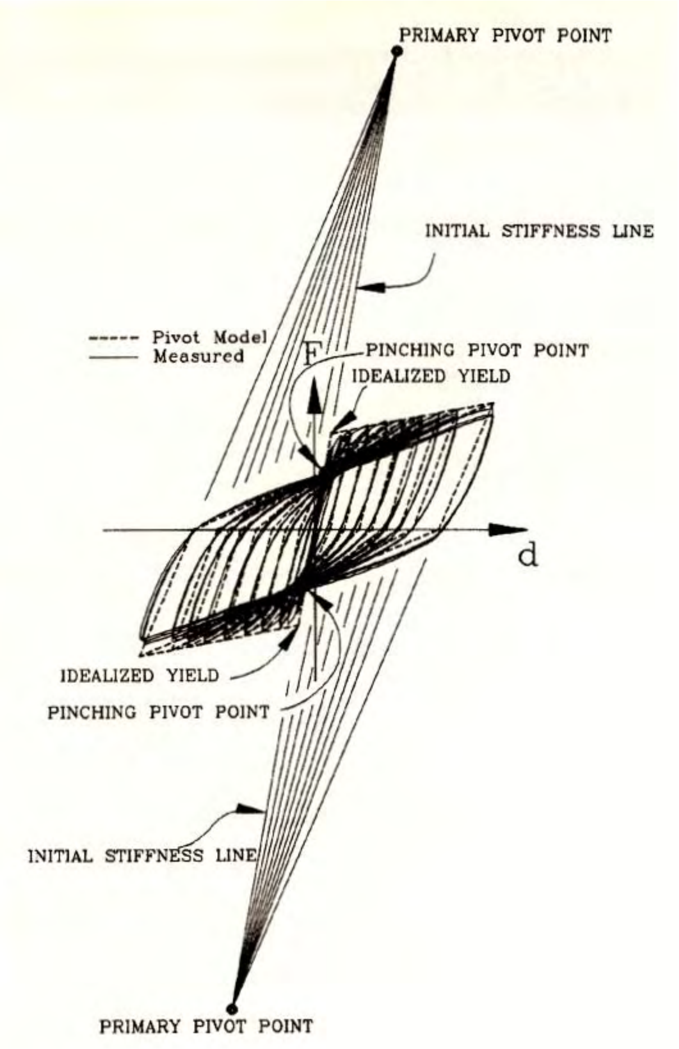

Figure 2.31 - Pivot hysteresis model (Dowel et. al 1998)

2.2.1.5 Members in Biaxial Flexure

During a seismic action, the direction of the loading is permanently changing. Thus, very seldom, if ever, is a structural member submitted to a state of stress corresponding to bending in one of the principal directions. This applies especially to columns. This indicates the importance of the inelastic response of a member submitted to biaxial flexure. However, the interest in this subject is recent and the available experimental results are rather limited. This is due to complications arising from adding an extra parameter corresponding to the manner in which the histories of bending moments in two directions are combined. Thus current knowledge of the inelastic behaviour of reinforced concrete members in biaxial flexure is far behind the understanding of the behaviour under uniaxial cyclic flexure.

The primary effect of biaxial flexure is strength degradation in one direction after an inelastic action in the orthogonal direction. (Otani, S. Cheung, V.W.T. and Lai, S.S., 1980) carried out a test series intending to investigate the effect of biaxial lateral load reversals on the cyclic response of reinforced concrete columns. They tested several specimens representing the part of the first-storey's columns between the foundation

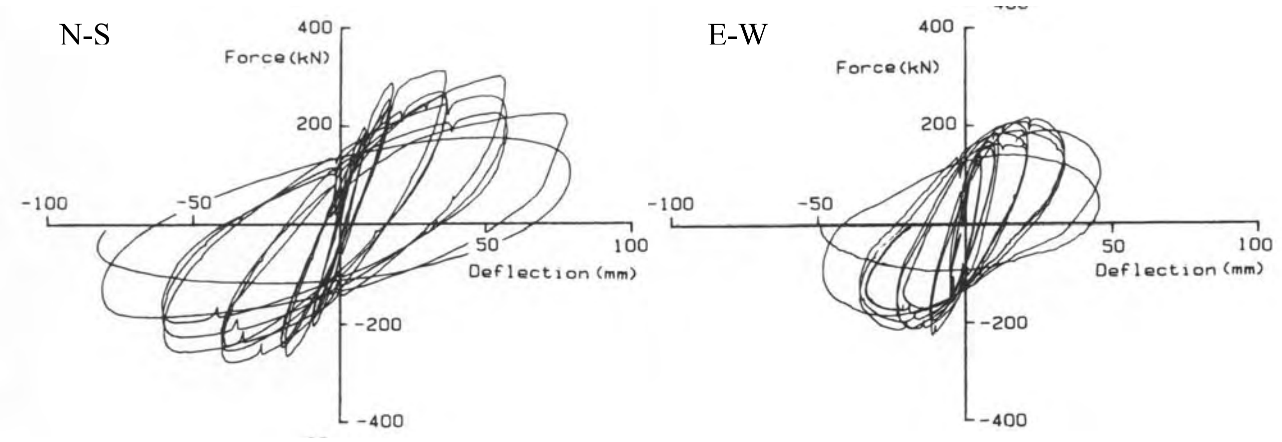

Figure 2.32 - Tests results of specimens B1 (Saatcioglu and Ozcebe, 1989)

and the inflection point in the moment diagram. Specimen SP4 was first submitted to two uniaxial cycles slightly past yield (displacement ductility ratio, μ_y, of about 2.0). Afterwards the same specimen was loaded with eight uniaxial cycles at $\mu_y = 4.5$. When cycling was repeated in the former direction at the same ductility ratio as before ($\mu_y = 2.0$), a very noticeable degradation of strength in comparison to the last cycle was observed.

(Staacioughu and Ozcebe, 1989) also reached the same conclusion: Despite the fact that deformations prior to yielding do not noticeably affect the response in the orthogonal direction, inelastic cycles in one direction drastically reduce column strength in the other direction. In Figure 2.32, a significant drop in capacity in direction E-W may be observed compared with that for direction N-S, despite the member B1 being designed to have the same capacity in both directions. The authors estimated a drop of strength of approximately 20- 30% in column B1.

The authors also showed that a member submitted to a deformation path in its diagonal direction significantly reduces the capacity in each of the directions of the principal axes, even if the deformation path is meant to produce the same bending and shear in the two principal directions.

However, when comparing the lateral load – top deflection hysteretic relationships in the direction of loading, it is observed that the overall hysteretic characteristics are similar in terms of strength, stiffness and ductility (compare in Figure 2.27 the shape of the hysteretic curves for specimens U and specimens D). This feature was also observed by (Umehara and Jirsa, 1982). This led to the conclusion that the maximum capacities of the columns with diagonal unidirectional loading could be estimated by an interaction circle in case of a fully symmetric cross-section or by an ellipse, if the loading capacities are different in each principal direction. This inelastic diagram connects the maximum capacities of the columns under unidirectional loading along the principal axes.

In all experimental investigations mentioned above, severe stiffness decay was observed after post-yield deformations in one of the two principal directions. This feature is well demonstrated in the hysteretic curve of specimen B1 tested by Saatcioglu and Ozcebe (Figure 2.32). A speedy decay in stiffness leads to the unfavourable effect of larger lateral displacements, hence to a more pronounced second order effect (P-Δ *effect*).

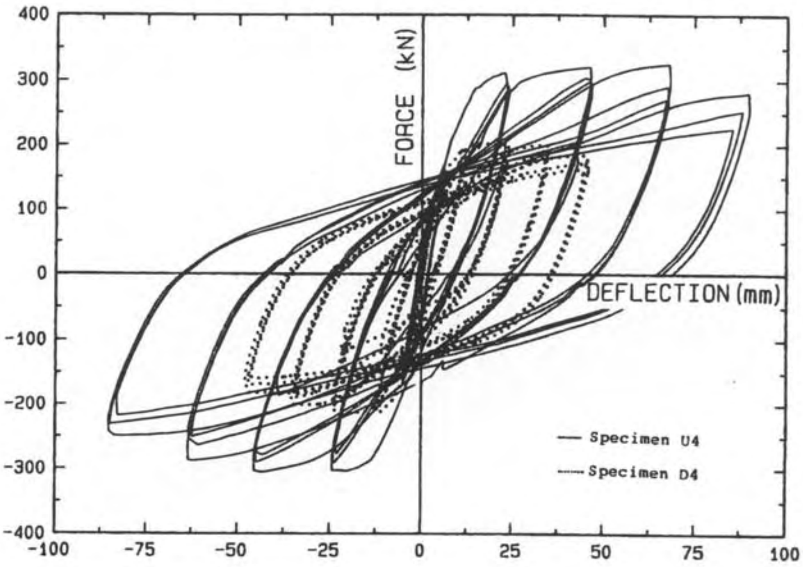

Figure 2.33 - Comparison of the responses of specimens U4 and D4 in the N-S direction (Staaciouglu and Ozcebe, 1989)

The high rate of damage in biaxial flexure inducing significant drops in strength and stiffness after each cycle may be explained referring to the cracking mechanism. It is well known that, in the course of seismic action, the direction of loading is permanently changing. Consequently, for a significant period of time, parts of the cross-section will be in tension and others will be in compression. This accelerates the degradation of stiffness and strength of the member due to the *Bauschinger effect* in the steel and due to crushing of the concrete and consequent spalling of the concrete cover in the compression face. Also, shear cracks will develop in both directions, increasing the rate at which they intercept, causing a quicker degradation of the concrete core. Thus, the rules for proper reinforcement detailing for ductile behaviour described in the previous sections must be strictly observed in the case of members subjected to biaxial flexure.

2.2.2 Members with shear-dominated behaviour

The discussion so far has referred to flexure-dominated members, i.e. to slender members. If the slenderness of the element drops to a certain level, the ultimate load is governed by shear forces. It is known that this type of behaviour is characterised by very low ductility and, in general, by poor performance under cyclic loading. This has been confirmed in the field after the spectacular shear failures of short columns observed after the 1968 Tokachi-Oki and the 1972 Managua earthquakes, which showed rather brittle behaviour of these type of members.

The slenderness parameter l/h, in which l is the length of the member and h its depth, is often used to trace the border between these two types of structural members regarding their structural behaviour. The reference value for slenderness that separates the two types of behaviour is approximately 4. In frame structures, low slenderness elements are either deep beams (high *h*) or short columns (low *l*). Modern seismic design philosophy requires a limitation of the strength of beams (weak beam / strong

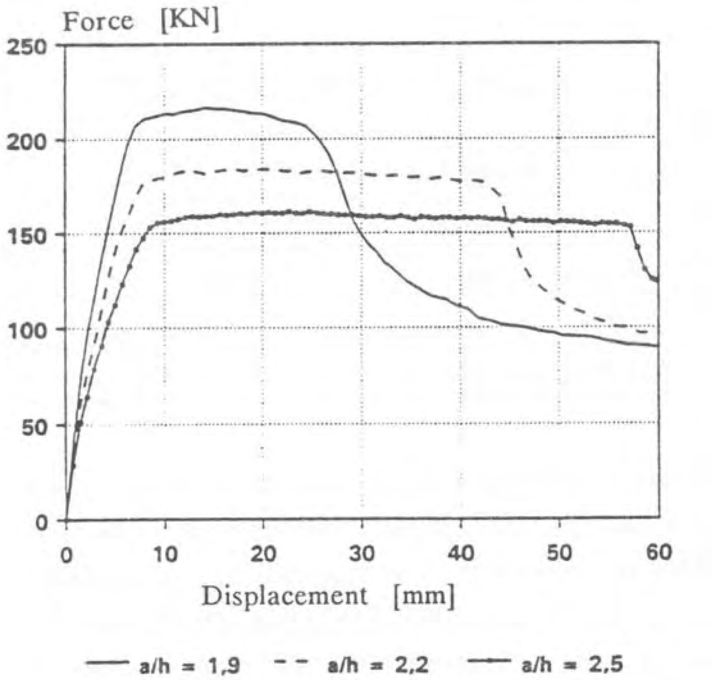

Figure 2.34 - Monotonic force-deflection curves at different shear span ratios (Garstka, B, W.B. Krätzig and F. Stangeberg,1993)

column criterion, see section 2.4.2). Therefore deep beams are very uncommon. On the other hand, short columns appear in frames frequently. This is done intentionally in the design of the frame, or unintentionally as is the case of slender columns, the effective lengths of which are reduced by infill masonry walls up to certain height in the frame. The latter case has dangerous consequences since the behaviour of shear–dominated members is substantially different from those described in the previous section, as will be shown below.

Authors often designate members with shear-dominated behaviour as members of *low shear span ratio*. The shear span ratio α, is defined as α=M/Vh.

(Garstka *et al*., 1993) showed that as the shear span ratio decreases below the critical value of approximately 2.0, the monotonic load-deformation curve gradually shifts from the ductile mode of the flexure-dominated behaviour to the brittle mode of the shear-dominated behaviour. In fact it may be seen in Figure 2.34 that for members with low shear span ratio (in the figure, *a* stands for the length of the member) the load-deformation curve exhibits a long, almost linear initial branch that softens smoothly to a well-defined ultimate peak strength, which is followed by a rather steeply descending branch. However, the differences between those three specimens were only seen in the shape of the deformation response, as all three specimens failed at the same value of the end moment. It is therefore evident that the lower the shear span ratio of the member, the closer the shape of the monotonic load-deformation curve resembles that of concrete in compression. This relates to the effect of the compressed diagonal strut, which carries the shear force. The damage imposed on the member, i.e. crushing after the occurrence of yielding of the longitudinal bars and gradual reduction in the depth of the compression zone, still takes place at the end section, but not normal to it, as in slender members, but as a sliding failure along the compressed diagonal. As the shear span ratio drops well below the limiting value of

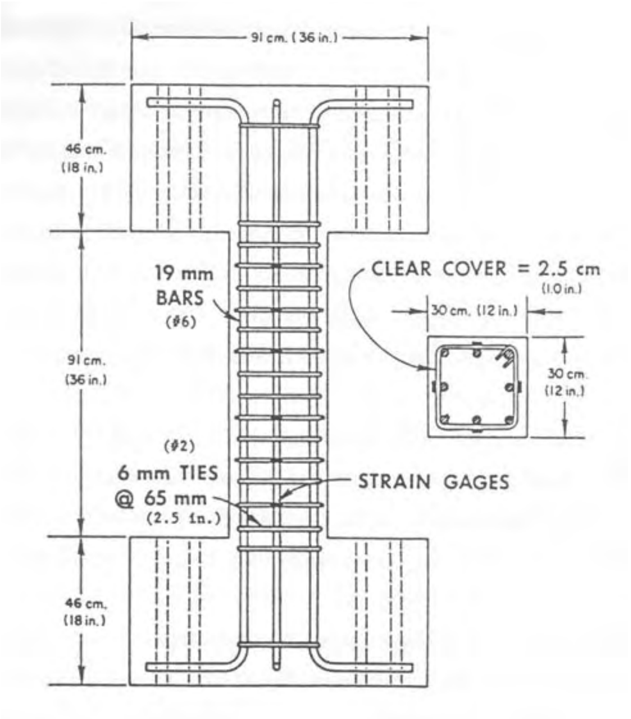

Figure 2.35 - Geometry of the specimens tested (K. Maruyama, H. Ramirez and J.O. Jirsa,1984)

2.0, the behaviour is more and more controlled by the concrete along the compressed diagonal (CEB, 1994).

(K. Maruyama, H. Ramirez and J.O. Jirsa 1984) undertook a test series with the purpose of investigating the behaviour of short-columns subjected to different cyclic lateral loading histories. The geometry of the specimens was not changed (see Figure 2.35).

In Figure 2.36, the test result for specimen O-U is shown in terms of force-deflection relationship of a column without axial load submitted to unidirectional loading. The load history consisted of three cycles in which the peak displacement was Δ_y followed by another three cycles in which the peak displacement was $2\Delta_y$ and so on until the last three cycles had a peak displacement of $4\Delta_y$.

It is evident that the hysteresis loops are narrower than in the flexure-dominated slender members and attain a pronounced inverted *S*-shape, i.e. pronounced pinching. This indicates a very poor hysteretic energy dissipation capacity.

The shape of the force-deflection relationships for members where behaviour is shear-dominated, relates to the role of the stirrups (CEB, 1994). Until the first inclined cracks form, the stirrups do not carry any shear. Therefore unloading and reloading prior to the opening of the cracks is almost elastic. After the yield deflection, the shear transferred across the crack consists of contributions of the compressed concrete above the crack, stirrups crossing the inclined crack and aggregate interlock forces on the surface of the crack (Wight and Sozen, 1973). Dowel forces may have a small effect. Also the bond deterioration between stirrups and the surrounding concrete contributes to larger tensile forces on the stirrups. After yielding, tensile strains tend to accumulate with cycling, which means that the inclined cracks remain open for a longer period. This increase in strain means that the inclined cracks open wider in

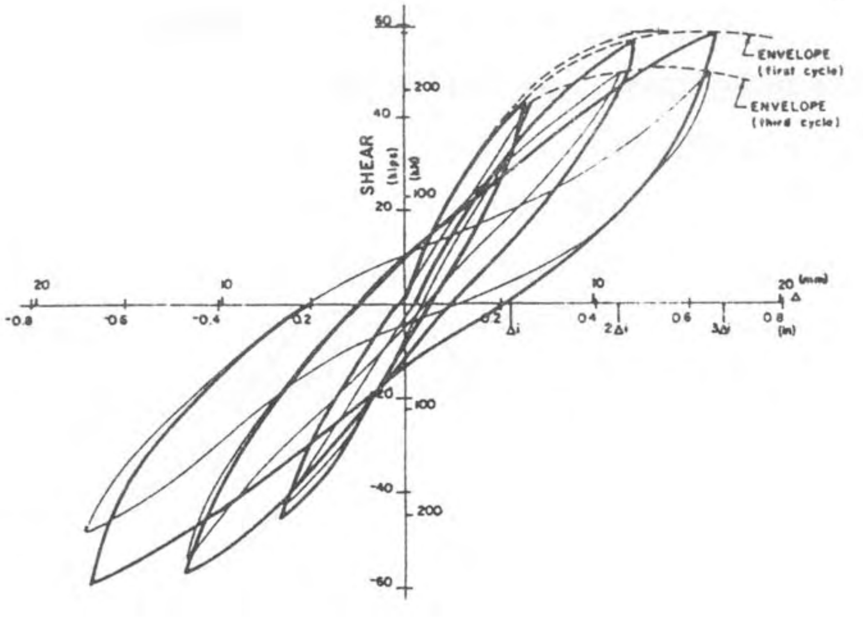

Figure 2.36 - Force-deflection response in test O-U without axial load (K. Maruyama, H. Ramirez and J.O. Jirsa, 1984)

each successive cycle, and as the width of the inclined cracks increases, the pinching effect becomes more and more pronounced, leading to a corresponding decrease in shear strength and stiffness, and reduction in the energy dissipation capacity of the member.

The fact that the loops are narrow relates to the fact that the behaviour is controlled by the concrete along the compressed diagonal, which leads to a rather limited capacity of deformation compared to flexure-dominated members in which the longitudinal reinforcement has a larger contribution to the overall deformation.

The work carried out by Woodward and Jirsa, 1984, at the University of Texas, is useful for understanding the effect of both transverse and longitudinal reinforcement on the behaviour of shear-dominated members. These authors concluded that increasing the ratio of transverse reinforcement increases the energy dissipation capacity and the deformation capacity at ultimate strength as for slender members. However, the parameter ultimate strength is left unaffected, or improves slightly. This indicates that the transverse reinforcement has a rather indirect role on the cyclic behaviour of short elements. Most of the ultimate strength is developed before the formation of the inclined cracks. After cracking, the shear resistance of the member is strongly related to the effectiveness of the aggregate interlock along the inclined cracks (Figure 2.37). The primary function of the stirrups is to control the widths of the inclined cracks to maintain the effectiveness of the aggregate interlock (Woodward and Jirsa, 1984). Thus, the monotonic force-deformation curve is an upper-bound envelope of the cyclic response.

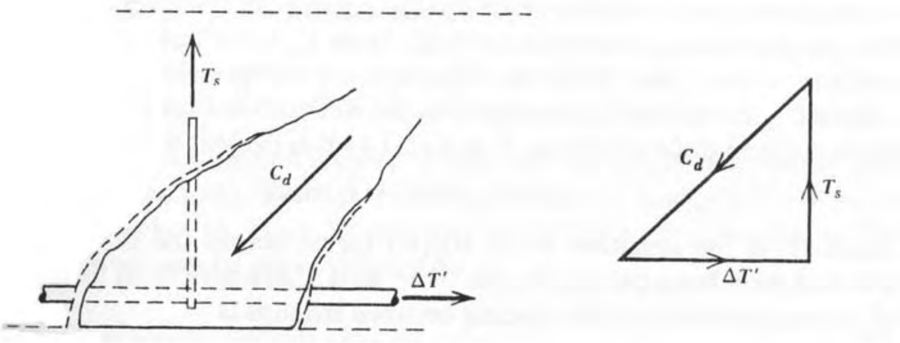

Figure 2.37 - The mechanism of shear resistance (Park and Paulay, 1975)

It was also concluded in this experimental investigation that, for the same reasons as in slender members, an increase of the longitudinal reinforcement leads to larger stiffness and strength degradation and also reduces the energy dissipation capacity.

An important observation from the experimental investigation carried out by (K. Maruyama, H. Ramirez and J.O. Jirsa, 1984) was the spreading of damage throughout the whole length of the member, rather than it being concentrated in the regions with high bending moments, as in slender members. With no axial load, severe diagonal shear cracks formed at both ends of the column. With added cycles or an increase in the deflection magnitude, cracks extended and new cracks appeared. At failure, the entire column was covered with cracks and several large cracks dominated the pattern (K. Maruyama, H. Ramirez and J.O. Jirsa, 1984).

The above-mentioned observation leads to the conclusion that failure may happen in any region of a low shear span ratio member. The failure of this type of element takes place firstly due to splitting of the concrete along the compressed diagonals and crushing of the outermost concrete fibres. Interception of the cracks in the course of cycling contributes to the stiffness and strength deterioration. Typically, failure is associated with the collapse of the member due to the excess of the load-carrying capacity of one of the compressed diagonals, which takes place in a rather brittle and explosive way.

Research has been carried out in recent years with the intention of improving seismic performance of low span ratio members by finding new arrangements of reinforcement. The greater effectiveness of the inclined shear reinforcement compared with the vertical one is well known, since the former is in the principal direction of the diagonal stress field of the shear-dominated member. (Park and Paulay, 1975) have proposed the use of cross-inclined diagonal bars (Figure 2.38b)) and (Tegos & Penelis, 1988) suggested the use of multiple cross-inclined bars, forming a rhombic truss (Figure 2.38c)). In Figure 2.38, the arrangements of reinforcement and the corresponding crack pattern at failure are depicted. Test results have indicated an improvement on the shear capacity, as well as in stiffness and energy dissipation (Penelis and Kappos, 1997). It appears that even better behaviour would be achieved by means of closely spaced diagonal reinforcement.

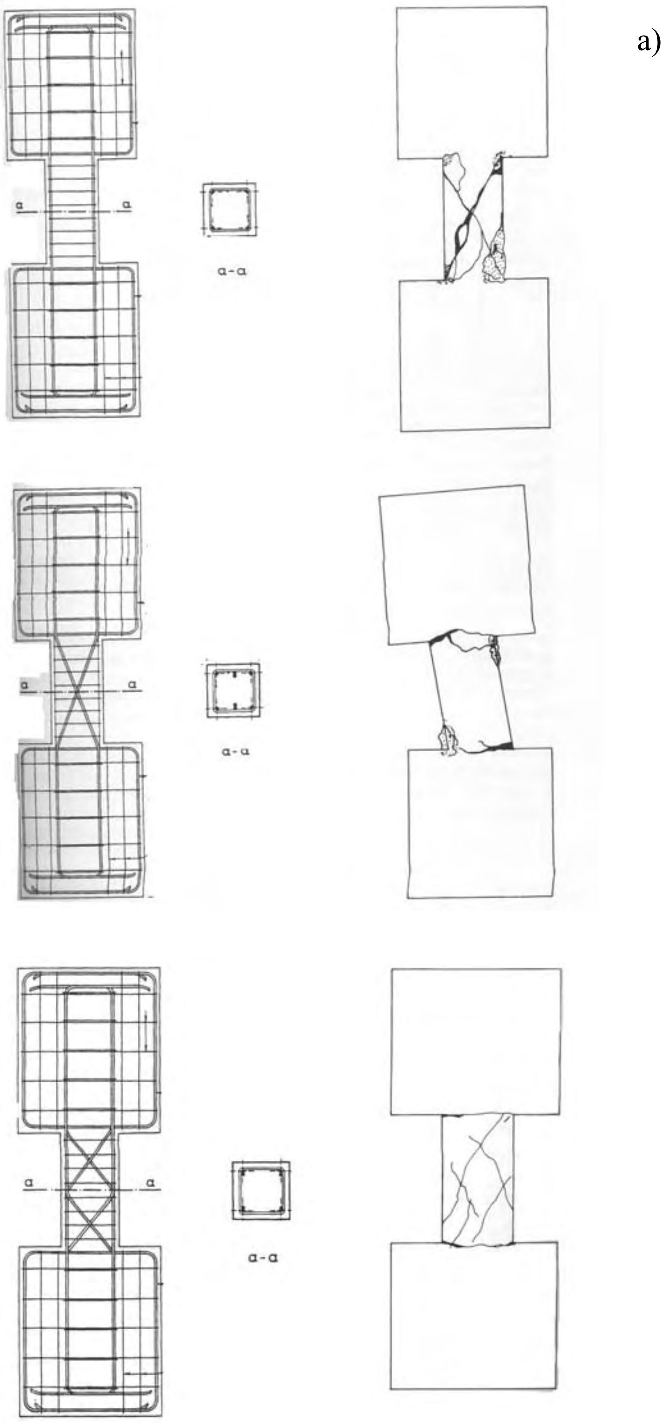

Figure 2.38 - a) Conventional reinforcement (closed spaced ties); b) Bidiagonal reinforcement and c) Rhombic reinforcement (Penelis and Kappos, 1997)

The effect of axial forces

The tests carried out by (K. Maruyama, H. Ramirez and J.O. Jirsa, 1984) also clarify the effect of axial force. The specimens (Figure 2.39) were submitted to the same loading history as the specimen in Figure 2.36, but with different levels of axial forces applied.

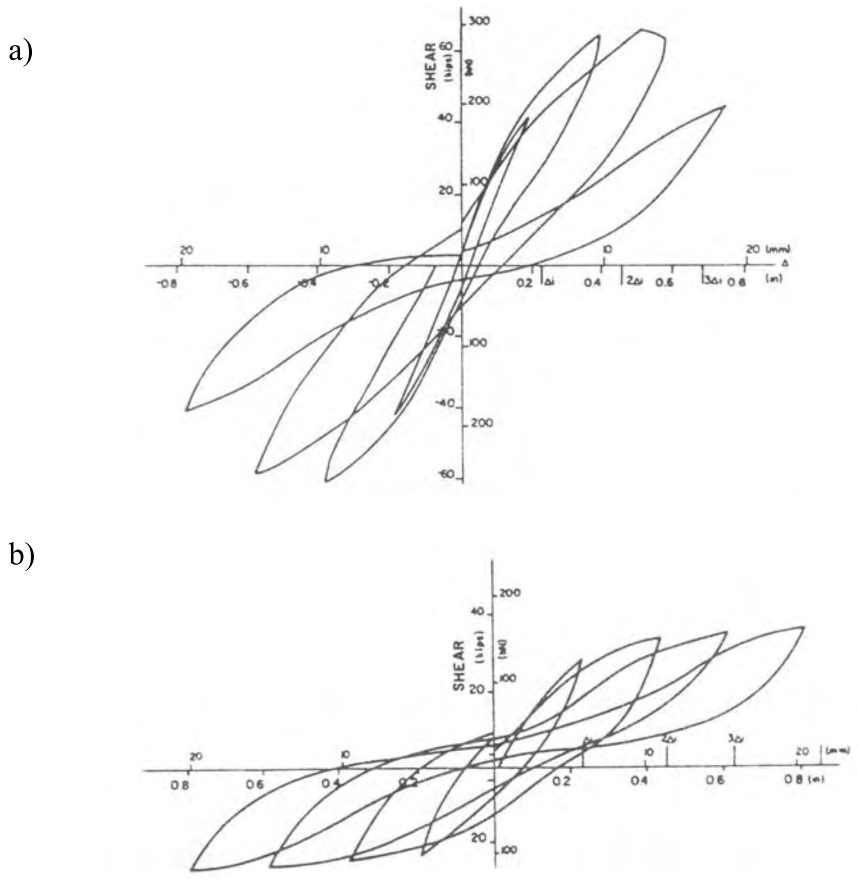

Figure 2.39 - Effect of axial load on cyclic response a) $\nu = -0.19$ (compression) and b) $\nu = 0.12$ (tension) (K. Maruyama, H. Ramirez and J.O. Jirsa, 1984)

It may be concluded by comparing Figure 2.36 with Figure 2.39a) that the presence of low-to-medium compressive forces increase the ultimate strength of a low shear span ratio member. This is due to the increase in the depth of the compression zone, and so in this zone, the shear may be transferred by inclined compression. However, this seems to be the only favourable effect since the rate of stiffness and shear strength decay is much larger in the post-yield deflections for the compressed member. Furthermore the capacity of energy dissipation is severely affected, as seen in Figure 2.39, noting that the axial compressed specimen has a larger *pinching effect*. An explanation for this lies in the fact that added compression on the compressed diagonal strut further accelerates splitting along the diagonal cracks and spalling of the concrete cover. Moreover the stirrups are already in tension due to lateral expansion from the compressive axial load. Thus, the stirrups are not as effective in providing confinement to the core at high levels of deformation and maintaining the shear capacity as in members without axial load. As a consequence, the rate of degradation of the inner structure of the member is higher for compressed members.

Axial tension has the reverse effects of axial compression for low shear span ratio members under cyclic loading. In fact, it may be concluded by comparing Figure 2.36 and Figure 2.39 b) that the shear force required to attain a given deformation decreases for members in tension. This may be explained by the fact that axial tension diminishes the contribution of the effect of the aggregate interlock in the shear resistance mechanism after the inclined cracks have formed. This also explains the reduced stiffness of the response, even for the first cycle. However less degradation of stiffness, strength and energy dissipation capacity are observed. In fact the shape of the hysteresis loops resemble those of the flexure-dominated members. This is because the forces in the stirrups are not mobilised until large lateral deformations close the horizontal cracks from tension, and diagonal cracks form. Therefore, the shape of the hysteresis loops is more stable, enabling the member to reach higher levels of ductility but at lower levels of strength and stiffness.

Members in biaxial shear

The tests performed at the University of Texas also included a series of biaxial tests to investigate the effect on biaxial shear in low span ratio reinforced concrete members. The tests, as reported below, were of two types according to the direction of the load:

- Alternate cyclic loading in both directions (Test O-B4). This test was conducted to examine the influence of previous cyclic loading in an orthogonal direction
- Cyclic loading in one direction with permanent deflection in the orthogonal direction (Tests O-U2 and O-U4)

Figure 2.41 exhibits the response for the three specimens in terms of the hysteretic relationships.

As previously mentioned, the geometry of the specimens tested was kept unchanged. However, according to the loading histories, the cyclic response was different. This fact is evident when comparing the responses referring to the N-S direction for the three specimens and the response curve of the control specimen O-U (Figure 2.18).

- It appears that the N-S strength of specimen O-B4 was only a fraction of the strength under unidirectional loading as shown in Figure 2.36. The only difference between these two specimens was that Specimen O-B4 had already been submitted to cyclic loading in the orthogonal direction with a magnitude of $4\Delta_y$, since the loading in the N-S direction was developed in the same way as for the control specimen O-U. Moreover, the response of Specimen O-B4 in the N-S direction showed lower strength than that of specimen O-U4 and with a more pronounced pinching effect. This leads to the same conclusion as for the biaxial flexure case (section 2.2.1.5): cycling in one direction with a magnitude larger than the yield displacement, Δ_y severely affects the strength and energy dissipation capacity in the orthogonal direction. The cycling nature of the load is the governing factor for the strength degradation in the orthogonal direction. This may be concluded referring to the fact that specimen O-U4, with a superior response, had also been exposed to a deflection in the orthogonal direction of $4\Delta_y$, but of a

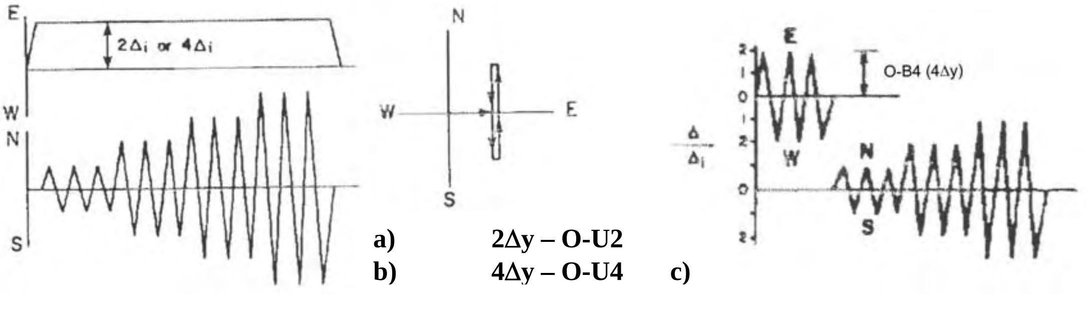

a) **2Δy – O-U2**
b) **4Δy – O-U4** **c)**

Figure 2.40 - Loading histories a) O-U2 b) O-U4 and c) O-B4 (K. Maruyama, H. Ramirez and J.O. Jirsa, 1984)

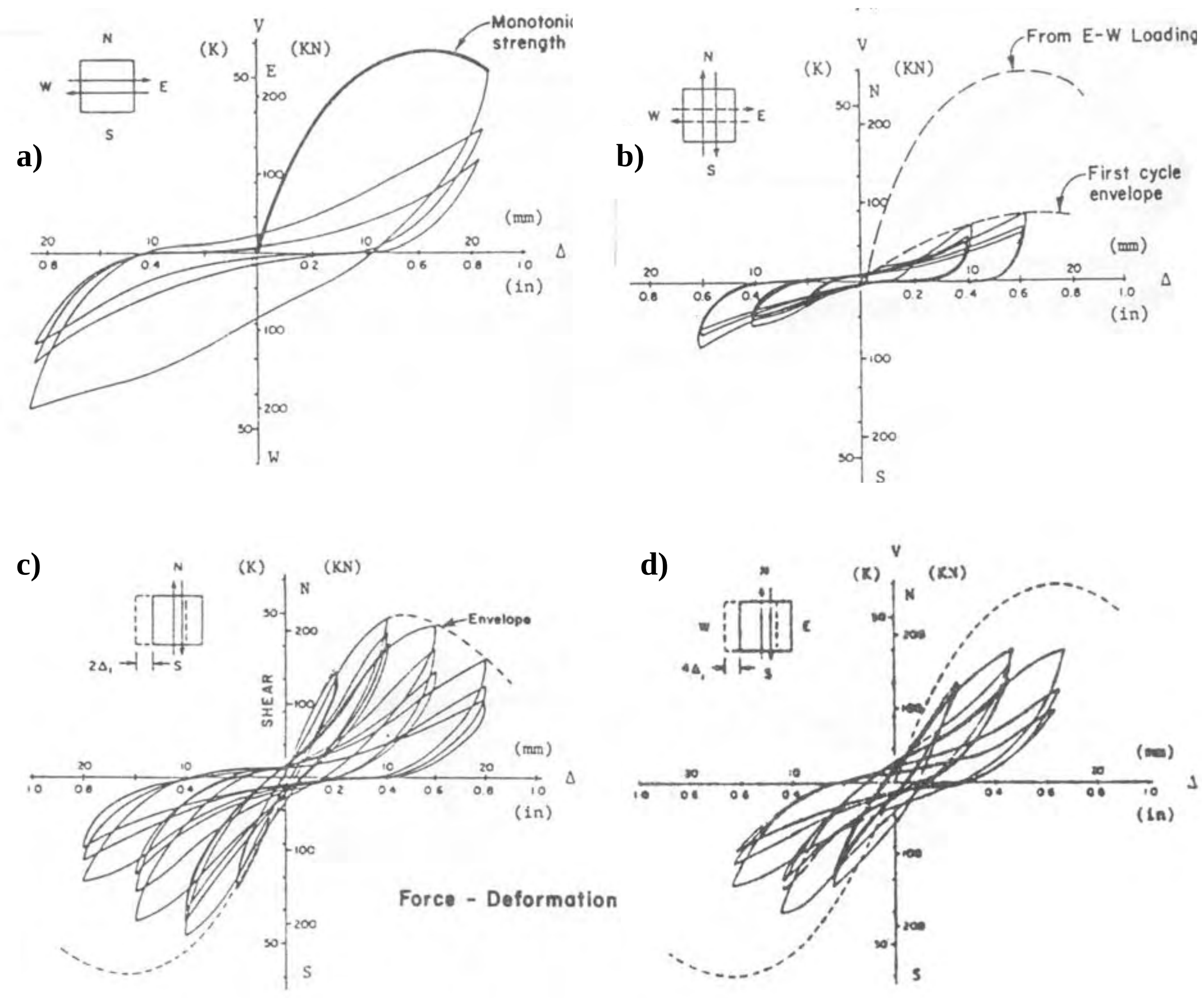

Figure 2.41 - Force-deflection response a) O-B4 (E-W direction) b) O-B4 (N-S direction) c) O-U2 and d) O-U4 (K. Maruyama, H. Ramirez and J.O. Jirsa, 1984)

permanent nature instead of cycling. This has to do with the fact that cycling not only contributes to increasing the damage already induced in the members on the previous cycle by the successive opening of the cracks, but also spreads further damage as new cracks form.

- The strength in the N-S direction for specimen O-U2 is larger than that of specimen O-U4. The only difference between these two tests lies in the magnitude of the permanent deflection in the E-W direction. The specimen with larger permanent deflection exhibited larger strength decay in the N-S direction. Thus, it can be concluded that the larger the inelastic action in one direction, the larger the strength decay in the orthogonal direction.

(Umehara and Jirsa, 1984) also concluded that previous loading in perpendicular directions does not significantly affect the maximum shear strength of the short low shear span ratio members unless the maximum deflection in the previous loading exceeds the deflection at which the maximum shear strength of the members under unidirectional loading is reached. Moreover, they reached the same conclusion as in 1982 (already referred to in the discussion regarding the biaxial state of flexure, section 2.2.1.5): as in slender members, the maximum capacity for low shear span ratio members with diagonal unidirectional loading may be estimated using an interaction circle or ellipse (for asymmetric cross-sections) connecting the maximum capacities of the columns under unidirectional loading along the principal axes.

2.2.3 Joints

The term *joint* refers to the regions where structural elements (columns and beams) intercept. It is now recognised that joints might be critical regions in reinforced concrete frames submitted to cyclic loading. However up until the late 1970's, the seismic provisions in all countries were based on the erroneous assumption that conditions within the joint, which often have somewhat larger dimensions than the members it joins, were not critical (Park and Paulay, 1975). This assumption was supported by observations in the field after strong earthquakes that showed little evidence of the contribution of joint failures for the major damage or collapse of structures. (Paulay and Priestley, 1992) explained these observations referring to the inferior standard of beam design and particularly to poor detailing of columns rather than attributing *apriori* a non-critical performance to the joints.

While the behaviour of joints for static loading is in a rather advanced state (Nielsen, 1998), only in recent years has the behaviour of joints submitted to seismic action been a subject of interest. There is still much debate regarding joint resistance mechanisms under cyclic loading, as present knowledge is far behind that of linear members. Moreover, experimental data relating to the cyclic behaviour of reinforced concrete joints is very scarce, since detailed experimental investigations are very recent. This is reflected in the significant differences both in the design approach and reinforcement detailing in modern codes.

Thus in the following, a qualitative description of the cyclic behaviour of concrete will be given with the intention of providing information about its main features and the parameters influencing it. Bonacci, Filippou and Pantazopoulou, (CEB, 1994) provided a critical compilation of available experimental results and design recommendations from several countries with the purpose of establishing the current state of the art.

2.2.3.1 Qualitative description of mechanics

The behaviour of a joint is characterised by a complex interaction where shear, bond and confinement mechanisms take place in a quite limited area. Until now, significant differences still exist among seismic codes with regard to the shear transfer mechanisms assumed. In the following, the simple approach suggested by (Paulay and Priestley, 1992) and adopted by the Standards Association of New Zealand is going to be presented.

Considering the overall statics of a given two-dimensional frame as shown in Figure 2.42, it can be understood that lateral loading imposes such a bending moment field in the beams and columns, that moments with the same magnitude but of opposite signs will take place on parallel faces of the joint. As a consequence, the joint region is subjected to horizontal and vertical shear forces whose magnitude is l_c/d_b times the maximum shear force in the columns and l_b/d_c times the maximum shear force in the beams, respectively (see the meaning of the symbols in Figure 2.42).

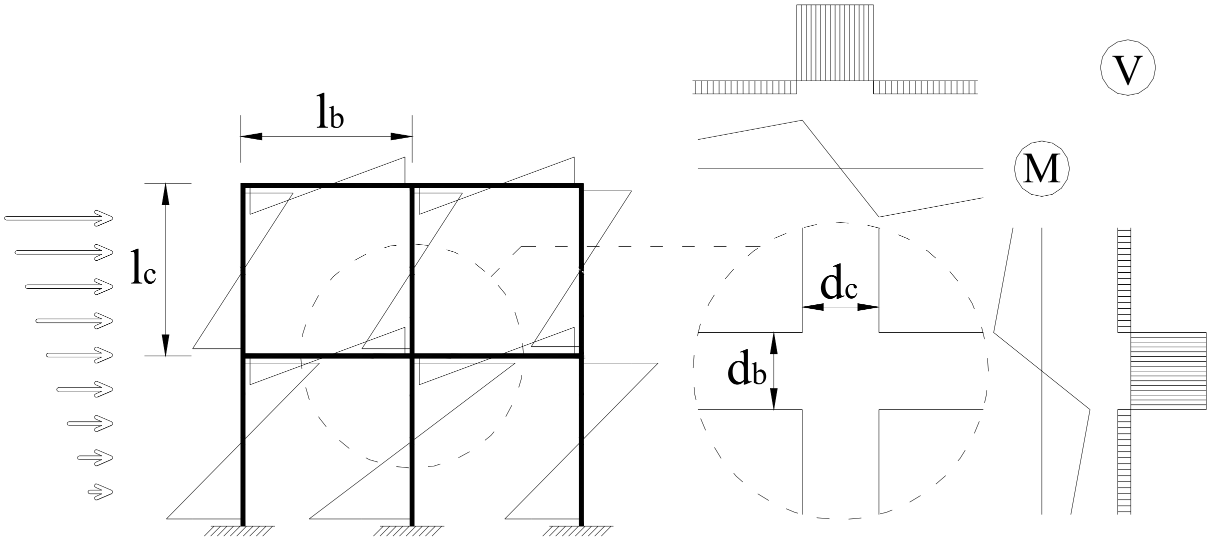

Figure 2.42 - Statics of laterally loaded frame; Detail: Moments and shear gradient through an interior joint

Consider now the equilibrium of the interior of the joint, represented in Figure 2.43 a). It may be seen that the joint core is submitted to two types of actions that when combined are generally known as the *joint shear*:

- Concrete flexural compression from beams and columns at the opposite corner of the joint (Figure 2.43b))
- Shear flow along its perimeter from beam and column bars by means of bond forces (Figure 2.43c))

The resistance mechanism is composed of a compressed diagonal of concrete roughly limited by the neutral axes of the end sections of the members (Figure 2.43d)) and of diagonal compression field– truss mechanism – consisting of horizontal hoops, intermediate column bars (Figure 2.43f)) and inclined compressed concrete between shear cracks (Figure 2.43e)).

The main component of the resistance mechanism is the compressed diagonal strut, which carries a substantial portion of the joint shear. The rest of the joint shear, transmitted to joint core through the bond between the longitudinal reinforcement of beams and columns and the surrounding concrete, is absorbed by the truss mechanism. Depending on the magnitude of the bond forces, diagonal tension cracking takes place. The main crack is developed along the compresses strut but other cracks parallel to it also form. In Figure 2.44 a crack pattern typical of joint shear is clearly seen.

To prevent shear failure both horizontal and vertical reinforcement are required. Such reinforcement enables a diagonal compression field to be mobilised as shown in Figure 2.43e). This leads to the conclusion that the amount of reinforcement may be significantly greater than would normally be provided by the extension of the reinforcement of beams and columns into the joint core. This is particularly true in the case of joints whose columns are low axially loaded.

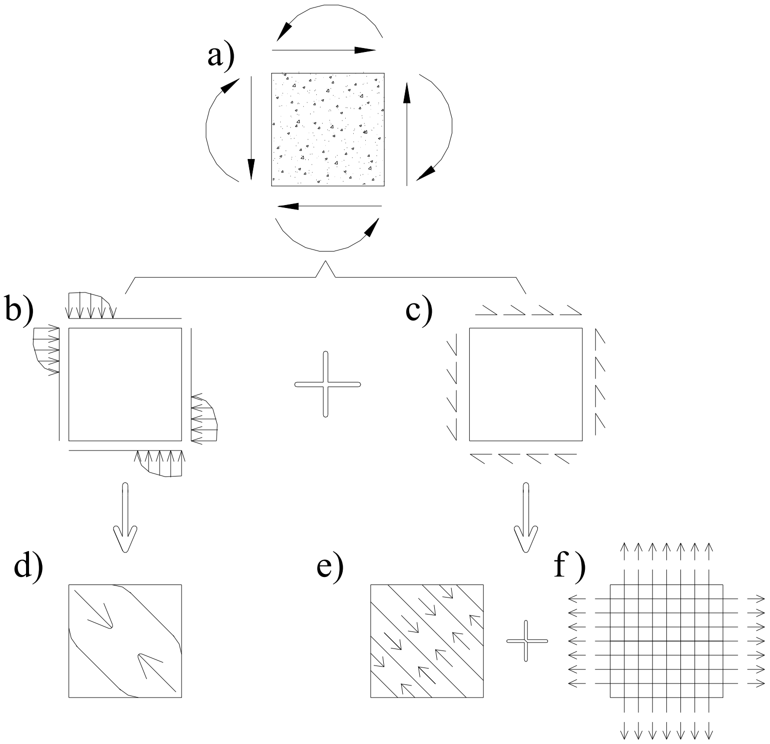

Figure 2.43 - Actions on a interior joint and the corresponding resistance mechanism according to (Paulay and Priestley, 1992)

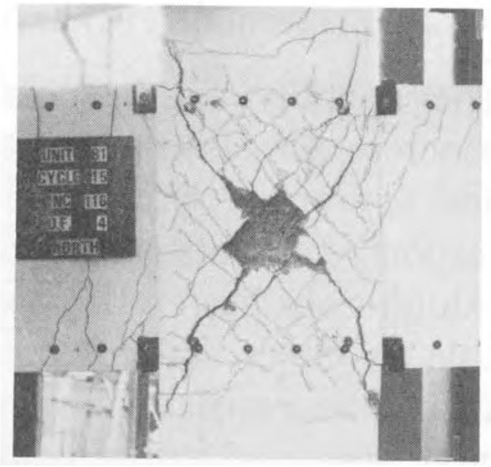

Figure 2.44 - Crack pattern of a joint (Paulay and Priestley, 1992)

2.2.3.2 Influence of cyclic loading

As per the previous section, the joint resistance mechanism depends on bond forces along its perimeter so that a truss mechanism can be mobilised, and on a compressed diagonal strut between corners. These are rather brittle modes of behaviour, which explains the very limited capacity that joints have in dissipating energy and maintaining their strength.

The contribution of the diagonal compressed strut is significant during the first cycle in the inelastic range. However it deteriorates with increases in the inelastic loading cycles. This is due to the fact that cycling at high levels of inelastic deformation causes permanent elongation on the beam bars and leads to full depth open cracks at the beam-joint interface. This was previously discussed in section 2.2.1. Under these conditions flexural compression from the beams become negligible. The compressive forces are then transmitted to the longitudinal bars of the beams, which significantly increases the bond stresses along the horizontal perimeters of the joint core. The foregoing leads to a drastic reduction in the contribution of the concrete strut to the transfer of horizontal joint shear and a consequent increase in the contribution of the truss mechanism. The mobilisation of the truss mechanism depends intimately on the effectiveness of bond between the steel bars and the surrounding concrete. As discussed in section 2.1.3, bond has a very poor response in terms of energy dissipation, stiffness and strength degradation under inelastic cycling. Thus, it can be concluded that the development of plastic hinges in the end sections of the beams seriously affects the ability of the joint to resist the induced shear forces in a stable manner. Again, joints whose columns are low axially loaded are the most sensitive to bond deterioration since compression helps to maintain the bond mechanism.

This serves to emphasise the need to take special precautions to prevent premature bond deterioration in joints under seismic loads. Adequate confinement of the joint core significantly improves the bond performance under seismic conditions (Paulay and Priestley, 1992). Confinement may be provided by axial compression of the column and/or by means of reinforcement using the intermediate column bars, as these members are supposed to remain in the elastic domain. Moreover, confinement improves the performance of the compressed diagonal strut.

Yielding of the longitudinal bars of the beam leads to another form of degradation of the shear resistance of the joint: As the horizontal bars yield on tension, the shear cracks due to diagonal tension tend to remain open, locked on the extended steel bars. This contributes to a rapid degradation of the shear resistance in the truss mechanism with cycling due to the successive drop on the friction forces along the shear cracks. Once again this effect may be diminished by taking advantage of the intermediate column bars which are intended to remain in the elastic range and therefore can contribute to the closing of the shear cracks throughout the whole seismic action.

The reversals in the loading also contribute to the spreading of the cracks in orthogonal directions. As seen in the case of members, this leads to successive degradation of the strength of the compressive diagonal struts, since the closing of the cracks is not completely effective given that the surfaces may not come into full contact. The damage induced by cross-inclined cracking also adversely affects the bond conditions of the longitudinal bars intercepting the concrete core. To control this effect, confinement plays an important role as well as keeping the inner structure of the concrete member preserved, controlling sliding along the cracks.

Failure of the joint is due to the inability of any of the “sub-mechanisms” depicted in Figure 2.43 d), e) and f) to successfully carry the load they are meant to sustain. It follows then that three different sources for joint failure can be pointed out:

- Failure of the compressed diagonal strut
- Failure due to loss of bond resistance along the joint boundary
- Failure due to an inability to develop a truss mechanism that can carry the diagonal tension by the premature yielding of the longitudinal bars intercepting the core (Figure 2.45).

A method by which to control the first and the second mode of failure is the obvious impact of increasing the joint dimensions. As previously explained, the current design

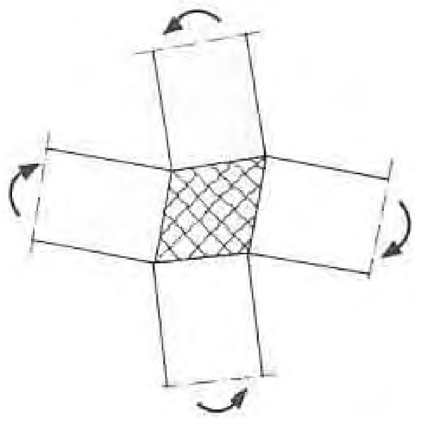

Figure 2.45 - Shear failure due to premature yielding of the joint reinforcement (Penelis and Kappos, 1997)

philosophy leads to the weak beam/strong column concept. Therefore it is reasonable to increase the joint dimensions by means of greater depth of columns. This has the dual effect of leading to less shear stresses in the joint core and also lowering bond demand along the beam bars passing through the joint.

Additionally to adequate confinement, good anchorage of the longitudinal beam bars is a decisive factor in the maintenance of the bond strength throughout the seismic loading. This is achieved by an appropriate anchorage length and configuration, and by limiting the diameter of the bar.

2.3 Available rotation capacity

Rotation capacity refers to the maximum value of the relative plastic rotation in a hinge. From the discussion in section 1.1 on modern displacement-based seismic design philosophy, it is understood that this is a crucial parameter in evaluating structural seismic performance. Unfortunately, it is difficult to calculate the rotation capacity accurately. Therefore, one must rely on tests and simple estimates.

Here we present a simple conservative method to evaluate the available rotation capacity of plastic hinges dominated by flexural behaviour, which, as may be understood from previous discussion, should be preferred over the failure modes relying on shear and bond deformations. Basically, the ultimate rotation capacity, θ_u, is derived from the integration of the curvature along the plastic hinge length, Δl.

Consider the bilinear idealisation of the stress-strain curve for reinforcement steel shown in Figure 2.46a). In this case, flexural yielding starts when the stress at the tensile reinforcement, σ, reaches $f_{y,min}$ and flexural failure takes place for $\sigma = f_{y,max}$ at an ultimate strain ε_{su}.

Consider the length of a beam with positive moment M and positive shear force V (the sign conventions are shown in Figure 2.46b). According to the lower bound solution, the diagonal compression stress field in the concrete implies that the tensile reinforcement has to carry the force (Nielsen, 1998):

$$T = \frac{M}{d} + \frac{1}{2} V \cot \alpha \tag{2.3}$$

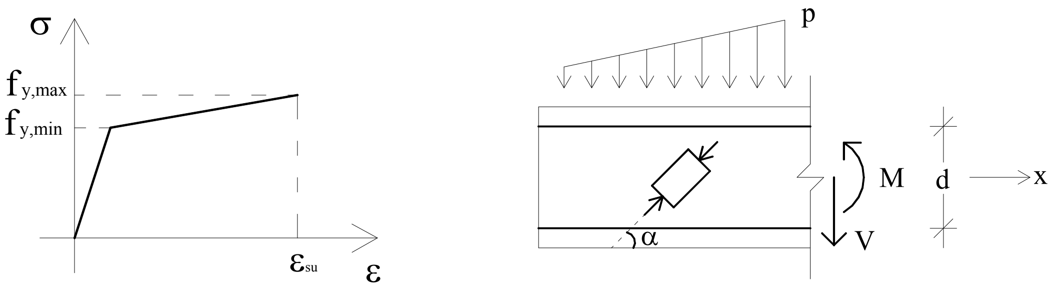

a) **b)**

Figure 2.46 - a) Stress-strain curve for reinforcement with strain hardening and b) Beam with shear zone. Bending moment M and shear force V

Here, d is the internal moment arm and α is the angle between the beam axis (the x-axis) and the diagonal compression stresses in the concrete. Hence:

$$\frac{dT}{dx} = \frac{V}{d} - \frac{1}{2} p \cot \alpha \tag{2.4}$$

p being the load per unit length of the beam.

Consider a beam loaded by a concentrated force at a plastic hinge, i.e. that p=0 and V=Constant=V_1. The tensile reinforcement has a constant area A_s along the plastic hinge length. If the plastic zone on the left-hand side of the hinge has the length Δl_1, we have the following change of force in the tensile reinforcement along Δl_1:

$$\Delta T = A_s \cdot (f_{y,max} - f_{y,min}) \tag{2.5}$$

Applying (2.4) we find that Δl_1 should be:

$$\Delta l_1 = \frac{d \cdot A_s \cdot (f_{y,max} - f_{y,min})}{V_1} \tag{2.6}$$

If M_P is the plastic moment in the hinge we have $A_s = M_P/(d \cdot f_{y,min})$. Note that A_s must be determined for the tensile force T at the hinge according to (2.3). Then (2.6) renders:

$$\begin{aligned} \Delta l_1 &= \frac{f_{y,max} - f_{y,min}}{f_{y,min}} \cdot \frac{M_P}{V_1} \Leftrightarrow \\ \Leftrightarrow \Delta l_1 &= \eta \cdot \frac{M_P}{V_1} \end{aligned} \tag{2.7}$$

The parameter η is solely dependent on the type of steel used. For instance, for the ductile steel class Grade B400 or B500 Tempcore, mentioned in section 2.1.2, we have η=0.20.

$M_P/V_1$is the left-hand shear span. We also receive a contribution from the right-hand shear span, which means that the total plastic zone length Δl is:

$$\Delta l = \Delta l_1 + \Delta l_2 \tag{2.8}$$

Obviously, to account for Δl_2 one should use the same value of M_P, but the corresponding value of V_2 for the part of the hinge on the right-hand side.

Since even a concentrated force will spread out from the point of application, a small term proportional to the height of the cross-section may be added to (2.7) and (2.8). If, in the middle of a beam depth, the concentrated force is assumed to be uniformly distributed along h/2 (spreading ratio 2:1), we get in each side of the hinge a length h/4 along which we may have yielding even without a constitutive relationship for the steel with strain hardening. Thus, the final version of (2.7) may be taken as the sum of two contributions, i.e.:

$$\Delta l_1 = 0.25h + \eta \cdot \frac{M_P}{V_1} \tag{2.9}$$

and then (2.8) reads

$$\Delta l = 0.5 \cdot h + \eta \cdot M_P \cdot \left(\frac{1}{V_1} + \frac{1}{V_2} \right) \tag{2.10}$$

These formulae are in close agreement with an empirical formula suggested by (Sawyer, 1964) if η in our formula is set to 0.075, cf. equation (2.11)

$$\Delta l_1 = 0.25 \cdot d + 0.075 \cdot \frac{M_P}{V_1} \tag{2.11}$$

For a uniformly loaded beam with transverse shear reinforcement, plastic theory has shown that the length $2 \cdot h \cdot \cot\alpha$ around the maximum moment point does not require any shear reinforcement, which means that T=constant along this length. Thus in this case the plastic zone is at least

$$\Delta l = 2 \cdot h \cdot \cot\alpha \tag{2.12}$$

The inclination α of the diagonal compression may be chosen freely as long as the diagonal compression stress does not exceed the effective compression strength of the concrete. To Δl, according to (2.12), could be added a length depending on h and η, but often this is not needed. The parameter $\cot\alpha$ is normally chosen between 1 and 2, or 2.5 for conventional reinforcement to avoid excessive cracking in the serviceability limit state.

For a hinge in a fixed end, formula (2.9) may be used for any loading taking M_P as the plastic moment in the hinge and V_1 as the absolute value of the shear force in the hinge.

When the plastic zone length Δl has been estimated, the rotation capacity θ_P may be calculated as

$$\theta_P = \frac{\varepsilon_{su}}{2 \cdot d} \cdot \Delta l \tag{2.13}$$

On the safe side, we have made the following assumptions to determine θ_P:

- The ultimate curvature, ϕ_u is computed considering that the compression strain in the upper stringer is zero, i.e. $\phi_u=\varepsilon_{su}/d$.
- The yield curvature at the ends of the plastic hinge away from the cross-section corresponding to M_P is negligible when compared to ϕ_u.

Considering that $d=0.9 \cdot h$, which is a common assumption for the length of the internal moment arm at flexural capacity, (2.13) is re-written in terms of the height of the cross-section:

$$\theta_P = \frac{\varepsilon_{su}}{1.8 \cdot h} \cdot \Delta l \tag{2.14}$$

For sections with compression normal force, (2.14) should not be used for normal forces larger than half the compression capacity of the concrete section (disregarding cover).

In order to estimate the ductility capacity in terms of rotation at the plastic hinge, $\mu_{\theta,max}$, we must first calculate the corresponding yield rotation, θ_y. This will be carried out assuming that the neutral axis remains in the same position from the onset of the yield curvature, ϕ_y, to the onset of the ultimate curvature. Thus:

$$\phi_y = \frac{\varepsilon_{sy}}{0.8 \cdot h} \tag{2.15}$$

The curvatures at the ends of the plastic hinge, ϕ_1' and ϕ_2', may be estimated considering linear variation of curvature along the plastic hinge length with the bending moment. Therefore, ϕ_1' and ϕ_2' are the ratio of the yield curvature according to the bending moment on the left-hand side and right-hand side, respectively:

$$\text{Cross-section at the left-hand side } \phi_1' = \frac{M_P - V_1 \cdot \Delta l_1}{M_P} \cdot \frac{\varepsilon_{sy}}{0.8 \cdot h} \tag{2.16}$$

$$\text{Cross-section at the right-hand side: } \phi_2' = \frac{M_P - V_2 \cdot \Delta l_2}{M_P} \cdot \frac{\varepsilon_{sy}}{0.8 \cdot h} \tag{2.17}$$

The yield rotation is obtained by integrating the curvature along the plastic hinge length:

$$\theta_y = \frac{\varepsilon_{sy}}{1.6 \cdot h} \cdot \left[\Delta l_1 \cdot \frac{2 \cdot M_P - V_1 \cdot \Delta l_1}{M_P} + \Delta l_2 \cdot \frac{2 \cdot M_P - V_2 \cdot \Delta l_2}{M_P} \right] \tag{2.18}$$

Finally, the estimate of the rotation ductility, μ_θ, is given:

$$\mu_{\theta,max} = 0.89 \cdot \frac{\varepsilon_{su}}{\varepsilon_{sy}} \cdot \frac{M_P \cdot (\Delta l_1 + \Delta l_2)}{\Delta l_1 \cdot (2 \cdot M_P - V_1 \cdot \Delta l_1) + \Delta l_2 \cdot (2 \cdot M_P - V_2 \cdot \Delta l_2)} \tag{2.19}$$

If the plastic hinge is located at the end of beam, e.g. the left-hand end, which is the most common location in ductile frames, (2.19) has a simpler expression:

$$\mu_{\theta,max} = 0.89 \cdot \frac{\varepsilon_{su}}{\varepsilon_{sy}} \cdot \frac{M_P}{2 \cdot M_P - V_1 \cdot \Delta l_1} \tag{2.20}$$

Example

Consider the case of a beam with rectangular cross-section in a ductile frame subjected to strong ground motion. The beam is 5m long and at the time of the earthquake, the sum of the dead and live loads is 10tonf/m. The plastic hinges are located at the ends, the bending moment capacities are the same for both directions and equivalent to 400kNm. The maximum shear force at the plastic hinges, V_{max}, is:

$$V_{max} = \frac{10 \times 9.81 \times 5}{2} + \frac{2 \times 400}{5} = 405.25\text{kN} \tag{2.21}$$

Consider further that the tensile reinforcement ratio, ρ_T, is 1% of the gross cross-section and that the steel class is Grade B500 Tempcore, cf. Table 2.4.

i. To solve this problem, we first have to find the value of the cross-section height, h. If we assume that the width of the cross-section b is given as a ratio β of the height, we have:

$$\begin{cases} b = \beta \cdot h \\ A_s = \rho_T \cdot b \cdot h \\ A_s = \dfrac{M_P}{d \cdot f_{y,min}} \\ d = 0.9 \cdot h \end{cases} \Rightarrow h = \sqrt[3]{\frac{M_P}{0.9 \cdot \alpha \cdot \rho_T \cdot f_{y,min}}} \tag{2.22}$$

Assuming that β=0.60 we find that h=0.53m. Rounding up the latter value we have

$$h = 0.55\text{m} \tag{2.23}$$

The resulting tensile reinforcement ratio is found to be

$$\rho_T = \frac{400}{0.9 \times 0.6 \times 0.55^3 \times 500 \times 10^3} = 0.89\% \tag{2.24}$$

which is considered to be an appropriate vale of ρ_T to assure ductile behaviour.

ii. The plastic hinge is located at the end of the beam. This implies expression in (2.9) to evaluate the length of the plastic hinge Δl:

$$\Delta l = 0.25 \times 0.55 + 0.20 \times \frac{400}{405.25} = 0.33\text{m} \tag{2.25}$$

iii. The rotation capacity is then given by (2.14):

$$\theta_P = \frac{0.1}{1.8 \times 0.55} \times 0.33 = 3.33 \times 10^{-2}\,\text{rad} \tag{2.26}$$

iv. To calculate the maximum ductility capacity in terms of rotation at the plastic hinge, $\mu_{\theta,max}$, we use expression (2.20):

$$\mu_{\theta,max} = 0.89 \times \frac{0.1}{0.0025} \times \frac{400}{2 \times 400 - 405.25 \times 0.33} \approx 21 \tag{2.27}$$

Table 2.4 - Properties of Grade B500 Tempcore steel

Grade B500 Tempcore	
$f_{y,min}$ (MPa)	500
$f_{y,max}$ (MPa)	600
E_s (GPa)	200
ε_{sy} (%)	0.25
ε_{su}(%)	10
η	0.2

2.4 Implications on seismic design

2.4.1 Principles of member design

As seen throughout section 2.2.1, as long as adequate reinforcement detailing is assigned, flexural yielding mechanisms have greater potential for developing and maintaining ductile response against cyclic loading. Conversely, mechanisms characterised by exhaustion of shear capacity or anchorage failure tend to present rather brittle modes of failure. The obvious implication for the case of seismic design is that modes of failure in flexural behaviour should be pursued and those exploring inelastic shear and bond-slip deformations should be avoided.

Some good rules of practise towards design for ductile response at the plastic hinges may be briefly summarized:

- To limit the compressive strength of concrete, as lower strength concrete classes are more ductile
- To adopt close spacing of transverse reinforcement and most specially proper hoop configurations to increase the beneficial effect of confinement
- To avoid asymmetry of cross-section lay-out as this leads to higher pinching effects in the weak “direction” and consequently, lower energy dissipation capacity
- To use low tensile reinforcement ratios to prevent high rates of strength and stiffness degradation
- For the case of columns, to design for moderate levels of normalized compressive axial force.

2.4.2 Weak beam / strong column concept for ductile frames

The review on cyclic behaviour of reinforced concrete elements presented in this chapter serves also to justify the so-called *weak-beam strong column concept*. This concept is the corollary of modern seismic design philosophy and is of fundamental importance in the design of structures for which seismic resistance systems are composed of ductile frames. Attending to the structural functions and modes of behaviour of beams and columns, this concept establishes that the energy dissipation mechanism of the structure is composed of flexural plastic hinges is occurring in beams (typically at the ends), and avoided as far as possible in columns. Therefore it follows that the strength of the beams is limited to the plastic hinge capacity and columns are intended to remain in the elastic domain. Column design moments are, according to this concept, derived at beam-column joints with respect to the actual resisting moments of the plastic hinges in the beams.

Columns are traditionally designed to withstand axial loads from the weight of the structure and from “live loads”, whereas beams have the function of carrying those mainly by flexure. During an earthquake, columns are additionally submitted to lateral loading to which they respond with flexural strength. Beams, however, roughly conserve their flexural mode of behaviour and this, as seen in section 2.2.1, enables them to maintain their strength even at significant levels of ductility, provided that adequate detailing of the reinforcement is used. Thus, it is expected that most of the dissipation capacity of the structure is allocated in the beams.

As seen in section 2.2.3, the behaviour of beam-column joints is dominated both by shear forces and bond mechanism, which have rather brittle modes of failure. Therefore these structural elements should always remain in the elastic domain, i.e. they should be provided with strength greater than the maximum demand corresponding to development of the adjacent plastic hinges. The larger the flexural capacity at the beams, the larger the shear force at the joint, cf. Figure 2.42, and thus, the more difficult it is to assure elastic behaviour during the whole period of ground excitation.

Avoiding joint failure also eliminates the need for repair in a relatively inaccessible region of the structure and prevents potential degradation of the capacity of the column due to degradation within the joint. Moreover, inelastic deformation of joints increases the overall story drifts of the frame leading to larger P-Δ effects.

2.4.3 Overstrength factors

The task of ensuring that only the desired collapse mechanism takes place, and all the other brittle modes of failure are prevented, is carried out by assessing the highest probable strength capacity at the plastic hinges and assigning enough corresponding strength in the remaining part of the structure so that it remains in the elastic domain during the whole ground motion, for all kinds of strength demand.

There are three main sources for overstrength at the plastic hinges:

1. Deviations due to calculation assumptions in specifying the reinforcement steel, dimensions and detailing and necessity to round off these quantities in practice
2. Deviations due to actual nominal material strength, other than those accounted for at the design phase
3. Strength enhancement in plastic behaviour due to strain hardening effects of the reinforcing steel and additional compressive strength of concrete due to confinement

It is obvious that the first two sources for overstrength at the plastic hinges also affect the other parts of the structure outside the hinges. Therefore, according to (Paulay and Priestley, 1992) the corresponding overstrength factor should be 10% of order of magnitude.

Strength enhancement in beams may differ from columns. In fact, the flexural strength of beams is relatively insensitive to concrete compressive strength. Therefore, strength enhancement in plastic behaviour is mainly due to strain hardening of the reinforcement steel. For normal steel classes (400 to 600 MPa), the overstrength factor is typically 25% of order of magnitude (Paulay and Priestley, 1992). For columns however, confinement and the favourable effect of axial loading may increase flexural strength up to 50% (Bachman, 1994).

It should be noted that significant engineering judgement and experience is required in the evaluation of the overstrength factors. For instance, shear modes of failure in columns and joints must be strictly avoided, and therefore it may be that the designer requires higher overstrength factors to define shear strength in those structural elements.

Finally, it is noteworthy that the economic advantages of plastic design are not compromised by the use of overstrength factors. There are of course further costs associated with appropriate detailing of the plastic hinges, and with over-design of the remaining part of the structure. However, this is outweighed by the significant reduction in earthquake design forces due to large ductility capacity.

3. The rigid-plastic seismic design method

3.1 General assumptions of the RPSD method

3.1.1 Rigid-plastic structures

The main idea of the RPSD method is to assume that the dynamic response is in no way influenced by the elastic properties of the structure. Therefore, we deal with rigid-plastic structures.

In this type of structure, one has rigid-plastic behaviour in the plastic hinges and rigid behaviour in the remaining part of the structure. Consequently, if rigid-plastic structures are designed to develop a chosen collapse mechanism, they are treated as assemblages of rigid bodies where the only source of internal displacements is due to deformations at the plastic hinges.

3.1.1.1 Plastic hinges

The assumption regarding rigid-plastic behaviour at the plastic hinges is worthy of closer examination.

The discussion in Section 2 showed that the cyclic behaviour of reinforced concrete members in flexure is dominated by the so-called pinching effect, which is mainly due to crack closing and the Baushinger effect. Pinching mainly affects the capacity of yield zones to dissipate energy. As this effect increases, energy dissipation capacity decreases, and thus seismic performance becomes poorer. However, provided that some rules are observed, high levels of ductility can be achieved throughout the period of seismic loading, as is the case of Figure 3.1.

Based on these types of observations, and for engineering purposes, when considering rigid-plastic relationships, it follows that a great deal of simplicity may be introduced in the treatment of the hysteretic behaviour of flexural plastic hinges subjected to large ductility demand.

Figure 3.2 depicts the rigid-plastic hysteretic relationships in terms of strength demand *vs.* deformation, F *vs.* δ, assumed herein for the plastic hinges.

In Figure 3.2a), the classic rigid-plastic relationship (Nielsen, 1998) is shown. As may be seen, no change of deformation occurs at all for strength demand within the yield strength limits $-f_P$ or f_P. The hinge is therefore said to display *rigid behaviour*. When the strength demand in one direction is the yield strength, deformations take place. This corresponds to *plastic behaviour*.

In Figure 3.2b), a modified rigid-plastic hysteretic relationship is introduced. It is clear that the same conditions as in the classic case apply. However, we can further assume that when the sign of the strength demand changes, the residual deformation at the end of the previous period of plastic behaviour is “lost” without any resistance from the plastic hinge. In the following, this type of behaviour will be referred to as *slip behaviour*.

The additional assumption of slip behaviour primarily affects the ability of the system to dissipate energy. Comparing both models in Figure 3.2, it is evident that the model contemplating slip behaviour has less capacity to dissipate energy induced by the

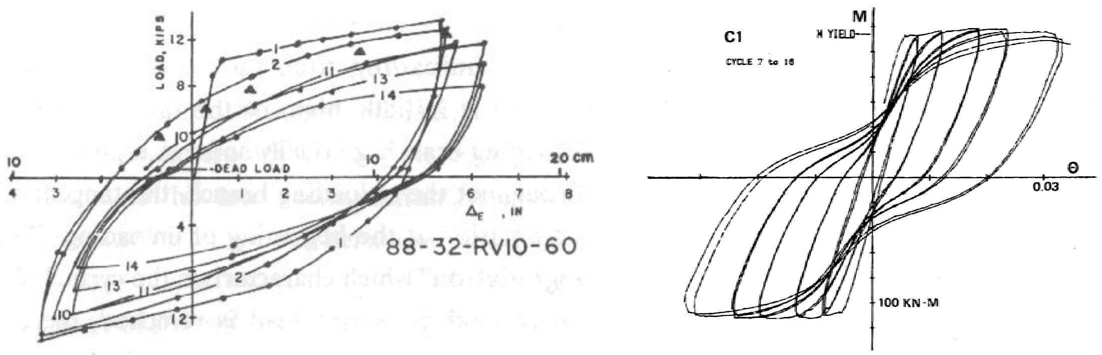

a) **b)**

Figure 3.1 -Members with symmetric cross-section and reinforcement under cyclic loading: a) Beam (Brown and Jirsa 1971) (1 kip=4.45kN;1 in.=2.54 cm), cf. section 2.2.1.1; b) Column with moderate axial force (Abrams, 1987), cf. section 2.2.1.3

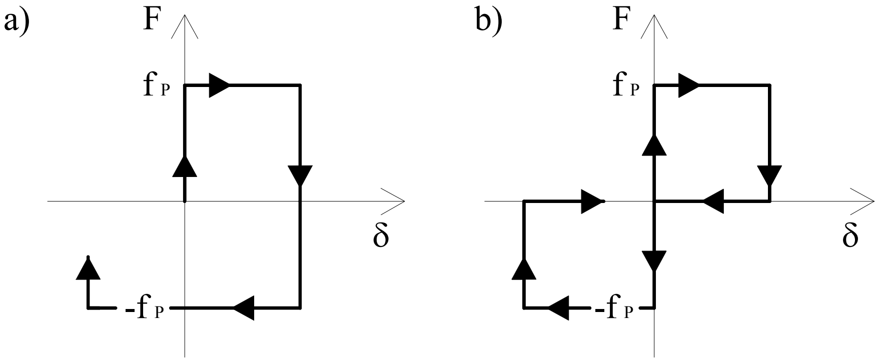

Figure 3.2 - a) Classic rigid-plastic relationship and b) Modified rigid-plastic relationship with consideration of pinching

ground motion. As we are dealing with reinforced concrete structures, this seems to be the most adequate rigid-plastic model to take into account the behaviour of most of the yield zones in a structural system.

In this work we conservatively assume that all the hinges in reinforced concrete structures will have this type of behaviour, even those with larger energy dissipation capacity, such as hinges in beams, the hysteretic behaviour of which could also be approximated by the classic rigid-plastic model in Figure 3.2a).

It should be noted that despite the differences in terms of hysteretic behaviour between the idealisations shown in Figure 3.2, to define both curves we need only to determine the strength limits. This makes the rigid-plastic models for hysteretic behaviour the simplest choice.

The magnitude of plastic deformations in the rigid-plastic models is alone related to the strength capacity. This seems to be an adequate assumption on the treatment of structural systems expected to develop significant levels of ductility under strong ground motion.

Figure 3.3 represents part of the lateral strength *vs.* deformation relationship of an elastoplastic oscillator under ground motion. Here, F is in force units and d in

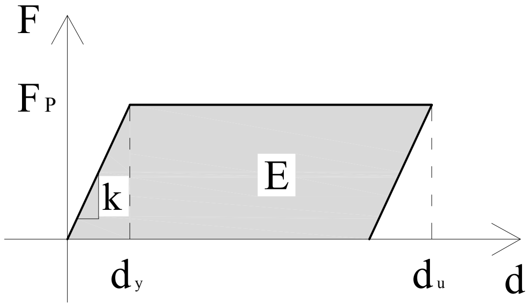

Figure 3.3 -Part of a hysteretic loop for an elastoplastic oscillator under ground motion

displacements units. It is assumed that significant levels of ductility, μ, may develop. In Figure 3.3, k is the stiffness of the system and d_y and d_u are the yield displacement and the displacement demand respectively. Viscous damping is disregarded here.

The energy inputted in this system due to ground motion is mostly dissipated by the onset of plastic behaviour and therefore close to the area E in Figure 3.3. Clearly, the greater the energy input, the greater the ultimate deformation, d_u, as F_P and d_y are exclusive properties of the system. The energy dissipated in the system is given by:

$$\begin{cases} E = F_P \cdot (d_u - d_y) \\ d_y = \dfrac{F_P}{k} \\ d_u = \mu \cdot d_y \end{cases} \Leftrightarrow E = \frac{F_P^2}{k} \cdot (\mu - 1) \tag{3.1}$$

From the discussion above and attending to the result in (3.1), it seems that the magnitude of plastic deformations imposed by the ground motion in elastoplastic systems able to develop significant levels of ductility is highly dependent on the lateral strength capacity of the system. In rigid-plastic systems, this dependency is exclusive to the lateral strength capacity. Therefore, the accuracy of the rigid-plastic models increases with the expected ductility.

3.1.1.2 Global behaviour as a function of local behaviour

Finally, it is important to mention that in rigid-plastic structures, as long as the mode of failure and of external loading are known, the displacement and force fields are solely related to the behaviour at the plastic hinges. This is a very important characteristic of rigid-plastic structures in the formulation of the RPSD method, and therefore deserves special attention.

Consider the case of the rigid-plastic SDOF systems in Figure 3.4. In the following, we refer to rigid-plastic SDOF systems as rigid-plastic oscillators. Figure 3.4a) represents a rolling mass connected to a wall on the side by a rigid-plastic spring that can only resist axial deformations. Its hysteretic behaviour is expressed in terms of axial force *vs.* displacements, i.e. N *vs.* d, and it is assumed to be of the classic type. N_P is the ultimate axial force. Figure 3.4b) depicts a rigid column supporting a mass and having a flexural hinge at the base. The latter is assumed to be concentrated in a single cross-section and to have a bending moment *vs.* rotation relationship, M *vs.* θ, of the rigid-plastic type including pinching. M_P is the flexural capacity of the plastic

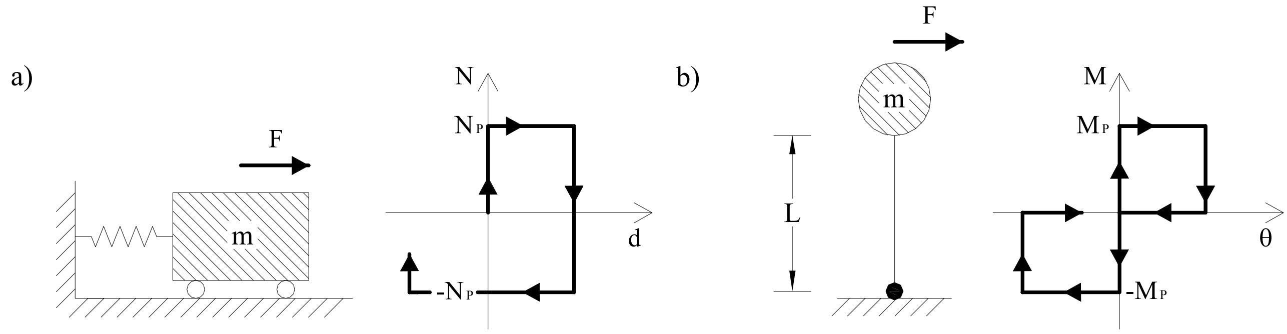

Figure 3.4 -Rigid-plastic oscillators

hinge in both directions. Both masses are subjected to a force F and may only move horizontally.

In both oscillators it is clear that the relative displacement of the mass, d_{mass} is given by the deformation at the yield zones since it is only there that internal deformations take place: In Figure 3.4a), the displacement of the rolling mass is the same as the spring connecting it to the wall, and in Figure 3.4b) one has $d_{mass}=-\theta \cdot L$, with θ being the rotation of the plastic hinge.

In addition, it is clear that equilibrium implies the external force F be written as a function of the strength demand at the plastic hinges: for the case of the rolling mass oscillator, we have F=N and for the column oscillator, F=-M/L. The maximum admissible values of F are $F=N_P$ and $F=M_P/L$. Therefore it is evident that in any rigid-plastic oscillator, the relationship of external force *vs.* displacement is of the same type as the corresponding plastic hinge.

Similar features are observed in rigid-plastic MDOF systems. Henceforth, rigid-plastic MDOF systems are simply referred as rigid-plastic structures.

Consider the 4-story plane rigid-plastic frame, as in Figure 3.5. Assume further that the structure is designed such that the mechanism shown on the right-hand side of the figure takes place when subjected to the set of external forces, $F \cdot \lambda_i$. Here the plastic hinges are of the flexural type and concentrated in the cross-sections at the ends of the beams and at the base of the columns. Their constitutive relationships are of the same type as in Figure 3.2b). The magnitude and orientation of the external forces are exclusively dependent on the load parameter F.

The displacement field in the structure has only one degree of freedom since only one mode of vibration is allowed, i.e. that associated with the collapse mechanism. Therefore, the relative displacement d_i, in any arbitrary floor i of this structure may be written as a function of the plastic rotations in the hinges, θ.

$$d_i = \theta \cdot h_i \tag{3.2}$$

Furthermore, as for the cases of rigid-plastic oscillators, the relationship of external forces *vs.* displacements is of the same type as for the plastic hinges. This may be proven by considering equilibrium in any rigid-plastic structure.

For the frame in Figure 3.5, equilibrium may be expressed by writing the virtual work equation for virtual displacement δθ:

$$-\sum_{j=1}^{10} \left| M_j \right| \cdot \delta\theta + F \cdot \sum_{i=1}^{4} \lambda_i \cdot h_i \cdot \delta\theta = 0 \tag{3.3}$$

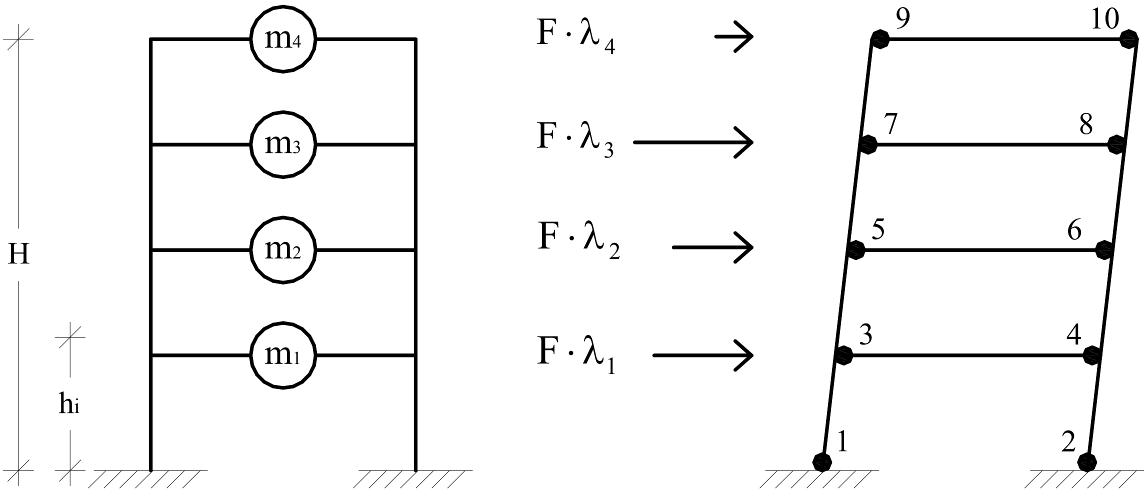

Figure 3.5 – 4 story rigid-plastic frame and corresponding collapse mechanism

where M_j is the bending moment at the j-th plastic hinge. Cancelling $\delta\theta$ yields:

$$F = \frac{\sum_{j=1}^{10} |M_j|}{\sum_{i=1}^{4} \lambda_i \cdot h_i} \tag{3.4}$$

from which it may be concluded that the value of the load parameter F is specified by the bending moment field at the plastic hinges.

Figure 3.6 depicts the relationship between external forces and displacements for the rigid-plastic frame in Figure 3.5. The curve is given in terms of the load parameter F and the displacement of the top floor.

Consider that the loads $F \cdot \lambda_i$ are applied slowly on the structure. As soon as F reaches a certain magnitude, all the plastic hinges undergo plastic behaviour – zone A. It is said then that the frame exhibits *plastic behaviour*. From (3.4) it follows that F at the onset of plastic behaviour is

$$F = \frac{\sum_{j=1}^{10} |M_{P,j}|}{\sum_{i=1}^{4} \lambda_i \cdot h_i} \tag{3.5}$$

where $M_{P,j}$ is the flexural capacity at hinge j. Here, for the sake of simplicity, we assume that the sum $M_{P,j}$ is the same regardless of orientation of the collapse mechanism.

As soon as F decreases, the strength demand on the plastic hinges is relieved, which means that they begin to exhibit rigid behaviour – zone B. Obviously at this stage, no internal deformations occur, and therefore there are no relative displacements. Therefore the frame has *rigid behaviour*.

When F changes sign, all the plastic hinges display slip behaviour, as the entire residual deformations are recovered without any resistance. The structure is not able to resist any lateral forces until it returns to its original position – zone C. At this point it is said that the structure has *slip behaviour*.

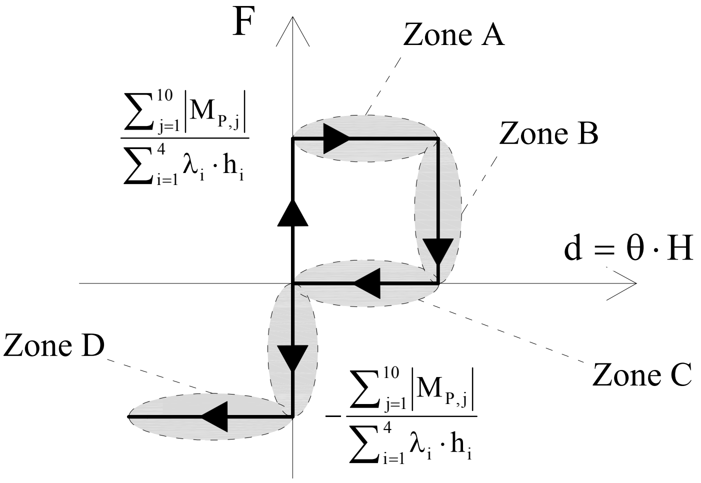
F
Zone A
Zone B
Zone C
Zone D
$\frac{\sum_{j=1}^{10}|M_{P,j}|}{\sum_{i=1}^{4}\lambda_i \cdot h_i}$
$-\frac{\sum_{j=1}^{10}|M_{P,j}|}{\sum_{i=1}^{4}\lambda_i \cdot h_i}$
$d = \theta \cdot H$

Figure 3.6 –External forces vs. displacements of the rigid-plastic 4-story frame in Figure 3.5

If F reaches the symmetric value as expressed in (3.5), all the plastic hinges undergo plastic behaviour again, albeit in the opposite direction. The structure starts to move to the left-hand side of the figure – zone D.

The properties of the rigid-plastic structures discussed here will be of extreme usefulness for the treatment of the dynamic response, as will be seen in the following chapters. As the reader may already understand, the main advantage of the rigid-plastic approach is the fact that structures with more than one degree of freedom may easily be treated as SDOF systems.

3.1.2 Disregard for viscous damping

Another important assumption of the RPSD method is that of neglecting the contribution of viscous damping for the dynamic response of structures. The primary reason for this is that the method applies to systems developing significant levels of ductility under strong ground motion. For this type of system, it is clear that the majority of the energy from the ground motion is dissipated at the plastic hinge regions by the onset of plastic behaviour.

Secondly, it is seen that viscous damping does not represent actual behaviour of reinforced concrete structures submitted to dynamic loading (Paulay and Priestley, 1992). The use of viscous damping in the treatment of the dynamic response of reinforced concrete systems is a matter of mathematical convenience rather than structural accuracy. Unfortunately, our knowledge regarding the physical nature of damping phenomena is still at a very primitive level.

Consider the case of an elastic system subjected to a sinusoidal displacement history, d(t), as in the following:

$$d(t) = d_{max} \cdot \sin(\omega \cdot t) \tag{3.6}$$

Here, d_{max} is the displacement amplitude and ω is the circular frequency of vibration.

The damping force, f_D, has the following expression. See section 1.2.1.1:

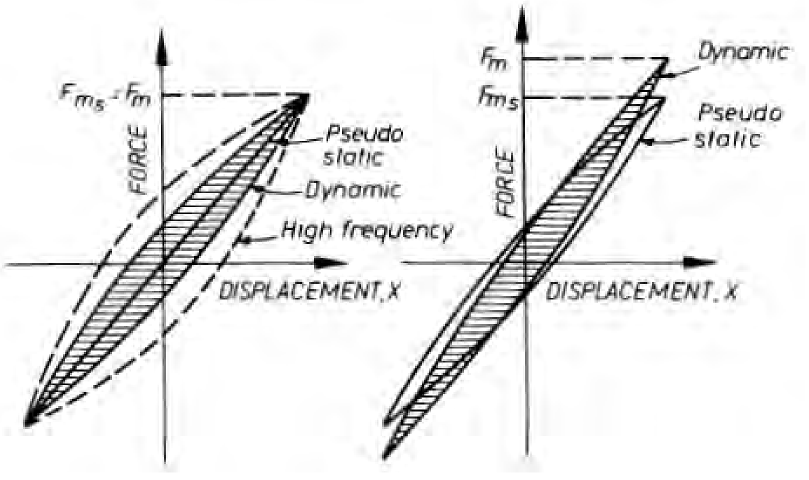

a) **b)**

Figure 3.7 - a) Viscous damping of a linear elastic system and b) Elastic behaviour of a concrete element (Paulay and Priestley, 1992)

$$\begin{aligned} & f_D = c \cdot v(t) \quad \Leftrightarrow \\ \Leftrightarrow \; & f_D = \omega \cdot c \cdot d_{max} \cdot \cos(\omega \cdot t) \end{aligned} \tag{3.7}$$

where it follows that the maximum damping force, $f_{D,max}$ is:

$$f_{D,max} = \omega \cdot c \cdot d_{max} \tag{3.8}$$

When examining expression (3.8), it is clear that the maximum damping force in an elastic system increases with the frequency of vibration: If the displacements are applied very slowly, (ω→0), the damping forces are effectively zero and so the resisting force *vs*. displacement relationship is given by a straight line (the pseudostatic line in Figure 3.7a), as it is solely due to elastic restitution forces. On the other hand, for high frequency motion, damping forces increase, as does the width of the hysteretic loop. Nevertheless, the maximum resisting force, F_m in Figure 3.7a) remains the same regardless of the frequency of vibration, as for maximum displacement the velocity is always zero.

Figure 3.7b) is a sketch of the typical behaviour of reinforced concrete systems. It is found that the width of the hysteretic loop is higher for the pseudostatic application of displacements than for the dynamic case, which is in direct contradiction to the predictions yielded by the elastic approach. Also, the peak resistance changes with the frequency of the applied displacement history.

Further assumptions for ductile frames

As previously mentioned, despite the RPSD method being quite general, special emphasis is devoted to the case of regular reinforced concrete ductile frames in this work. Therefore, we can make standard assumptions (Paulay and Priestley, 1992):

1. The in-plane stiffness of the floor system is infinitely large, which is a reasonable assumption for frame systems with normal length to width ratios.
2. The analysis of the frame system is subdivided into a series of plane frames, which are analysed separately

3. The mass at each floor is lumped at its centre of mass
4. The lateral resistance is the same for both horizontal directions. This is the case for the overwhelming majority of design problems in Earthquake Engineering, since the direction of maximum demand due to ground motion is unknown.

It should be noted that assumptions 1 and 2 must be observed in order for the RPSD method to be applied, as it only deals with dynamic response in one direction. Consideration of simultaneous earthquake loading even for the two horizontal directions would compromise the simplicity of the RPSD method, as this requires an extra dynamic parameter in the analysis, i.e. the angle of the horizontal plane of the structural displacement shape vector. Therefore the validity of assumptions 1 and 2 must be checked in advance, thus for irregular structures, or structures whose plane dimensions are such that assumption 1 is invalid, other methods such as refined NLTHA should be employed.

On the other hand, as explained below, the RPSD method does not require assumptions 3 and 4 to be satisfied. They are only considered in this work to avoid superfluous complexity of the explanations, and because they do not compromise the accuracy of the results provided.

3.2 Rigid-plastic dynamics

3.2.1 Rigid-plastic oscillators

3.2.1.1 Formulation of the equation of motion

In Chapter 1, the formulation of the equation of motion of the SDOF systems under ground motion at any time t was presented:

$$m \cdot a_r(t) - R(t) = -m \cdot a_g(t) \tag{3.9}$$

or in a more convenient form:

$$a_r(t) = \frac{R(t)}{m} - a_g(t) \tag{3.10}$$

In classic Structural Dynamics, R(t) accounts for viscous damping forces and internal forces opposing lateral motion of the mass, thus according to the notation in section 1.2.1.1 $R(t)=-c \cdot v_r(t)-k \cdot d_r(t)$. However, in this work we only deal with rigid-plastic structural systems in which the only source of energy dissipation occurs due to plastic deformations at the yield zones. Therefore for the case of rigid-plastic oscillators, R(t) is simply formulated on the basis of the internal force mechanism that opposes lateral motion of the mass. The latter, as seen in chapter 3.1.1.2, is specified by the behaviour at the yield zone. Therefore, the task of writing the equations of motion of rigid-plastic oscillators simply comprises of identifying the resisting force mechanism and its association with the dynamic state of the system.

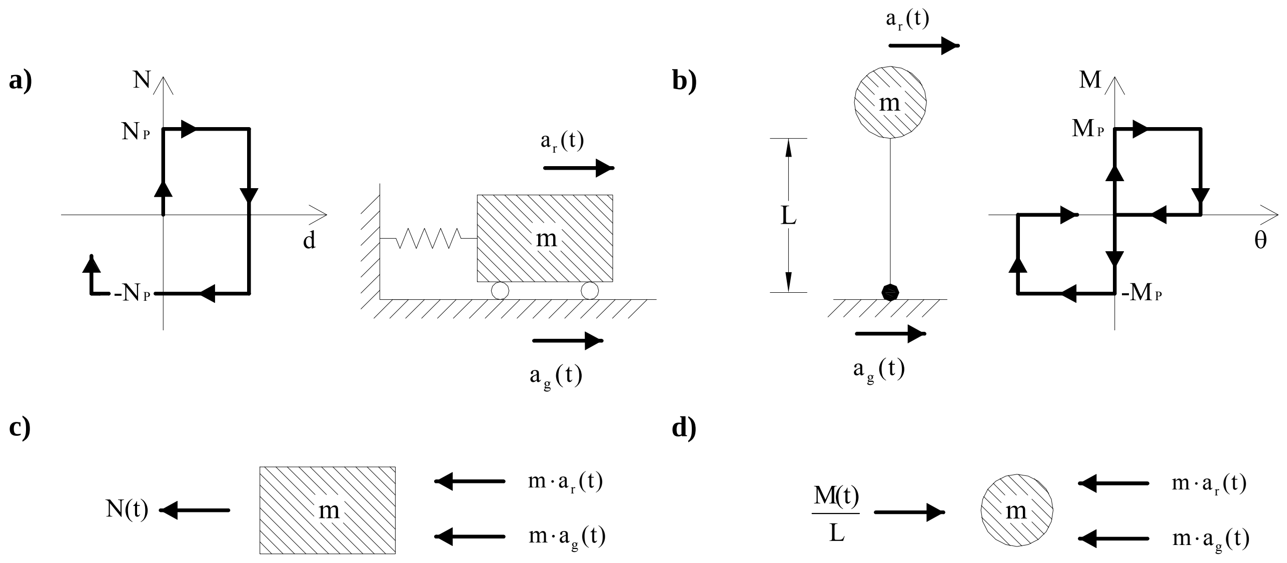

Figure 3.8 -Rigid-plastic oscillators subjected to positive ground motion and the corresponding free-body diagrams at the masses when their motion is with positive relative acceleration

For illustrative purposes, consider again the case of the rigid-plastic oscillators of section 3.1.1.2 reproduced again in Figure 3.8a) and b). Assume that these are subjected to a positive ground acceleration and that their masses are moving with positive relative acceleration. Assume further that the rigid-plastic spring on the rolling mass oscillator is in tension, and that the bending moment in the plastic hinge of the column oscillator is positive.

To express dynamic equilibrium, d'Alembert's principle is used. This is easily carried out attending to the free-body-diagram of the mass in each system, Figure 3.8c) and d).

Thus one reaches the following expressions for each of the rigid-plastic oscillators in Figure 3.8.

Rolling mass oscillator	Column oscillator
$a_r(t) = -\dfrac{N(t)}{m} - a_g(t) \qquad (3.11)$	$a_r(t) = \dfrac{M(t)}{m \cdot L} - a_g(t) \qquad (3.12)$

Here, N(t) is the axial force on the rigid-plastic spring at the time t, and M(t) is the bending moment at the plastic hinge at time t.

Observing the expressions in (3.11) and (3.12), it appears that the dynamic response of rigid-plastic oscillators submitted to base motion is only determined by the internal force mechanism able to resist lateral deformations, which in turn is exclusively dependent on the plastic hinges.

To complete the formulation of the equations of motion, one only has to associate the dynamic state of the system with the behaviour at the plastic hinges. This is carried out attending to the relative velocity of the mass and the strength demand at the yield zone for each time instant t, referred to in general terms as f(t). For the oscillators considered here, f(t)=N(t) in the rolling mass oscillator and f(t)=M(t) for the column oscillator.

It is clear that when f(t) lies between the yield strength limits, no relative deformations will occur. It is said that the system has *rigid behaviour*. Therefore, the following conditions apply:

Rolling mass oscillator	Column oscillator
$\text{if } N(t)\in\,]\text{-}N_P,N_P[\;\Rightarrow\begin{cases}a_r(t)=0\\ v_r(t)=0\\ d_r(t)=\text{constant}\end{cases}$ (3.13)	$\text{if } M_P\in\,]\text{-}M_P,M_P[\;\Rightarrow\begin{cases}a_r(t)=0\\ v_r(t)=0\\ d_r(t)=\text{constant}\end{cases}$ (3.14)

When the strength capacity at the plastic hinges is exhausted in one direction, it is said that the system has *plastic behaviour*. The energy from the earthquake is dissipated by plastic deformations at the yield zone of the system. When this energy is fully dissipated, the system again reverts to rigid behaviour. Therefore the condition determining whether the energy has been fully dissipated or not has to be included. This is simply carried out by attending to the velocity of the mass. In basic terms, the strength demand at the plastic hinge determines the onset of plastic behaviour, but it is the dynamic state of the system, specified by the relative velocity of the mass, that controls the end of it.

Rolling mass oscillator	Column oscillator
$\text{if}\begin{cases}N(t)=N_P\\ v_r(t)>0\end{cases}\Rightarrow a_r(t)=-\frac{N_P}{m}-a_g(t)$ or (3.15) $\text{if}\begin{cases}N(t)=\text{-}N_P\\ v_r(t)<0\end{cases}\Rightarrow a_r(t)=\frac{N_P}{m}-a_g(t)$	$\text{if}\begin{cases}M(t)=-M_P\\ v_r(t)>0\end{cases}\Rightarrow a_r(t)=-\frac{M_P}{m\cdot L}-a_g(t)$ or (3.16) $\text{if}\begin{cases}M(t)=M_P\\ v_r(t)<0\end{cases}\Rightarrow a_r(t)=\frac{M_P}{m\cdot L}-a_g(t)$

It should be noted that according to the sign convention adopted in this work, when the column oscillator has plastic behaviour, the sign of the relative velocity of the mass is always opposite to the sign of the rotations at the plastic hinge.

Finally, with regard only for the column oscillator, there is the case of *slip behaviour*, since this is contemplated in the hysteretic relationship of the plastic hinge. Here, one must also take into account the velocity of the mass as, if this is annulated, it would mean that the residual deformation in the system was not fully recovered. Under these circumstances, the system once again experiences rigid behaviour. The additional condition corresponding to *slip behaviour* is:

Column oscillator
$\text{if}\begin{cases}M(t)=0\\ v_r(t)\cdot d_r(t)<0\end{cases}\Rightarrow a_r(t)=-a_g(t)$ (3.17)

As previously pointed out in section 3.1.1.1, when the plastic hinge has slip behaviour, no resistance can be developed there. For the dynamic response of the system, this is translated in a period of zero lateral resistance against ground motion. Therefore, the dynamic response of the system is symmetrical to the ground motion.

It should be noted that when the residual deformation is recovered, it is highly unlikely that the relative velocity of the mass is zero. In other words, at the end of a period of slip behaviour in which the residual deformations have been fully recovered, the system has most likely accumulated kinetic energy that has to be dissipated. The only source of energy dissipation in rigid-plastic oscillators is due to plastic deformations in the yield zone. Therefore after a period of slip behaviour, there is an immediate transition to plastic behaviour. The relative velocity of the mass at the beginning of the new period of plastic behaviour is the velocity at the end of the previous period of slip behaviour.

From the discussion above, it appears that, in order to determine the dynamic response of a rigid-plastic oscillator, one must simply know the lateral capacity of the system against horizontal forces, here with the symbol F_y. If F_y is known, writing the equations of motion is an automatic process. In fact, the only time this parameter appears in the equations of motion is during periods of plastic behaviour. Here, the sign of F_y is opposite to the relative velocity of the mass, which physically means that the force mechanism against horizontal forces always resists rate of changes in the position of the mass.

For the rolling mass oscillator, it is clear the $F_y=N_P$,while for the column oscillator, $F_y=M_P/L$.

However, to fully assess the dynamic response of a rigid-plastic oscillator, one has to establish the conditions concerning the strength demand at the plastic hinges.

Consider that the previous rigid-plastic oscillators have rigid behaviour for the time t, i.e. $a_r(t)=0$. Observing equations (3.11) and (3.12), one finds that for periods of rigid behaviour, $N(t)=m\cdot a_g(t)$ for the rolling mass oscillator and $M(t)= m\cdot a_g(t)\cdot L$ for the column oscillator. Thus, the strength capacity at the plastic hinge is exhausted for values $a_g(t)=\pm N_P/m$ or $a_g(t)=\pm M_P/m\cdot L$, respectively.

Introducing F_y, one may generalise with regard to the previous statements and define the ground acceleration at the onset of plastic behaviour, a_y:

$$a_y = \frac{F_y}{m} \tag{3.18}$$

Thus:

- If the rigid-plastic oscillator starts from rest, which in general is the case for most of the problems in Earthquake Engineering, then plastic behaviour will take place as soon as the ground acceleration exceeds a_y in one of the directions.
- If the system has rigid behaviour and $|a_g(t)|<a_y$, then it remains with rigid behaviour.
- For the case of oscillators with hysteretic relationship accounting for the effect of pinching, it is clear that the change of sign on the strength demand at the plastic hinges takes place when $a_g(t)=0$.

In consequence, the equations of motion according to the type of behaviour at the plastic hinge in any rigid-plastic oscillator may be given in the general form as in (3.19).

Note that one could use a_y directly in the equations of motion. However, as will be seen, it is convenient to retain the format in (3.19), as it explicitly considers the strength capacity of the system against horizontal forces.

$$\begin{array}{ll}
\text{Plastic behaviour:} & \begin{cases} a_r(t) = -\dfrac{F_y}{m} - a_g(t) & \text{if} \quad |f(t)| = f_P \quad \text{and} \quad v_r(t) \geq 0 \\ a_r(t) = +\dfrac{F_y}{m} - a_g(t) & \text{if} \quad |f(t)| = f_P \quad \text{and} \quad v_r(t) \leq 0 \end{cases} \\
\text{Slip behaviour:} & a_r(t) = -a_g(t) \quad \text{if} \quad f(t) = 0 \quad \text{and} \quad v_r(t) \cdot d_r(t) < 0 \\
\text{Rigid behaviour:} & a_r(t) = 0 \quad \text{if} \quad |a_g(t)| < \dfrac{F_y}{m}
\end{array} \tag{3.19}$$

3.2.1.2 Computational procedure to perform rigid-plastic non-linear time-history analysis.

In the following, a step-by-step integration procedure for the computation of the dynamic response of a rigid-plastic oscillator subjected to any type of base motion is presented. The response is evaluated at each successive time interval i with length Δt being sufficiently small to justify that $a_g(t)$ is assumed constant and equal to the average, $a_{g,i}$, between the value at the beginning and end of that time interval, $a_g(t_i)$ and $a_g(t_i+\Delta t)$, respectively. Thus:

$$a_g(t) = a_{g,i} = \frac{a_g(t_i) + a_g(t_i + \Delta t)}{2} \qquad \text{for} \qquad t \in \left] \, t_i ; t_i + \Delta t \right] \tag{3.20}$$

Classic rigid-plastic oscillators

Table 3.1 summarises the conditions to be considered when computing the dynamic response of oscillators with plastic hinges of the type sketched in Figure 3.2a). The equations presented allow the assessment of the dynamic state of the system for any time t in any time step i.

Table 3.1 - Procedure to derive the dynamic response of rigid-plastic oscillators against any ground motion

Condition	End of time step i-1	Time step i	Time step i+1
1	Rigid behaviour	If $\lvert a_{g,i} \rvert < a_y$, then $\begin{cases} a_r(t) = 0 \\ v_r(t) = 0 \\ d_r(t) = d_{r,i-1} \end{cases}$	Rigid behaviour (apply 1,2 or 3)
2	Rigid behaviour	If $a_{g,i} \geq a_y$ then $\begin{cases} a_r(t) = +\dfrac{F_y}{m} - a_{g,i} \\ v_r(t) = \left(+\dfrac{F_y}{m} - a_{g,i} \right) \cdot (t - t_i) \\ d_r(t) = \left(+\dfrac{F_y}{m} - a_{g,i} \right) \cdot \dfrac{(t-t_i)^2}{2} + d_{r,i-1} \end{cases}$	Plastic Behaviour (apply 4 or 5)

Table 3.1 - Procedure to derive the dynamic response of rigid-plastic oscillators against any ground motion (cont.)

Condition	End of time step i-1	Time step i	Time step i+1
3	Rigid behaviour	If $a_{g,i} \leq -a_y$ then $\begin{cases} a_r(t) = -\frac{F_y}{m} - a_{g,i} \\ v_r(t) = \left(-\frac{F_y}{m} - a_{g,i}\right) \cdot \left(t - t_i\right) \\ d_r(t) = \left(-\frac{F_y}{m} - a_{g,i}\right) \cdot \frac{\left(t - t_i\right)^2}{2} + d_{r,i-1} \end{cases}$	Plastic behaviour (apply 4 or 5)
4	Plastic behaviour	▪ If $v_r(t_i)>0$ and $v_r(t_i+\Delta t)>0$ then $\begin{cases} a_r(t) = -\frac{F_y}{m} - a_{g,i} \\ v_r(t) = \left(-\frac{F_y}{m} - a_{g,i}\right) \cdot \left(t - t_i\right) + v_{r,i-1} \\ d_r(t) = \left(-\frac{F_y}{m} - a_{g,i}\right) \cdot \frac{\left(t - t_i\right)^2}{2} + v_{r,i-1} \cdot \left(t - t_i\right) + d_{r,i-1} \end{cases}$ ▪ If $v_r(t_i)<0$ and $vr(t_i+\Delta t)<0$ then $\begin{cases} a_r(t) = +\frac{F_y}{m} - a_{g,i} \\ v_r(t) = \left(+\frac{F_y}{m} - a_{g,i}\right) \cdot \left(t - t_i\right) + v_{r,i-1} \\ d_r(t) = \left(+\frac{F_y}{m} - a_{g,i}\right) \cdot \frac{\left(t - t_i\right)^2}{2} + v_{r,i-1} \cdot \left(t - t_i\right) + d_{r,i-1} \end{cases}$	Plastic behaviour (apply 4 or 5)
5	Plastic behaviour	If there is a time τ in the time step for which $v_r(\tau)=0$, then keep $d_r(\tau)$: ▪ If $v_r(t_i)>0$ then $d_r(\tau) = \left(-\frac{F_y}{m} - a_{g,i}\right) \cdot \frac{\left(\tau - t_i\right)^2}{2} + v_{r,i-1} \cdot \left(\tau - t_i\right) + d_{r,i-1}$ ▪ If $v_r(t_i)<0$ then $d_r(\tau) = \left(+\frac{F_y}{m} - a_{g,i}\right) \cdot \frac{\left(\tau - t_i\right)^2}{2} + v_{r,i-1} \cdot \left(\tau - t_i\right) + d_{r,i-1}$	Rigid Behaviour (apply 1,2 or 3)

The quantities $v_{r,i-1}$ and $d_{r,i-1}$ refer to the relative velocity and displacement of the mass at the end of time step i-1, respectively.

Rigid-plastic oscillators with consideration of pinching

The equations and conditions presented in Table 3.1 also apply to rigid-plastic oscillators where the yield zones have hysteretic behaviour, as in Figure 3.2b). Thus the computational procedure is the same as in the case of "classic" rigid-plastic oscillators but with additional conditions concerning slip behaviour. These are presented in Table 3.2.

Table 3.2 –Procedure to derive the dynamic response of rigid-plastic oscillators with pinching against any ground motion (extension to table 3.1)

Condition	Time step i-1	Time step i	Time step i+1
6	Rigid behaviour	If $a_{g,i-1} \cdot a_{g,i} < 0$ then $\begin{cases} a_r(t) = -a_{g,i} \\ v_r(t) = -a_{g,i} \cdot (t - t_i) \\ d_r(t) = -a_{g,i} \cdot \frac{(t-t_i)^2}{2} + d_{r,i-1} \end{cases}$	Slip behaviour (apply 7,8 or 9)
7	Slip behaviour	If $d_r(t_i+\Delta) \cdot v_r(t_i+\Delta) < 0$ then $\begin{cases} a_r(t) = -a_{g,i} \\ v_r(t) = -a_{g,i} \cdot (t - t_i) + v_{r,i-1} \\ d_r(t) = -a_{g,i} \cdot \frac{(t-t_i)^2}{2} + v_{r,i-1} \cdot (t - t_i) + d_{r,i-1} \end{cases}$	Slip behaviour (apply 7,8 or 9)
8	Slip behaviour	If there is a time τ in the time step for which $v_r(\tau)=0$, then keep $d_r(\tau)$: $d_r(\tau) = -a_{g,i} \cdot \frac{(\tau-t_i)^2}{2} + v_{r,i-1} \cdot (\tau - t_i) + d_{r,i-1}$	Rigid Behaviour (Apply 1,2 or 3)
9	Slip behaviour	If there is a time τ in the time step for which $d_r(\tau)=0$, then keep $v_r(\tau)$: $v_r(\tau) = -a_{g,i} \cdot (\tau - t_i) + v_{r,i-1}$	Plastic behaviour (Apply 4 or 5)

Conclusions

In this section it was shown that the rigid-plastic approach yields significant advantages over the standard methods to evaluate the dynamic response of oscillators under ground motion.

- The dynamic response is solely controlled by the behaviour at the plastic hinge, which not only simplifies the computational procedure but also enables the direct correlation between the displacements in the system and the deformation demand at the yield zone. The latter is crucial for the evaluation of the damage induced by the ground motion.
- It was seen that to perform NLTHA, the user must simply identify the force mechanism able to resist horizontal forces, which in rigid-plastic oscillators is solely dependent on the strength demand at the yield zones. Writing the equations of motion is thus a straightforward process using the equations in (3.19)
- The computational procedure shown here is far simpler than the traditional one. It is also always stable, as it is not dependent on the frequency of vibration of the oscillator.

3.2.2 Basic study on the dynamic response of rigid-plastic oscillators

The dynamic response of rigid-plastic oscillators under ground motion will be investigated below. The purposes of this study is to explain the trends in which their dynamic response develops and at the same time provide comparisons with oscillators having more sophisticated types of behaviour. Therefore, we use three simplified ground motions where the explanations are at simpler levels and where it is easier to identify the different phenomena controlling the dynamic response. The work presented here was carried out at the Nagoya Institute of Technology, Japan, in cooperation with the research group of Professor Toshikatsu Ichinose. Two papers were published about this study. The first, (Marubashi *et. al*, 2005) in Japanese, was published in the Transactions of the Architectural Institute of Japan and the second in the Proceedings of the 2006 U.S. National Earthquake Conference (Marubashi *et. al*, 2006).

3.2.2.1 Definition of the oscillators

The oscillator considered in this study is of the same type as presented in Figure 3.4b) It is a rigid column with length 3m that supports a mass of 1.0 ton. The latter may only move in the horizontal direction. At the base of the column there is a rigid-plastic hinge with M_P=6.0kNm. From the discussion held in the last section it is concluded that $F_y=M_P/L$=2.0kN, implying a_y=2.0m/s^2, i.e. the ground acceleration at the onset of plastic behaviour is 2.0m/s^2 assuming that the system will start from rest; Both cases of rigid-plastic behaviour at the plastic hinge, i.e. with and without consideration of pinching are considered. See Figure 3.2a) and b). For simplicity, in this section the later model is also referred as rigid-slip model.

For comparison purposes, we also consider the cases in which the hysteretic behaviour of the plastic hinge is described by the elastic-perfectly-plastic model, as shown in Figure 3.3, and by the Takeda stiffness degradation model in Figure 2.30. The same magnitude, M_P, is assigned for the bending capacity in both directions. In previous models, damping is disregarded. Additionally, with the purpose of illustrating the influence of elastic stiffness on the dynamical response, two levels of fundamental period are regarded:

- Short Period (SP), T = 0.2 s and
- Long Period (LP), T = 0.6 s.

3.2.2.2 Ground motions

Two simplified periodic ground motions are considered. Their representation is depicted in Figure 3.9 in terms of time-histories for the ground accelerations, a_g, velocities, v_g, and displacements, d_g. Both are derived so that the peak ground velocity is 0.6m/s, the period, T_g, is 0.8s and the ground velocities and displacements at the end of the ground motion are 0. The shape of this ground motion is determined by the ratio between the time lengths a and b, as shown in the curves of Figure 3.9 concerning ground velocities. For the first one, denominated *Symmetric*, this ratio is 1, yielding symmetric values for the ground acceleration. For the second, *Asymmetric*, it is assumed that a/b=3, leading to different values for the ground acceleration in each direction.

Also, the response of the oscillators subjected to part of a real accelerogram is included in this study. One considers the JMA NS record of the Kobe Earthquake, 1995 between t=7.2s and t=8.8s. This ground motion is also represented in the same format as for the simplified ground motions and is superimposed in the figures concerning the Asymmetric ground motion.

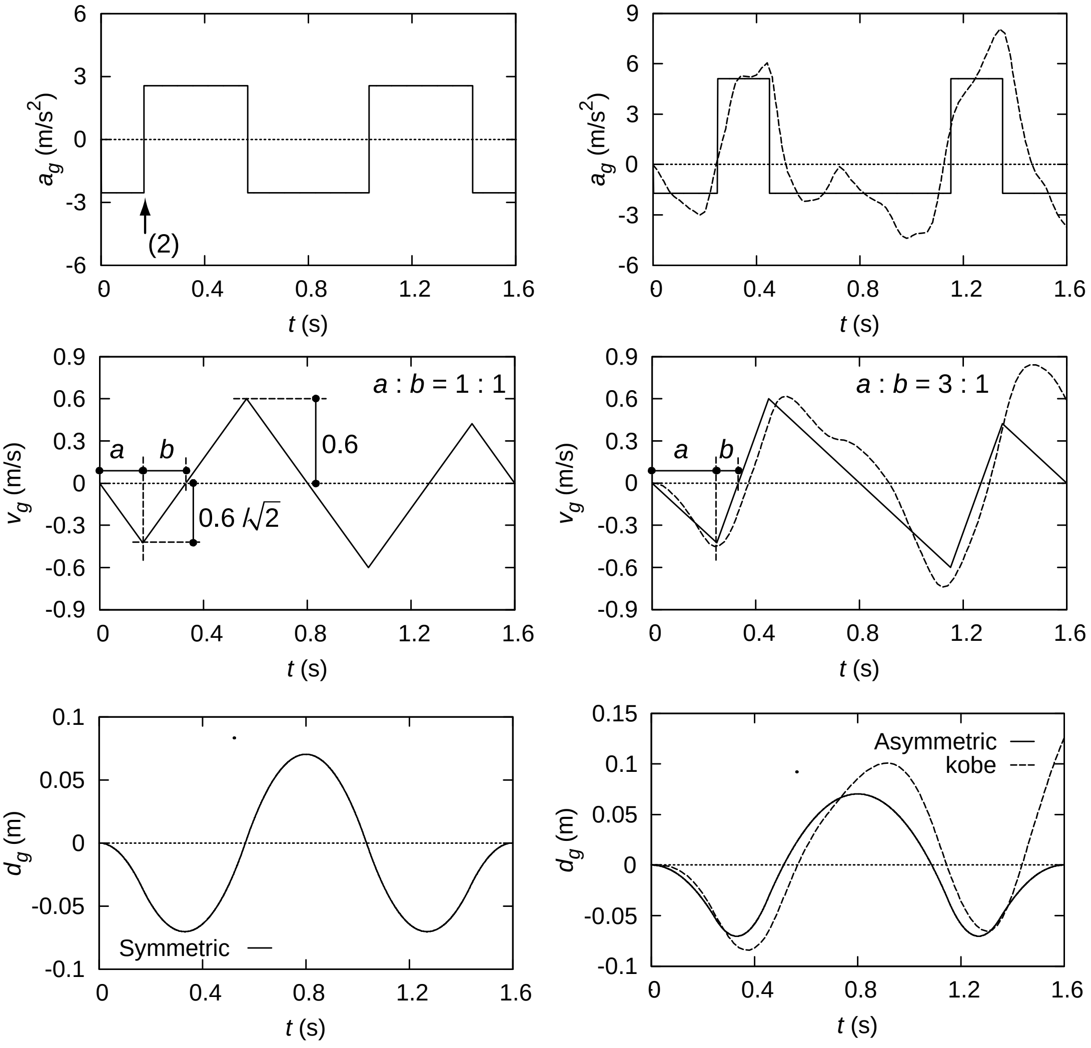

Figure 3.9 –Time-history curves for the input ground motion

3.2.2.3 Dynamical response of the rigid-plastic and elastoplastic models

Symmetric Accelerogram

Figure 3.11 shows the time-history curves that describe the dynamical response of the rigid-plastic and elastoplastic models to the Symmetric accelerogram for the time interval $t \in [0;1.6]$.

From the time-history curves concerning the displacements of the mass, Figure 3.11d), it may be observed that the three models present an “oscillatory” type of response around the time axis, i.e. a dynamical response with reversal of motion. However, for both levels of fundamental period, the elastoplastic model provides time-history curves of wider amplitudes than that corresponding to the rigid-plastic model. The detail of the time-history curves shown in Figure 3.10, comparing the response of the rigid-plastic model and elastoplastic model with short fundamental period, may help explain these observations:

- For the rigid-plastic model, the capacity at the plastic hinge is exceeded instantaneously from the onset of the actuation of the ground motion. The relative acceleration of the mass at t=0.0s is $a_r(0)=-2.0/1.0-(-2.56)=0.56$ m/s^2 (see the first equation in (3.19)), and remains constant during the initial period at which the ground acceleration is -2.56 m/s^2 (the solid line in Figure 3.10b)).On the other hand, when the elastoplastic model starts from rest, the bending moment at the plastic hinge is 0 as there are no relative displacements of the mass d_r, thus there are no rotations in the plastic hinge. Therefore, dynamical equilibrium implies that $a_r(0)=-a_g(0)=2.56$ m/s^2. As the mass begins to move, the bending moment at the plastic hinge increases until its capacity is exhausted (the broken line in Figure 3.10a)). This leads to a smooth decrease in the relative acceleration in the elastoplastic model shown in Figure 3.10b) between the points (0) and (1). Until this point, the latter is always larger in the case of the elastoplastic model. This is reflected in the time-history curve of relative velocity of the mass, v_r, (Figure 3.10c)), which has a higher slope for the same period compared with the constant slope of the rigid-plastic model. When the capacity at the plastic hinge is exhausted, the relative acceleration remains constant and equal to that of the rigid-plastic model, until there is a reversal in the direction of the ground motion, point (2) in Figure 3.10b), leading to parallel slopes between the two models for the time-history curves concerning the relative velocity, see Figure 3.10c).
- When there is a reversal in the ground motion (shortly before t=0.2s), both models still have plastic behaviour, and the relative velocity is still greater than zero. As they have the same capacity, the relative acceleration is the same: $a_r=-2.0/1.0-2.56=-4.56$ m/s^2 (we still apply the first equation in (3.19)). However, it should be noted that the peak relative velocity at this instant is, according to the explanation above, higher for the case of the elastoplastic model. This explains the “delay” of the latter regarding the time instant at which the kinetic energy is fully dissipated, i.e. $v_r=0$, the time interval between points (3) and (4) in Figure 3.10c).
- The dynamical response of both models has the same pattern as explained above, after the relative velocity is zero, point (3) for the rigid-plastic model and point (4) for the elastoplastic model in Figure 3.10c). In fact, for the case of the former, the ground acceleration at that time is sufficiently high to cause immediate exhaustion of the capacity of the plastic hinge in the opposite direction. In the latter model, for the sake of dynamic equilibrium when considering the elastic forces at the

spring, the unloading proceeds continuously along the elastic branch between points (4) and (5) in Figure 3.10e). This has the same implication as previously: a higher initial slope for the relative velocity in the elastoplastic model corresponding to the period of elastic behaviour. Obviously, when the capacity of the plastic hinge is reached, the elastoplastic model exhibits the same relative acceleration of the rigid-plastic model, yielding parallel slopes in the time-history curves for the relative velocity, see time instant $t \approx 0.24$s in Figure 3.10c).

The dynamical response of the three models develops in the same way for the rest of the period.

Therefore, it seems that the "oscillatory" pattern of the dynamical response of both models is connected with the ability of the Symmetric ground motion to induce deformations in both directions.

The wider amplitude of motion observed for the elastoplastic models is due to the fact that lateral capacity of the system against horizontal forces is quite high. Note that $a_y=2.0\text{m/s}^2$, i.e. the onset of plastic deformations only takes place for ground motions higher than 80% of the PGA. Thus the elastic behaviour in the elastoplastic systems will dominate the overall response. In fact, it was seen that the "smooth" transitions due to elastic behaviour between phases of plastic behaviour play an important role for the elastoplastic oscillators opposing the case of the rigid-plastic model, where these transitions take place instantaneously.[1]

Asymmetric accelerogram

The dynamical response of the elastoplastic and rigid-plastic models under the Asymmetric ground motion for the period $t \in [0;1.6]$ is depicted in terms of time-history curves in Figure 3.13 and a detail corresponding to the first 0.3s of the response is given in Figure 3.12.

The difference between the dynamic response for the Asymmetric ground motion compared with the Symmetric one is evident: for the latter the response is of the oscillatory type, whereas for the Asymmetric accelerogram the response takes place mainly in one direction, i.e. clearly asymmetric. The primary reason for this is that the ground acceleration is of the pulse type with a magnitude higher than a_y in one direction only. On the other hand the PGA of this record is much higher than the Symmetric accelerogram: $a_y/\text{PGA}=40\%$. This indicates that for this wave, plastic deformations will control the dynamic response, which explains the superior agreement between the elastoplastic models and the rigid-plastic model.

---

[1] **The influence of the fundamental period of the system for elastoplastic analyses**

From Figure 3.10 and Figure 3.11 it seems that the larger the fundamental period of the elastoplastic model, the larger the amplitudes on the dynamical response. In fact, observing Figure 3.10b), one may see that the "smooth" transition from point (4) to point (5) for the elastoplastic model with short period happens in 0.045s, which approximately corresponds to ¼ of its fundamental period. In the case of the elastoplastic model with long period, the same transition takes 0.136 s, which again is very close to ¼ of the corresponding fundamental period. Therefore, the longer the fundamental period of the system, the slower the transitions corresponding to elastic behaviour, leading to larger areas on the time-history curves of relative accelerations (see, for instance, the highlighted area in Figure 3.10b)) and successively larger areas on the curves regarding the relative velocities and displacements. It was seen in this example that the displacement demand in the elastoplastic model with larger period is 100% higher than for the case of the elastoplastic model with shorter period. Thus, in elastic-based seismic design procedures, it seems of fundamental importance to accurately estimate the fundamental period of the structure for the initial assessment of the seismic demand on the structure. This is arguably achieved using the simplified formulas available, which represent the first step in those design procedures.

As may be seen in ground acceleration curve in Figure 3.9 for the Asymmetric ground motion, the initial value of the ground acceleration is 1.71 m/s^2. Thus for this period, the rigid-plastic model will not experience plastic deformation, as this value is lower than a_y. Initially therefore, there is no relative motion for this model which may be confirmed observing the detail given in Figure 3.12b), c) and d). For the case of the elastoplastic models, there is limited motion due to the onset of elastic behaviour: As a consequence of dynamical equilibrium, the initial value of the relative acceleration is –1.71m/s^2, decreasing as the restitution forces increase with the relative displacement; The kinetic energy accumulated during this period is dissipated when the capacity of the plastic hinge is reached, point (1) in Figure 3.12a).

The first time there is a reversal of the ground motion, the rigid-plastic model experiences relative deformations due to the onset of plastic behaviour in the opposite direction of the ground acceleration. The relative acceleration is then given by a_r=+2.0–5.12=–3.12m/s^2. Conversely, the elastoplastic models had been in the plastic domain in the positive direction, which means that at the time of the reversal of the ground motion, point (2) on Figure 3.12b), a_r=–2–5.12=–7.12 m/s^2.

The development of the relative accelerations from the first to the second reversal of ground motion is similar to that of the Symmetric accelerogram: Initially, point (2) on Figure 3.12a), the elastoplastic model presents a “smooth” transition until the capacity of the plastic hinge is exhausted in the opposite direction, point (3) in Figure 3.12b). From this point until there is a new reversal in the motion of the ground, the relative acceleration remains constant, point (4) in Figure 3.13c) and d). On the other hand, the rigid-plastic model exhibits a constant value for the relative acceleration during the whole period. After the second reversal of ground motion, the relative acceleration is given by a_r=2.0+1.71=3.71 m/s^2 for the three models, as they were in plastic behaviour in the same direction. The relative acceleration remains constant for the three models until relative velocity is zero. At this instant, the ground acceleration is again 1.71 m/s^2, and is therefore insufficient to induce plastic behaviour on the rigid-plastic model, i.e. insufficient to induce relative motion of the mass, point (5) in Figure 3.13b). The elastoplastic models perform a transition similar to the initial period from (0) to (1), but in this case starting from a plastic state instead of from rest conditions. This induces a reversal in the motion of these models, as seen in the time-history curve referring to relative displacements, Figure 3.13d), the magnitude of which is directly related to the period of the structure as explained in the previous paragraph.

Kobe Record

Observing the plots on the right-hand-side of Figure 3.9, it may be concluded that the record of the Kobe Earthquake used in this study has a clear asymmetric pattern. This explains why the results concerning the dynamical response to the ground motion of the rigid-plastic and elastoplastic models have striking similarities with the results corresponding to the Asymmetric accelerogram, compare Figure 3.14 and Figure 3.16.

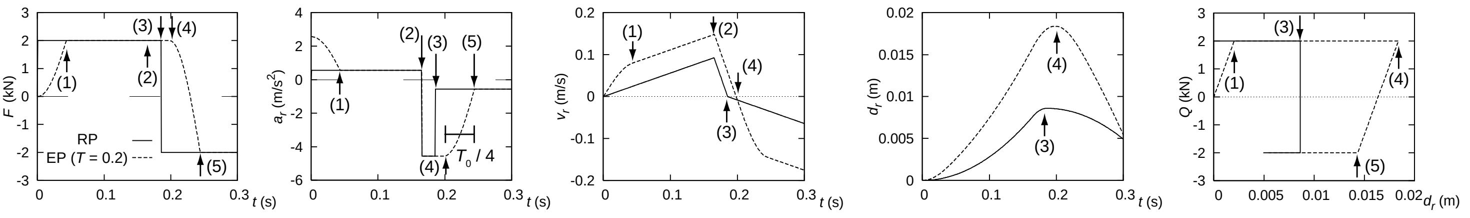

a) Resisting force

b) Relative accelerations

c) Relative velocities

d) Relative displacement

e) Resisting forces vs. relative displacements

Figure 3.10 -Dynamical response from t=0s to t=0.3s of the rigid-plastic model and of the elastoplastic model with fundamental period of 0.2s subjected to the Symmetric ground motion

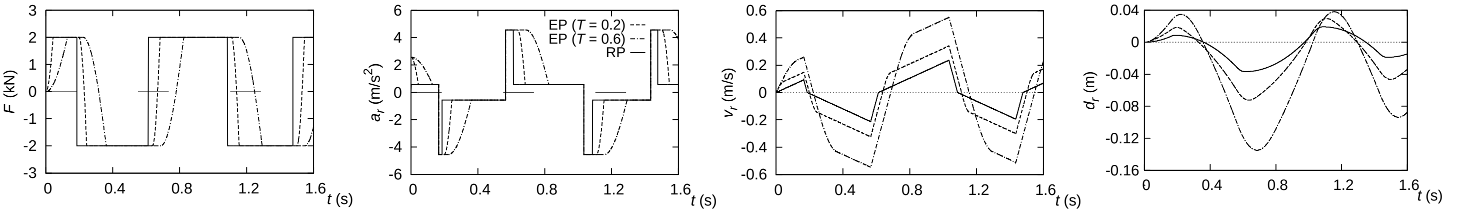

a) Resisting force

b) Relative accelerations

c) Relative velocities

d) Relative displacement

Figure 3.11 -Dynamical response of the rigid-plastic and elastoplastic models until t=1.6s subjected to the Symmetric ground motion

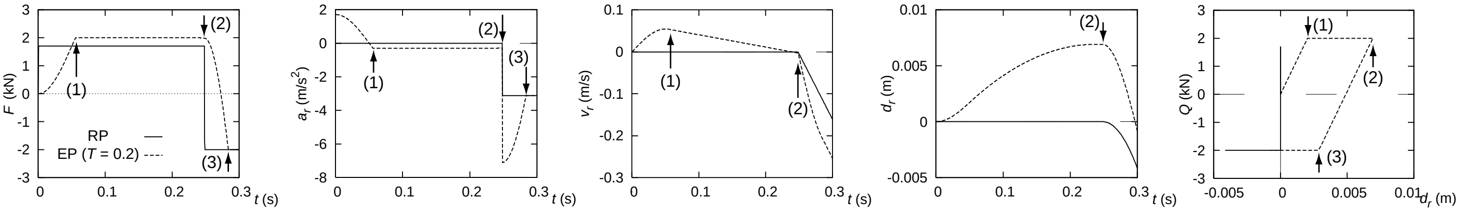

a) Resisting force

b) Relative accelerations

c) Relative velocities

d) Relative displacement

e) Resisting forces vs. relative displacements

Figure 3.12 -Dynamical response from t=0s to t=0.3s of the rigid-plastic model and of the elastoplastic model with fundamental period of 0.2s subjected to the Asymmetric ground motion

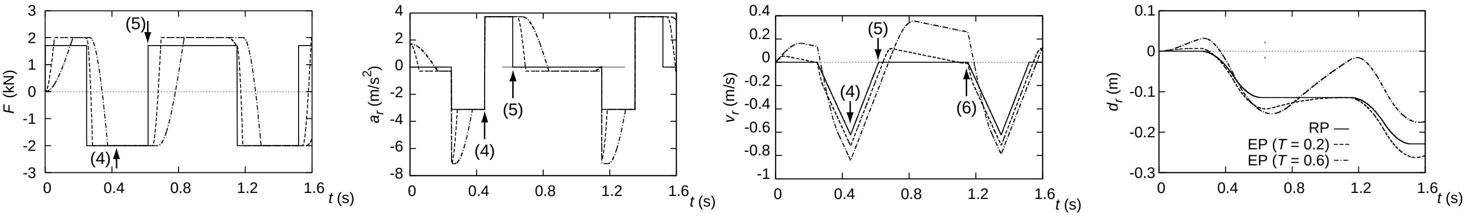

a) Resisting force

b) Relative accelerations

c) Relative velocities

d) Relative displacement

Figure 3.13 - Dynamical response of the rigid-plastic and elastoplastic models until t=1.6s subjected to the Asymmetric ground motion

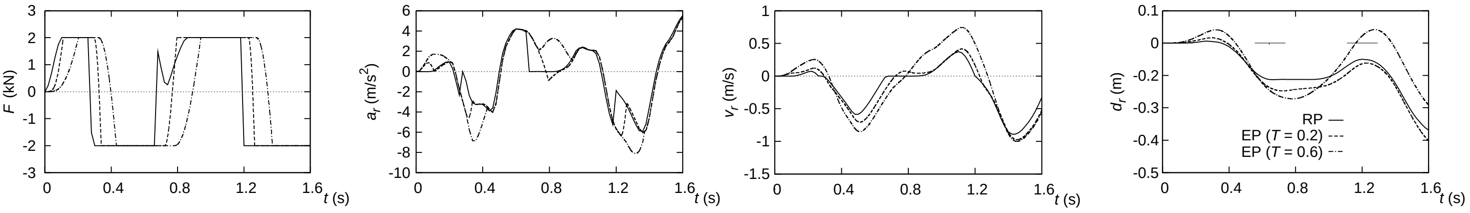

a) Resisting force

b) Relative accelerations

c) Relative velocities

d) Relative displacement

Figure 3.14 - Dynamical response of the rigid-plastic and elastoplastic models until t=1.6s subjected to the Kobe ground motion

3.2.2.4 Dynamical response of the rigid-slip model and Takeda model

It is well known that the hysteretic models discussed previously allow only crude estimations of the dynamical response of structures built with materials with limited energy dissipation capacity, such as reinforced concrete. Here, the dynamic response of the rigid-plastic model with pinching is presented and its results compared with the more sophisticated Takeda model.

Symmetric accelerogram

The dynamical response to the Symmetric ground motion of the rigid-plastic model with pinching and of the Takeda model with short and long period are depicted in terms of time-history curves in Figure 3.16. It may be observed that these models yield much closer results to one another for this ground motion than those discussed in the previous section. This is mainly due to the hysteretic behaviour of the present models, which have similar performances in terms of energy dissipation capacity. In fact, observing their hysteretic curves in Figure 3.2b) and Figure 2.30, it may be concluded that the consideration of pinching effect implies periods of significantly smaller resistance (non-existent for the case of the rigid-slip model) to imposed deformations from the ground motion. Therefore, these models are more prone to accumulate kinetic energy that has to be dissipated mainly by plastic behaviour at the hinges. Therefore, they more easily tend to experience a reversal in relative motion of the mass. This leads to larger amplitudes of motion, as observed when comparing Figure 3.11and Figure 3.16.

In Figure 3.15 one may see a detail of the response for the first 0.3s of the rigid-plastic model with pinching and of the Takeda model with short period, conveniently explaining the deviations between these two models:

- From the beginning of the actuation of the ground motion, until shortly after its first reversal, points (2) and (3) in Figure 3.15, the rigid-plastic model with pinching and the Takeda model develop the same response as the rigid-plastic model and the elastoplastic model respectively (compare with Figure 3.10): The rigid-plastic model immediately undergoes plastic behaviour because the magnitude of the ground motion, 2.56 m/s^2, is larger than a_y, 2.0m/s^2. When there is a reversal in the ground motion, the models remain in the plastic domain until the kinetic energy is dissipated, point (2) in Figure 3.15c). The Takeda model initially displays elastic behaviour, which explains the "smooth" transition from point (0) to (1) in Figure 3.15a) and e). When the capacity of the plastic hinge is exhausted, the model experiences plastic behaviour and proceeds until point (3), with the same value for the relative accelerations as in the rigid-slip model.
- When the rigid-plastic model with pinching again undergoes rigid-behaviour, the ground acceleration is large enough to immediately impose a change of sign in the bending moment at the plastic hinge. This means that there will be a period during which the model is not able to resist the external forces associated with ground motion. The length of this period is directly related with the residual deformation previously imposed, as resistance resumes only when the model is back to its original position. In this particular case, the period corresponds to the time interval between points (2) and (5) in Figure 3.15a), during which dynamical equilibrium imposes $a_r(t)$=-$a_g(t)$=–2.56m/s^2 (see the equation (3.19) corresponding to slip behaviour). On the other hand, the Takeda model performs a smooth transition, as

for the case of the elastoplastic model, but with two different slopes, as may be seen in Figure 3.15e) between points (3) and (5).

The models proceed with the same value for relative acceleration until there is a reversal of ground motion, point (6) in Figure 3.16b). Until point (7) in the same figure, their behaviour is of the same type as explained above. It should be noted in the time-history curve for the relative accelerations, Figure 3.16b), that during this period the areas above the time-axis are very similar for the three models, despite their differing shapes. This explains the consequent agreement between both models on the dynamical response in terms of relative velocities and displacements.

Asymmetric ground motion

The time-history curves depicting the response of the rigid-plastic model with pinching and of the Takeda models with short and long period subjected to the Asymmetric ground motion are shown in Figure 3.17.

As for the case of the Symmetric ground motion, the first part of the dynamical response to the Asymmetric ground motion of the rigid-plastic model with pinching, from point (0) to point (2) (in Figure 3.17a), b) and c)), is identical to the rigid-plastic model. The same similarity is found between the Takeda and the elastoplastic models. As explained above, the response develops in different patterns at the start of the first unloading branch, point (2). At this instant, the ground acceleration is sufficiently large to induce a change of sign on the bending moment at the plastic hinge for the rigid-plastic model with pinching. Therefore, the relative acceleration has an intermediate plateau symmetrical to the value of the ground acceleration at that time, 1.71 m/s^2. When the model is back to its original position, point (3), it immediately experiences plastic deformations in the opposite direction, due to the kinetic energy developed during the previous period of zero resistance. This explains the onset of plastic behaviour in both directions despite the magnitude of the ground acceleration being smaller than a_y in one direction, converse to what happens in the “classic” rigid-plastic model, see section 3.2.2.3. When there is a new reversal in ground motion, shortly before t=1.2s, the rigid-plastic model with pinching and the Takeda models had been experiencing plastic behaviour in the same direction. Therefore, they will proceed with the same value of relative acceleration of the mass, $a_r = -2-5.12 = -7.12$ m/s^2. In fact, as one may see comparing Figure 3.17 and Figure 3.16, from this point on, the dynamical response of the three models to the Asymmetric ground motion is quite similar to that corresponding to the Symmetric ground motion.

Kobe record

The results describing the response of the rigid-plastic model with pinching and Takeda models to the Kobe record may be appreciated in Figure 3.18. The dynamical response to this record is similar to the Asymmetric ground motion. As referred to previously, this relates to the similarity between both accelerograms. However, here the results associated with the rigid-plastic approach are much closer to the reference model, which is the Takeda model. Also, it may be observed that this similarity is found for both levels of fundamental period considered. This relates to the intensity of the ground motion, which is able to induce significant levels of plastic deformations, reducing the role of elastic behaviour on the overall response of the models.

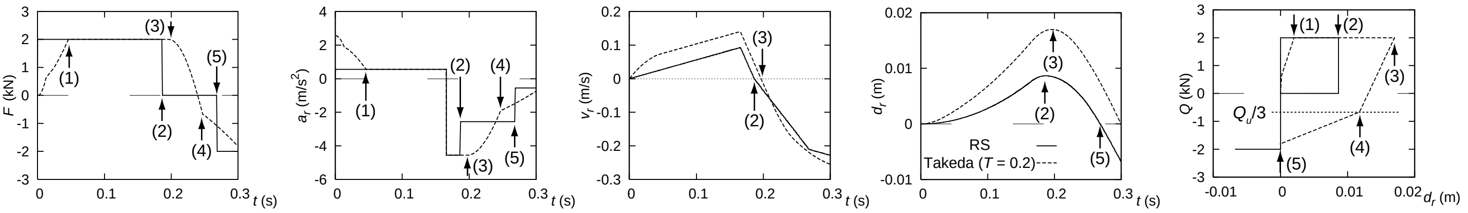

a) Resisting force

b) Relative accelerations

c) Relative velocities

d) Relative displacements

e) Resisting forces vs. relative displacements

Figure 3.15 -Dynamical response from t=0s to t=0.3s of the rigid-slip model and of the Takeda model with fundamental period of 0.2s subjected to the Symmetric ground motion

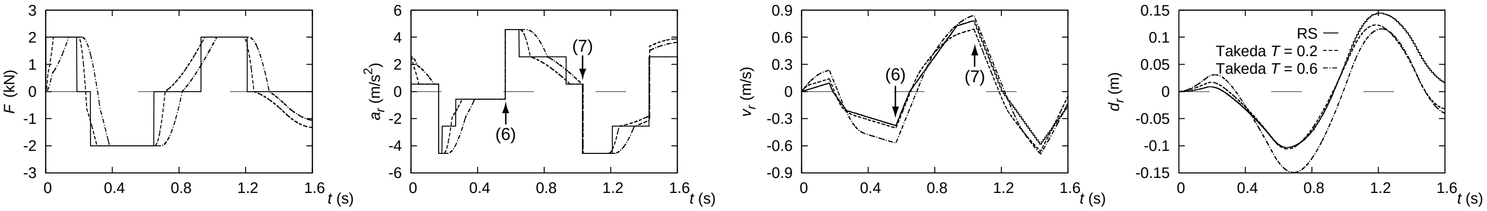

a) Resisting force

b) Relative accelerations

c) Relative velocities

d) Relative displacements

Figure 3.16 -Dynamical response of the rigid-slip and Takeda models until t=1.6s subjected to the Symmetric ground motion

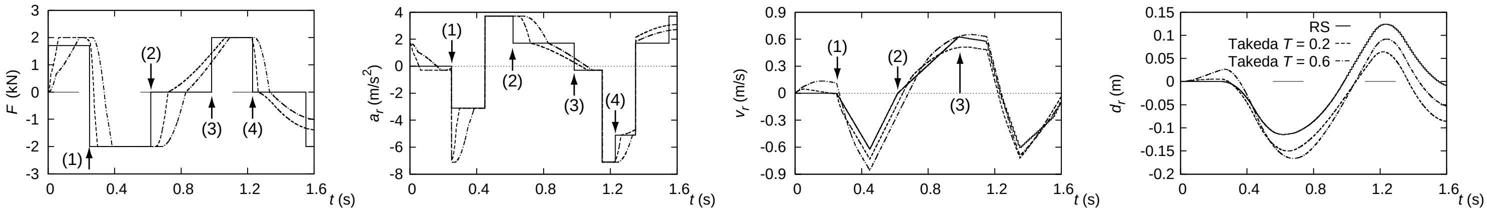

a) Resisting force

b) Relative accelerations

c) Relative velocities

d) Relative displacements

Figure 3.17 -Dynamical response of the rigid-slip and Takeda models until t=*1.6s subjected to the Asymmetric ground motion*

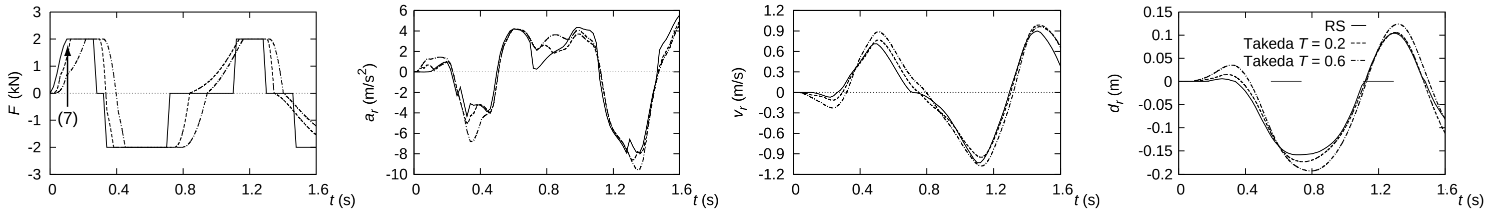

a) Resisting force

b) Relative accelerations

c) Relative velocities

d) Relative displacements

Figure 3.18 -Dynamical response of the rigid-slip and Takeda models until t=*1.6s subjected to the Kobe ground motion*

3.2.2.5 Conclusions

The simple study presented here regarding the dynamic response of rigid-plastic oscillators provides the following conclusions:

- The rigid-plastic model provides accurate results as long as the dynamic response is controlled by plastic behaviour. This was observed through poor agreement between this model and the elastoplastic model for the Symmetric ground motion. This is unsurprising given the large capacity of the oscillators to resist horizontal forces relative to the ground motion demand. When the ground motion intensity (in terms of acceleration) increased (Asymmetric and Kobe accelerograms), agreement between the elastoplastic and rigid-plastic models improved significantly, reaching quite satisfactory levels.
- Such results could be anticipated using the ratio a_y/PGA. This seems to provide an effective estimate of the accuracy of rigid-plastic models predicting dynamic response of oscillators. In fact, a_y/PGA expresses the lateral strength capacity of the oscillator in terms of the maximum demand from ground motion. The larger this parameter, the poorer the predictions from the rigid-plastic model. In the case of the Symmetric ground motion a_y/PGA is 80%, for the Symmetric ground motion it is 40%, and for the part of the Kobe accelerogram it is 25%.
- The rigid-plastic model with pinching appears to be a very accurate tool in predicting the dynamic response of rigid-plastic oscillators with limited energy dissipation capacity, such as reinforced concrete oscillators. The correlation with the Takeda model was remarkably close, both in terms of predicting maximum demand and trend in which the dynamic response develops. These results are even more satisfactory attending to the simplicity of formulation and reduced computational effort required to perform NLTHA using the rigid-plastic model with pinching. As for the rigid-plastic model, the accuracy of the rigid-plastic model with pinching worsens as the ratio a_y/PGA increases. However, the fact that has lower energy dissipation capacity increases the influence of plastic behaviour on the overall dynamic response even at higher levels of a_y/PGA.
- The higher the degree of asymmetry of the ground motion, the higher the displacement demand induced in the inelastic system. In fact, all 4 hysteretic models used in this study reported higher displacement demand for the Asymmetric and Kobe ground motions, especially those with higher dissipation capacity. It was seen that asymmetric waves are less prone to induce reversal of motion in the system and therefore have a higher potential for “magnifying” the deformations in one direction after each cycle.

3.2.3 Rigid-plastic structures

In the following, the treatment of the dynamic response of rigid-plastic structures designed to develop a chosen collapse mechanism is presented.

In section 3.1.1, two important properties of these systems were discussed:

- The displacement field in the structure may be given as a function of a single displacement amplitude, as there is only one mode of vibration considered, i.e. that associated with the shape of the collapse mechanism.

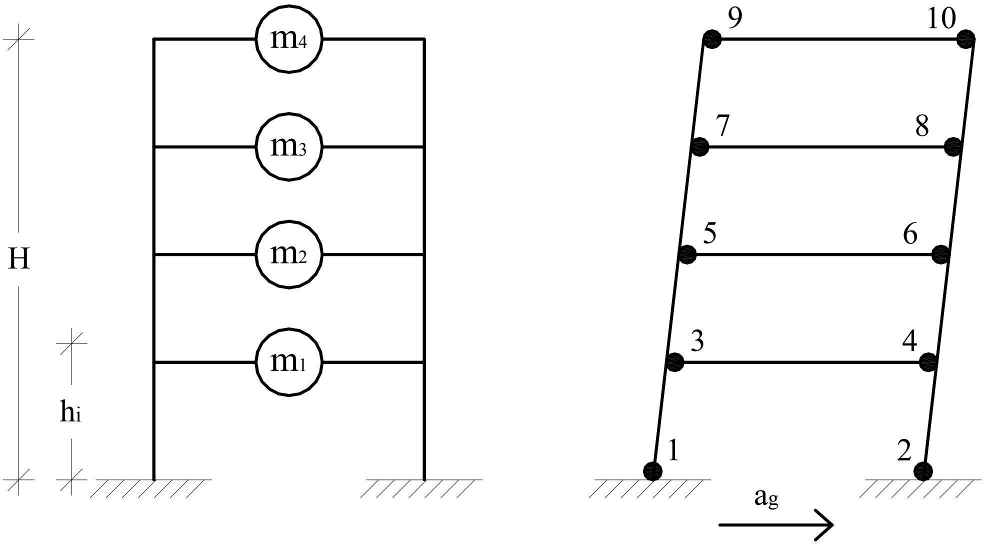

Figure 3.19 - a) Example of a 4-story-plane frame and b) Suitable collapse mechanism

- The relationship between lateral strength demand *vs.* displacements is of the same type as the hysteretic relationships at the plastic hinges, i.e. rigid-plastic with or without the consideration of pinching according to the assumptions at the plastic hinges.

Bearing this in mind, rigid-plastic structures designed to develop a collapse mechanism may be conceived as assemblages of rigid bodies where the only source of internal displacements is due to plastic deformations at the yield zones. Thus, they can be treated as rigid-plastic oscillators and benefit from the corresponding advantages in the treatment of the dynamic response.

For illustration purposes, consider again the case of the reinforced concrete plane frame of section 3.1.1.2. We assume that the only lateral demand is due to base motion, Figure 3.19a). Since we are dealing with a reinforced concrete structure, we further assume that the behaviour at the plastic hinges is of the rigid-plastic type with the consideration of pinching, Figure 3.2b). This decision is justified by the ability of this hysteretic relationship to successfully predict the behaviour of reinforced concrete plastic hinges in cyclic loading, as seen in the previous section.

The structure is designed to develop the collapse mechanism in Figure 3.19b), i.e. that associated with the formation of flexural plastic hinges at the ends of the beams and at the base of the columns on the first floor.

The first step towards the formulation of the equation of motion of a rigid-plastic structure is to choose a displacement amplitude so that the displacement field may be fully defined. Here, we choose to represent any relative displacement in the deformed shape of the structure proportional to the relative displacement at the top floor, d_r.

Therefore, the displacement shape vector is given by

$$\phi_i = \frac{h_i}{H} \tag{3.21}$$

and the displacement at each floor i by:

$$d_{r,i} = \phi_i \cdot d_r \tag{3.22}$$

Of course, the relative velocity and accelerations at each floor i are expressed as in (3.22):

$$v_{r,i} = \phi_i \cdot v_r \tag{3.23}$$

$$a_{r,i} = \phi_i \cdot a_r \tag{3.24}$$

In (3.23) and (3.24) v_r and a_r represent the relative velocity and acceleration of the top floor, respectively.

It is obvious that the frame has rigid behaviour when all the plastic hinges are in the rigid domain. From this it follows:

$$\text{If } \left|M_j\right| < M_{P,j} \Rightarrow \text{ Rigid behaviour } \Rightarrow a_r(t) = 0 \tag{3.25}$$

When the collapse mechanism is activated, two situations may take place:

- The system has plastic behaviour, i.e. all plastic hinges are in the plastic branch, or
- The systems has slip behaviour, i.e. all plastic hinges are in the branch of zero resistance

For each time t of plastic or slip behaviour, dynamic equilibrium may be expressed considering the virtual work equation accounting for the external work from the inertia forces, $m_i \cdot a_{r,i}(t)$, the external work from the base motion loading, $m_i \cdot a_g(t)$, and the internal work at the plastic hinges for virtual displacement δ.

Figure 3.20 depicts the external forces field in this frame, in the coordinate system moving with the ground, when the collapse mechanism is activated in the positive direction assuming that the system is subjected to positive ground motion and moving with positive relative acceleration. The virtual displacement field, δ_i, is also shown for positive increments.

From Figure 3.20 one can write the virtual work equation in this system according to

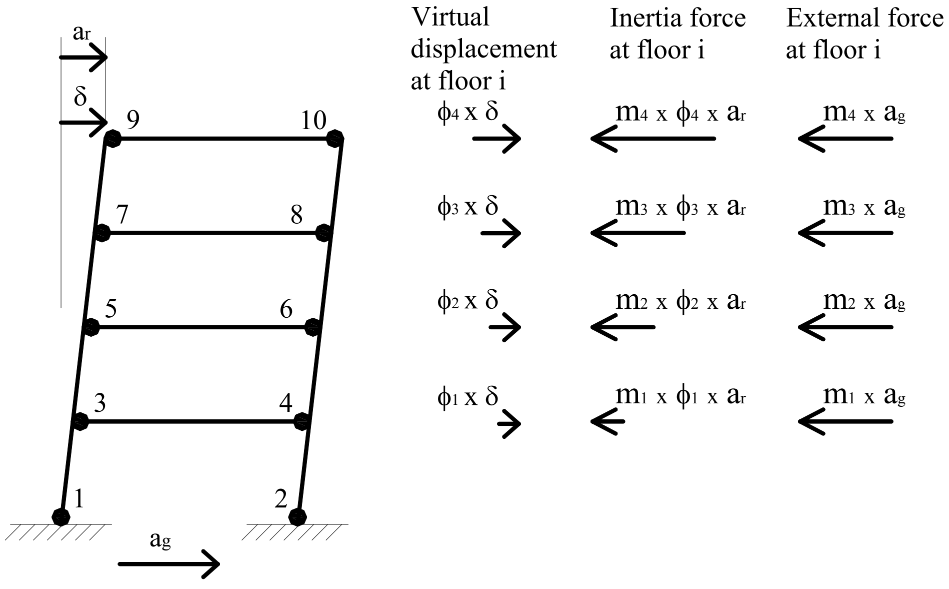

Figure 3.20 -External force field in the 4-storey frame when the collapse mechanism in the positive direction is activated

the sign of the displacement increments:

$$
\begin{aligned}
&-\sum_{j=1}^{10}\left|M_j\right|\cdot\frac{\delta}{H}-\sum_{i=1}^{4}m_i\cdot\phi_i^2\cdot a_r(t)\cdot\delta-\sum_{i=1}^{4}m_i\cdot\phi_i\cdot a_g(t)\cdot\delta=0 \quad \text{if} \quad \delta>0\\
&-\sum_{j=1}^{10}\left|M_j\right|\cdot\frac{\delta}{H}+\sum_{i=1}^{4}m_i\cdot\phi_i^2\cdot a_r(t)\cdot\delta+\sum_{i=1}^{4}m_i\cdot\phi_i\cdot a_g(t)\cdot\delta=0 \quad \text{if} \quad \delta<0
\end{aligned}
\tag{3.26}
$$

It should be noted in equations (3.26) that the value of M_j depends on which direction the collapse mechanism is activated, and of the type of behaviour at the plastic hinges. For instance, in the situation depicted in Figure 3.19, i.e. when the collapse mechanism is activated in the positive direction and there is plastic behaviour, the bending moment at plastic hinges 3, 5, 7 and 9 is the corresponding positive bending capacity, whereas on the opposite side of the beams it is the negative one. If the collapse mechanism were to be activated in the negative direction, i.e. to the left-hand side of the figure, then the bending moments in the left-hand end of the beams would be the negative flexural capacities and the bending moments on the right-hand side of the beams would be the positive bending capacities. Either way, according to our assumptions concerning same lateral capacity of the structure regardless of the direction of the loading, the sum of bending capacities $\sum_{j=1}^{10}\left|M_j\right|$ is the same in both directions of the collapse mechanism.

Of course, if the system is in slip behaviour, then all the bending moments at the plastic hinges are zero regardless of the direction of the collapse mechanism.

It should be noted that as for the case of rigid-plastic oscillators, the condition in which plastic or slip behaviour takes place is based on the relative velocity and the strength demand at the plastic hinges:

- The system undergoes plastic behaviour when all the plastic hinges reach their strength capacities, and it remains in plastic behaviour until the kinetic energy is dissipated.
- The system undergoes slip behaviour when the strength demand at the plastic hinges changes sign and remains in slip behaviour until the residual internal deformations are not recovered.

Bearing this in mind, the equations in (3.26) may be re-written according to the type of behaviour at the structure, see (3.27).

Here $\sum_{j=1}^{10}\left|M_{P+,j}\right|$ and $\sum_{j=1}^{10}\left|M_{P-,j}\right|$ are the sum of the bending capacities when the collapse mechanism in the positive and in the negative direction are activated, respectively. As referred to above, we assume that these quantities are the same regardless of the direction of the collapse mechanism, since this yields the same “overall” strength capacity of the structure against horizontal forces.

$$
\text{Plastic behaviour}\begin{cases}
\sum_{i=1}^{4} m_i \cdot \phi_i^2 \cdot a_r(t) = -\dfrac{\sum_{j=1}^{10}\left|M_{P+,j}\right|}{H} - \sum_{i=1}^{4} m_i \cdot \phi_i \cdot a_g(t) \quad \text{if} \quad v_r(t) > 0 \\
\sum_{i=1}^{4} m_i \cdot \phi_i^2 \cdot a_r(t) = +\dfrac{\sum_{j=1}^{10}\left|M_{P-,j}\right|}{H} - \sum_{i=1}^{4} m_i \cdot \phi_i \cdot a_g(t) \quad \text{if} \quad v_r(t) < 0
\end{cases}
$$

$$
\text{Slip behaviour:} \quad \sum_{i=1}^{4} m_i \cdot \phi_i^2 \cdot a_r(t) = -\sum_{i=1}^{4} m_i \cdot \phi_i \cdot a_g(t)
$$

$$
\text{if} \quad M_j(t) = 0 \ \text{with}\ j \in [1,10] \quad \text{and} \quad v_r(t) \cdot d_r(t) < 0 \tag{3.27}
$$

Introducing the terms in (3.28), the equation in (3.27) can be simplified:

$$
\begin{gathered}
m^* = \sum_{i=1}^{4} m_i \cdot \phi_i^2 \\
\kappa = \frac{\sum_{i=1}^{4} m_i \cdot \phi_i}{\sum_{i=1}^{4} m_i \cdot \phi_i^2} \\
F_y^* = \frac{M_P^*}{H}, \ \text{with}\ M_P^* = \sum_{j=1}^{10}\left|M_{P+,j}\right| = \sum_{j=1}^{10}\left|M_{P-,j}\right|
\end{gathered} \tag{3.28}
$$

Thus for this system,

$$
\text{Plastic behaviour}\begin{cases}
a_r(t) = -\dfrac{F_y^*}{m^*} - \kappa \cdot a_g(t) \quad \text{if} \quad v_r(t) \geq 0 \ \text{and}\ \left|M_j\right| = M_{P+,j} \ \text{with}\ j \in [1,10] \\
a_r(t) = +\dfrac{F_y^*}{m^*} - \kappa \cdot a_g(t) \quad \text{if} \quad v_r(t) \leq 0 \ \text{and}\ \left|M_j\right| = M_{P-,j} \ \text{with}\ j \in [1,10]
\end{cases}
$$

$$
\text{Slip behaviour:} \quad a_r(t) = -\kappa \cdot a_g(t) \quad \text{if} \quad M_j = 0 \ \text{with}\ j \in [1,10] \ \text{and}\ v_r(t) \cdot d_r(t) < 0 \tag{3.29}
$$

The analogy between equations in (3.19) and (3.29) is obvious, in accordance to the fact that rigid-plastic structures may be treated as rigid-plastic oscillators. However, two important points should be made before proceeding:

- The parameters m* and κ are solely dependent on the shape of the collapse mechanism and the mass distribution. The corresponding expression given in (3.28) is valid for any lumped mass structure designed to develop a chosen collapse mechanism. For continuous systems, it is easy to understand from the discussion above that the expressions would be as a function of integrals rather than sums (cf. the discussion in section 4.2 about equations 4.13 and 4.14).
- The parameter F_y*=M_P*/H in equation (3.28) is characteristic of this frame alone, where the dissipation takes place at flexural plastic hinges, all of them submitted to the same rotation demand, d_r/H at the same time. Other types of structural systems have different mechanisms of energy dissipation. However, the equations of motion in any rigid-plastic structure may be derived in the same way, as in

(3.26), where one could conclude that the parcel corresponding to the dissipation is always in the form $F_y^* \cdot \delta$.

Therefore, only two steps are necessary in determining the dynamic response of a rigid-plastic structure designed to develop a collapse mechanism.

- From the shape of the collapse mechanism, determine m* and κ and
- Identify the energy dissipation mechanism to determine F_y^*.

Writing the equations of motion of the structure under ground motion is thus an automatic process.

However, we must still determine the condition describing the transition from rigid to plastic behaviour and from rigid to slip behaviour. Consider that the system starts from rest and that the ground motion increases with time. It is obvious that at the onset of plastic behaviour we have $a_r(t)=0$. Attending to the equations regarding plastic behaviour in (3.29), one finds that the ground acceleration at the onset of plastic behaviour, a_y, in rigid-plastic structures is given by:

$$a_y = \frac{F_y^*}{\kappa \cdot m^*} \tag{3.30}$$

In rigid-plastic structures, a_y has exactly the same characteristics as in rigid-plastic oscillators:

- If the structure starts from rest, then plastic behaviour takes place as soon as the ground acceleration exceeds a_y in one of the directions,
- If the system has rigid behaviour and $|a_g(t)|<a_y$, then the lateral strength demand is insufficient for all plastic hinges to undergo plastic behaviour and activate the collapse mechanism.
- If pinching is considered, then the change of sign on the strength demand at the plastic hinges takes place when $a_g(t)=0$

Thus, the general formulation of the equations of motion for rigid-plastic structures is:

$$\begin{array}{ll}
\text{Plastic behaviour:} & \begin{cases} a_r(t) = -\dfrac{F_y^*}{m^*} - \kappa \cdot a_g(t) \ \text{ if } \ \left|f_j(t)\right| = f_{P+,j} \quad \text{and} \quad v_r(t) \geq 0 \\ a_r(t) = +\dfrac{F_y^*}{m^*} - \kappa \cdot a_g(t) \ \text{ if } \ \left|f_j(t)\right| = f_{P-,j} \quad \text{and} \quad v_r(t) \leq 0 \end{cases} \\
\text{Slip behaviour:} & a_r(t) = -\kappa \cdot a_g(t) \ \text{ if } \ f_j(t) = 0 \text{ with } j \in \left[1, n\right] \quad \text{and} \quad v_r(t) \cdot d_r(t) < 0 \\
\text{Rigid behaviour:} & a_r(t) = 0 \ \text{ if } \ \left|a_g(t)\right| < \dfrac{F_y^*}{\kappa \cdot m^*}
\end{array} \tag{3.31}$$

where

n is the number of yield zones

$f_j(t)$ is the strength demand at the j-th plastic hinge.

$f_{P+,j}$, $f_{P-,j}$ are the capacities at the j-th plastic hinge when the system is moving in the positive or in the negative direction, respectively.

Comparing the system of equations in (3.19) and (3.31), it is seen that the analogy between the dynamic response of rigid-plastic oscillators and rigid-plastic structures is complete. This result is the very basis of the RPSD method. In fact, we can conclude that the dynamic response of a rigid-plastic structure to a ground motion $a_g(t)$ is the same as for a rigid plastic oscillator having $F_y=F_y^*$, $m=m^*$ and submitted to the same ground motion magnified by a factor κ.

Figure 3.21 resumes the procedure for the determination of the dynamic response of a rigid-plastic structure from an equivalent rigid-plastic oscillator, applied to the structure under consideration. In the following, m* will be called *generalised mass* and F_y^* the *generalised yield strength*.

Conclusions

It was seen in this section that rigid-plastic structures designed to develop a chosen collapse mechanism might be treated as rigid-plastic oscillators. Therefore, one may benefit from the simplicity of rigid-plastic NLTHA discussed in section 3.2.1.2 to

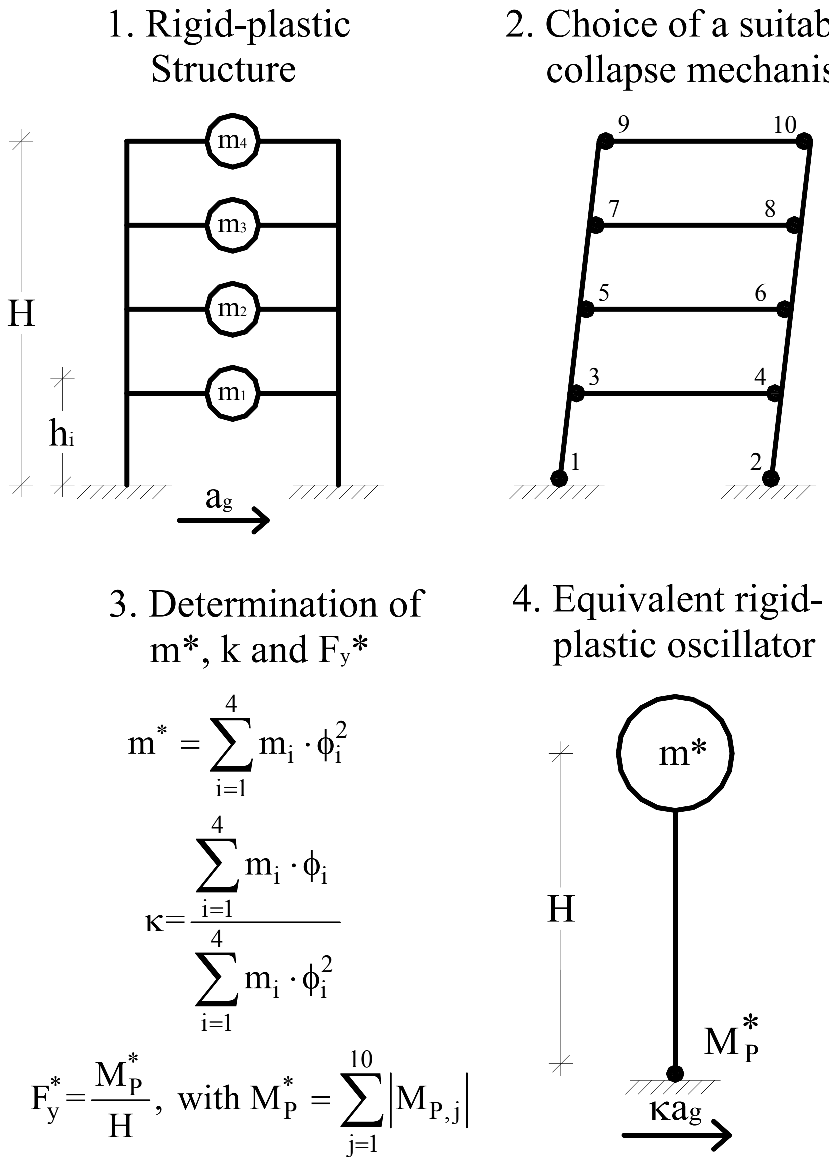
1. Rigid-plastic Structure
m4
m3
m2
m1
H
hi
ag
2. Choice of a suitable collapse mechanism
9
10
7
8
5
6
3
4
1
2
3. Determination of m*, k and Fy*
4. Equivalent rigid-plastic oscillator
m*
H
M*P
κag

$$m^* = \sum_{i=1}^{4} m_i \cdot \phi_i^2$$

$$\kappa = \frac{\sum_{i=1}^{4} m_i \cdot \phi_i}{\sum_{i=1}^{4} m_i \cdot \phi_i^2}$$

$$F_y^* = \frac{M_P^*}{H}, \text{ with } M_P^* = \sum_{j=1}^{10} \left| M_{P,j} \right|$$

Figure 3.21 -From a rigid-plastic structure to a rigid-plastic oscillator.

assess the dynamic behaviour of rigid-plastic structures.

The dynamic response of the structure may be assessed as soon as the collapse mechanism is chosen and the dissipation capacity at each yield zone is known. Moreover, as in the case of rigid-plastic oscillators, the magnitude of displacements in the structure is directly related with the extension of plastic deformations at the yield zones. Therefore, one may easily relate the magnitude of dynamic response to the extension of damage, which as detailed below, yields significant advantages in relation to performance-based design philosophy.

3.3 Seismic demand

In this section, the basis for the estimation of seismic demand on reinforced concrete structures designed according to the RPSD method will be discussed. The concept of rigid-plastic spectrum will be introduced as well as a conservative procedure to define the strength distribution in structures subjected to strong ground motion.

Since the discussion will refer to reinforced concrete structures, we shall only consider the rigid-plastic model with consideration to pinching, see Figure 3.2b) in section 3.1.1.1. In section 3.2.2 it was shown that this is the rigid-plastic model that most adequately describes the hysteretic behaviour of reinforced concrete yield zones.

3.3.1 Rigid-plastic response spectra

The initial task in modern seismic design philosophy deals with the selection of a suitable collapse mechanism ensuring ductile behaviour during ground motion, cf. section 1.1. This decision is constrained by a large number of parameters, such as the avoidance of brittle modes of failure, extensive distribution of dissipation capacity throughout the structure and possible limitations of ductility in the yield zones, which in turn are directly related to the level of damage accepted after the earthquake event. However, at the start of the design process, a significant proportion of the data leading to the choice of a suitable collapse mechanism is available, since it is highly dependent on the geometry of the structure and its mass distribution. The latter parameters are often out of the scope of the structural engineer since they relate more to architectural considerations.

In rigid-plastic dynamics, the major implication for the above deals with the fact that after the engineer chooses a suitable collapse mechanism, the remaining unknown quantity to define the equations of motion of the structure is the generalised yield strength of the structure, F_y*. The generalised mass, m* and the factor κ are automatically given after the choice of the suitable collapse mechanism, see expressions (3.28).

Bearing this in mind and attending to the reduced computational effort required to perform NLTHA in rigid-plastic dynamics, one possible way to determine F_y* is to follow the procedure:

1. Define a performance criterion able to describe the level of damage accepted in the structure during strong ground motion.
2. Consider a sufficient number of records representative of the seismicity at the implementation site.

3. Carry out a number of rigid-plastic NLTHA adjusting the parameter F_y^* until the performance criterion is reached within acceptable tolerance.

However, in the RPSD method this is not necessary.

Consider again the equations of motion of a rigid-plastic oscillator.

$$\text{Plastic behaviour:}\quad \begin{cases} a_r(t) = -\dfrac{F_y}{m} - a_g(t) & \text{if} \quad |f(t)| = f_P \quad \text{and} \quad v_r(t) \geq 0 \\ a_r(t) = +\dfrac{F_y}{m} - a_g(t) & \text{if} \quad |f(t)| = f_P \quad \text{and} \quad v_r(t) \leq 0 \end{cases}$$

$$\text{Slip behaviour:}\quad a_r(t) = -a_g(t) \quad \text{if} \quad f(t) = 0 \quad \text{and} \quad v_r(t) \cdot d_r(t) < 0 \qquad (3.19)$$

$$\text{Rigid behaviour:}\quad a_r(t) = 0 \quad \text{if} \quad |a_g(t)| < \frac{F_y}{m}$$

It is clear that the dynamic response of rigid-plastic oscillators is solely dependent on the parameter $a_y=F_y/m$. Rigid-plastic oscillators with the same value for a_y will develop same dynamic response.

This property of rigid-plastic oscillators yields the possibility for constructing a spectrum that can express any maximum dynamic response parameter, R_{max}, as a function of a_y for any ground motion. R_{max} may be maximum relative acceleration, velocity or displacement. In the following, this spectrum will be called the *rigid-plastic spectrum* and will have the designation RPS in figures.

The dashed lines in Figure 3.22a) and b) show two rigid-plastic spectra in terms of peak relative displacement, d_{max}. The hysteretic model considered here is the rigid-plastic with slip behaviour. The first refers to the N-S component of the JMA record of the Kobe Earthquake, 1995. The second refers to the 360-component of the Sylmar record of the Northridge, California Earthquake, 1994. The corresponding accelerograms are given in the Appendix.

As may be observed, the rigid-plastic spectrum intercepts the a_y-axis at the value of

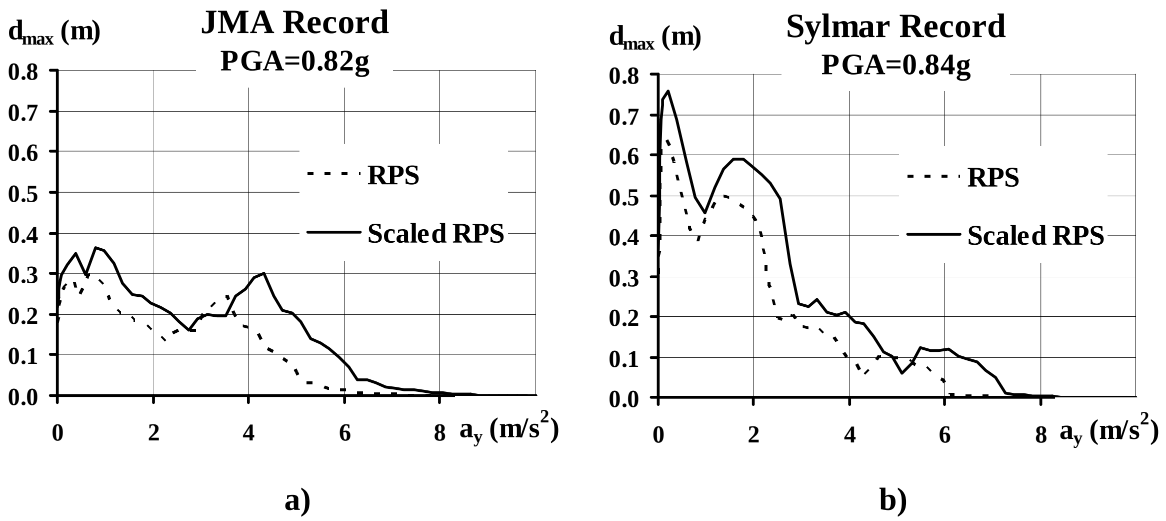

a) b)

Figure 3.22 -Rigid-plastic spectra in terms of peak relative displacement, d_{max}, for the a) JMA N-S record of the Kobe Earthquake, 1995 and b) Sylmar 360 record of the Northridge Earthquake, 1994

PGA, since any oscillator having $a_y \geq PGA$ remains in the rigid domain, which implies no relative deformations whatsoever during the whole ground motion.

On the other hand, if $a_y=0$, then the dynamic response of the oscillator is solely given by the equation corresponding to slip behaviour in (3.19). Therefore the motion of the mass is symmetric to the ground motion. This implies that in Figure 3.22a) and b) the values of d_{max} for $a_y=0$ are the peak ground displacement of the Kobe and Northridge records, respectively. Of course, if the spectra in Figure 3.22a) and b) were given in terms of maximum relative velocities, v_{max}, or accelerations, a_{max}, then one would read either the peak ground velocity or PGA for each ground motion for $a_y=0$.

The rigid-plastic spectra are of great practical value due to the following properties:

1. The rigid-plastic spectrum of a ground motion scaled by a factor α is given by the original curve scaled by the same factor α in both R_{max} and a_y directions. This is easily recognised by affecting the expressions in (3.19) by a factor α, whereby it appears that the dynamic response of an oscillator with $\alpha \cdot a_y$ subjected to $\alpha \cdot a_g(t)$ is α times the dynamic response of an oscillator with a_y and subjected to $a_g(t)$. Thus, the rigid-plastic spectra of the records mentioned above, scaled up so that the PGA equals 1g (the solid lines in Figure 3.22a) and b)), are obtained by magnifying the scale of both axes of the corresponding broken lines by the factors $1/PGA_{Sylmar}$ and $1/PGA_{JMA}$ respectively, with PGA in g units.
2. If one were to reproduce the seismicity of a region by a sufficient number of accelerograms, then the envelope of all the corresponding rigid-plastic spectra would give the rigid-plastic spectrum characteristic for that region. Figure 3.23 shows the envelope of the rigid-plastic spectra corresponding to the scaled records in Figure 3.22a) and b).

The problem now regards the use of the rigid-plastic spectra in the case of rigid-plastic structures. Clearly, the solution is to be found in the complete analogy between rigid-plastic oscillators and rigid-plastic structures.

Consider again the system of equations of motion for rigid-plastic structures:

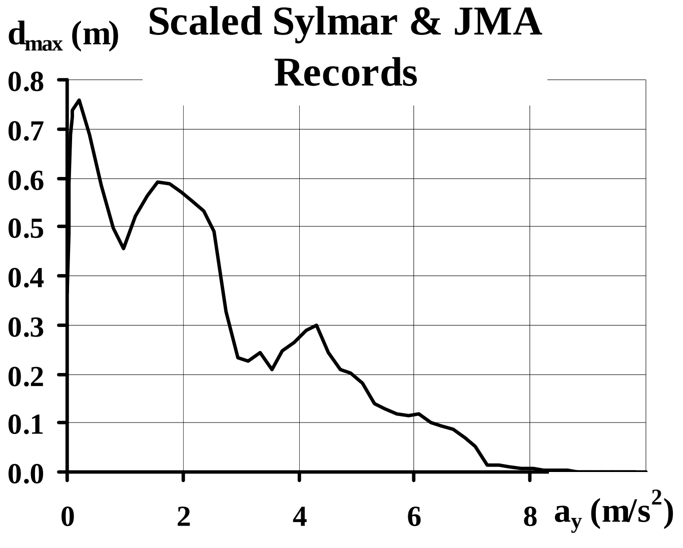

Figure 3.23 -The GRPS of the scaled Sylmar and JMA records so that PGA=1g in terms of peak relative displacement, $d_{r,max}$

$$
\begin{array}{ll}
\text{Plastic behaviour:} & \begin{cases} a_r(t) = -\dfrac{F_y^*}{m^*} - \kappa \cdot a_g(t) \ \text{ if } \left|f_j(t)\right| = f_{P+,j} \ \text{ and } \ v_r(t) \geq 0 \\ a_r(t) = +\dfrac{F_y^*}{m^*} - \kappa \cdot a_g(t) \ \text{ if } \left|f_j(t)\right| = f_{P-,j} \ \text{ and } \ v_r(t) \leq 0 \end{cases} \\
\text{Slip behaviour:} & a_r(t) = -\kappa \cdot a_g(t) \ \text{ if } f_j(t) = 0 \text{ with } j \in [1,n] \ \text{ and } \ v_r(t) \cdot d_r(t) < 0 \\
\text{Rigid behaviour:} & a_r(t) = 0 \ \text{ if } \left|a_g(t)\right| < \dfrac{F_y^*}{\kappa \cdot m^*}
\end{array}
\qquad (3.31)
$$

Dividing the expressions in (3.31) by a factor κ, we conclude that the dynamic response against a ground motion $a_g(t)$ of a rigid plastic structure with $a_y=F_y^*/m^*$ divided by κ is the same of an equivalent rigid-plastic oscillator with $a_y=F_y^*/(m^* \cdot \kappa)$. In other words, the dynamic response of a rigid-plastic structure with $a_y=F_y^*/ m^*$ subjected to ground motion $a_g(t)$ is κ times larger than the dynamic response of a rigid-plastic oscillator with $a_y=F_y^*/(m^* \cdot \kappa)$ subjected to the same ground motion.

In practical terms, this means that the rigid-plastic spectrum of a structure designed to develop a chosen collapse mechanism during a given ground motion is reached by scaling, by a factor κ, the rigid-plastic spectrum corresponding to the case of the oscillators in the R_{max}-direction.

In the following, for the sake of simplicity, we attribute the designation of GRPS to the rigid-plastic spectra corresponding to the oscillators case. The letter *G* refers to *general*, since these spectra are solely dependent on the ground motion; The rigid-plastic spectra which refers to the dynamic response of a *specific* structure designed to develop a *specific* collapse mechanism is designated as SRPS.

Figure 3.24a) depicts the procedure to convert a GRPS into a SRPS.

From the discussion above, it seems clear that the determination of the generalised yield strength in the structure, F_y^*, may easily be carried out after the SRPS for a given structure and collapse mechanism has been determined: In fact, having the SRPS, one needs only to define the performance criterion in terms of the maximum dynamic response parameter, R_{max} and read off the corresponding value of F_y^*. The procedure is shown in Figure 3.24b).

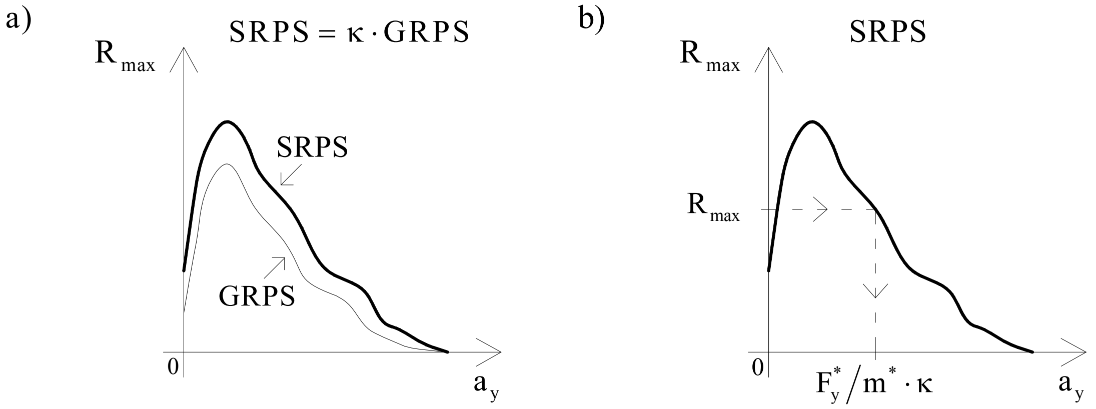

Figure 3.24 -a) Transition from GRPS to SRPS and b) Determination of F_y from R_{max}*

At this stage it is possible to give the procedure in the RPSD method leading to the determination of the generalised yield strength, F_y*, if the GRPS characteristic of the seismicity at the implementation site is available.

1. Definition of a performance criterion in terms of a maximum response parameter R_{max}.
2. Determination of the factor κ from the collapse mechanism.
3. Definition of the SRPS from the GRPS, see Figure 3.24a).
4. Read off the value of a_y in the SRPS associated with R_{max}, the graphical procedure in Figure 3.24b).
5. Use equation (3.30) to derive F_y*:

$$F_y^* = \kappa \cdot m^* \cdot a_y \tag{3.32}$$

Clearly, a large proportion of the simplicity and practical value of the RPSD method lies on the use of rigid-plastic spectra. In fact, if the GRPS characteristic of the seismicity is known, there is no need to perform NLTHA in order to derive the value of the generalised yield strength, F_y*, that makes the dynamic response completely defined.

Most importantly however, is the fact that the rigid-plastic spectra avoid the use of any sort of artificial coefficients intended to adjust the dynamic response of the structure according to empirical observations, while lacking physical meaning. This is because the values read from the SRPS are the actual values of the dynamic response of the structure. There is no need for any modal combination rules, since there is only one possible mode of vibration – that associated with the collapse mechanism. Also, reduction coefficients are unnecessary, as the results computed in the rigid-plastic spectra are derived after rigid-plastic NLTHA. From the author's point of view, this is a major advantage over the simplified design procedures currently available, i.e. those that, in one way or the other, still make use of elastic spectra.

In the following, the discussion proceeds with the use of the rigid-plastic spectra for design purposes. A study evaluating the range of application of the rigid-plastic spectra in the a_y domain will be given, and some recommendations will be proposed.

Rigid-plastic spectra for design purposes

The single most important feature of any spectrum used for design purposes is that a sufficient number of records are accounted for, so that the seismicity at the implementation site can be effectively reproduced. Generally, this number has to be rather high, as our knowledge of ground motion prediction is still rather limited. Therefore, the best way to increase the reliability of the spectrum for design purposes is to increase the number of records accounted for in it.

However, identifying records typical of the regional seismicity is not an easy task at all. (Priestley et al., 1996) suggested the following basic procedure to define a reliable ground motion scenario that can be used for design purposes:

1. Identification of earthquakes sources in the region, i.e. active faults and their potential energy release
2. Use of attenuation laws to predict expected ground acceleration intensity at the implementation site

3. Definition of the ground motion according to the source mechanism and travel path along different layers of soil filtering different types of waves
4. Identification of maxima components such as duration, PGA, peak ground velocity (PGV), etc.
5. Consideration of local soil conditions, expected directional effects and geographical amplification.

Furthermore, according to the importance of the structure and the risk accepted, one has to define the design intensity of the ground motion scenario. Economic and structural safety considerations have to be addressed simultaneously in this decision.

It is out of the scope of this work to discuss in detail the aspects mentioned above, since these have more to do with seismic hazard analysis than with structural design.

In the following, we discuss the characteristics of rigid-plastic spectra, assuming that they are composed of a sufficient number of records that represent the seismicity at the implementation site, and therefore can be used for design purposes.

Consider for instance, the GRPS in Figure 3.25 in terms of peak relative displacement. This was computed from 15 artificially generated records based on the Friuli Earthquake, Italy, 1976. The records were generated at ICIST-IST, The Technical University of Lisbon, Portugal (Falcão, 2002) and they comply with the elastic response spectrum in EC8 (CEN, 2003) for intermediate soil (profile B), a viscous damping ratio equal to 5% and 0.3g<PGA<0.4g. The accelerograms are depicted in the Appendix.

Clearly, the GRPS presents a different development than that shown in Figure 3.23. Generally, the GRPS in Figure 3.25 is given by a smooth, continuous descending line, opposing the spectrum in Figure 3.23 where lower levels of response for lower levels of a_y are found. This is because the GRPS of Figure 3.25 accounts for the response of 15 records, and therefore the tendency of lower response for higher lateral capacity is

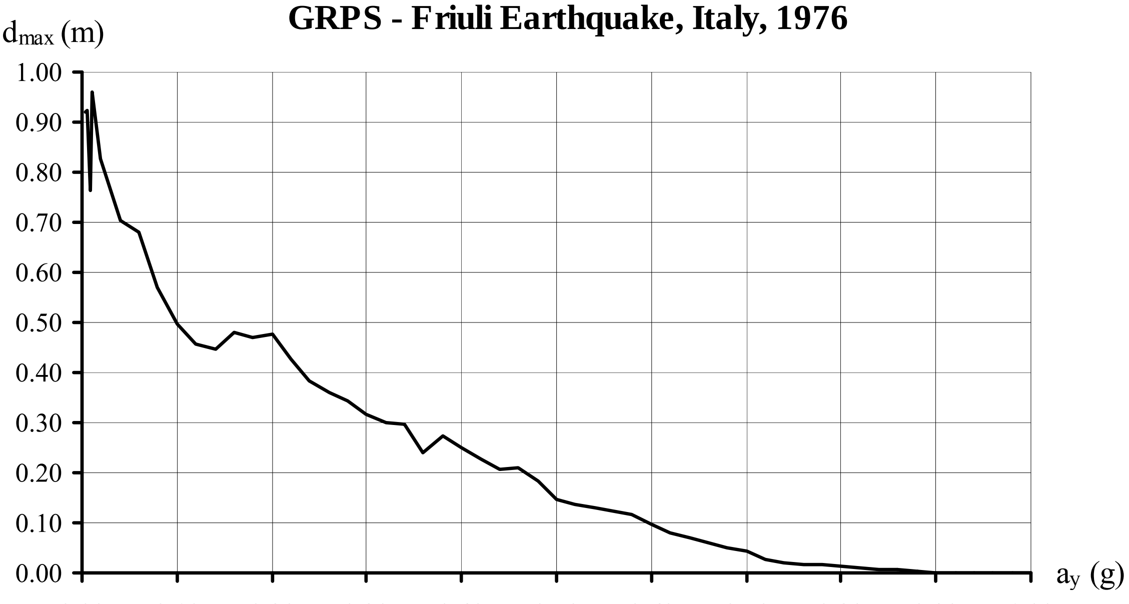

Figure 3.25 -GRPS based on the Friuli Earthquake, Italy, 1976

effectively captured.

However, some values of a_y are still seen in the GRPS of Figure 3.25, for which the maximum relative displacement is lower than the maximum relative displacement corresponding to higher values of a_y, i.e. in the following intervals:

- $0.12g \leq a_y \leq 0.18g$
- $0.34g \leq a_y \leq 0.38g$
- $0.44g \leq a_y \leq 0.46g$

This implies that potentially, there is more than one solution of a_y for the same value of R_{max} associated with the chosen performance criterion for the structure in the resulting SRPS. Obviously, in a design situation one would normally choose the lowest possible value of a_y, since in this way the performance criterion would be met at the lowest cost. However, there are two reasons to consider the highest value of a_y:

1. As discussed in the beginning of this section, the degree of uncertainty regarding an earthquake that might hit the structure is still considerable. In other words, there is still a significant probability that the "actual" ground motion would impose a higher response demand in the region of a_y than the structure was designed for.
2. Potential enhancement of dissipation capacity in the structure due to strength enhancement at the plastic hinges will translate in a higher a_y value for the structure and therefore higher response demand, which in turn compromises the fulfilment of the performance criterion.

From this it follows that whenever the designer is faced with a SRPS having successive descending and ascending branches, a safe estimation of the maximum deformation demand in the corresponding domain of a_y is attained by drawing a line between the successive peaks. Figure 3.26 shows the corrected GRPS of the ground

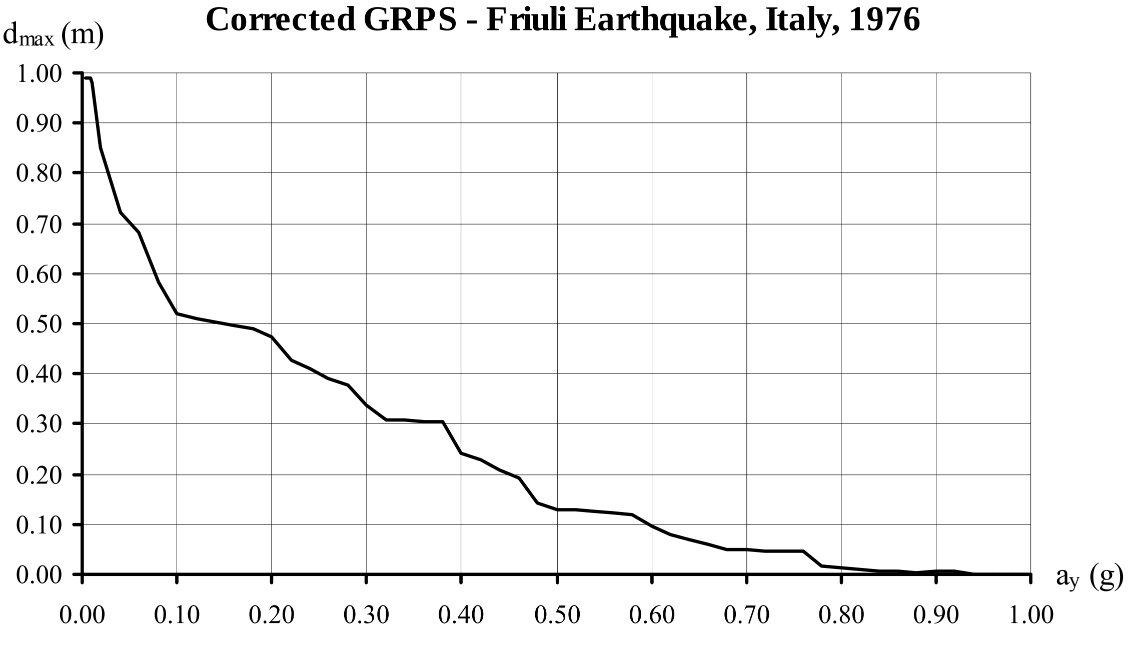

Figure 3.26 -Corrected GRPS based on the Friuli Earthquake, Italy, 1976

motion scenario based on the Friuli Earthquake, Italy, 1976.

Finally, there is the problem of establishing the limits within which rigid-plastic spectra are expected to provide accurate results. In section 3.2.2 it was seen that the lower the value of a_y, the more accurate the predictions based on rigid-plastic oscillators. This is explained by the fact that, for the same displacement demand, the lower the lateral strength, the higher the magnitude of plastic deformations compared with elastic deformations, and therefore, the more accurate the rigid-plastic approach. In other words, the higher the expected ductility demand at the yield zones, the better the results we can expect from the rigid-plastic spectra.

For the case of structural systems designed to develop collapse mechanisms with flexural hinging, the expected ductility demand in terms of rotation in each plastic hinge, $\mu_{\theta,exp}$, may be defined:

$$\mu_{\theta,\mathrm{exp}} = \frac{\theta_{u,RPS}}{\theta_y} \tag{3.33}$$

where,

$\theta_{u,RPS}$ is the maximum rotation demand at the plastic hinge predicted from the rigid-plastic spectra and

θ_y is the corresponding yield rotation.

If the ductility demand at all plastic hinges is sufficiently high, then the rigid-plastic spectra are able to provide accurate results. The problem now arises in determining the minimum requirement for the expected ductility demand.

With this purpose in mind, a series of refined NLTHA were conducted to investigate the dynamic response of elastoplastic column oscillators, as in the sketch of Figure 3.8b). For each elastoplastic oscillator, one would plot the curve d_{max} *vs.* a_y and compare it with the GRPS shown in Figure 3.26. Therefore, each elastoplastic oscillator with the corresponding level of a_y was subjected to the 15 records of the Friuli Earthquake, Italy, 1976, scaled up so that PGA=1g. In this study we tacitly assumed that all the plastic hinges had enough rotation capacity to sustain the displacement demand introduced by the ground motion scenario.

The study was carried out as follows:

- Two column oscillators were considered. The product m·L was identical for both, and equal to 50ton·m. Thus, for the same value of a_y the same bending capacity M_P had to be assigned at the plastic hinge, cf. section 3.2.1.1. In the following, each of the column oscillators is designated by Col.#, # being the number corresponding to the length of the column in m. Table 3.3 refers to the mass and length of each of the column oscillators used in this study.

  It should be noted that the relation between vibration periods of both oscillators is expected to be the same regardless of the corresponding value of a_y. In fact, the relation between the base shear, V, and top displacement, d, for elastic cantilever

Table 3.3 -Mass and length of the column oscillators

	Col. 2	Col. 5
Mass (ton)	25	10
Length of the column (m)	2	5

column oscillators is $V=EI/L^3 \cdot d$. Noting that for the same a_y we have the same bending moment distribution in the cantilever and in turn, EI, we find that $T_{Col.5}/T_{Col.2}=2.5$:

$$\frac{T_{Col.5}}{T_{Col.2}} = \sqrt{\frac{m_{Col.5}}{m_{Col.2}} \cdot \frac{L^3_{Col.5}}{L^3_{Col.2}}} = \sqrt{\frac{10 \times 5^3}{25 \times 2^3}} = 2.5 \tag{3.34}$$

- 20 different bending capacities for each column oscillator were considered. These cover the range corresponding to $a_y=0.05g$ to $a_y=1.00g$.
- The design of each column oscillator follows the procedure as seen in the example in section 2.3. The tensile reinforcement ratio at the plastic hinges is set to 0.8% and the width to height ratio of the cross-section, β, to 0.6. As discussed in section 2.4.3, the overstrength factor to design the column outside the hinge is 1.4. We assume equal geometry for the cross-sections along the whole column, therefore the tensile reinforcement ratio outside the hinges is 1.4x0.8=1.12%. The reinforcement steel used is the same as investigated by (Pipa and Vercesi, 1998), and has similar ductile properties to Grade B500 Tempcore steel.

Table 3.5 summarises the structural properties of the plastic hinge at the base of the elastoplastic oscillators as well as plastic hinge length, Δl, yield rotation, θ_y and expected rotation ductility, $\mu_{\theta,exp}$, according to the type of oscillator and the a_y parameter. Δl and θ_y were calculated according to the procedure discussed in section 2.3. $\mu_{\theta,exp}$ is given by the expression:

$$\mu_{\theta,exp} = \frac{d_{max,GRPS}}{H \cdot \theta_y} \tag{3.35}$$

where

$d_{max,GRPS}$ is maximum displacement read from the GRPS in Figure 3.26 according to a_y and

H is the height of the column oscillator.

As we can see in Table 3.5, it is expected that the shortest column oscillator will be subjected to a much higher ductility demand (approximately 5 times higher in the whole range of a_y). This is explained by the fact that Col.2 is 2.5 times shorter than Col.5, cf. equation (3.35). Moreover, the plastic hinge length, to which the θ_y is directly proportional, is approximately halved in Col.2 for the whole range of a_y. The latter is due to the fact that in these oscillators, Δl is essentially dependent on the shear span length, which is the column's own length. Thus, attending to the equation in (2.10), we have the following ratio between plastic hinges lengths:

$$\frac{\Delta l_{Col.5}}{\Delta l_{Col.2}} = \frac{0.25 \cdot h + \eta \cdot 5}{0.25 \cdot h + \eta \cdot 2} \approx 2 \tag{3.36}$$

Table 3.4 -Properties of reinforcement steel

$f_{y,min}$ (MPa)	519
ε_{sy} (%)	0.26
η	0.15

- The dynamic response of the column oscillators was calculated by direct integration of the equation of motion using the commercial program SAP2000 with the following features:
  a) The Newmark method with γ=0.5 and β=0.25 as the numerical integration procedure.
  b) 0.05 for the damping ratio of the vibration mode.
  c) The flexural behaviour of the plastic hinge described the pivot hysteresis model with α and β set to 4 and 0.55, respectively. This is in agreement with the experimental work carried out by (Abrams, 1987) cf. section 2.2.1.3.

Table 3.5 -Expected rotation ductility at the plastic hinge for the different elastoplastic oscillators according to the value of a_y

	a_y (g)	M_P (kNm)	h (m)	V (kN)	Δl (m)	θ_y ($x10^{-2}$ rad)	T (s)	$\mu_{\theta,exp}$
Col.2	0.05	24.5	0.222	12.3	0.355	0.47	1.416	74.3
Col.5				4.9	0.805	1.08	3.480	13.0
Col.2	0.10	49.1	0.280	24.5	0.370	0.39	0.899	66.6
Col.5				9.8	0.820	0.87	2.199	11.9
Col.2	0.15	73.6	0.320	36.8	0.380	0.35	0.690	71.8
Col.5				14.7	0.830	0.77	1.682	13.0
Col.2	0.20	98.1	0.352	49.1	0.388	0.32	0.572	73.2
Col.5				19.6	0.838	0.71	1.391	13.4
Col.2	0.25	122.6	0.380	61.3	0.395	0.30	0.494	66.0
Col.5				24.5	0.845	0.66	1.200	12.1
Col.2	0.30	147.2	0.403	73.6	0.401	0.29	0.439	58.2
Col.5				29.4	0.851	0.63	1.064	10.8
Col.2	0.35	171.7	0.425	85.8	0.406	0.28	0.397	55.0
Col.5				34.3	0.856	0.60	0.962	10.3
Col.2	0.40	196.2	0.444	98.1	0.411	0.27	0.364	44.9
Col.5				39.2	0.861	0.57	0.881	***8.4***
Col.2	0.45	220.7	0.462	110.4	0.415	0.26	0.338	38.2
Col.5				44.1	0.865	0.56	0.815	7.2
Col.2	0.50	245.3	0.478	122.6	0.420	0.25	0.315	25.3
Col.5				49.1	0.870	0.54	0.760	4.8
Col.2	0.55	269.8	0.494	134.9	0.423	0.25	0.296	25.2
Col.5				54.0	0.873	0.52	0.714	4.8
Col.2	0.60	294.3	0.508	147.2	0.427	0.24	0.280	20.0
Col.5				58.9	0.877	0.51	0.674	3.8
Col.2	0.65	318.8	0.522	159.4	0.430	0.24	0.266	13.6
Col.5				63.8	0.880	0.50	0.640	2.6

Table 3.5 -Expected rotation ductility at the plastic hinge for the different elastoplastic oscillators according to the value of a_y (Cont.)

	a_y (g)	M_P (kNm)	h (m)	V (kN)	Δl (m)	θ_y ($x10^{-2}$ rad)	T (s)	$\mu_{\theta,exp}$
Col.2	0.70	343.4	0.535	171.7	0.434	0.23	0.253	10.4
Col.5				68.7	0.884	0.49	0.609	2.0
Col.2	0.75	367.9	0.547	183.9	0.437	0.23	0.243	***10.2***
Col.5				73.6	0.887	0.48	0.582	2.0
Col.2	0.80	392.4	0.559	196.2	0.440	0.23	0.233	3.3
Col.5				78.5	0.890	0.47	0.558	0.6
Col.2	0.85	416.9	0.571	208.5	0.443	0.22	0.224	1.5
Col.5				83.4	0.893	0.46	0.536	0.3
Col.2	0.90	441.5	0.582	220.7	0.445	0.22	0.216	1.3
Col.5				88.3	0.895	0.45	0.517	0.2
Col.2	0.95	466.0	0.592	233.0	0.448	0.22	0.208	0.1
Col.5				93.2	0.898	0.45	0.499	0.0
Col.2	1.00	490.5	0.603	245.3	0.451	0.22	0.202	0.0
Col.5				98.1	0.901	0.44	0.482	0.0

The results of the study can be seen in Figure 3.27. This represents the corrected GRPS of Figure 3.26 together with the curves d_{max} *vs.* a_y for both Col.2 and Col.5

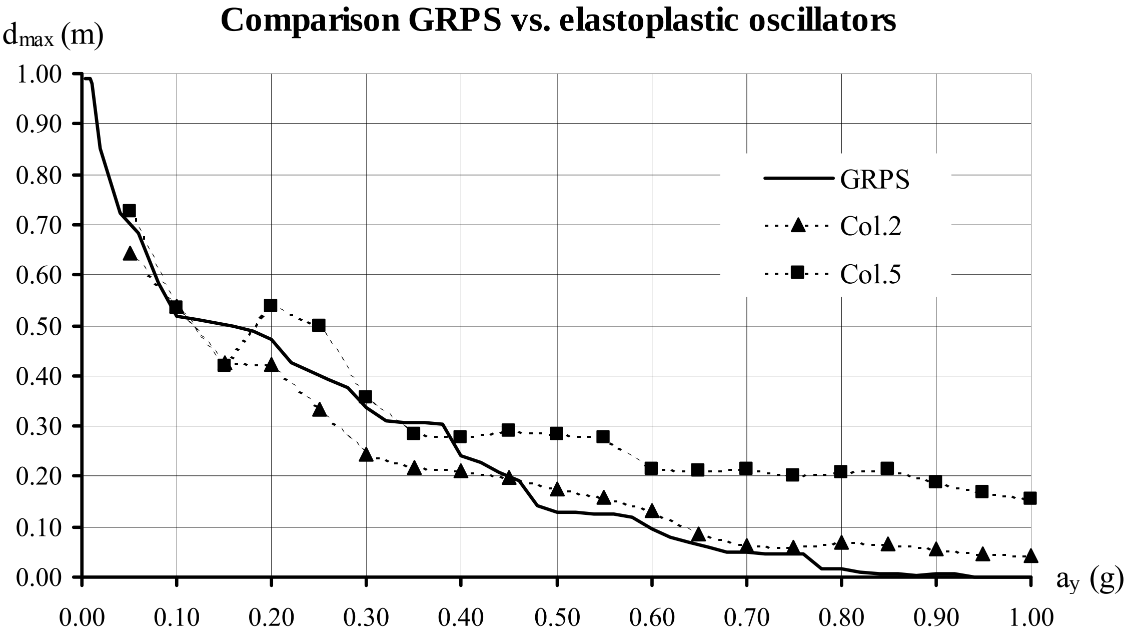

Figure 3.27 - Comparison between the GRPS and corresponding curves for each of the column oscillators

oscillators.

Let us concentrate first on the development of the two elastoplastic curves alone. For low levels of a_y ($a_y \leq 0.45g$), the agreement between both curves is quite satisfactory considering the difference in stiffness between both oscillators. In fact, for $a_y \leq 0.15g$ there is virtually no difference between the displacement demand in both systems, and for $0.15 \leq a_y \leq 0.45g$, the ration $d_{max,Col.2} / d_{max,Col.5}$ does not exceed 2/3. From Table 3.5, it is seen that the expected ductility demand, $\mu_{\theta,exp}$, is at least 7 for both oscillators when $a_y \leq 0.45g$, thus confirming the hypothesis of the RPSD method, i.e. the disregard of the elastic properties of the structural system for the dynamic response dominated by plastic deformations at the yield zones. For $a_y > 0.70g$, the above-mentioned ratio is below 1/2, while for $a_y > 0.85g$ it is below 1/3.

Regarding the agreement between the elastoplastic curves and the GPRS, we can point out two different regions for each oscillator in the range of a_y: Region 1, where the estimates provided by the GRPS are either conservative or not exceeded by 25%; Region 2, where the estimates by the GRPS are considerably lower, thus unsafe, than the maximum displacement demand observed in the elastoplastic oscillators. Obviously, the first region is of interest when defining the limits regarding the application of rigid-plastic spectra for design purposes.

For the Col.5 oscillator, good agreement with the GRPS is reached for $a_y \leq 0.4g$ whereas for the Col.2 oscillator this range is extended to $a_y \leq 0.75g$. For the first oscillator we have for $a_y = 0.4g$, $d_{max} = 0.28m$, which is 15% higher than the prediction of the GRPS. For the Col.2 oscillator we have $d_{max} = 0.06m$ for $a_y = 0.75g$, which is 25% higher than the value estimated by the GRPS.

Notably, from Table 3.5 we find that $\mu_{\theta,exp}$ at those values of a_y is remarkably close for both oscillators: 8.4 for Col.5 oscillator and 10.2 for Col.2 (the bold-faced values). Thus, it seems that the ability of the GPRS to accurately predict maximum dynamic response on oscillators with flexural yielding is assured if the expected rotation ductility demand is at least in the range of the values mentioned above. This is indeed an important conclusion as it provides the user of the RPSD method with a quantitative parameter to assess beforehand the validity of the assumption concerning disregard for elastic behaviour on the overall dynamic response, and therefore, on the reliability of the estimations of the GRPS.

3.3.2 Strength distribution in the RPSD method

Until now we have been dealing with the dynamic response of rigid-plastic structures, accepting without reservations that the structure is designed so that only the chosen collapse mechanism is formed for periods of plastic or slip behaviour. The enforcement of the chosen collapse mechanism is the subject treated below.

From the discussion held in section 1.3, it is concluded that in plastic design, to ensure that a specific collapse mechanism takes place when the structure is subjected to a given load, the strength demand outside the hinges must not exceed the local strength capacity.

In rigid-plastic structures subjected to ground motion, this is carried out by determining only one safe stress field from all the possible safe stress fields outside the hinges after the lower bound theorem of Plasticity. There are only two requirements for these stress fields:

a) Dynamic equilibrium must be satisfied at all times, taking into account both lateral loading due to ground motion and other loads at the time of the earthquake (e.g. dead or live loads)

b) Yielding does not take place at any point in the structure outside the hinges.

Clearly, there will be a number of possible safe stress fields in the structure. Therefore, once again, the engineer must make one more decision, related to the way the structure is going to carry the stresses imposed by the ground motion. The decision must be carried out according to engineering judgement after weighing up considerations with respect to structural performance and economy of design. Depending on the complexity of the structure, this task might be repeated until a satisfactory solution is found. There is no silver bullet for this problem, only engineering judgement and experience.

The determination of a safe stress field consists of three main steps:

1. To choose a number of point values that make the structure statically determined. In structures under dynamic loading, the simplest way is probably to choose the yield capacities at the plastic hinges.
2. Imposing dynamic equilibrium leading to the strength demand in the remaining part of the structure.
3. Finally, the strength capacity in the part of the structure outside the hinges is determined on the basis of the choice of an appropriate overstrength factor applied to the strength demand derived in the previous step.

However, one problem remains for the determination of the safe stress field. This is the determination of the lateral external force field in the structure so that point 2 above may be carried out. Obviously, here we assume that other loads present at the time of the earthquake remain constant with time.

The lateral external force field in the structure is given by the general expression:

$$F_i(t) = -m_i \cdot \left[\phi_i \cdot a_r(t) + a_g(t) \right] \qquad (3.37)$$

Once the generalised strength, F_y*, has been derived, the dynamic response of the structure against *any* ground motion is fully determined. Therefore, considering (3.31) and (3.32), the expression in (3.37) may be expanded according to the type of behaviour at the structure:

$$\begin{array}{ll} \text{Plastic behaviour:} & \begin{cases} F_i(t) = -m_i \cdot \left[-\phi_i \cdot \kappa \cdot a_y + a_g(t) \cdot \left(1 - \phi_i \cdot \kappa\right) \right] \text{ if } v_r(t)>0 \\ F_i(t) = -m_i \cdot \left[+\phi_i \cdot \kappa \cdot a_y + a_g(t) \cdot \left(1 - \phi_i \cdot \kappa\right) \right] \text{ if } v_r(t)>0 \end{cases} \\ \text{Slip behaviour:} & F_i(t) = -m_i \cdot a_g(t) \cdot \left(1 - \phi_i \cdot \kappa\right) \qquad (3.38) \\ \text{Rigid behaviour:} & F_i(t) = -m_i \cdot a_g(t) \end{array}$$

From (3.38) it is concluded that if a_y is known, then the lateral external force field in the structure is dependent on the ground motion, $a_g(t)$, and in the case of plastic behaviour, the direction of the collapse mechanism.

Thus, it seems clear that in a design situation, one may find the lateral external force field in the structure if one knows the ground motion records included in the rigid-plastic spectra used to determine a_y. However, despite the simplicity in carrying out rigid-plastic NLTHA, it is clear that this option is not practical from a user perspective. Firstly, these records might not be available, and secondly, if they are, determining the dynamic response of the structure to each ground motion record (part of the GRPS), seems to be a highly cumbersome task to undertake, given the number of records necessary to adequately define the rigid-plastic spectra.

Therefore, one needs to find a simplified approach to determine the lateral external force field required for design purposes.

The extreme loading scenarios approach

Before discussing the application of the extreme loading scenarios approach in the determination of the required loading cases for design purposes, an important remark must be added.

When a rigid-plastic structure has rigid behaviour, all the yield zones are below the yield point and therefore the stress field is undetermined. This means that the last expression in (3.38) is irrelevant for the purpose of determining the local strength demand on the structure for periods of rigid behaviour. However, for design purposes, this is not a serious setback of the rigid-plastic formulation simply because periods of rigid behaviour do not correspond to periods of maximum demand on the structure.

From previous discussions, cf. section 3.1.1, it is obvious that when the structure has rigid behaviour, the strength demand at the yield zones does not exceed the local capacity. Bearing in mind that rigid behaviour is only possible for $|a_g(t)| \leq a_y$ (see again (3.31)), and observing the last expression in (3.38), it follows that the maximum strength demand outside the yield zones for periods of rigid behaviour takes place precisely when the structure is about to undergo plastic behaviour in the positive or in the negative direction.

From the above discussion it is concluded that only for periods of plastic or slip behaviour will one find the maximum strength demand at any point in the structure. This is highly convenient since for these periods the collapse mechanism is activated and thus, the stress field is fully determined.

The first assumption must be that at this point we have already determined a_y following the procedure described in the previous section. Examining expression (3.38), it is concluded that when the collapse mechanism is activated, the lateral external force field in the structure depends on the ground motion $a_g(t)$, and in the case of plastic behaviour, the direction of the collapse mechanism. When the structure has plastic or slip behaviour, the strength demand at the yield zones does not change with time, as it equals the local yield capacity or zero, respectively. Consequently, the maximum strength demand at any point of the structure is linearly dependent on the ground motion, and in the case of plastic behaviour only, the direction of the collapse mechanism.

Therefore, the extreme values of strength demand at a point in the structure outside the hinges are definitely reached when the ground acceleration reaches its peak value, i.e. the PGA value, and the collapse mechanism is activated. However, we do not know the direction of the ground motion that will hit the structure, nor the type of behaviour that the structure experiences at the time of $a_g(t)$=PGA. Moreover, maximum strength demand at different points of the structure outside the hinges does not necessarily take place for the same value of ground acceleration.

From this, and with the aim of covering all possible scenarios, one must consider a set of lateral external force fields corresponding to $a_g(t)$=+PGA and $a_g(t)$=—PGA in each of the expressions in (3.38) for plastic or slip behaviour.

The diagram in (3.39) shows each of the so-called extreme loading scenarios.

$$\bullet\text{Plastic behaviour}\begin{cases}\text{Collapse mechanism in the positive direction}\begin{cases}a_g(t)=+PGA\\ a_g(t)=-PGA\end{cases}\\ \text{Collapse mechanism in the negative direction}\begin{cases}a_g(t)=+PGA\\ a_g(t)=-PGA\end{cases}\end{cases}$$

$$\bullet\text{Slip behaviour}\begin{cases}a_g(t)=+PGA\\ a_g(t)=-PGA\end{cases} \tag{3.39}$$

In Table 3.6 we summarise the application of the extreme loading scenarios approach to the case of the structure considered in section 3.2.3. The inclination of the frame there refers to the sign of the relative velocity, $v_r(t)$.

Examining the expression of Table 3.6, we conclude that the extreme loading scenarios approach yields a set of three symmetrical loading cases, which may induce the idea that only consideration of three loading cases is enough to find the maximum strength demand at any point of the structure. However, this is not generally valid, as the strength demand at any point of the structure depends also on the choices on the safe stress field.

The extreme loading scenarios approach yields a conservative set of external forces in the structure as the PGA only takes place in one direction and at a single time instant t. However, this is not considered a setback in the formulation since we are aiming at determining design values, which of course have to be safe.

It should be noted that the expressions in Table 3.6 are derived on the basis of the equation of motion. As seen in section 3.2.3, the latter were derived using the virtual work principle, which is a statement of equilibrium. Thus, any external force field resulting from the expressions in Table 3.6 respects equilibrium.

For the RPSD method, the extreme loading scenarios approach is a very convenient tool, due to the simplification introduced in the task of determining a safe stress field in the structure. The first advantage clearly deals with the fact that the user does not have to perform NLTHA. The second advantage is that the stress field found is always safe regardless of the shape of the ground motion. The latter advantage deserves further explanation:

In reality, the assumption of considering PGA values for the ground acceleration makes the above-mentioned task independent of the ground motion, as the quantity PGA is normally given at the beginning of the design process as a specification on the performance criterion (for instance, one might say that a given structure has to perform within a specified limit when subjected to ground accelerations up to a PGA value). Bearing this in mind and examining the expression in Table 3.6, it is seen that the lateral forces used for design purposes depend only on the choice of the collapse mechanism, which is reflected in the parameters κ and ϕ_i, and on the choice of the performance criterion in the local seismicity, given by parameter a_y. They are independent of the specific shape of the ground motion. Therefore, we conclude that:

a) if one finds a stress field which is safe for all the extreme loading scenarios in Table 3.6

b) if the ground motion that will actually hit the structure is such that $a_y \leq |a_g(t)| \leq PGA$

c) if the ductility capacity of the structure is not exceeded under that ground motion then the chosen collapse mechanism is formed and the structure is able to carry out the lateral strength demand independently of the shape of the ground motion that will actually hit the structure.

Table 3.6 - The extreme loading scenarios approach

Plastic Behaviour	Mechanism in the positive direction	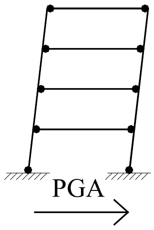 $F_i(t) = -m_i \cdot \left[-\phi_i \cdot \kappa \cdot a_y + PGA \cdot \left(1 - \phi_i \cdot \kappa\right)\right]$
		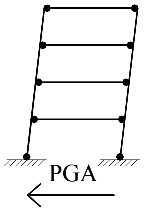 $F_i(t) = -m_i \cdot \left[-\phi_i \cdot \kappa \cdot a_y - PGA \cdot \left(1 - \phi_i \cdot \kappa\right)\right]$
	Mechanism in the negative direction	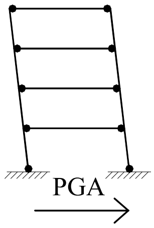 $F_i(t) = -m_i \cdot \left[\phi_i \cdot \kappa \cdot a_y + PGA \cdot \left(1 - \phi_i \cdot \kappa\right)\right]$
		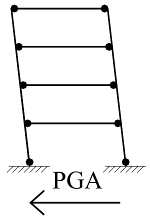 $F_i(t) = -m_i \cdot \left[\phi_i \cdot \kappa \cdot a_y - PGA \cdot \left(1 - \phi_i \cdot \kappa\right)\right]$
Slip behaviour	The stress field depends only on the direction of the ground acceleration	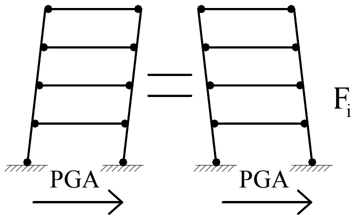 $F_i(t) = -m_i \cdot PGA \cdot \left(1 - \phi_i \cdot \kappa\right)$
		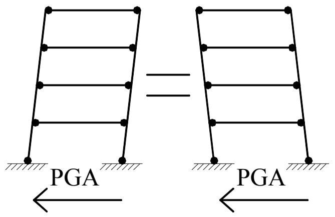 $F_i(t) = m_i \cdot PGA \cdot \left(1 - \phi_i \cdot \kappa\right)$

It is further observed that the lateral external force field yielded by the extreme loading scenarios approach is independent of the choices regarding the safe stress field that initiate the procedure determining the force demand at any point of the structure (see point 1 in page 117) . In fact, the lateral external forces in the structure are completely defined immediately after one has determined ϕ_i, κ and a_y. This yields two important features for the RPSD method:

- There is an effective separation between strength distribution in the structure and dynamic response. It was seen that the dynamic response of the structure is solely dependent on the generalised strength, F_y*, which is related to the dissipation capacity. Therefore, regardless of the choices made on the safe stress field, as long as F_y* is kept constant, the structure develops the same dynamic response.
- The task of calibrating the final design of the structure is simplified to a great extent since the equilibrium conditions defining the force demand outside the yield zones may be expressed in terms of a number of parameters that reflect the choices of the designer regarding the safe stress field. From a practical point of view, this is seen as a highly valuable feature of the RPSD method.

3.3.3 Conclusions

In this section the procedures to determine the seismic demand on the RPSD method were discussed.

The first was the determination of the generalised yield strength, F_y*, using the rigid-plastic spectra. F_y* is decided on the basis of desired performance against ground motion following a simple graphical procedure. It was seen that this is a rational procedure according to the main assumption of the RPSD method, which is to consider the dynamic response of the structure controlled by plastic behaviour at the yield zones.

The rigid-plastic spectra are a valuable tool for design purposes for the following reasons:

- The GRPS can easily be scaled up or down according to ground motion intensity expected at the implementation site.
- The seismic demand associated with a number of ground motion records is simply given by the envelope of each of the corresponding GRPS.

It was seen that the GRPS tends to be a continuous descendent line in the a_y-range as the number of records accounted for increases. Conservatively, if more than one value of a_y is found for the same value of R_{max}, the highest a_y value should be considered in the design process.

The study presented in section 3.3.1 showed that the GRPS may effectively predict the maximum dynamic demand on reinforced concrete oscillators with flexural hinging when the expected rotation ductility demand is at least of the order of 8-10 if calculations are carried out according to section 2.3. Given the full analogy between rigid-plastic oscillators and rigid-plastic structures, similar figures are expected for the case of MDOF systems.

In the RPSD method, strength is distributed on the basis of the lower bound theorem of plasticity, i.e. on the choice of a safe stress field. The lateral force demand is conservatively estimated using the extreme loading scenarios approach.

The latter approach releases the designer from performing NLTHA and is explicitly expressed in terms of his/ her decisions for a suitable collapse mechanism and the desired performance of the structure in the local seismicity of the region. This makes the dynamic response of the structure independent of the choices regarding strength distribution and to a great extent facilitates calibration of the final design.

The combination of both rigid-plastic spectra and of the extreme loading scenarios approach yields a straightforward procedure towards final design and allows an effective separation between the properties of the structure and those of the ground motion. This has been one of the most difficult challenges in Earthquake Engineering, to which elasticity based seismic design procedures have not been able to provide satisfactory solutions:

As referred in the beginning of this section, in the overwhelmingly majority of the design cases, the information initially available refers to the mass distribution, geometry of the structure and the desired target performance against the expected ground motion scenario. Additionally, the designer has information about the seismicity at the implementation site. This may be the elastic spectrum if he/ she prefers to use the Elastic Spectrum Method, the GRPS if the RPSD method is to be used, or local accelerograms if the design is based on NLTHA.

In design methods where the elastic properties of the structure play a role, in order for the seismic demand on the system to be determined, one has to know the strength capacity and stiffness distribution beforehand in the design process. However, these are obviously unknown. Strength capacity and stiffness distribution are of course the properties up to the structural engineer to define. So, initially the engineer is forced to “guess” those parameters normally using simplified empirical relations that may only provide crude estimations and then undergo an iterative process between assessing the seismic demand and changing the design in terms of strength capacity and stiffness distribution until the performance criteria are met within desired limits. Every time the design changes, a new structure has to be checked against the ground motion scenario at the implementation site, in turn changing the performance of the new structure.

In the RPSD method, the information initially available is necessary to determine with significant levels of certainty the suitable collapse mechanism. From this, it follows that κ is known. The designer then uses the GRPS which is characteristic of the ground motion alone and magnifies it by κ, which is characteristic of the structure and the chosen collapse mechanism. At this point, the designer is able to assess the maximum dynamic demand on the structure for any value F_y^*. Therefore, using the SRPS, the designer considers the performance criterion and determines the energy dissipation capacity of the system, expressed by F_y^*. At this point, the dynamic response of the structure is fully determined. The designer can proceed to the final design of the structure by determining first the lateral force demand, which is made independent of the ground motion by means of the extreme loading scenarios approach. The final distribution of strength and hence of stiffness throughout the structure is carried out making choices regarding the most appropriated stress field, until a satisfactory solution is reached.

3.4 P-Δ effects in the RPSD method

Until now, we have tacitly assumed that the equations of motion are written disregarding the effect of change of geometry. Of course, this may lead to unconservative estimations of the dynamic response of the structure if this is loaded to levels close to instability. This is the case of structures with large normal compression forces or with reduced lateral resistance.

Here, we treat geometric non-linearity only for the case of P-Δ effects. The change of geometry due to large displacements is not considered in this work. We assume that for design situations, the magnitude of maximum displacement demand is "small" enough to consider the estimations to be accurate on the dynamic response without the effect of change of geometry due to large displacements.

3.4.1 The case of rigid-plastic oscillators

From classical beam-column theory, it is well known that the effect of change of geometry may be taken into account by adding a fictitious external moment per unit length $\pm N\partial u/\partial x$, the sign depending on the sign conventions used, (Timoshenko et al., 1961), (Nielsen et al., 1973) and (Nielsen, 2000). Here, N is the normal force, u the deflection and x a coordinate along the beam axis. For a column with constant normal force N, the external moment for any selected length is statically equivalent to two transverse opposite forces at the ends: $\pm N\cdot\psi$, ψ being the inclination relative to the beam axis of a straight line connecting the end points of the length considered. The result is independent of the actual deflection shape along the length.

In the case of the column oscillator in section 3.2.1, see Figure 3.4b), the axial force in the column is the weight of the mass, m·g. Therefore, the transverse forces at the columns ends will be:

$$\pm N\cdot\psi(t)=\pm m\cdot g\cdot\frac{d_r(t)}{L} \tag{3.40}$$

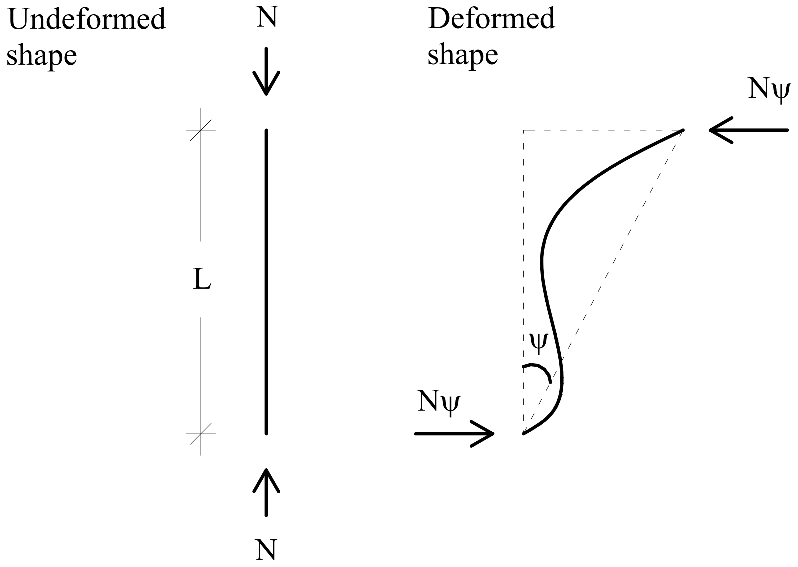

Figure 3.28 - The consideration of P-Δ effects on a single column

It is clear that the force applied at the mass has the same sign as the relative displacements, $d_r(t)$, according to the adopted sign convention. Thus, to take into account P-Δ effects, the general formulation of the equation of motion in (3.12) is transformed into:

$$a_r(t) = \frac{M(t)}{m \cdot L} - a_g(t) + g \cdot \frac{d_r(t)}{L} \tag{3.41}$$

Following the explanations regarding the formulation of the equations of motion according to the type of behaviour at the plastic hinges given in section 3.2.1.1, it is concluded that for any column oscillator with length L, one has:

$$\begin{array}{ll}
\text{Plastic behaviour:} & \begin{cases} a_r(t) = -\dfrac{F_y}{m} - a_g(t) + g \cdot \dfrac{d_r(t)}{L} & \text{if} \quad |f(t)| = f_P \quad \text{and} \quad v_r(t) \geq 0 \\ a_r(t) = +\dfrac{F_y}{m} - a_g(t) + g \cdot \dfrac{d_r(t)}{L} & \text{if} \quad |f(t)| = f_P \quad \text{and} \quad v_r(t) \leq 0 \end{cases} \\
\text{Slip behaviour:} & a_r(t) = -a_g(t) + g \cdot \dfrac{d_r(t)}{L} \quad \text{if} \quad f(t) = 0 \quad \text{and} \quad v_r(t) \cdot d_r(t) < 0 \\
\text{Rigid behaviour:} & a_r(t) = 0 \quad \text{if} \quad |a_g(t)| < \dfrac{F_y}{m}
\end{array} \tag{3.42}$$

Physically, the "P-Δ forces" will resist any tendency of the system to return to its original undeformed position. This is captured in the equations in (3.42). Therefore, when the oscillator experiences plastic behaviour, the P-Δ forces increase the magnitude of plastic deformations. On the other hand, if the hysteretic relationship at the plastic hinge accounts for the effect of pinching and the system has slip behaviour, then these forces will oppose the motion towards the undeformed position. If the yield zone in the oscillator has the classic rigid-plastic hysteretic relationship, it is seen that P-Δ forces resist the motion of the mass while the system is recovering residual deformations in plastic behaviour, i.e. cf. Figure 3.2a), if the hysteretic curve is in the 2nd or 4th quadrant then the P-Δ forces have opposite signs to the velocity of the mass.

Examining the system of equations in (3.42), it is concluded that the dynamic response is now dependent on the relative displacement quantity. This implies that we must now deal with non-linear equations of motion, which are of much higher complexity. Therefore, the computational procedure given in section 3.2.1.2 is no longer valid. One possible solution to this problem is to proceed with direct integration of the equation of motion using the linear acceleration step-by-step method, see section 1.2.1.1. The only change we have to make is on the parameter $\bar{k}_i$, cf. equation (1.17)

$$\bar{k}_i = -\frac{g}{L} + 6 \cdot \frac{m}{\Delta t^2} \tag{3.43}$$

It is further observed in equations in (3.42) that the dynamic response of oscillators is no longer solely due to the parameter $a_y = F_y/m$. This is because a new geometric term characteristic of the oscillator is introduced, the length of the column L. Therefore, it is no longer valid that rigid-plastic oscillators with the same value for a_y develop the same dynamic response. This makes it impossible to construct a rigid-plastic spectrum solely dependent on the ground motion. For this reason, in the RPSD method, the evaluation of P-Δ effects is done after the determination of F_y* using the procedure illustrated in Figure 3.24b). Hereafter, a rigid-plastic NLTHA including P-Δ effects should be carried out using the procedure described above. If the latter reveals that P-Δ effects introduce further severe displacements, additional lateral resistance has to be assigned to the system, which may be reflected by increasing the parameter F_y*.

3.4.2 The case of rigid-plastic structures

In this section it is seen that the analogy between rigid-plastic structures and rigid-plastic oscillators is still valid when determining the dynamic response against ground motion.

The idea remains the same, i.e. to consider a set of equivalent horizontal forces that adequately reproduce the influence of P-Δ effects in the dynamic response.

An explanation will be provided for the case of frame structures with lumped mass at each floor. However, formulation of the equations of motion follows the same reasoning as described here for other types of structural systems.

For illustration purposes, consider that the 12-storey plane frame of Figure 3.29 is designed to develop the collapse mechanism shown in the right hand side of the figure.

Figure 3.30 depicts the axial forces and the corresponding equivalent transverse forces in two consecutive columns in the deformed shape. Note that the inter-storey drift is the same at each floor, which implies that the inclination ψ is the same for each floor.

It is initially observed that the magnitude of the axial forces at each column of each floor, N_i and N_{i+1} in Figure 3.30, is no longer statically determined, as this depends on the choices on the safe stress field. Note that in the RPSD method, the dynamic response of the system is to be first treated based on the assumption of the collapse mechanism and then one proceeds to the distribution of strength. However, considering equilibrium, we know that the sum of the axial forces at each floor has to

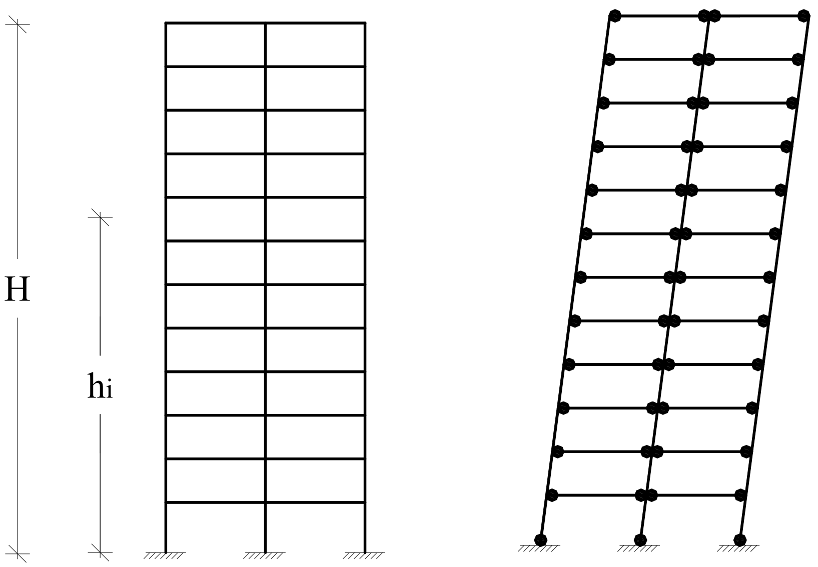

Figure 3.29 -12-storey plane frame and corresponding collapse mechanism

be the weight of the floor plus the weight of the structure above it.

This means that the equivalent horizontal force at each floor i is given by the product of the inclination ψ and the subtraction between the total vertical load at floor i and the total vertical load at the floor above. The latter is the product of the weight of floor i and the inclination ψ. See Figure 3.30.

If we again choose to represent any relative displacement in the deformed shape of the structure proportional to the relative displacement at the top floor, d_r, then $\psi=d_r/H$. Thus, the horizontal external force field in the structure due to P-Δ effects, F_i, is given by:

$$F_i = m_i \cdot g \cdot \frac{d_r}{H} \tag{3.44}$$

Consider the choice of a collapse mechanism with upper rigid floors. Then, since $\psi=0$ for these floors, between each rigid floor there will be no horizontal force applied. However, in the uppermost non-rigid floor, the j-th floor, the horizontal force is given by $N_j \cdot g \cdot \psi$ (imagine that in Figure 3.30, the upper column would remain in the undeformed shape. For this case, $N_{i+1}=0$). Therefore, the horizontal force in the uppermost non-rigid floor is given by:

$$F_j = \sum_{i=j}^{n} m_i \cdot g \cdot \frac{d_r}{H} \tag{3.45}$$

Please note that in equation (3.45), n is the total number of floors in the frame, d_r is

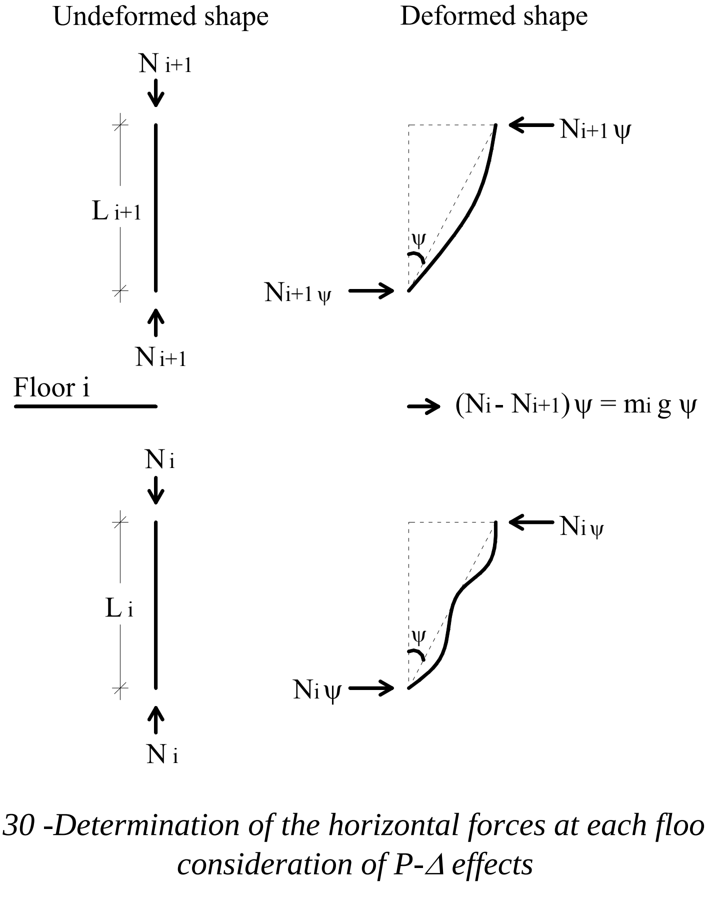

Figure 3.30 -Determination of the horizontal forces at each floor i for the consideration of P-Δ effects

the relative displacement of the j-th floor, and H the corresponding height. The horizontal forces in the floors below are given by expression (3.44)

Having determined the external force field due to P-Δ effects, the corresponding virtual work for the displacement increment δ is derived and added to the virtual work equation of the structure using the same format as in (3.26) of section 3.2.3. Examining expressions (3.44) and (3.45), it is concluded that regardless of the consideration of upper rigid floors or not, the contribution of the equivalent horizontal forces for the virtual work equation is:

$$\begin{aligned} &+\sum_{i=1}^{12} m_i \cdot g \cdot \frac{d_r(t)}{H} \cdot \phi_i \cdot \delta = 0 \quad \text{if} \quad \delta > 0 \\ &-\sum_{i=1}^{12} m_i \cdot g \cdot \frac{d_r(t)}{H} \cdot \phi_i \cdot \delta = 0 \quad \text{if} \quad \delta < 0 \end{aligned} \tag{3.46}$$

Applying the same reasoning from (3.26) to (3.31) in section 3.2.3 leads to the following system of equations of motion for rigid-plastic structures with the consideration of P-Δ effects.

$$\text{Plastic behaviour:} \quad \begin{cases} a_r(t) = -\dfrac{F_y^*}{m^*} - \kappa \cdot a_g(t) + \kappa \cdot g \cdot \dfrac{d_r(t)}{H} \quad \text{if} \quad \left|f_j(t)\right| = f_{P+,j} \quad \text{and} \quad v_r(t) \geq 0 \\ a_r(t) = +\dfrac{F_y^*}{m^*} - \kappa \cdot a_g(t) + \kappa \cdot g \cdot \dfrac{d_r(t)}{H} \quad \text{if} \quad \left|f_j(t)\right| = f_{P-,j} \quad \text{and} \quad v_r(t) \leq 0 \end{cases}$$

$$\text{Slip behaviour:} \quad a_r(t) = -\kappa \cdot a_g(t) + \kappa \cdot g \cdot \frac{d_r(t)}{H} \quad \text{if } f_j(t) = 0 \text{ with } j \in \left[1, n\right] \quad \text{and} \quad v_r(t) \cdot d_r(t) < 0$$

$$\text{Rigid behaviour:} \quad a_r(t) = 0 \quad \text{if} \quad \left|a_g(t)\right| < \frac{F_y^*}{\kappa \cdot m^*} \tag{3.47}$$

As expected, the P-Δ effects do not play a role in the analogy between rigid-plastic oscillators and rigid-plastic structures. Therefore, the dynamic response of rigid-plastic structures with P-Δ effects is determined applying the same procedure as for rigid-plastic oscillators. The computational procedure after Paz, cf. section 1.2.1.1, may be used again to derive the dynamic response of rigid-plastic structures against a specific ground motion. The parameters $\bar{k}_i$ and ΔF_i are as follows:

$$\bar{k}_i = -\kappa \cdot \frac{g}{H} + 6 \cdot \frac{m^*}{\Delta t^2} \tag{3.48}$$

$$\Delta F_i = -\kappa \cdot m \cdot \Delta a_g + m^* \cdot \left(6 \cdot \frac{v_r(t_i)}{\Delta t} + 3 \cdot a_r(t_i) \right) \tag{3.49}$$

Note that, as in the case of rigid-plastic oscillators, the dynamic response also depends on the geometry parameter H. Therefore, the closing remarks of the previous section also apply to the case of rigid-plastic structures. In the design process, P-Δ effects are to be checked after the determination of F_y^* using the procedure described in section 3.3.1.

3.4.3 Conclusions

In this section, an explanation was given for how P-Δ effects may be taken into account in the dynamic response of rigid-plastic structures designed to develop a chosen collapse mechanism. It was seen that the analogy between rigid-plastic oscillators and rigid-plastic structures is still conserved.

The equations of motion considering P-Δ effects are of the non-linear type and therefore the complexity of the computational procedure increases. However, rigid-plastic NLTHA still display greater simplicity than the standard ones.

Moreover, it was seen that the seismic demand on the structure cannot be determined based on the rigid-plastic spectra, which implies that P-Δ effects must be checked after the determination of F_y* (without P-Δ effects). If the displacement criteria are substantially violated by the P-Δ effects, the lateral resistance must be increased and a new calculation must be done.

3.5 The Rigid-Plastic Seismic Design method step-by-step

In the following, the formulation of the RPSD method in a step-by-step format is given.

Step 1 – Choice of a suitable collapse mechanism

Clearly this is the most important step in the RPSD method, as this choice is reflected in all subsequent steps. Essentially, the designer chooses the most adequate way for the structure to dissipate energy during strong ground motion. In practical terms, the output of this initial step is the determination of ϕ_i, m* and κ.

Previously it was concluded that the data available at the beginning of the design process (mass distribution, geometry and desired performance) is necessary to decide the shape of a suitable collapse mechanism.

The guidelines leading to the choice of an appropriate collapse mechanism have already been discussed in detail throughout sections 1.1 and 2.4:

- Extensive distribution of plastic dissipation throughout the structure.
- The target displacement demand must be reached with the smallest non-linear deformation demand at the plastic hinges.
- Local flexural modes of failure should be enforced and allocated in parts of the structure with accessibility for repairing work after the earthquake event.
- Local brittle failure must be prevented. Therefore, a significant part of the energy dissipation must be allocated in structural elements where ductile behaviour may be provided more easily (beams and columns in low shear and axial stresses).

Step 2 – Choice of a dynamic performance criterion, R_{max}

The extent of damage in the structure is related to the extent of plastic deformation at the yield zones, which in turn is related to the magnitude of the relative displacements in the structure. Therefore the criterion P, representing the desired performance of the structure, should be expressed in terms of displacement based quantities (e.g. top floor displacement or inter-storey drift in building structures). In this way, global dynamic behaviour may be conveniently related to local damage.

Step 3 – Definition of the required dissipation capacity using the rigid-plastic spectra

After steps 1 and 2, κ and R_{max} are known. Therefore, the required dissipation capacity related to F_y* is determined following the procedure.

1. Definition of the SRPS curve scaling the GRPS curve in the R_{max} – direction by a factor κ, cf. Figure 3.24a) in section 3.3.1.
2. Determination of a_y based on performance criterion, the graphical procedure in Figure 3.24b) of section 3.3.1.
3. Determination of F_y* using expression (3.32) in section 3.3.1.

At this point, the structure may be checked for P-Δ effects by carrying out a number of rigid-plastic NLTHA using the procedure described in section 3.4. If it is found that the magnitude of extra displacements is enough to violate the performance criterion, then the lateral strength must be increased. This is reflected by increasing the parameter a_y until the influence of the P-Δ effects in the dynamic response of the structure are negligible.

It should be noted that after the conclusion of this step, the parameters m*, κ and F_y* are known. Thus, the designer has all the information necessary to write the equations of motion of the structure, cf. expression (3.31) in section 3.2.3, and consequently to assess the dynamic response of the structure against any ground motion.

Step 4 - Choice of an appropriate safe stress field using the extreme loading scenarios approach

This step is subdivided into 3 sub-steps:

1. Application of the extreme loading scenarios approach for the definition of the lateral external force fields of Table 3.6.
2. Choice of a number of requirements for the internal stress field to make the system statically determined
3. Equilibrium of each of the lateral force fields derived in sub-step 1 and other loads at the time of the earthquake and determination of the maximum strength demand at any point of the structure.

Depending on the complexity of the structure, sub-steps 2 and 3 might be repeated until a satisfactory strength distribution is reached. However, it is emphasised that the lateral loading cases of sub-step 1 are not affected by the decisions on the shape of the safe stress field made in sub-step 2.

It is further observed that the lateral external force fields from the extreme loading scenarios approach do not take into account P-Δ effects. This is due to the fact that in step 3 we have assured that P-Δ effects have a negligible influence on the dynamic response. This reduces the change in the lateral external force fields regarding the formulation in Table 3.6, which in fact is already a conservative estimation of the lateral force demand. Moreover, in the final design of the structure, cf. step 5, we use overstrength factors which are intended to deal with any unexpected increase in the strength demand outside the hinges.

Step 5 – Final structural design

At the end of the previous step, the seismic demand at any point of the structure is determined both in terms of displacement and strength demand. Hence, cross-sectional detailing may be carried out.

This may be done on the basis of expected ductility at the yield zones and by ensuring rigidity in the remaining part of the structure. The latter makes use of overstrength factors, cf. section 2.4.3.

Finally, the design may be checked by considering the serviceability limit states for more moderate and frequent ground motions and higher mode effects. Evidently, the rigid-plastic approach cannot provide an accurate solution for these problems, since it neglects the contribution of elasticity in the dynamic response. Therefore, a number of standard NLTHA may be carried out using accelerograms characteristic of moderate ground motion at the implementation site. This may result in an increase in structural stiffness. However, in structures designed according to the RPSD method, the dynamic response against lifetime earthquake events is controlled by the strength demand at the yield zones, which implies that enhancement of stiffness has a rather limited role in the case of ultimate limit states. This has been confirmed by the study in section 3.3.1, where it was shown that oscillators with flexural yielding and with significantly different levels of stiffnesses develop similar dynamic response for rotation ductility demand higher than 7.

3.6 Final remarks

It was seen in this chapter that the RPSD method is a *simple* and *straightforward* design procedure: Simple because almost no computational effort is required and there is no need for pre-design of the structure; Straightforward due to the fact that in the RPSD method, there is an effective separation between the dynamic response of the structure and the strength distribution. In fact, according to the complexity of the structure, there might be some iteration in steps 3 and 4. However, as discussed in section 3.3.2, the shape of the safe stress field found in step 4 in no way affects the dynamic performance of the structure, which is defined after the conclusion of step 3. The same is applied to step 5 where change of stiffness may be required so that the structure satisfies serviceability limit states or the demand arising from higher mode effects. Nevertheless, this does not affect the dynamic performance of the structure against an extreme earthquake event. So, in the RPSD method, whenever the designer proceeds to the following step, there is no need to return to the previous one.

Another important feature of the RPSD method highlighted here is that the user has full control over the design process, especially when selecting the collapse mechanism and the means by which the structure is to carry the stresses during strong ground motion. Therefore, significant engineering judgement is required to weigh up structural performance and economic considerations leading to appropriate choices. The consequence of this lies in the exclusion of any artificial/ empirical considerations unrelated to the physical nature of the response of structures subjected to strong ground motion.

4. Applications of the RPSD method to frame structures

In this section two reinforced concrete frames are designed according to the RPSD method.

The first structure is rather simple. The main purpose of this example is to give a straightforward application of the RPSD method. Concurrently, it will be shown that the dynamic response of a structure designed according to the RPSD method lies within the desired limits and performs as expected, i.e. on the formation of the chosen collapse mechanism and having the response controlled by the behaviour at the yield zones.

In the second example we design a more realistic structure, i.e. a 12-storey three-dimensional frame. Special attention is given to the choice of the ground motion scenario and collapse mechanism using the concept of rigid-plastic spectra. Also the complexity of the structure allows a better illustration of the economic and structural performance considerations leading to the choice of an appropriate safe stress field. The response of both structures in terms of displacement and strength demand is compared by means of refined NLTHA.

The first example has been included in a paper published by the Journal of Earthquake Engineering and Structural Dynamics, while the second is included in a paper written in cooperation with the Ichinose Lab, Nagoya Institute of Technology, Japan, and published in the Proceedings of the 1st European Conference on Earthquake Engineering and Seismology.

4.1 Design of a 4-storey plane frame.

Consider the 4-storey plane frame as in Figure 3.19a). The frame is again reproduced in Figure 4.1 and its specific geometry and mass distribution properties are synthesised in Table 4.1.

The performance criterion upon which the design is based is such that the maximum

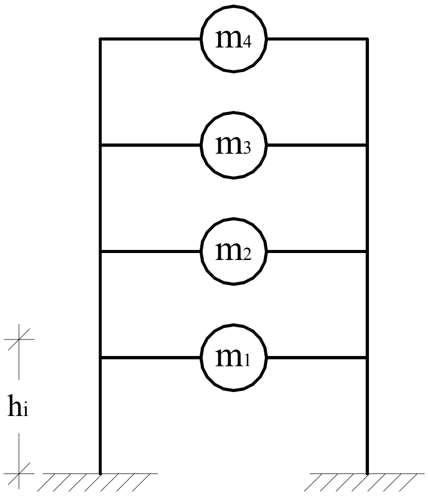

Figure 4.1 - 4-storey reinforced concrete plane frame

Table 4.1 -Mass and height for each floor

Floor i	Mass, m_i (ton)	Height, h_i (m)
1	50	4
2	50	7
3	50	10
4	50	13

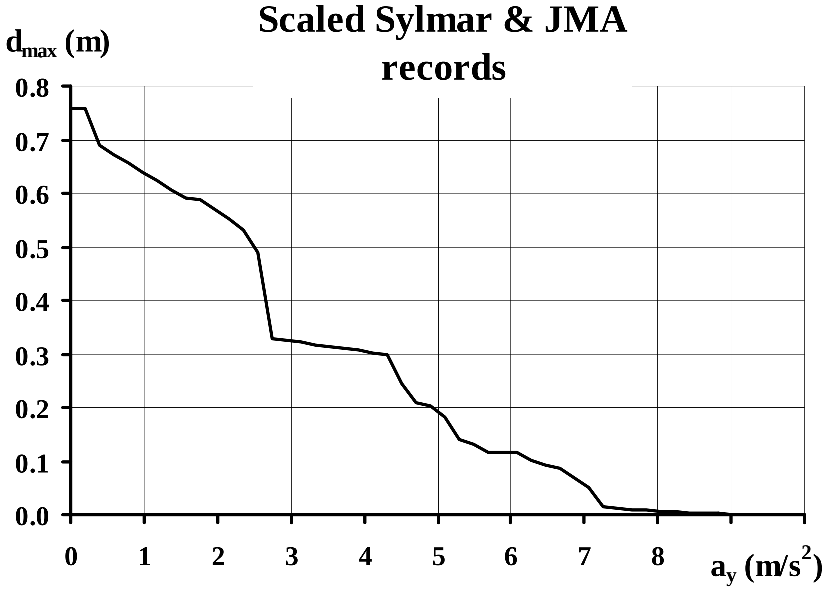

Figure 4.2 - Corrected GRPS of the scaled Sylmar and JMA records so that PGA=1g in terms of maximum displacement, $d_{r,max}$.

inter-storey drift is 2.5% for ground motion up to 1g.

For the sake of simplicity, it is further assumed that the ground seismicity at the implementation site of this structure is conveniently represented by the N-S component of the JMA record of the Kobe Earthquake, 1995, and by the 360 component of the Sylmar record of the Northridge Earthquake, California, 1994. In the future, these records will be referred to as JMA and Sylmar records, respectively.

Since the performance criterion specifies maximum ground acceleration of 1g, we use the GRPS of Figure 3.23 to account for both the Sylmar and JMA records, scaled up so that the PGA value of each record equals 1g. However, we must still apply the correction mentioned in section 3.3.1, *Rigid-plastic spectra for design purposes*, as there can be more than one value of a_y for the same value of performance criterion. The corrected GRPS is shown in Figure 4.2

Step 1 – Choice of a suitable collapse mechanism

For this simple structure, it is evident that the most suitable collapse mechanism is that depicted in Figure 3.19b). In fact with this choice, a significant part of the dissipation capacity is allocated in beam elements with limited axial force, and global displacement demand is reached with minimum deformation demand at the plastic hinges.

Hence, we have:

$$\{\phi\}=\left\{\frac{h_i}{H}\right\}=\{\ 0.31\ ,\ 0.54\ ,\ 0.77\ ,\ 1.00\ \} \tag{4.1}$$

$$m^* = \sum_{i=1}^{4} m_i \cdot \phi_i^2 = 50\times\left(0.31^2+0.54^2+0.77^2+1.00^2\right)=98.82\ \text{ton} \tag{4.2}$$

$$\kappa=\frac{\sum_{i=1}^{4} m_i \cdot \phi_i}{\sum_{i=1}^{4} m_i \cdot \phi_i^2}=\frac{50\times\left(0.31+0.54+0.77+1.00\right)}{98.82}=1.32 \tag{4.3}$$

Step 2 – Choice of a dynamic performance criterion, R_{max}

Due to the shape of the collapse mechanism, the dynamic performance criterion, R_{max}, may be written in terms of the maximum displacement at the top, d_{max}.

$$\text{Maximum drift} = 2.5\% \quad \Rightarrow \quad R_{max}=0.33\text{m} \tag{4.4}$$

Step 3 – Definition of the required dissipation capacity using the rigid-plastic spectra

Firstly, in order to determine maximum dynamic response in the a_y domain of this structure against the Sylmar and JMA record, we magnify the curve in Figure 4.2 in the d_{max} – direction by κ=1.32. The SRPS for this structure is reproduced in the solid line in Figure 4.3.

Reading off from the SRPS, in order for the performance criterion to be met, i.e.

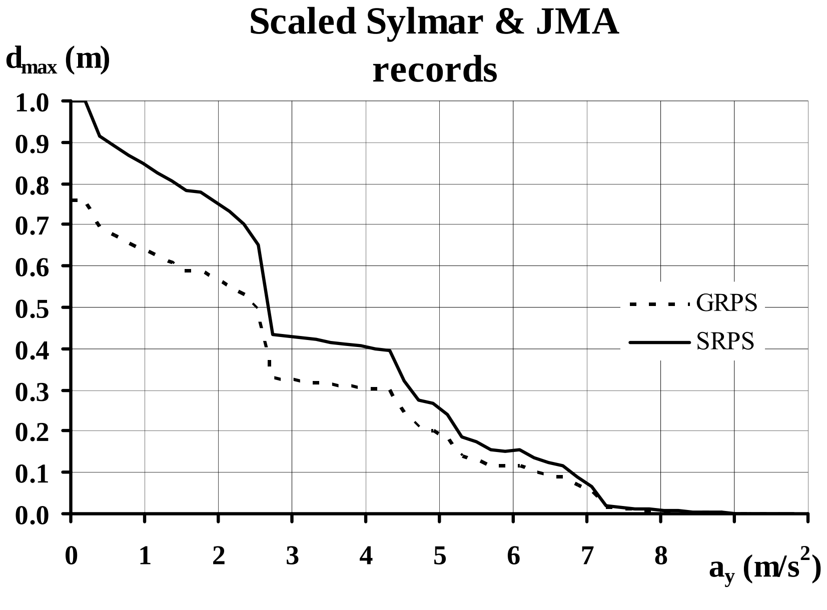

Figure 4.3 -Transition from GRPS to SRPS

R_{max}=0.33m, we find that:

$$a_y = 4.51 \text{ m/s}^2 \tag{4.5}$$

Finally, the parameter F_y*, related with the energy dissipation capacity of this structure is thus defined:

$$F_y^* = \kappa \cdot m^* \cdot a_y = 1.32 \times 98.82 \times 4.51 = 588.3\text{kN} \tag{4.6}$$

Step 4 - Choice of an appropriate safe stress field using the extreme loading scenarios approach

The lateral external force fields to be used for design purposes are defined by introducing the quantities found in (4.1), (4.3) and (4.5) into the expressions in Table 3.6. The result for the six extreme loading scenarios is shown in Table 4.2.

In the present case, we shall make the following considerations regarding the safe stress field:

- All yield moments in the plastic hinges at the ends of the beams, M_P^B, have the same magnitude, M.
- The yield moment at the base of the columns, M_P^C, is related to M by a factor X.
- The base shear force at each floor is equally distributed by both columns.

This yields a symmetric design for the beams and columns.

Since the lateral force demand on the structure is already determined, a particular choice of X is sufficient to determine the stress field in the structure at collapse. Thus,

$$\begin{aligned} M_P^B &= M \\ M_P^C &= X \cdot M \end{aligned} \tag{4.7}$$

As discussed in section 3.2.3, cf. equations (3.28), for this particular structure and collapse mechanism, we have:

$$F_y^* = \frac{M_P^*}{H}, \text{ with } M_P^* = \sum_{j=1}^{10} \left| M_{P+,j} \right| = \sum_{j=1}^{10} \left| M_{P-,j} \right| \tag{4.8}$$

with H being the total height of the structure. Then, M_P* is found to be:

$$M_P^* = F_y^* \cdot H = 588.3 \times 13 = 7648\text{kNm} \tag{4.9}$$

Table 4.2 -Lateral force fields for design purposes (kN)

Floor	Plastic Behaviour				Slip Behaviour	
	Mechanism in the positive direction		Mechanism in the negative direction			
	+PGA	-PGA	+PGA	-PGA	+PGA	-PGA
4	455	141	-140	-455	157	-157
3	237	221	-221	-237	8	-8
2	18	302	-302	-18	-142	142
1	-200	383	-383	200	-291	291

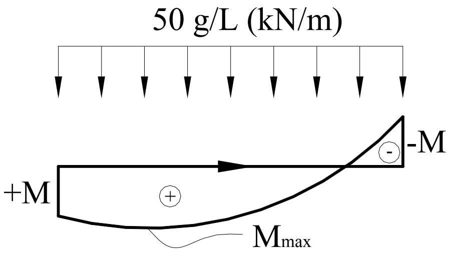

Figure 4.4 -Bending moment field in the beams when the collapse mechanism in the positive direction is activated

Hence,

$$M = \frac{M_P *}{8 + 2 \cdot X} \tag{4.10}$$

Evidently the assumption on lumped masses at each floor is only valid for estimation of the dynamic response of the structure. For the purpose of estimating the strength demand at the beams, we consider that the gravitational forces are uniformly distributed along the length of these elements. Then, when the choice of X has been made, it is a simple matter to determine the entire moment field.

One means of selecting the magnitude of X is to make some requirements on the bending moment field in the beams: static analysis of these beams shows that if X equals 4, then the maximum positive bending moment in the beams, M_{max} in Figure 4.4, is only 9% higher than M. This allows for an economic design as there is no need to use significantly different longitudinal reinforcement throughout the length of the beam. Therefore:

$$X = 4 \quad \Rightarrow \quad \begin{cases} M_P^B = 478 \text{ kNm} \\ M_P^C = 1912 \text{ kNm} \end{cases} \tag{4.11}$$

The system is now statically determined. This implies that the strength demand at any point of the structure may be determined by means of equilibrium of each of the lateral external force fields in Table 4.2 and the distributed vertical load in the beams. In the third to fifth columns of Table 4.3, one finds the maximum strength demand at the critical cross-sections in the columns, i.e. the top and bottom cross-sections at each floor, for X=4. Thus M, V and N are the bending moment, shear force and compressive axial force, respectively. The minimum compressive axial force in the columns is also provided, as this is an important parameter in evaluating the variation of the axial force in the column and in turn the dissipation capacity in the plastic hinges at the base of these structural elements. It should be noted that the values for flexural and shear strength demand in Table 4.3 are written irrespective of the sign, as we have chosen the safe stress field so that the design of the frame will be symmetric.

To enforce the weak beam – strong column concept, cf. section 2.4.2, one might wish to increase the value of X to 6, which yields:

$$X = 6 \quad \Rightarrow \quad \begin{cases} M_P^B = 382 \text{ kNm} \\ M_P^C = 2294 \text{ kNm} \end{cases} \tag{4.12}$$

Table 4.3 - Required strength in the columns for two values of X (kN-m)

Column	Cross-section	X=4				X=6			
		M	V	N_{max}	N_{min}	M	V	N_{max}	N_{min}
4th Floor	Top	478	228	405	86	382	228	373	118
	Bottom	267				300			
3rd Floor	Top	745	346	809	172	554	346	745	236
	Bottom	763				954			
2nd Floor	Top	680	355	1214	258	571	355	1118	354
	Bottom	1349				1636			
1st Floor	Top	871	524	1618	344	1253	524	1490	472
	Bottom	1912				2294			

The maximum positive bending moment in the beams is now 22% higher than the yield moment at the plastic hinges, which is still considered an economic design. The corresponding strength demand is summarised in the first four columns from the left in Table 4.3.

It should be noted in Table 4.3 that the required shear strength per floor is the same irrespective of the choice of X. This is because the lateral external force fields from the extreme loading scenarios approach do not depend on the choice of the safe stress field. In fact, the values in Table 4.3 are easily derived by summing up the forces in Table 4.2 above each floor, divided by 2.

It should also be noted that the shear strength demand increases dramatically in the columns of the first floor. This is the source of many structural failures of building during strong ground motion, leading to so-called “soft-storey mechanisms”. The conservative nature of the estimation of the required strength at any point of the structure in the RPSD method, explained in section 3.3.2, provides greater safety in the prevention of this type of failure.

Another interesting aspect reflected in Table 4.3 is that concerned with the range of variation of the axial forces in the columns. It is seen that the stronger the beams (X=4), the larger this range of variation, resulting in larger compression forces at some periods and rather low axial force for other periods of earthquake loading. It was discussed above in section 2.2.1.3, *Members with varying axial force*, that hinges placed in columns with wide range of variation of the axial forces have poor performance in terms of dissipation capacity during cyclic loading due to restraint in crack closure and increased risk of failure due to sliding shear. Moreover, the flexural strength may be seriously reduced. Therefore, if the design of the structure is made according to the choice X=4, then the dimensions of the column would have to increase in order to prevent large variations in the axial load ratio, ν, and to avoid excessive compressive strains in the concrete. A higher level of confinement should also be attributed in order to maintain the ductile behaviour of the hinges in cyclic loading. For these reasons, the above-mentioned economy achieved in the design of beams may be compromised by the greater safety that should be attributed in the columns.

Bearing this in mind, it seems that the design of the structure according to the choice of X=6 provides a better compromise between structural safety and economy. For illustration purposes however, we consider both lay-outs below.

Step 5 – Final structural design

The design of the structure is carried out assuming that the onset of plastic behaviour in the hinges is due to yielding of the reinforcement. Following the discussion in section 2.4.3, the overstrength factor is set to 1.4. For the sake of simplicity, the geometry of the cross-sections outside the hinges in the beams and of the columns is identical to the corresponding plastic hinges. Furthermore, to assure ductile behaviour, we assume that the maximum tensile reinforcement ratio at the plastic hinges is r_T=0.85%. We further assume the width/ height ratio, β, to be 0.6 for beams and 1 for columns, see the example in section 2.3.

The compressive cylinder strength of the concrete is 25MPa and the reinforcement steel used is Grade B500 Tempcore, cf. Table 2.4.

Table 4.4 refers to the detailing of the different cross-sections in the structure according to the two values of X, as well as expected ductility demand following the procedure discussed in section 2.3. It also provides information regarding the resulting fundamental period of the structure, T, after a modal analysis performed

Table 4.4 -Cross-section detailing

Design	X =4 ; T=0.53s				X =6 ; T=0.55s			
Cross-section	PHC	PHB	C	B	PHC	PHB	C	B
Flexural demand (kNm)	1912	478	2677	669	2294	382	3212	535
Height (m)	0.8	0.6	0.8	0.6	0.85	0.55	0.85	0.55
Width (m)	0.8	0.35	0.8	0.35	0.85	0.35	0.85	0.35
Tensile Reinforcement steel area (mm^2)	5311	1770	7436	2478	5997	1543	8397	2162
Tensile reinforcement ration (%)	0.83	0.82	1.16	1.15	0.83	0.85	1.16	1.19
Shear force demand (kN)	524	405	734	567	524	373	734	522
Plastic hinge length (m)	0.93	0.39	-	-	1.09	0.34	-	-
Rotation capacity (x10^{-2}rad)	6.46	3.57	-	-	7.11	3.46	-	-
Yield Rotation (x10^{-2}rad)	0.32	0.17	-	-	0.35	0.16	-	-
Expected rotation ductility demand	8	15	-	-	7	15	-	-

PHC – Plastic hinges in columns; PHC – Plastic hinges in beams; C – Rest of the columns; B – Rest of the beams

with the commercial FEM programme SAP2000 (Computers and Structures, Inc., 2004).

Referencing Table 4.4, it is seen that all the plastic hinges have enough rotation capacity to cope with maximum displacement demand corresponding to 2.5% drift. Consequently, the expected rotation ductility demand in those elements is at least 7, which indicates that the dynamic response shall be controlled by plastic behaviour. It is therefore expected that the RPSD method will provide accurate estimations for the seismic response of this building against the ground motion scenario accounted for in the GRPS of Figure 4.2.

Comparison with refined NLTHA analysis

In this section, the performance of the structure previously designed according to the RPSD method is assessed by means of NLTHA. For comparison purposes, we use rigid-plastic and refined NLTHA using the first 15 seconds of the scaled accelerograms of the Sylmar and JMA records so that PGA=1g.

The latter is carried out using the commercial FEM program SAP2000, (Computers and Structures, Inc., 2004) in the following way:

- The response is calculated by direct integration of the equations of motion using the Newmark method, with $\gamma=0.5$ and $\beta=0.25$.
- The damping matrix is directly proportional to the stiffness and mass matrixes in such a way that the damping ratio of the first mode equals 0.05.
- The pivot hysteresis model, cf. section 2.2.1.4, has been used to reproduce the flexural behaviour at the plastic hinges: in the columns, the parameters α and β of this model were set to 4 and 0.55, respectively. This is in agreement with the experimental work carried out by (Abrams, 1997), cf. section 2.2.1.3. In the beams, we used $\alpha=8$ and $\beta=0.65$ based on the tests by (Brown and Jirsa, 1971), cf. section 2.2.1.1.
- The remaining part of the structure is modelled using elastic linear elements, the stiffness of which is derived on the basis of the internal forces in Table 4.3 magnified by the overstrength factor[1].

Figure 4.5 shows the relation between the flexural demand and the top displacement for the plastic hinges at the base of the column on the left-hand side (PHC), and at the left end of the beam of the 4th floor (PHB) for the structure designed according with X=4. The curves correspond to the refined NLTHA and refer to the period between t=6.72s and t=9.42s of the JMA record, this imposing maximum displacement demand in the structure.

Although not shown, the behaviour of the hinge in the right-hand side column and the hinges on the left end of the beams is identical to their counterparts in Figure 4.5. The curve representing the hysteretic behaviour of the hinges located in the right end of the beams is symmetric with respect to the top displacement axis to the dashed curve in Figure 4.5.

---

[1] In connection to the discussion held in section 1.2.2 in this example we will not regard the solution of the FEM programme in terms of distribution of strength demand for the sake of comparison between the internal forces derived in the RPSD method based on the extreme loading scenarios approach and refined NLTHA.

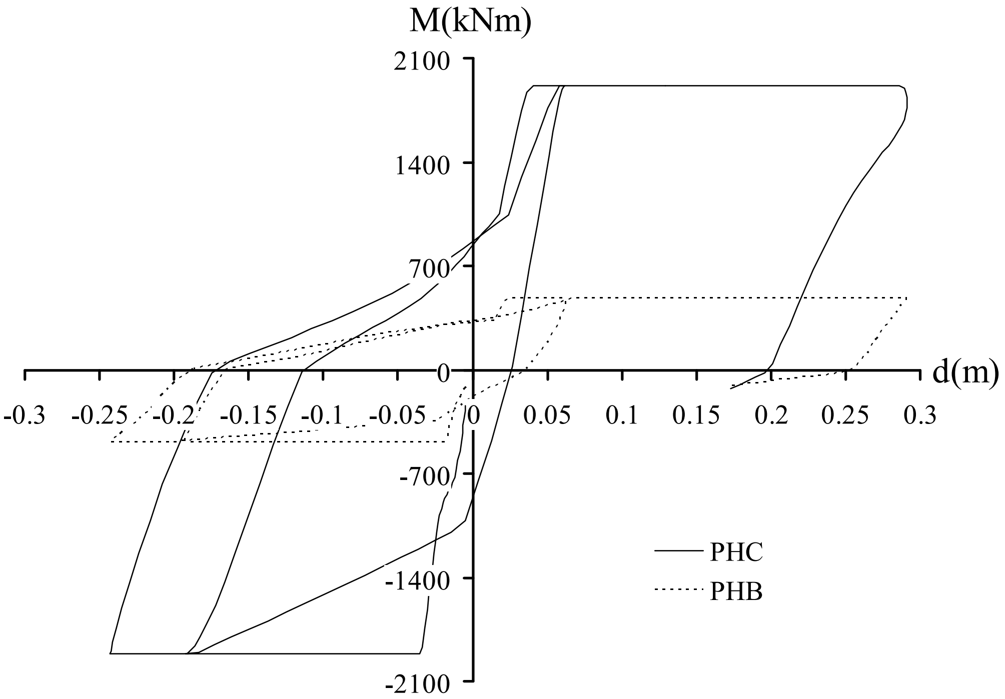

Figure 4.5 - Bending moment at the plastic hinges vs. top displacement from t=6.72s to t=9.42s for the frame with X=4 and subjected to the JMA record.

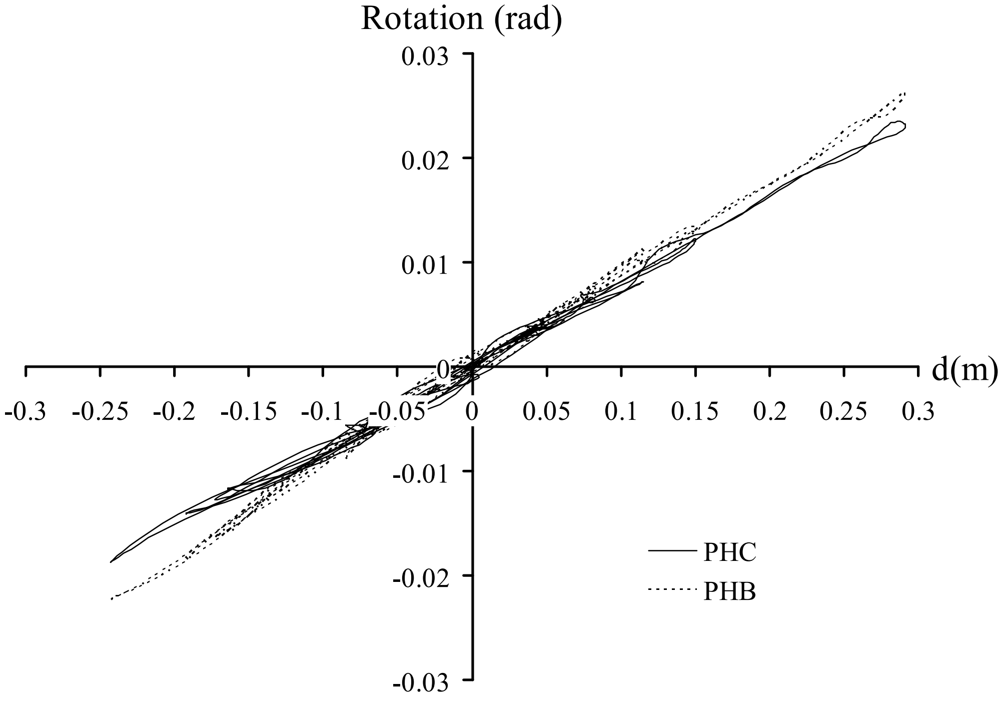

Figure 4.6 - Relation between rotations in the plastic hinges of Figure 4.6 and top displacement of the frame designed according to X=4 during the whole JMA record

In Figure 4.6, we represent the relation between the rotations in the same plastic hinges as in Figure 4.5 and the top displacement in the structure designed according to X=4 for the whole period of the JMA record.

It is initially observed in Figure 4.5 that the curve corresponding to the plastic hinges in the columns is virtually a scaled version of that corresponding to the plastic hinge in the beams. Clearly, the scale factor is the ratio of the flexural capacity at the hinges in the columns to that in the beams. This indicates that the hinges are in the same phase of behaviour for the same periods of time. Another observation is that the curves in Figure 4.5 have the same shape as the hysteretic relationships at the plastic hinges, i.e. bending moment *vs.* rotation.

From Figure 4.6, it is seen that there is a linear variation between deformations at the plastic hinges and global displacements in the structure. This is as expected since the displacement field has only one degree of freedom – the one associated with the collapse mechanism.

These observations confirm the basic hypothesis upon which the RPSD method is based, i.e. on the direct relation between local behaviour and global behaviour in structures designed to develop a specific collapse mechanism and subjected to large ductility demand.

Furthermore, examining Figure 4.5, we find that the yield displacement in the structure, defined as the displacement at the time of onset of plastic behaviour at all plastic hinges for the first time, is 0.042m. Therefore, observing that the maximum displacement is 0.291m, we reach a global displacement ductility factor of 7.

The rotation demand found for the plastic hinges in the columns is 2.35×10^{-2}rad, while for those in the beams, 2.63×10^{-2}rad, which yields, with reference to Table 4.4, an actual ductility demand of 7.3 and 15.3, respectively. This is consistent with the values of expected rotation ductility demand found in the same table.

Given that the structure fulfils the assumption of the RPSD method, good agreement is expected in terms of maximum displacement and strength demand between rigid-plastic and refined NLTHA.

Figure 4.7a) and b) shows the displacement-history for both records at periods of maximum demand in terms of top displacement.

A quick examination of the curves in Figure 4.7 shows that there is good agreement regarding the estimation of maximum displacement demand for both records between the rigid-plastic and the refined analysis. In fact, for both designs, according to the choice of X, the refined NLTHA yields a maximum top displacement only 10% lower and 15% higher than that estimated by the RPSD method for the JMA and Sylmar records, respectively. For engineering purposes, this is considered to be a small deviation and a remarkable achievement of rigid-plastic NLTHA, given their simplicity regarding the NLTHA from the FEM program.

Another important observation is that the dynamic response of both structures in the refined NLTHA is practically identical regardless of the choice of the internal stress field. This is consistent with the feature of the RPSD method regarding the effective separation between dynamic response, solely dependent on the dissipation capacity (thus proportional to F_y*) and the choices on the safe stress field. In fact, both designs correspond to the same value of F_y*, cf. step expression (4.6) in step 3 of previous section.

It should also be noted from Figure 4.7 that there is agreement between the time-history curves computed by the refined NLTHA and those corresponding to the RPSD method, particularly after the initial onset of plastic behaviour. The reasons for this are analogous to those discussed in section 3.2.2 for the case of oscillators: In reality, when the system initially undergoes plastic deformations, additional to the input

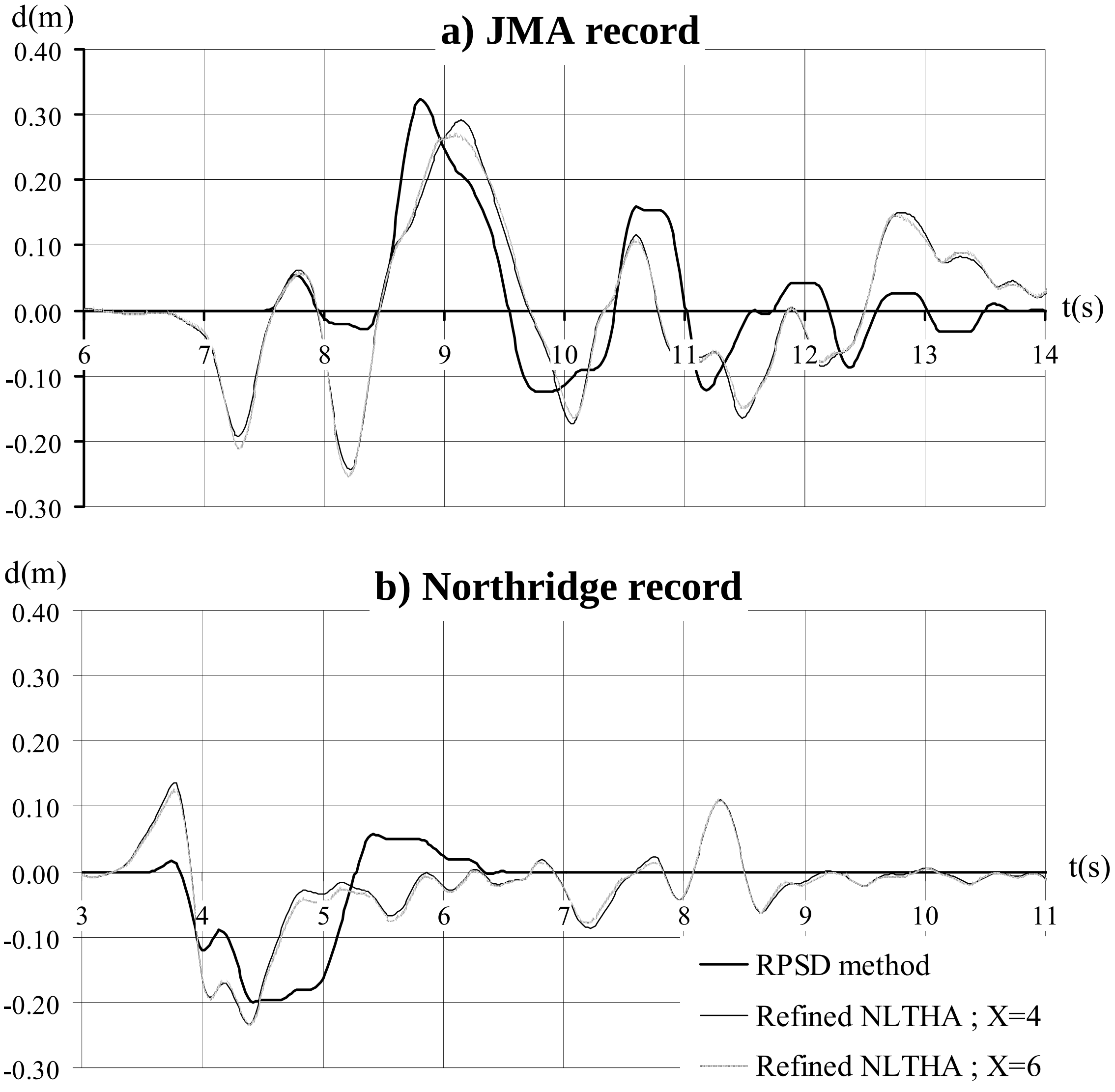

Figure 4.7 -Displacement-history curves for the top displacement for a) the JMA record and b) the Northridge record

energy from the ground motion, there is also an elastic energy input in the form of kinetic energy. Both forms of energy are later dissipated by the plastic hinges, which is taken into account in the refined NLTHA. The rigid-plastic behaviour assumed in the RPSD method implies that the system starts from rest when the first plastic deformations take place, thus initially there is no kinetic energy to be dissipated. This explains the discrepancy in the time-history curves shown in Figure 4.7a) and b) at the onset of plastic behaviour between the refined and the rigid-plastic NLTHA. In reality, the larger the parameter a_y, the larger the influence of the elastic behaviour on the dynamic response, and therefore the larger the discrepancy. The difference in behaviour is also characterised by some small oscillations found in the refined NLTHA curves. These oscillations are also related to the elastic behaviour and therefore irrelevant for the evaluation of damage to the structure.

Finally, we show the comparison in terms of base-shear between the rigid-plastic and refined NLTHA for periods of maximum demand, cf. Figure 4.8. The curves referring

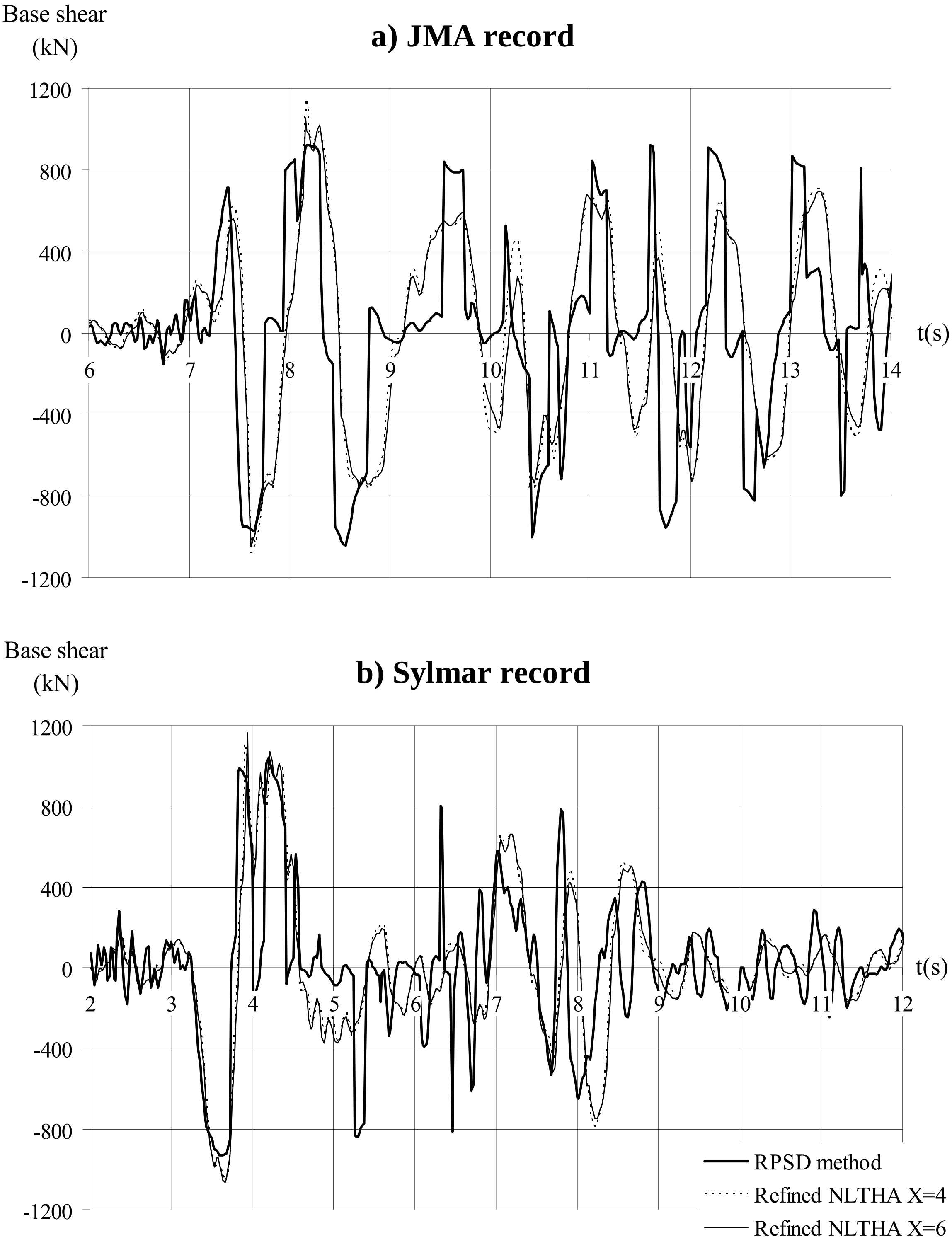
a) JMA record

b) Sylmar record

Figure 4.8 -Base-shear-history curves for a) the JMA record and b) the Northridge record

to the refined NLTHA are formulated from the output solution of the FEM program in terms of absolute accelerations at each floor.

Again, the same features are observed for the case of the displacement-history:

- The maximum base shear demand predicted by the RPSD method is only 10% lower than the one corresponding to the refined NLTHA.
- Generally, there is good agreement between the base-shear-history curves in the time domain. The deviations, the most obvious of which is that taking place for t≈6.5s of the Sylmar record, are attributed to the abrupt transitions between types of behaviour for the rigid-plastic model as opposed to smooth transition in the case of elastoplastic models. This has been discussed in detail in section 3.2.2.
- There are virtually no differences between the different designs according to the choice of X in the refined NLTHA.

4.2 Design of a 12-storey frame

In this example, the RPSD method is used to design the 12-storey frame depicted in Figure 4.9. The total height of the building is 42.5m. The height of the first floor is 4m, while for subsequent floors it is 3.5m. Each bay is 8m in length, in both horizontal directions. The distributed dead and live load at each floor at the time of the earthquake is 11.772kN/m^2. Therefore, the total "seismic" mass at each floor is 307.2ton.

The building is designed to withstand a lifetime earthquake event. Therefore the performance criterion upon which the design is based is such that the maximum inter-storey drift is 4.5% for ground motion up to 1g.

Given the symmetry in-plane and vertical regularity of the building, it is clear that this structure satisfies the assumption on the analysis of the frame system subdivided into

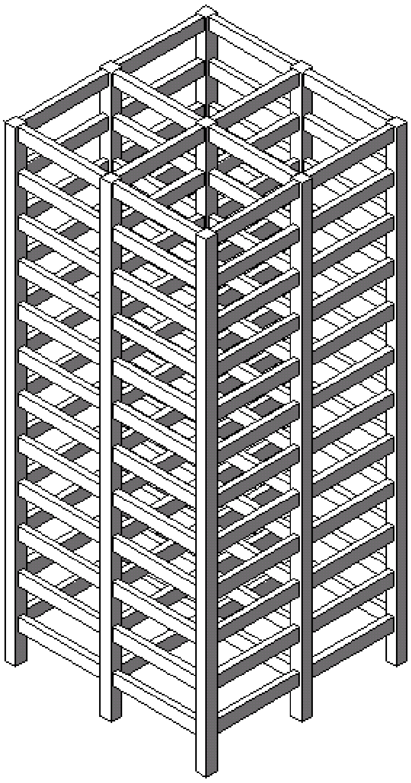

Figure 4.9 -12-storey frame.

a series of plane frames, which are treated separately, cf. section 3.1 – *Further assumptions for ductile frames*. Observing Figure 4.9 it is clear this implies the design for ground motion to be the same for both directions, meaning that we just have to analyse the structure in one of the principal horizontal directions.

Choice of a ground motion scenario for design purposes

It is well known that high-rise buildings are not as sensitive to earthquake motion as for instance, wind loading. This is mainly due to the fact that earthquakes induce limited deformation demand on structures, the magnitude of which is closely related with the level of ground motion displacement. This is effectively captured by the rigid-plastic spectra concept, cf. section 3.3.1.

From the examples of GRPS's given previously in this work, it is seen that the displacement demand characteristic of a certain ground motion is of the same order of magnitude as the peak ground displacement, the ordinate corresponding to a_y=0m/s^2. The SRPS is a magnification of the GRPS using the factor κ. High-rise buildings are typically characterised by uniform distribution of geometry and mass throughout the structure. Therefore, the expression in (3.28) for κ in section 3.2.3 approaches the solution for continuous systems. If the system is designed to develop a full-sway collapse mechanism as in Figure 3.29, we have:

$$\begin{aligned} m(h) &\approx m \\ \phi(h) &\approx \frac{h}{H} \end{aligned} \tag{4.13}$$

where m is the distributed mass along the building in kg/m units. H and h have the same meaning as in Figure 3.29. Then κ in (3.28) reads:

$$\kappa \approx \frac{\int_0^H m \cdot \frac{h}{H} dh}{\int_0^H m \cdot \left(\frac{h}{H}\right)^2 dh} \approx \frac{3}{2} \tag{4.14}$$

If the desired collapse mechanism is such that upper rigid floors will form, it may easily be shown that κ, as in (4.14) is lower than 1.5.

Figure 4.10 shows the SRPS in terms of maximum relative displacements of structural system with κ=1.5 for the scaled JMA record so that PGA=1g.

It is seen that for buildings higher than 55m and designed to develop full-sway collapse mechanism, the maximum drift demand is lower than 1% for any range of a_y. This indicates that the JMA record is unable to induce significant damage in high-rise ductile buildings. In fact, the majority of structural failures that occurred during the Kobe Earthquake, 1995, occurred in parts of the city dominated by lower housing structures. Generally, high-rise buildings in downtown Kobe city survived this event with limited damage.

The study carried out at the Nagoya Institute of Technology, cf section 3.2.2, showed that the higher the degree of asymmetry of the ground motion, the higher the displacement demand induced in the system. Although not investigated, it seems clear that the period of the ground motion waves also plays a role. In fact, the longer the period of the wave, the longer the time interval Δt, during which the system has plastic deformation in one of the directions. For rigid-plastic systems, the

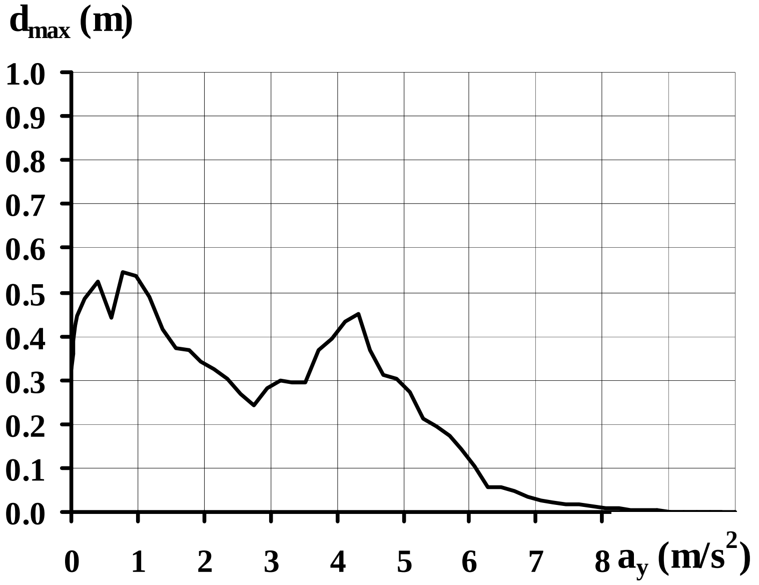

Figure 4.10 -SRPS in terms of maximum displacement demand for the N-S component of the JMA record of the Kobe Earthquake, 1995, for structural system with κ=1.5

displacement demand is proportional to $(a_y - a_g(t))\cdot\Delta t^2/2$, the strong dependence on the period of the ground motion waves is thus evident.

Thus, it seems reasonable that the seismic performance of the structure in Figure 4.9 should be checked against ground motion of the asymmetric type and dominated by seismic waves with long period as these have a higher potential for inducing severe displacement demand on the structure.

In consequence, we choose both horizontal components of the Erzikan Earthquake, Turkey, 1992, and of the Kobe Earthquake, 1995, recorded at the Takatori station. In the following, the records corresponding to the Erzikan Earthquake, 1992, will be simply designated by Erzikan plus the corresponding horizontal component, whereas the records from the Kobe Earthquake, 1995, will be referred to by the name of the station where they were recorded: Takatori plus the corresponding horizontal component. The records are shown in Appendix. Those corresponding to the Erzikan earthquake are single-shock ground motion with a high degree of asymmetry, particularly the N-S component, whereas the accelerograms of the Kobe earthquake recorded at the Takatori station are long and dominated by long periods of vibration due to the filtering effect of soft layers of soil.

Here of course, given the performance criterion, we deal with the scaled versions of these records so that PGA=1g. In Figure 4.11 the GRPS of each of the scaled records in terms of maximum displacement demand is shown. The envelope curve is simply designated GRPS, as it represents the ground motion scenario considered in this design case.

Finally, we simply apply the correction of the GRPS mentioned in section 3.3.1 – *Rigid-plastic spectra for design purposes*, in order to have a representation of the ground motion scenario adequate for design purposes, cf. Figure 4.12.

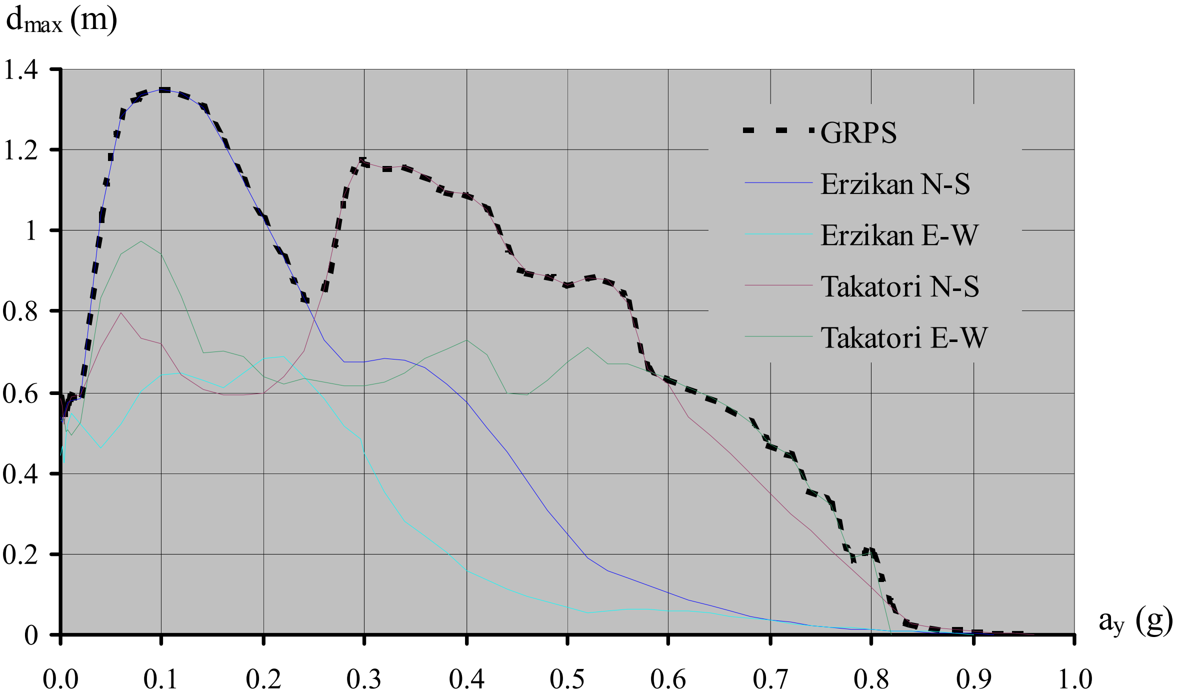

Figure 4.11 - GRPS's of each of the records used for the design of the 12-storey frame and the corresponding envelope curve.

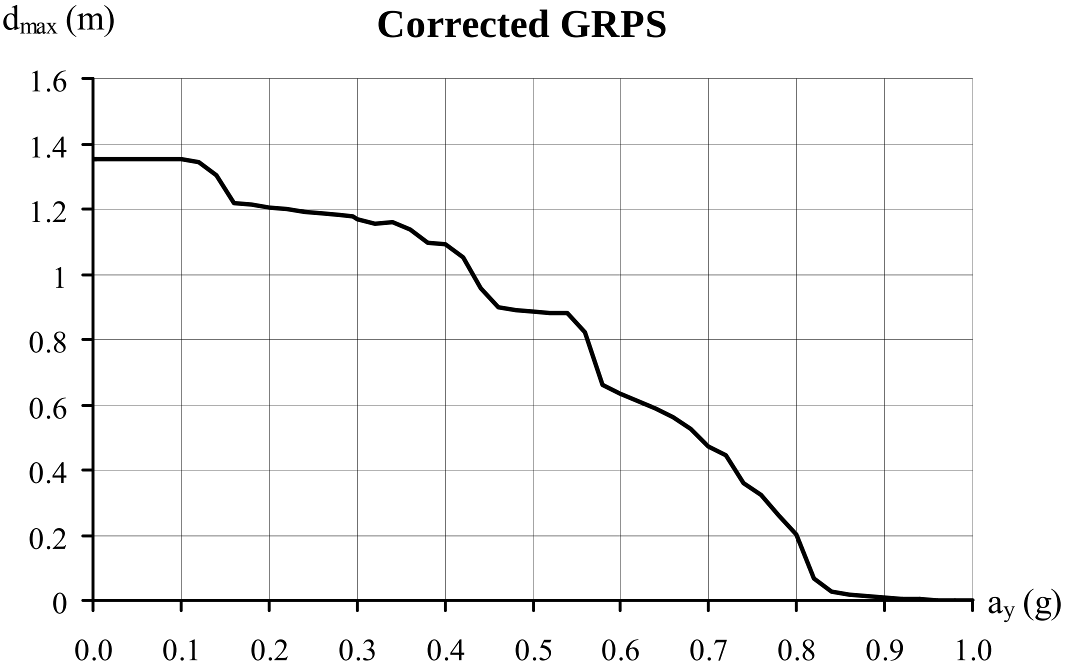

Figure 4.12 -Corrected GRPS in terms of maximum displacement demand for design purposes

Step 1 – Choice of a suitable collapse mechanism

In this case, the choice of the most suitable collapse mechanism is not as straightforward as for the previous design example. Of course the full-sway collapse mechanism shown in Figure 4.13a) is still considered to be a valid choice. On the other hand, it seems that a collapse mechanism with some upper rigid floors, as depicted in Figure 4.13b), would still assure adequate dissipation capacity throughout the structure despite an increase in the rotation demand at each plastic hinge. However, the advantage of such a choice is found in terms of the economy of the design in the rigid floors due to the avoidance of refined differentiated reinforcing detail at the plastic hinges.

For illustration purposes, in this design case we initially consider the full-sway collapse mechanism and the "partial" collapse mechanism involving the formation of plastic hinges in the ends of the beams up to the 8th floor, in the base of the columns on the ground floor, and in the top of the 8th floor, cf. Figure 4.13a) and b), respectively. It should be noted that in the latter mechanism, only 2/3 of the plastic hinges of the full-sway mechanism are required. The corresponding quantities m* and κ are also shown in the figure. In the future, the index F and P refer to the (F)ull-sway and to the (P)artial collapse mechanisms, respectively.

The maximum rotation demand at each of the plastic hinges, θ_{max}, in both collapse mechanisms is:

$$\theta_{max} = \frac{d_{max} \cdot \kappa}{H} \tag{4.15}$$

where H is the height of the upper "inclined" floor. Thus, H=42.5m for the full-sway mechanism and H=32.0m for the partial collapse mechanism.

From (4.15) it follows that if both collapse mechanisms are subjected to the same

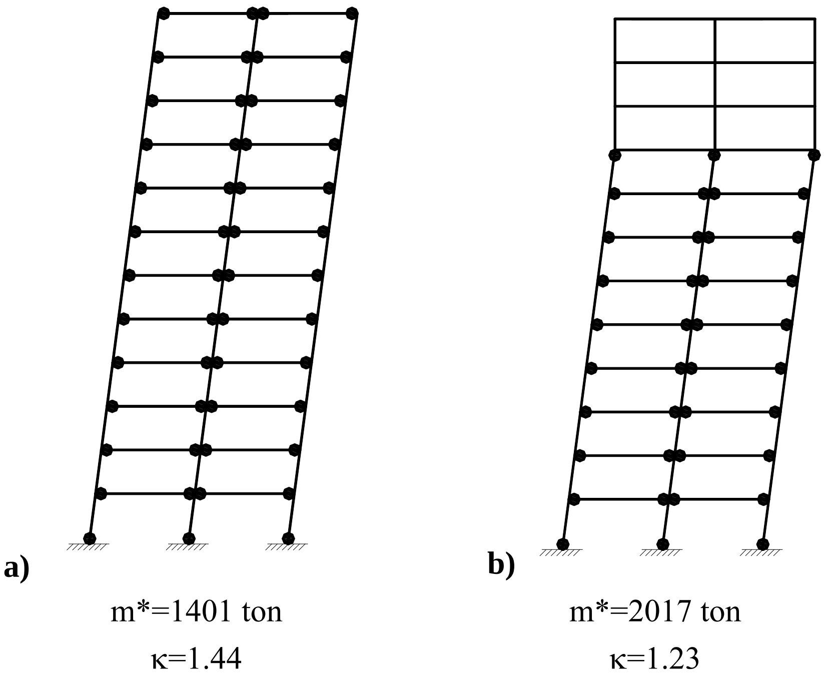
a) m*=1401 ton κ=1.44

b) m*=2017 ton κ=1.23

Figure 4.13 -Two possible collapse mechanisms for the 12-storey frame and corresponding m and κ quantities*

displacement demand d_{max}, then the relation between the rotation demand in the plastic hinges of the partial collapse mechanism, $\theta_{max,P}$, and of the full-sway mechanism, $\theta_{max,F}$, is only 13%:

$$\frac{\theta_{max,P}}{\theta_{max,F}} = \frac{\kappa_P / H_P}{\kappa_F / H_F} = \frac{1.23}{1.44} \times \frac{42.5}{32.0} = 1.13 \tag{4.16}$$

Given this small difference, it is expected that the value of a_y, read in the corresponding SRPS from the performance criterion, does not differ significantly for both collapse mechanisms. As previously discussed, in these frame structures the required dissipation capacity is associated with the sum M_P^* of all the plastic moments given by $M_P^*=\kappa \cdot a_y \cdot m^* \cdot H$.

For the same chosen value of a_y, it is seen that the partial collapse mechanism implies a value of M_P^* that is 7% lower than for the full-sway mechanism:

$$\frac{M^*_{P,P}}{M^*_{P,F}} = \frac{1.23 \times 2017 \times 32.0}{1.44 \times 1401 \times 42.5} = 0.93 \tag{4.17}$$

This difference in terms of required dissipation capacity may result in significant savings in terms of reinforcement quantities for the partial collapse mechanism.

Step 2 – Choice of a dynamic performance criterion, R_{max}

As we are considering two different collapse mechanisms, it is convenient to represent both SRPS's curves in terms of maximum rotation demand, as this allows both curves to be drawn in the same space. Therefore, the values in the GRPS of Figure 4.12 should be affected by the parameter κ/H, cf. (4.15), for each of the collapse mechanisms to perform the transformation from GRPS in terms of maximum displacement demand to SRPS in terms of maximum rotation demand.

Step 3 – Definition of the required dissipation capacity using the rigid-plastic spectra

Following the discussion in the previous step, the SRPS's in terms of maximum rotation demand, θ_{max}, for each collapse mechanism may be plotted. We use the following factors to perform the transformation:

$$\begin{aligned} &\text{Full-sway collapse mechanism:} && \kappa/H=\frac{1.23}{32.0}=0.038 \\ &\text{Partial collapse mechanism:} && \kappa/H=\frac{1.44}{42.5}=0.034 \end{aligned} \tag{4.18}$$

The intervals of a_y given for which the performance criterion is satisfied are according to the SRPS's of Figure 4.14.

$$\begin{aligned} &\text{Full-sway collapse mechanism:} && \theta_{max} \le 0.045 \text{ for } a_y \ge 0.12g \\ &\text{Partial collapse mechanism:} && \theta_{max} \le 0.045 \text{ for } a_y \ge 0.29g \end{aligned} \tag{4.19}$$

However, the determination of a_y is not concluded yet. In these types of structures, P-Δ effects have to be taken into account. This is especially pertinent if we decide to design the structure according to the choice of the full-sway mechanism where the value of a_y, and therefore of the required lateral strength is rather small.

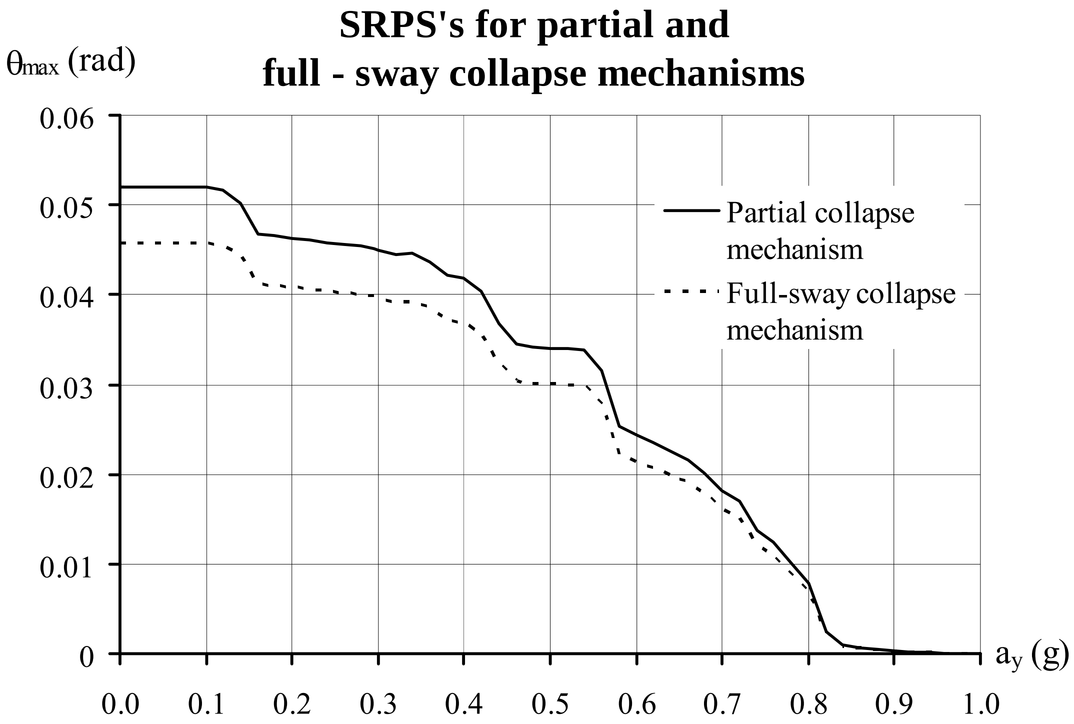

Figure 4.14 -SRPS's for the full-sway and partial collapse mechanisms in terms of maximum rotation demand at the plastic hinges.

Table 4.5 -Rigid-plastic NLTHA with the consideration of P-Δ effects in the structure chosen to develop the full-sway mechanism

	Maximum rotation demand, θ_{max} (rad)	
a_y (m/s^2)	Erzikan N-S	Takatori N-S
0.15	0.049	0.030
0.20	0.048	0.024
0.23	0.044	0.019

In fact, it is concluded that the performance criterion for a structure designed to develop the full-sway collapse mechanism is only satisfied for $a_y \geq 0.23$g. Table 4.5 summarises the results in terms of maximum rotation demand at the plastic hinges in the structure with the full-sway collapse mechanism for rigid-plastic NLTHA with the consideration of P-Δ effects for all the records in the GRPS carried-out until the performance criterion was met.[1]

In the case of the structure designed to develop the partial collapse mechanism, it was found that the maximum rotation demand corresponding to a_y=0.29g when P-Δ effects are taken into account is slightly reduced to 0.043rad. For this reason it is considered that a structure designed to develop a partial collapse mechanism, and with a_y=0.29g, is stable enough against P-Δ effects.

---

[1] In a real design situation, the GRPS would have accounted for far more records. Despite the simplicity of rigid-plastic NLTHA, this would make it impractical to evaluate the response of the structure against every record accounted for in the GRPS, as is done in this illustrative example. However, the purpose of this analysis is simply to check if the chosen value of a_y is high enough so that the structure is not greatly affected by P-Δ effects. According to engineering judgement, this can be carried out with a reduced amount of rigid-plastic NLTHA.

It is concluded that if one chooses the full-sway collapse mechanism, the dissipation capacity on the structure requires that a_y=0.23g, whereas if the structure is designed according to the partial collapse mechanism, a_y=0.29g.

Thus, the required lateral strength assigned to the structure according to each choice of the collapse mechanism is of the same order of magnitude and, consequently the advantages of the economy of design associated with the partial collapse mechanism are retained. For this reason we consider that the most suitable collapse mechanism, i.e. yielding a better compromise between structural performance and economy, is the partial collapse mechanism. Therefore, we proceed with the design of the structure according to this choice.

Step 4 - Choice of an appropriate safe stress field using the extreme loading scenarios approach

We first define the external lateral force fields by applying the equations in Table 3.6. Previously it was seen that if the structure is designed to develop the partial collapse mechanism and to meet the performance criterion of θ_{max}≤0.045rad, the quantities in (4.20) are reached, which yield the lateral loading cases in Table 4.6:

$$\begin{aligned} &\kappa = 1.23 \\ &a_y = 2.85\text{m}/\text{s}^2 \\ &\text{PGA} = 9.81\text{m}/\text{s}^2 \end{aligned} \tag{4.20}$$

Table 4.6 - Lateral force fields for design purposes (kN)

Floor	Plastic Behaviour				Slip Behaviour	
	Mechanism in the positive direction		Mechanism in the negative direction			
	+PGA	-PGA	+PGA	-PGA	+PGA	-PGA
12	1762	388	-388	-1762	687	-687
11	1762	388	-388	-1762	687	-687
10	1762	388	-388	-1762	687	-687
9	1762	388	-388	-1762	687	-687
8	1240	675	-675	-1240	282	-282
7	718	962	-962	-718	-122	122
6	195	1250	-1250	-195	-527	527
5	-327	1537	-1537	327	-932	932
4	-850	1824	-1824	850	-1337	1337
3	-1372	2111	-2111	1372	-1741	1741
2	-1894	2398	-2398	1894	-2146	2146
1	-2417	2685	-2685	2417	-2551	2551

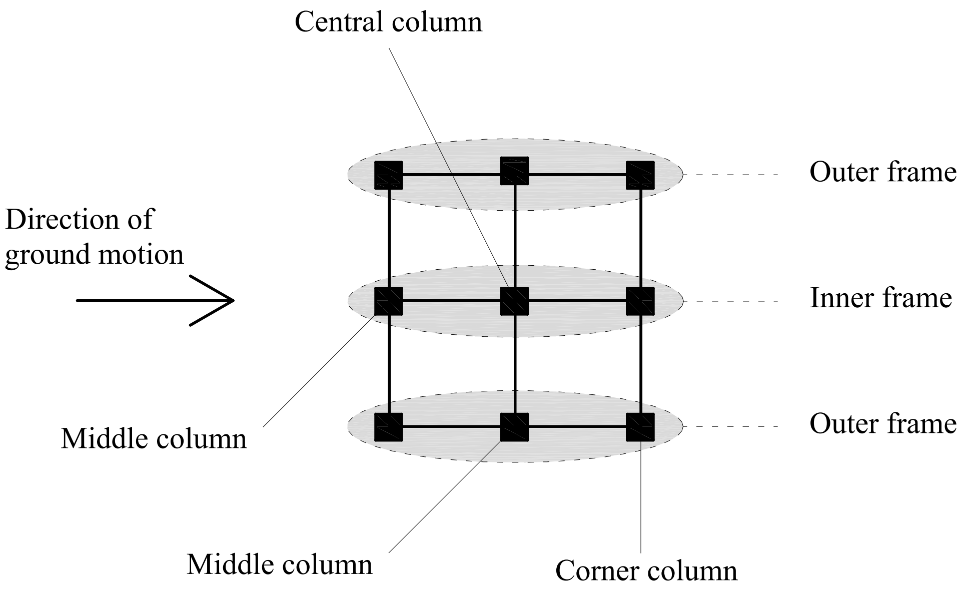

Figure 4.15 -Identification of the columns according to its location in plan

The choices on the safe stress field are more complex as in the case of the simple 4-storey plane frame of the previous design example. In fact, for high-rise buildings it seems obvious that the strength capacity at each structural element should decrease with the height of the corresponding floor. Moreover, the strength capacity of each column should be assigned according to its location in the plan.

Firstly we assume that the base shear per floor is equally distributed by the 3 sub-frames in the direction of the ground motion, cf. Figure 4.15.

Bearing this in mind, we make the following considerations to determine the required bending capacity in the beams:

- The plastic hinges in the ends of the beams on the same floor have the same flexural capacity in both directions. Let the bending capacity of the hinges in floor 1 be M.
- The flexural capacity of the plastic hinges in the beams of floors 4 to 8, $M^{B}_{P,4\sim8}$, is 75% of the flexural capacity of the plastic hinges in the beams of floors 1 to 3, $M^{B}_{P,1\sim3}$.
- To enforce the weak beam – strong column concept, 1/3 of the dissipation capacity is due to flexural behaviour at the plastic hinges in the columns, i.e. the sum of the flexural capacities of the hinges in the columns, ΣM^{C}_{P}, is 50% of the sum of the flexural capacities of the hinges in the beams, ΣM^{B}_{P}.

At this point we have enough information to determine the flexural capacity of the hinges in the first three floors, M, which is the variable required to determine the flexural capacities at all plastic hinges in the beams. This is carried out by expressing each of the conditions above and solving the system of equations:

$$\begin{cases} M^{B}_{1\sim3} = M \\ M^{B}_{4\sim8} = 0.75 \times M^{B}_{1\sim3} \\ \sum M^{C}_{P} = 0.50 \times \sum M^{B}_{P} \\ M^{*}_{P} = \sum M^{C}_{P} + \sum M^{B}_{P} \\ M^{*}_{P} = \kappa \cdot a_{y} \cdot m^{*} \cdot H \text{ cf. (4.6) and (4.9)} \end{cases} \tag{4.21}$$

where it follows that

$$\begin{gathered} 1.5 \times (12 \times M \times 3 + 12 \times 0.75 \times M \times 5) = 1.23 \times 2.85 \times 2017 \times 32 \Leftrightarrow \\ \Leftrightarrow M = 1862 \text{ kNm} \end{gathered} \tag{4.22}$$

Note that in the direction of the ground motion, there are 12 plastic hinges in each floor.

The following considerations lead to the determination of the flexural capacities of each plastic hinge in the columns:

- The sum of the flexural capacities of the plastic hinges at the top of floor 8, $\Sigma M^{C}_{P,8}$, is 50% of the sum of the flexural capacities at the base of the column in the ground floor, $\Sigma M^{C}_{P,GF}$.
- Cf. Figure 4.15. The flexural capacities in plastic hinges located in the corner columns, M_P^{Corner}, and in the middle columns, M_P^{Middle}, is 70% and 80%, respectively, of the flexural capacity of the plastic hinges located in the central column, $M_P^{Central}$.

Now we have:

$$\begin{cases} \sum M^{C}_{P,8} + \sum M^{C}_{P,G} = 0.50 \times \sum M^{B}_{P} \\ \sum M^{C}_{P,8} = 0.5 \times \sum M^{C}_{P,GF} \\ M^{Corner}_{P} = 0.7 \times M^{Central}_{P} \\ M^{Middle}_{P} = 0.8 \times M^{Central}_{P} \end{cases} \tag{4.23}$$

leading to the determination of the required bending capacity of the plastic hinge in the bottom of the central column:

$$\begin{gathered} 1.5 \times M^{Central}_{P} (1 + 4 \times 0.7 + 4 \times 0.8) = 0.5 \times (12 \times 1862 \times 3 + 12 \times 0.75 \times 1862 \times 5) \Leftrightarrow \\ \Leftrightarrow M^{Central}_{P} = 7182\text{kNm} \end{gathered} \tag{4.24}$$

The required flexural capacities at each plastic hinge are summarised in Table 4.7.

The stress field is fully determined in the beams, but not yet in the columns. In fact,

Table 4.7 - Bending capacities of the different plastic hinges (kNm)

Beams		Columns	$M_{C,Corner}$	$M_{C,Middle}$	$M_{C,Central}$
Floor 1-3	1862	Ground floor	5027	5746	7182
Floor 4-8	1397	Top of 8th floor	2514	2873	3591

for the latter case, we must still find a base shear distribution compatible with the flexural capacities shown in Table 4.7.

Consider the case of the corner column. When the structure has plastic behaviour we know the magnitude of the bending moments at the top of the 8th floor and at the ground floor. In addition, we know that these bending moments have opposite signs. Therefore, the variation of the bending moment from the top of the 8th floor to the ground floor in the corner column, $\Delta M_{GF\sim8}{}^{Corner}$, has to be the sum of the corresponding bending capacities plus the contribution from the bending moments at the ends of the beams. The latter is also determined. Thus,

$$\Delta M_{GF\sim8}^{Corner} = 5027 + 2514 + 3\times1862 + 5\times0.75\times1862 = 20110 \text{ kNm} \tag{4.25}$$

from which it follows that the average shear force in the corner column $\overline{V}_{GF\sim8}^{Corner}$ must be

$$\overline{V}_{GF\sim8}^{Corner} = \frac{\Delta M_{GF\sim8}^{Corner}}{H} = \frac{20110}{32} = 628 \text{ kN} \tag{4.26}$$

Applying identical reasoning to the middle column in the same sub-frame we have:

$$\Delta M_{GF\sim8}^{Middle} = 5746 + 2873 + 2\times\left(3\times1862 + 5\times0.75\times1862\right) = 33756 \text{ kNm} \tag{4.27}$$

Note that the column in the middle receives twice as much contribution from the beams.

$$\overline{V}_{GF\sim8}^{Middle} = \frac{\Delta M_{GF\sim8}^{Middle}}{H} = \frac{33756}{32} = 1055 \text{ kN} \tag{4.28}$$

From (4.26) and (4.28) it is found that in the outer sub-frames, the shear force in the middle column must be 70% greater than the shear force in the corner columns.

$$\frac{\overline{V}_{GF\sim8}^{Middle}}{\overline{V}_{GF\sim8}^{Corner}} = \frac{1055}{628} = 1.7 \tag{4.29}$$

The same relationship regarding the base shear distribution is found for the inner frame:

$$\frac{\overline{V}_{GF\sim8}^{Central}}{\overline{V}_{GF\sim8}^{Middle}} = \frac{\Delta M_{GF\sim8}^{Central}}{\Delta M_{GF\sim8}^{Middle}} = \frac{7182+3591+2\times\left(3\times1862 + 5\times0.75\times1862\right)}{5746 + 2873 + 3\times1862 + 5\times0.75\times1862} = 1.7 \tag{4.30}$$

We are now in a position to derive the strength demand at any point of the structure below the rigid floors by considering equilibrium of each of the lateral force fields in Table 4.6 and the gravitational forces. Table 4.8 shows the required flexural and shear strength for each of the columns and for each of the sub-frames identified in Figure 4.15.

To conclude this step, it is necessary to ensure that the upper rigid floors remain in the rigid domain throughout the entire ground motion event.

Bearing in mind that the lateral force field is also known in this part of the structure, rigidity is guaranteed by determining the required strength so that all the possible collapse mechanisms are prevented. This is carried out by applying the work equation for each of the possible collapse mechanisms by determining the required bending

Table 4.8 - Required flexural and shear strength in the columns identified in Figure 4.15 up to the 8th floor (kN-m)

Floor	Cross-section	Outer frames				Inner frame			
		Corner column		Middle column		Middle column		Central column	
		M	V	M	V	M	V	M	V
8	Top	2514	635	2873	1080	2873	635	3591	1080
	Bottom	2029		2050		2363		2726	
7	Top	3423	747	4839	1270	3757	747	5515	1270
	Bottom	2732		3665		3032		4282	
6	Top	4126	811	6453	1379	4426	811	7071	1379
	Bottom	3137		4772		3388		5305	
5	Top	4532	829	7560	1409	4782	829	8094	1409
	Bottom	3712		6454		3874		6621	
4	Top	4549	800	8009	1359	4731	800	8425	1359
	Bottom	5070		8344		5369		8745	
3	Top	4090	723	7647	1229	4179	723	7905	1229
	Bottom	6165		9787		6589		10400	
2	Top	4306	893	7253	1518	4729	893	7306	1518
	Bottom	6369		9577		6896		10365	
1	Top	4510	1109	5858	1885	5037	1109	6647	1885
	Bottom	5986		8368		6587		9281	
GF	Top	4127	1351	4650	2296	4728	1351	5563	2296
	Bottom	5027		5746		5746		7182	

capacities at the critical cross-sections so that the load parameter λ, affecting the external force field, is greater than 1.

To simplify the procedure, we assume that the flexural strength of the beams in the upper rigid floors, $M^B{}_{P,9\sim12}$, is 60% of the strength of the beams in the first 3 floors, $M^B{}_{P,1\sim3}$. Thus,

$$\begin{aligned} & M^B_{9\sim12} = 0.60 \times M^B_{1\sim3} \Leftrightarrow \\ \Leftrightarrow\ & M^B_{9\sim12} = 0.60 \times 1862 \Leftrightarrow \\ \Leftrightarrow\ & M^B_{9\sim12} = 1117 \text{ kNm} \end{aligned} \tag{4.31}$$

a)

$$\lambda = 2.77 \Rightarrow \begin{cases} M_{P,11}^{Central} = 529\ \text{kNm} \\ M_{P,11}^{Middle} = 423\ \text{kNm} \\ M_{P,11}^{Corner} = 370\ \text{kNm} \end{cases}$$

b)

$$\lambda = 1.88 \Rightarrow \begin{cases} M_{P,10}^{Central} = 1145\ \text{kNm} \\ M_{P,10}^{Middle} = 916\ \text{kNm} \\ M_{P,10}^{Corner} = 802\ \text{kNm} \end{cases}$$

c)

$$\lambda = 1.50 \Rightarrow \begin{cases} M_{P,9}^{Central} = 2184\ \text{kNm} \\ M_{P,9}^{Middle} = 1748\ \text{kNm} \\ M_{P,9}^{Corner} = 1529\ \text{kNm} \end{cases}$$

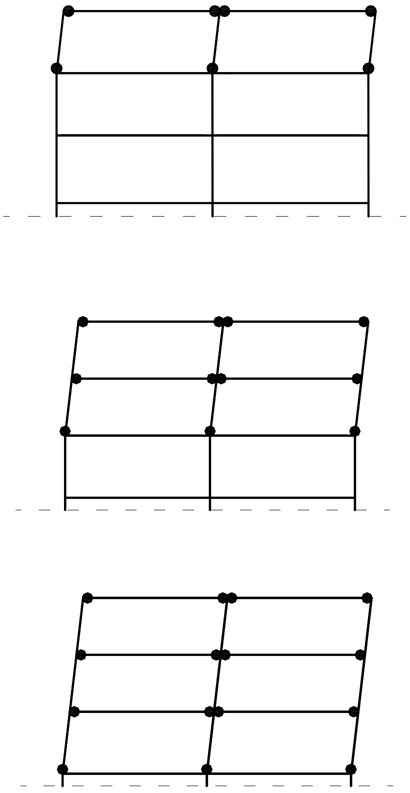

Figure 4.16 -Determination of the required bending capacity in the columns so that the 3 upper floors remain in the rigid domain throughout the entire ground motion

We further assume that the previous relationships between the flexural strengths at the different columns as in (4.23) as well as the ones concerning base shear distribution per each sub-frame in the direction of the ground motion still apply. The flexural capacity in a given column is constant throughout its length.

From Table 4.6 we find that the most severe loading cases for the 3 upper rigid floors are those when the structure has plastic behaviour in the same direction as the maximum expected ground acceleration, PGA. Therefore, the loading case considered corresponds to a rectangular force distribution with magnitude 1762 kNm per floor multiplied by a load parameter λ.

Given the distributed vertical load in the beams, we find that the maximum positive bending moment in the beams takes place in the end cross-section with positive bending moment equal to 1117kNm, consequently the cross-sections where potential plastic hinges may be located are those at the ends of the beams and of the columns. This leads to 8 collapse mechanisms, see Figure 4.16 and Figure 4.17.

In each of the collapse mechanisms, the external virtual work W_E is given by:

$$W_E = \lambda \cdot \sum F_i \cdot \theta \cdot h_i \qquad (4.32)$$

where F_i is lateral force applied at the displaced floor i, and h_i is the corresponding height to the highest rigid floor or, in the case of soft-storey mechanisms, the height of the own floor.

a)

$M_{P,11}^{Central} = 529 \text{ kNm} \Rightarrow \lambda = 1.20$

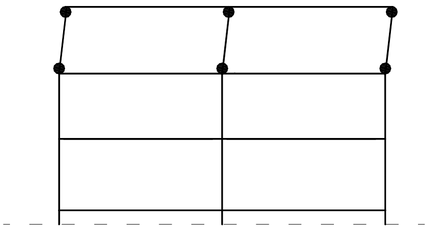

b)

$M_{P,10}^{Central} = 1145 \text{ kNm} \Rightarrow \lambda = 1.30$

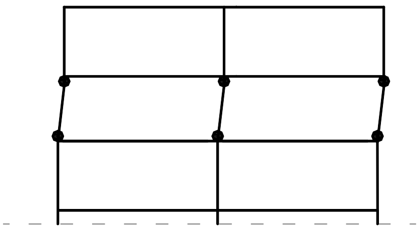

c)

$M_{P,9}^{Central} = 2184 \text{ kNm} \Rightarrow \lambda = 1.65$

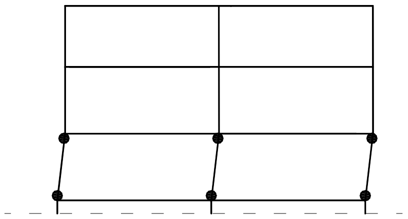

d)

$$\left\{\begin{matrix} M_{P,11}^{Central} = 529 \text{ kNm} \\ M_{P,10}^{Central} = 1145 \text{ kNm} \end{matrix}\right. \Rightarrow \lambda = 1.36$$

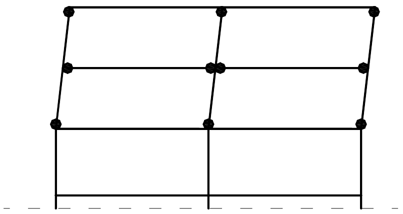

e)

$$\left\{\begin{matrix} M_{P,11}^{Central} = 529 \text{ kNm} \\ M_{P,10}^{Central} = 2184 \text{ kNm} \end{matrix}\right. \Rightarrow \lambda = 1.24$$

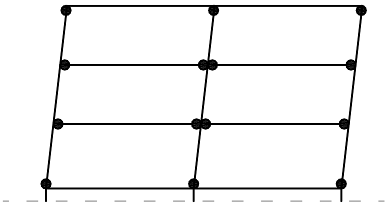

Figure 4.17 -Verification of the required bending capacity in the columns so that the 3 upper floors remain in the rigid domain throughout the entire ground motion

The internal virtual work, W_I, is given by the sum of the internal virtual work at the plastic hinges in the beams and in the columns.

$$W_I = W_I^B + W_I^C \tag{4.33}$$

where

$$W_I^B = 1117 \cdot N \cdot \theta \tag{4.34}$$

with N as the number of plastic hinges at the beams (which is a multiple of 12), and

$$W_I^C = \sum (1 + 4 \cdot 0.7 + 4 \cdot 0.8) \cdot M_{P,j}^{Central} \cdot \theta \tag{4.35}$$

in which $M_{P,j}^{Central}$ is the required bending capacity at the plastic hinges in the central column at level j.

The virtual work principle is successively applied to collapse mechanisms in sketches a), b) and c) of Figure 4.16 to determine the required bending capacity $M_{P,j}^{Central}$ at the base of floors 11, 10 and 9, respectively, ensuring that in each of the collapse mechanism $\lambda>1$:

$$M_{P,j}^{Central} = \frac{\lambda \cdot \sum F_i \cdot h_i - 1117 \cdot N}{(1+4\cdot 0.7+4\cdot 0.8)} \quad j=9,\ 10 \text{ or } 11 \tag{4.36}$$

By determining λ, the same principle is applied to verify the safety of the design against the formation of the collapse mechanisms, as in sketches a) to e) of Figure 4.17. Rigidity of the sub-frame is guaranteed when $\lambda>1$ for all the collapse mechanisms.

Finally, the remaining bending capacities at the corner and middle columns may be defined, see Table 4.9. At this point, the strength required at any point of the structure, ensuring that the collapse mechanism shown in Figure 4.13b) takes place, is fully determined. Thus, we can proceed to step 5.

Step 5 – Final structural design

The structure was designed by (Aono *et al*, 2006) at Ichinose Lab, Nagoya Institute of Technology assuming that only flexural collapse mechanisms may take place.

The compressive cylinder strength of the concrete is assumed to vary between 36MPa and 54MPa depending on the storey, cf. Table 4.10. The reinforcing steel used in

Table 4.9 -Required bending capacities in the columns of the 3 upper floors (kNm)

Columns	$M_{C,Corner}$	$M_{C,Middle}$	$M_{C,Central}$
11th Floor	370	423	529
10th Floor	802	916	1145
9th Floor	1529	1748	2184

Table 4.10 - Properties of concrete and reinforcing steel

Floor	Concrete		Reinforcing steel				
	Compressive strength, f_c, (MPa)	Tensile strength, f_t, (MPa)	Yield strength, f_y, (MPa)	Ultimate strenght, f_u, (MPa)	Yield strain, ε_y	Ultimate strain, ε_u	η[1]
9~12	36	1.8	490	613	0.025	0.12	0.20
6~8	42	2.1					
3~5	48	2.4					
GF~2	54	2.4					

---

[1] To estimate of the available rotation capacity at the plastic hinges following the procedure described in section 2.4.

Table 4.11 - Cross-section detailing for columns and beams according to the floor number

Floor	Columns	Beams
12	–	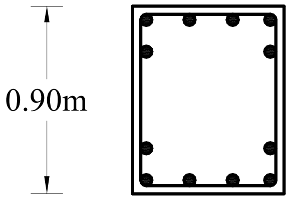 4 + 2 D29
11	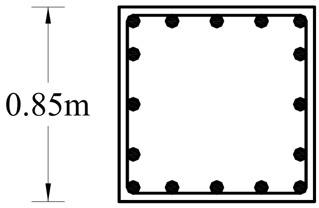 16 D32	
10		
9		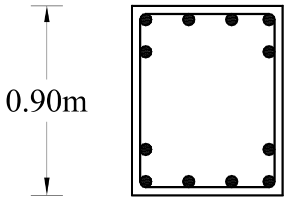 4 + 2 D32
8	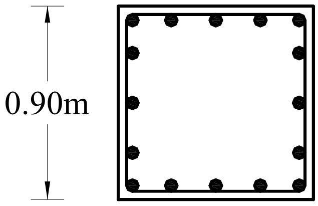 16 D35	
7		
6		
5	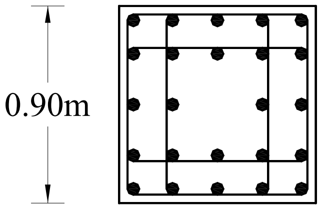 16 + 8 D35	
4		
3		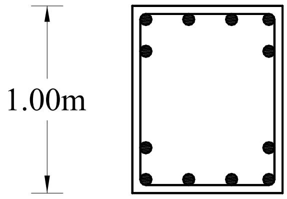 4 + 2 D35
2	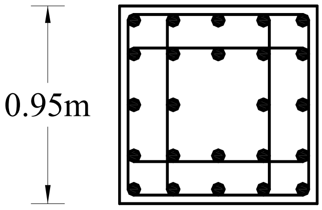 16 + 8 D38	
1		
GF		–

every structural element of this frame is comparable to European B500, see Table 2.4. The yield strength is 490MPa.

As in the previous example, the onset of plastic behaviour in the plastic hinges is associated with yielding of the tensile reinforcement. The cross-section detailing columns and beams is identical, irrespective of its location in the plan. In other words, cross-section detailing only changes with the floor number. To assure ductile behaviour, low tensile reinforcement ratios were chosen: between 0.8% and 1.1% for the beams and 0.6% and 1.2% for the columns. Table 4.11 shows the cross-section detailing in terms of longitudinal reinforcement according to the floor number for both columns and beams. The information regarding the longitudinal reinforcement is below the sketches: For instance, for the case of the columns in the first 3 floors, the outer layer of longitudinal reinforcement is composed of 16 bars, each with a diameter of 38mm, whereas the inner layer is composed of 8 bars with the same diameter, thus the designation, 16 + 8 D38. In the beams, the designation below the sketch refers only to the longitudinal reinforcement in one of the faces (top or bottom).

The problem now is to ascertain whether the structure designed by (Aono *et al.*, 2006) meets the particular specifications of this design case, as discussed in the previous steps and the general requirements of the RPSD method.

The flexural strength capacity of each of the cross-sections in the columns of Table 4.11 was determined using the commercial programme Canny (Canny Structural Analysis, 2004), using the so-called fibre model. The gravitational forces at the time of the earthquake were considered. Regarding the plastic hinges in the beams, a simple cross-section analysis was carried out. Table 4.12 shows the results of this analysis for the cross-sections at the ends of the beams and at the columns. The flexural capacities of the plastic hinges corresponding to the partial collapse mechanism are highlighted with a grey background.

Firstly, it is seen from Table 4.12 that the flexural strength of the plastic hinges in the structure designed by (Aono *et al.*, 2006) is practically the same as the requirements derived in step 4.

A further analysis of Table 4.12 shows that the strength demand in the columns above

Table 4.12 - Flexural capacities of the plastic hinges considering the gravitational forces at the time of the earthquake for the structure designed by (Aono *et al.*, 2006)

Floor	Columns			Beams
	Corner	Middle	Central	
12	–	–	–	1126
11	1979	2057	2210	
10	2057	2210	2502	
9	2134	2359	2776	1390
8	2772	3088	3676	1390
7	2853	3241	3947	
6	2932	3390	4203	
5	4234	4767	5711	
4	4313	4911	5951	
3	4390	5053	6179	1873
2	4911	5702	7075	
1	4993	5851	7317	
GF	5075	5998	7547	–

Table 4.13 - Available rotation capacity and expected ductility demand at the plastic hinges of the structure designed by (Aono *et al.*, 2006)

Plastic hinges			M (kNm)	V (kN)	h (m)	l_p (m)	θ_u (rad)	θ_y (rad)	μ_{exp}
Columns	Top of the 8th floor	Corner	2514	635	0.90	1.02	0.068	0.003	14
		Middle	2873	1080	0.90	0.76	0.050	0.002	19
		Central	3591	1080	0.90	0.89	0.059	0.003	16
	Base of the ground floor	Corner	5027	1351	0.95	0.98	0.062	0.003	15
		Middle	5746	2296	0.95	0.74	0.047	0.002	20
		Central	7182	2296	0.95	0.86	0.055	0.003	17
Beams	4~8		1397	600	0.90	0.69	0.046	0.002	21
	1~3		1862	717	1.00	0.77	0.046	0.002	21

the 9th floor of the structure designed by (Aono *et al.*, 2006) is always larger than the requirements found in Figure 4.16 and Figure 4.17, thus yielding will not take place at the 3 upper floors.

Additionally, we must verify whether the structure designed above complies with the general assumptions of the RPSD method, i.e. if there is enough rotation capacity at the plastic hinges and if the expected ductility demand in these elements is sufficient to consider that plastic behaviour will govern the dynamic response. Therefore we apply the procedure in section 2.3 to obtain a conservative estimation of the rotation capacity of each of the plastic hinges. Table 4.13 summarises the results of such an analysis. Note that the bending moment and shear force quantities were already determined in the previous design step, and that the expected ductility demand refers to the ratio of the maximum expected rotation, θ_u=0.045rad, to the yield rotation, θ_y.

From Table 4.13, it is seen that there is enough rotation capacity at all plastic hinges, i.e. θ_u>0.045 rad, and that the expected ductility demand is always greater than 10, leading to the conclusion that the dynamic response will be controlled by plastic behaviour.

Finally, comparing the existing flexural capacities in the columns, cf. Table 4.12 and the corresponding strength demand derived in step 4, cf. Table 4.8, it is expected that yielding will take place in some parts of the columns of the structure designed by (Aono *et al.*, 2006). However, it should be noted that this situation would be prevented using appropriate overstrength factors if the author had carried out the design. In practise this would translate into stronger and therefore stiffer cross-sections in the columns, implying different elastic properties assigned to the structure as a whole. Nevertheless, as mentioned above, it is expected that the structure designed by (Aono *et al.*, 2006) will have its dynamic response against the ground motion of the GRPS in Figure 4.12 controlled by plastic behaviour, which therefore minimises this discrepancy.

Comparison with refined NLTHA analysis

With reference to the previous section, we can expect that the dynamic response of the structure designed by (Aono *et al.*, 2006) against the ground motions in the GRPS

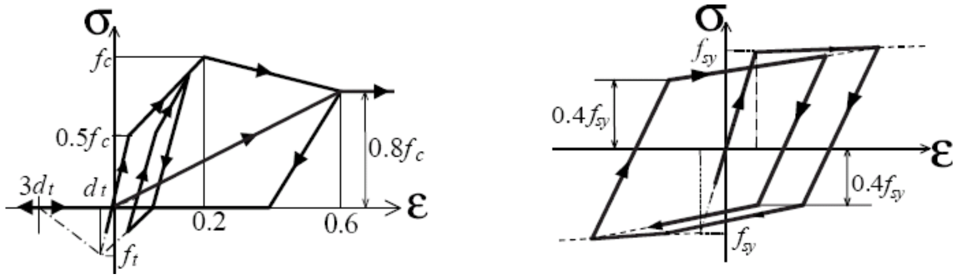

a) **b)**

Figure 4.18 -Stress-strain curves for a) confined concrete and b) reinforcing steel

of Figure 4.12 will develop within the limits discussed in steps 1 to 4, i.e. on the formation of the partial collapse mechanism of Figure 4.13b) and having maximum drift of 4.5%. To confirm this we have performed refined NLTHA's using the full records of both horizontal components of the Erzikan and Takatori ground motions, scaled up so that PGA=1g.

We used the commercial programme, Canny, based on the fibre-modelling approach to model the columns, cf. section 1.2.2. The properties of the materials are explicitly defined by the corresponding stress-strain curves, see Figure 4.18.

Figure 4.18 shows the stress-strain curves for the confined concrete and reinforcing steel in the columns adopted in this analysis. The first is the constant confinement trilinear model, and the second the bilinear steel model.

The beams are modelled as linear elastic elements with plastic hinges in the ends, the length of which are 0.80m (slightly larger than the values estimated in Table 4.13, and therefore with even larger rotation capacity). The hysteretic properties of the plastic hinges are simulated using the Takeda model.

The fact that the structural model makes use of the fibre modelling approach for the case of the columns allows an accurate estimation of damage along these structural elements. We must simply assign the properties of the materials. Furthermore, this allows for a comparison of the solution in terms of strength demand at the columns provided by the RPSD method and the refined NLTHA.

The damping was considered to be proportional to the stiffness matrix so that the damping ratio of the first mode equals 0.03.

As in the previous example, the response is calculated by direct integration of the equations of motion using the Newmark method, with $\gamma=0.5$ and $\beta=0.25$.

Figure 4.19 and Figure 4.20 show the first 15s of the displacement-history curves in terms of top displacement for the rigid-plastic and the refined NLTHA.

From the curves in Figure 4.19 and Figure 4.20 it is first noted that generally there is good agreement between the displacement-history curves computed by the rigid-plastic NLTHA and by the refined NLTHA. Again, we have virtually parallel curves for periods of large displacement demand after the onset of the first period of plastic behaviour. In the previous example, the explanation for the initial discrepancy between elastoplastic and rigid-plastic analysis was given.

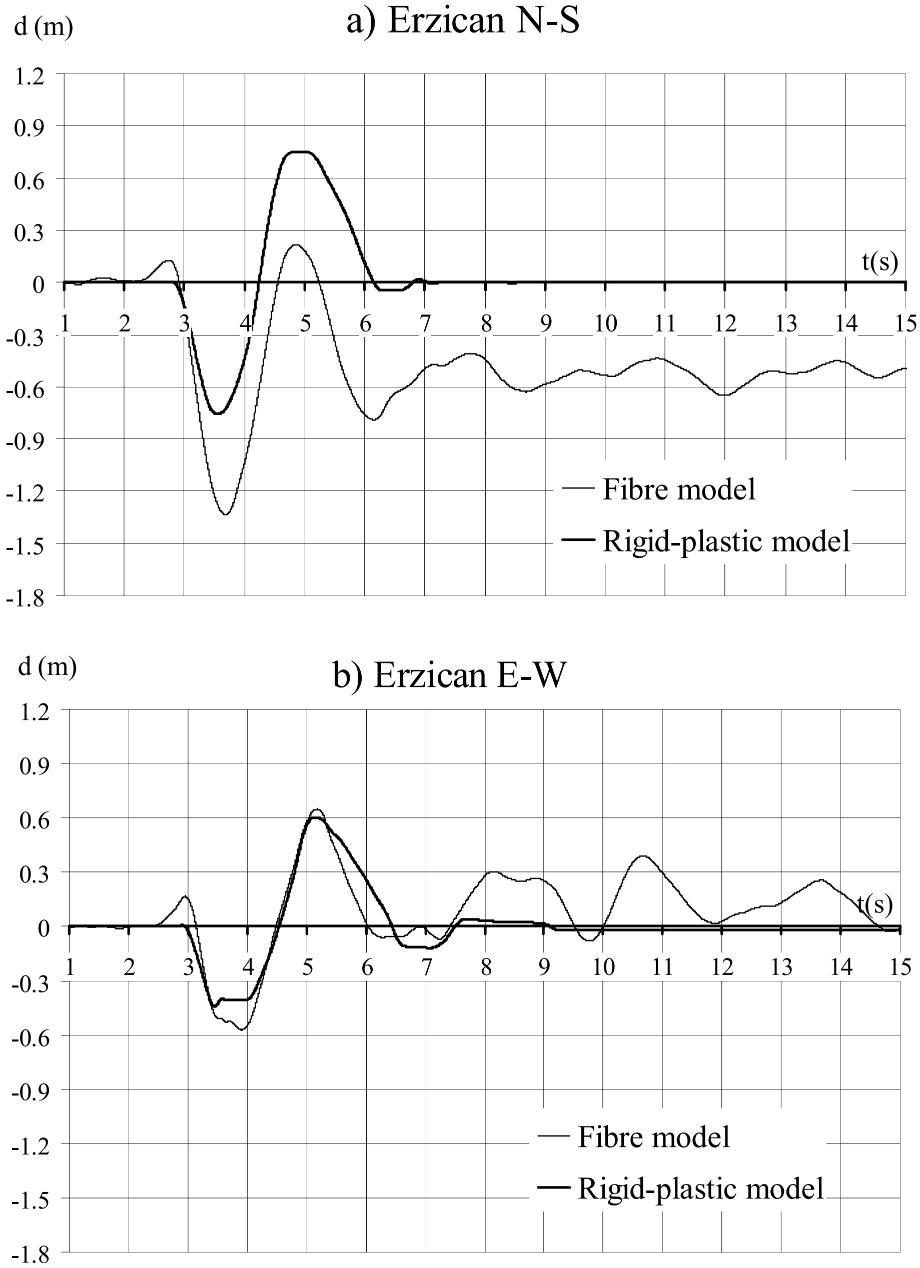

Figure 4.19 - Top displacement-history curves by the rigid-plastic and the refined NLTHA for both horizontal components of the Erzikan ground motion

Table 4.14 -Maximum displacement at the top for the rigid-plastic and fibre models (m)

	Erzikan N-S	Erzikan E-W	Takatori N-S	Takatori E-W
RPSD method	0.75	0.61	1.36	0.74
Refined NLTHA	1.34	0.65	1.15	1.06

On average, it is seen that the prediction of maximum displacement demand by the rigid plastic model is 15% lower than that provided by the fibre model, see Table

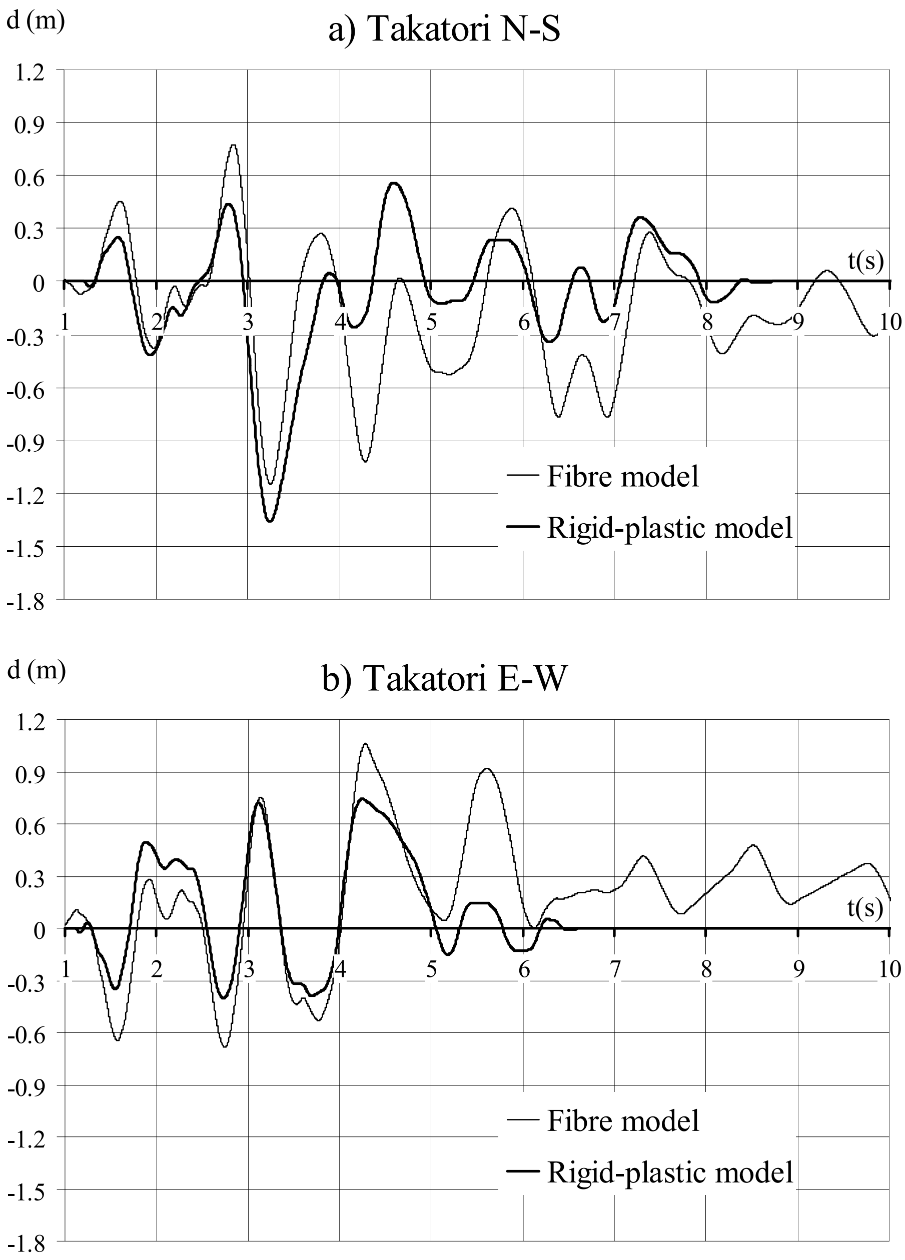

Figure 4.20 - Top displacement-history curves by the rigid-plastic and the refined NLTHA for both horizontal components of the Takatori ground motion

4.14. It is again stressed that from an engineering perspective, this is considered a small deviation.

However, it is more important to evaluate if the structure develops the partial collapse mechanism and whether the maximum drift is 4.5%, than it is to have good agreement between the displacement time-history curves. Figure 4.21 shows the inter-story drift development with the height for both horizontal records of the Erzikan ground motion obtained by the fibre model at the time of maximum displacement demand. Examining the last row of Table 4.14, it can be seen that these records define the range of maximum displacement demand predicted by the refined NLTHA.

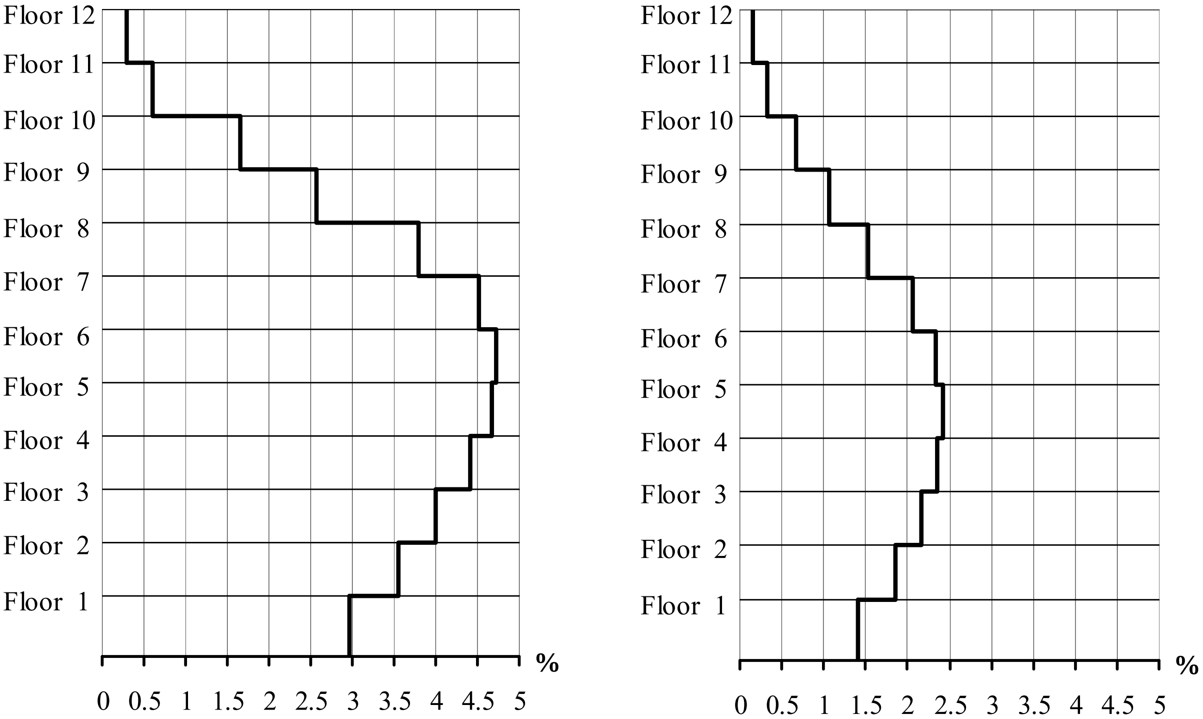

a) N-S component b) E-W component

Figure 4.21 -Inter-storey drift at time of maximum displacement demand for both components of the Erzikan ground motion

From the records analysed by the fibre model, the N-S component of the Erzikan ground motion yields maximum inter-story drift, i.e. 4.7% between floors 5 and 6. This is remarkably close to the prediction of the rigid-plastic approach.

Moreover, as one can see in Figure 4.21a) and b), the drift among the 3 upper floors is comparably lower than in the first 8 floors, for both records and for different levels of maximum displacement demand. This indicates that the structure designed by (Aono *et al.*, 2006) did indeed perform as expected, i.e. the structure developed the partial collapse mechanism of Figure 4.13b).

Finally, the results in terms of maximum strength demand from the refined NLTHA are compared with the predictions of the RPSD method after the application of the extreme loading scenarios approach, cf. Table 4.8. Figure 4.22 and Figure 4.23 show the maximum strength demand in terms of bending moments and shear forces in each of the columns of Table 4.8 up to the 8th floor from the refined NLTHA for all 4 records of ground motion. The curves representing the strength demand derived in step 4 are also shown.

Analysing Figure 4.22 and Figure 4.23 it is shown that the predictions of maximum strength demand by the RPSD method are close to the results from the refined NLTHA, particularly for the case of shear strength demand. In fact, the strength demand estimated by the RPSD method is on average 95% lower than the refined NLTHA for the shear case and 42% higher for the flexural case. The latter is as expected, judging by the conservative nature of the horizontal forces estimated on the basis of the extreme loading scenarios approach.

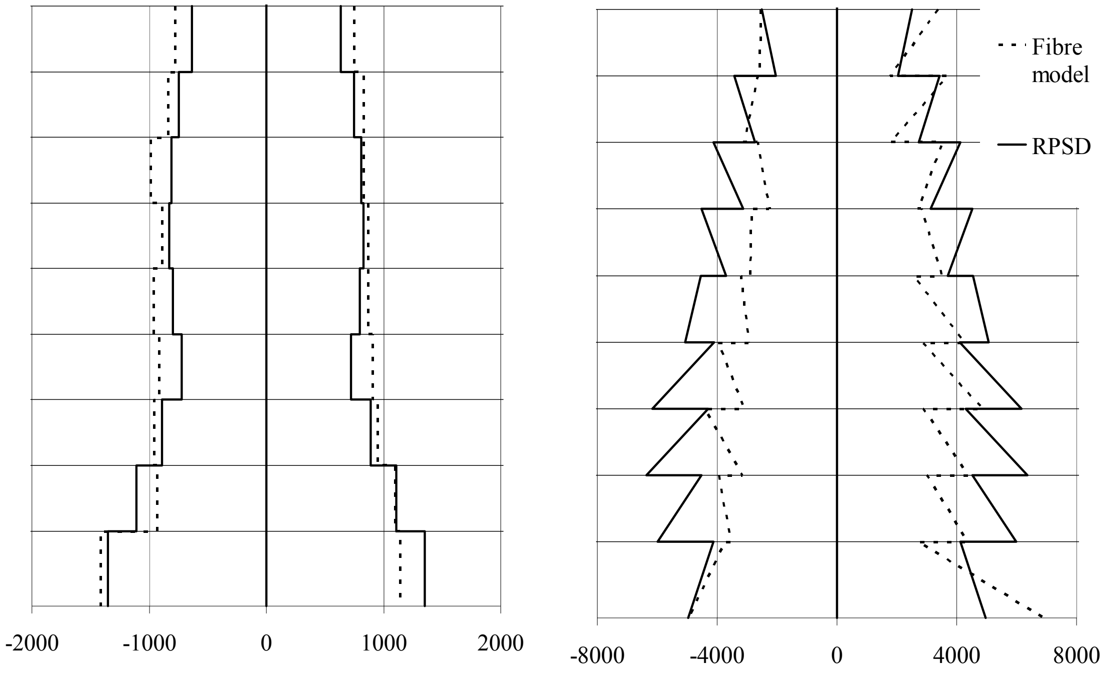

a) Corner Column / Outer frame
Shear strength demand

b) Corner column / Outer frame
Flexural strength demand

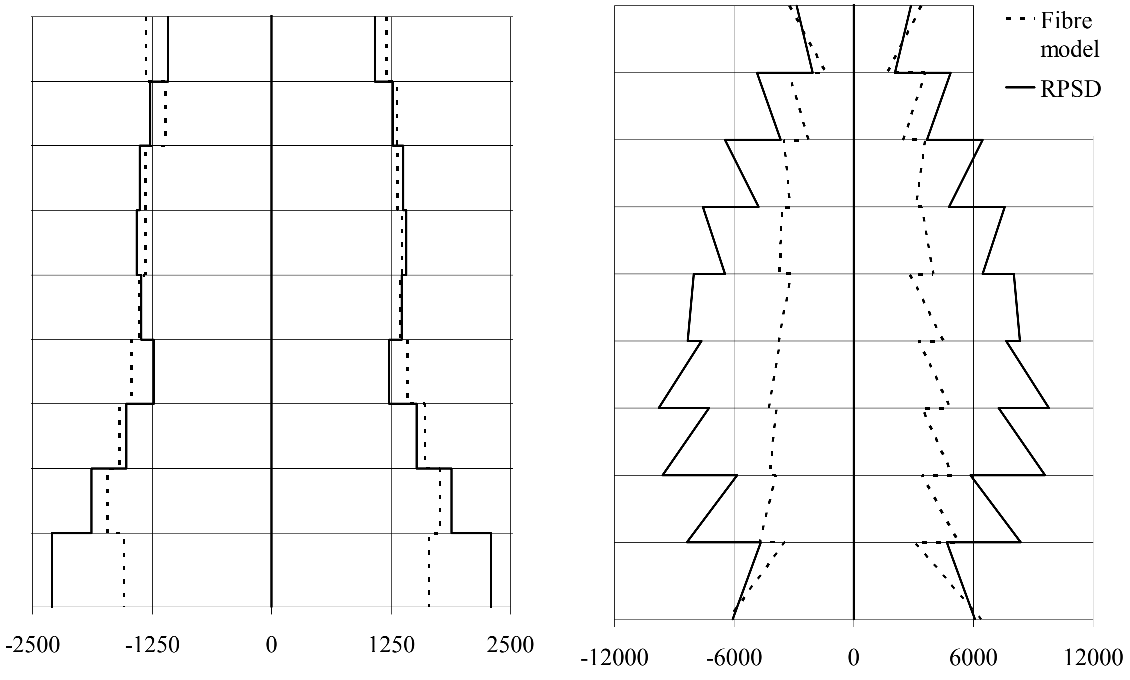

c) Middle column / Outer frame
Shear strength demand

d) Middle column / Outer frame
Flexural strength demand

Figure 4.22 -Maximum strength demand at the columns in the outer frame by the RPSD method and by the refined NLTHA in terms of shear force and bending moments

a) Middle column / Inner frame
Shear strength demand

b) Middle column / Inner frame
Flexural strength demand

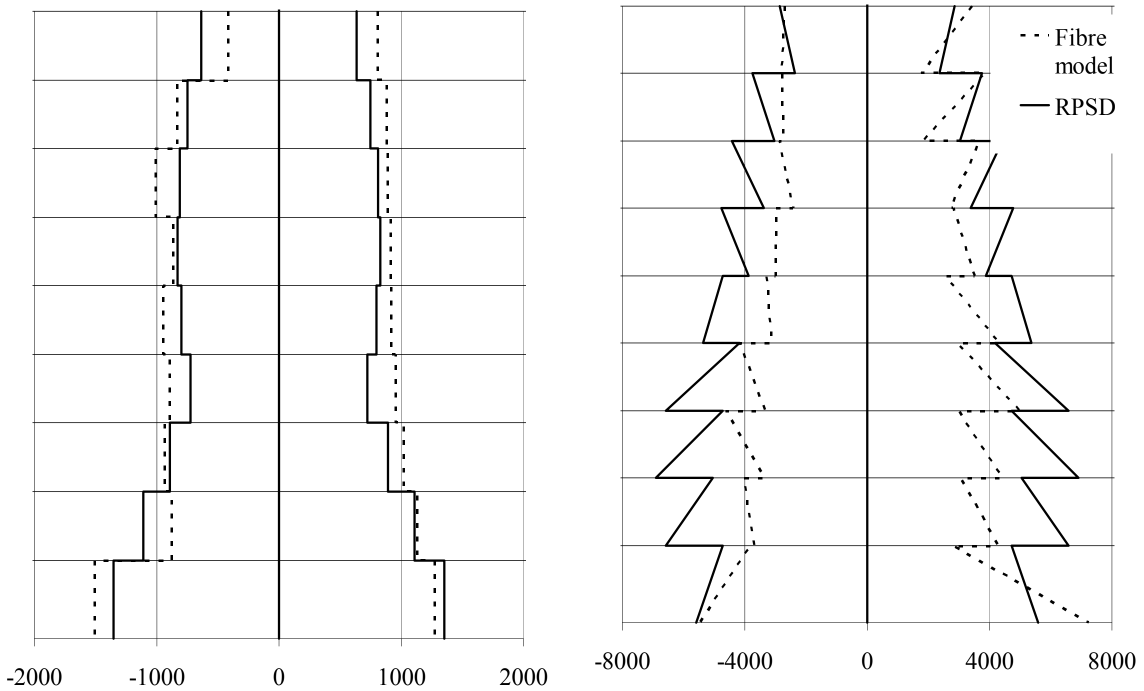

c) Central column / Inner frame
Shear strength demand

d) Central column / Inner frame
Flexural strength demand

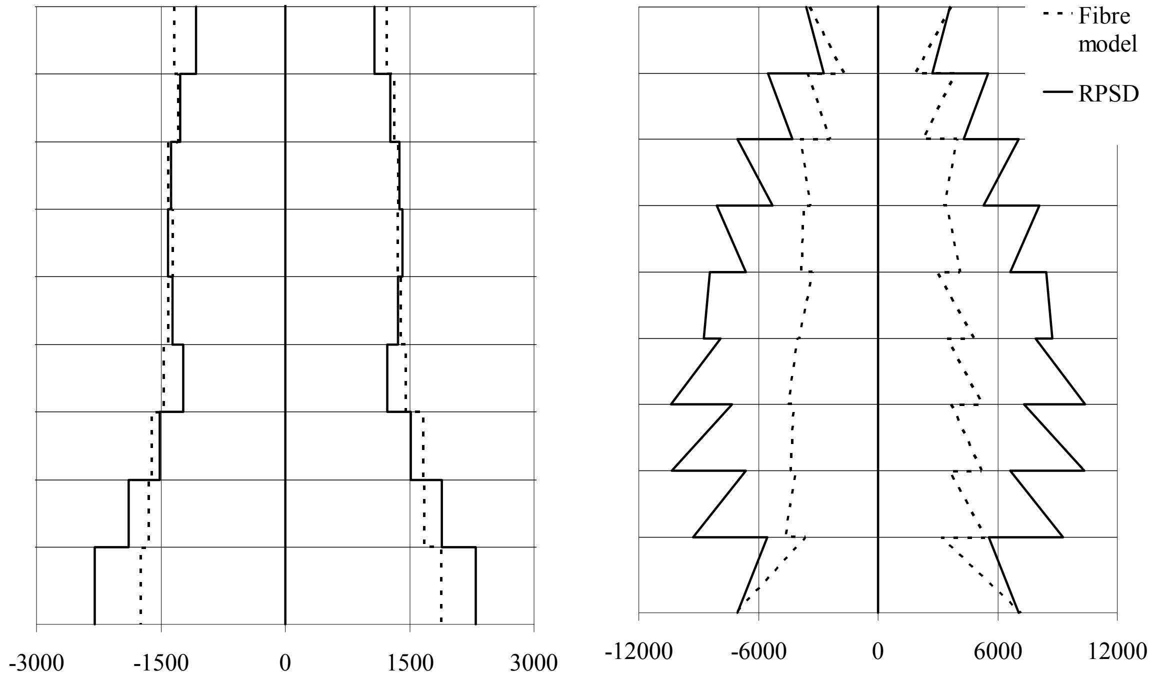

Figure 4.23 - Maximum strength demand at the columns in the inner frame by the RPSD method and by the refined NLTHA in terms of shear force and bending moments

Table 4.15 -Flexural strength demand determined by the refined NLTHA and the corresponding ration to the flexural capacity in the columns of the 3 upper floors

Floor	Cross-section	Corner Column		Corner Column		Corner Column	
		Demand, D	Ratio D/C	Demand, D	Ratio D/C	Demand, D	Ratio D/C
11	Top	1345	0.68	2239	1.09	2258	1.02
	Bottom	1536	0.78	1665	0.81	817	0.37
10	Top	2562	1.25	2619	1.18	2621	1.05
	Bottom	1949	0.95	2153	0.97	1339	0.54
9	Top	2698	1.26	2808	1.19	2821	1.02
	Bottom	2151	1.01	2304	0.98	1654	0.60

There are some cross-sections, particularly the one close to the plastic hinges in the columns, where the strength demand predicted by the RPSD method is lower than that predicted by the refined NLTHA. This relates to the overstrength phenomena at the plastic hinges due to the effect of axial compressive forces effectively captured by the fibre modelling approach. In reality this would not be a problem, as overstrength factors described in section 2.4.3 would be considered to magnify the strength demand at any point of the structure outside the hinges. In fact, it is noted that an overstrength factor of 1.3, which is perfectly within the limits discussed in section 2.4.3, is enough to assure safety at any point of the structure outside the hinges.

Finally, the flexural strength demand determined by the refined NLTHA at the columns in the 3 upper floors is shown in Table 4.15. The ratios D/C refer to the relation between the flexural strength demand, D, and the respective flexural capacity, C, cf. the 3 upper rows in Table 4.15.

Again it is found that flexural demand at some cross-sections is slightly exceeded. However, in Figure 4.21 it is shown that the drift in these floors is very limited, which in turn indicates small amounts of plastic deformations. Therefore, the fact that the flexural demand is exceeded in some cross-sections does not indicate the onset of plastic behaviour there, but the enhancement of flexural capacity due to additional compressive forces.

5. Final remarks

The main objective of this work is to present a new, rational and simplified design procedure that can help engineers faced with the task of designing reinforced concrete structures to withstand the effects of strong ground motion.

- Despite its rationality and superior accuracy, the use of conventional NLTHA for design purposes is beset with some important setbacks, the most notorious of all being the one related with the complete definition *a priori* of strength and stiffness distribution throughout the structure. On the other hand, current simplified design procedures, as the Elastic Spectrum and the Capacity Spectrum methods, may work directly with a spectrum, which allows a swift estimation of the seismic demand expected at the implementation site. However, as it was seen in section 1, these procedures rely on the use modal superposition and combination rules together with force reduction factors to assess the seismic demand in ductile structures. Not only this is inconsistent from the theoretical point of view, but also may lead to erroneous estimations of internal forces and displacements most especially when higher mode effects are important.
- The RPSD method, presented in this thesis, combines the
    a) The rationality of NLTHA for the estimation of the seismic demand solely based on the properties of the structure, and
    b) The simplicity and practical value of spectral analysis for the estimation of the required dissipation capacity.

  While significant engineering judgement is required, the designer has full control over the design process as a suitable collapse mechanism, required structural dissipation capacity and appropriate strength distribution throughout the structure are explicitly defined according to the desired performance criterion. Therefore, the procedure follows the modern seismic design philosophy, Performance Based-Seismic Design.
- The corresponding theoretical background is found on the extremum principles of the theory of Plasticity as the formation of the desired collapse mechanism is enforced by finding a statically admissible safe stress field outside the plastic hinges.
- In section 3.1 it was seen that the main assumptions of the RPSD method are:
    a) Disregard for the contribution of structural elastic properties in the dynamic response and
    b) Disregard for viscous damping given that the only source of energy dissipation is attributed to plastic behaviour.

  As a result, undamped rigid-plastic structures are considered i.e. structures with rigid-plastic behaviour at the plastic hinges and rigid behaviour in the remaining part. Therefore, the only source of deformation is due to plastic deformations at the plastic hinges, which in turn enables a direct relation between the global dynamic response with the local damage at the yield zones.
- The review on cyclic behaviour of reinforced concrete elements presented in chapter 2 showed that significant levels of ductility may be reached provided that the plastic hinges are properly detailed and explore flexural modes of failure. This

is on the basis of the rigid-plastic hysteretic relationships assumed at the plastic hinges.

- In section 2.3, a new simplified procedure to evaluate rotation capacity of flexural hinges was presented.
- Another important feature of rigid-plastic structures designed to develop a collapse mechanism is that there is only one mode of vibration, which means that they can be treated as rigid-plastic oscillators. As seen in section 3.2, this yields a great deal of simplification in the treatment of the dynamic response of the structure to any ground motion. In fact, for each time step of a direct integration procedure, there is only one equation of motion to be solved. The latter simply depends on the shape of the collapse mechanism and the dissipation capacity of the structure. In section 3.2.1 a computational procedure to perform NLTHA is presented.
- It was further seen in section 3.2.2 that the rigid-plastic hysteretic relationship with consideration of pinching provides accurate estimations of the dynamic response of ductile reinforced concrete systems given the close agreement with those provided by the Takeda model.
- In the RPSD method the required dissipation capacity on the structure, associated with the parameter F_y* (defined in section 3.2.3), is estimated considering a predefined performance parameter by means of the rigid-plastic spectra. These spectra were found to be very useful for design purposes for the following reasons:
    a) GRPS can easily be scaled up or down according to ground motion intensity expected at the implementation site.
    b) The seismic demand associated with a number of ground motion records is simply given by the envelope of each of the corresponding GRPS's.
    c) The GRPS is exclusively dependent on the ground motion scenario.
    d) The seismic demand at a specific structure imposed by a specific ground motion scenario is given by the SRPS, which is simply obtained multiplying the ordinates in the corresponding GRPS by the parameter κ (defined in section 3.2.3). The latter parameter is characteristic of the structure and of the collapse mechanism assumed.
- It was further concluded in the study on the dynamic response of reinforced concrete oscillators with flexure dominated behaviour of section 3.3.1, that the GRPS is an effective tool to estimate maximum dynamic seismic demand when the expected rotation ductility demand is at least of the order of 8-10 and if calculations are carried out according to section 2.3.
- The task of selecting the most appropriate way for the structure to withstand the stresses imposed by the ground motion is facilitated to a great extent by the extreme loading scenarios approach, cf. section 3.3.2. It was seen that this approach yields a conservative set of external forces
- The combination of both rigid-plastic spectra and of the extreme loading scenarios approach yields a straightforward procedure towards final design and allows an effective separation between the properties of the structure and those of the ground motion. In fact, the lateral loading cases upon which the design of the structure is based are solely dependent on the shape of the chosen collapse

mechanism and the desired structural performance in the local seismicity. They do not depend on the choices regarding the way the structure should carry the stresses imposed by the ground motion neither on the shape of the ground motion. On the other hand, as it was confirmed in the example shown in section 4.1, the dynamic response of the structure is independent of the choices regarding strength distribution, which to a great extent facilitates calibration of the final design.

- Another important feature of the RPSD method is the avoidance of any sort of artificial coefficients intended to adjust the dynamic response of the structure according to empirical observations, while lacking physical meaning. This is because the values read from the SRPS are the actual values of the dynamic response of the structure. There is no need for any modal combination rules, since there is only one possible mode of vibration – that associated with the collapse mechanism. Also, reduction coefficients are unnecessary, as the results computed in the rigid-plastic spectra are derived after rigid-plastic NLTHA.
- The simplified design procedure proposed in this paper follows the principles of rigid-plastic theory, which means that any phenomena regarding elastic behaviour of structures cannot be taken into account. Therefore, depending on the structural system and its performance requirements, final design may be adjusted considering higher mode effects and serviceability limit states against more frequent and moderate ground motion. This may be done checking the performance of the structure by means of other methods for dynamic analyses based on simplified linear elastic theory.
- The design examples of chapter 4 highlighted the simplicity of the RPSD method, and the comparison with a refined NLTHA showed that the structure indeed performed as expected, both in terms of seismic demand on the structure and formation of the chosen collapse mechanism.
- Future developments of the RPSD method should include the extension to the case of three-dimensional structures. Also, further investigations should focus on the application of the procedure to more complicated systems than the simple frames considered in the paper, such as shear wall systems and the systems with combined frame and shear wall action (dual systems).
- The shape of the GRPS in Figure 3.27, which corresponds to the Friuli earthquake records, is notably different than that in Figure 4.12, which corresponds to the Erzikan and Takatori records. The former has a concave contour and the latter a convex one. Observing the corresponding accelerograms in the Appendix, it is seen that the Friuli records are dominated by high frequency and symmetric vibration opposing the Takatori and Erzican records which are clearly asymmetric pulses. It seems that the GRPS may be used as an effective tool to characterize a specific ground motion and its potential damage induced in structures. Future research on this topic is also required.

Bibliography

Abrams, D., 1987 – Influence of axial force variation on flexural behaviour of reinforced concrete columns. Structural Journal of the ACI, Vol. 84 (May-Jun), pages: 246-254

Ang, B.G., Priestley, M.J.N. and Paulay, T., 1989 – Seismic shear strength of circular reinforced concrete columns. Structural Journal of the ACI, Vol.86 (Jan-Fev), pages: 45-58

Aoyama H. and Noguchi, H., 1979 – Mechanical properties of concrete under load cycles idealizing seismic actions. Bull. d'information CEB, Vol. 131, pages: 29-63

ATC, 1996 – Seismic evaluation and retrofit of concrete buildings, Applied Technology Council, Vol. 1, ATC-40, Redwood City.

Bachman, H., Linde, P. and Wenk, T., 1994 – Capacity design and nonlinear dynamic analysis of earthquake-resistant structures Proc. 10th Eur. Conf. Earthquake Engng., Vienna, Balkema, Rotterdam.

Bertero, V.V., Bresler, B. and Liau, H., 1969 – Stiffness degradation of reinforced concrete members to cyclic flexural moments. Earthquake Engineering Research Center, Univ. of California, Berkeley, Ca.

Biot, M.A., 1942 – Analytical and Experimental Methods in Engineering Seismology, ASCE Transactions, 108, pp 365-408

Bousias, S.N. Verzelleti, G., Fardis, M.N. and Magonette, G., 1992 – RC columns in cyclic biaxial bending and axial load, Proceedings of the 10th World Conference on Earthquake Engineering, Madrid, pages: 3041-46

Brinch Hansen, J., 1953 – Earth Pressure Calculation, Danish Association of Civil Engineers

Brown, R.H. and Jirsa, J.O., 1971 – Reinforced concrete beams under load reversals. Structural Journal of the ACI, Vol. 68 (May), pages: 380-390

Chopra, A.K, 2004 – Estimating seismic demands for performance-based engineering of buildings, Key-note lecture at the 13th World Conf. Earthquake Engng., Vancouver, Paper no. 5007

Chopra, A.K. and Goel, R.K., 1999 – Capacity-demand-diagram methods based on inelastic design spectrum, Earthquake Spectra, Earthquake Engineering Research Institute, vol. 15(4), 637-56

Chopra, A.K. and Goel, R.K., 2001 – Direct displacement-based design: Use of inelastic vs. elastic design spectra, Earthquake Spectra, Earthquake Engineering Research Institute, vol. 17(1), 47-64

Clough, R.W. and Penzien, J., 1993 – Dynamics of structures 2nd ed., McGraw-Hill, U.S.A.

Comite Euro-International du Beton, 1994 – Behaviour and analysis of reinforced concrete structures under alternate actions inducing inelastic response. Bulletin d'Information Nº 220, Volume 2.

Comite Euro-International du Beton, 1996 – RC elements under cyclic loading, State of the art report.

Computers and Structures, Inc., 2004 – CSI Analysis reference manual, Berkeley

Dansk ingeniørforening, 1908 – Normer for jærnbetonkonstruktioner, København, Denmark, in Danish

Darwin, D and Nmai, C.K., 1986 – Lightly reinforced concrete beams under cyclic load. Structural Journal of the ACI, Vol. 83 (Sept.-Oct.), pages: 777-783

Domingues Costa, J.L., 2003 – Reinforced concrete under large seismic action, BYG•DTU, Report R-076, Lyngby, Denmark

Domingues Costa, J.L., Bento R., Levtchitch V. and Nielsen M.P., 2005 – Simplified non-linear time-history analysis based on the Theory of Plasticity, Proceedings of the ERES 2005 Conference, Skiathos, Greece, WIT-Press, Southampton, UK, pp. 375-386

Domingues Costa, J.L., Bento R., Levtchitch V. and Nielsen M.P., 2006 – Rigid-plastic seismic design of reinforced concrete structures, Journal of Earthquake Engineering and Structural Dynamics, John Wiley&Sons, DOI: 10.1002/eqe.617

Domingues Costa., J.L., Aono, M., Ichinose, T., Bento, R., Nielsen, M.P., 2006 – The RPSD method and its application to the design of a 12-story R/C frame, Proceedings of the 1st European Conference on Earthquake Engineering and Seismology, Genéve, Switezerland

Dowel, R.K., Seible, F. and Wilson, E.L., 1998 – Pivot hysteresis model for reinforced concrete members, Structural Journal of the ACI, vol. 95(5), 607-17

European Committee of Standardization (CEN), 2003 – Eurocode 8, draft no:6, Brussels

Fajfar, P., 1999 – Capacity Spectrum Based on Inelastic Demand Spectra, Earthquake Engineering and Structural Dynamics, John Wiley&Sons, Vol. 28, pp. 979-993.

Falcão, S., 2002 – Performance based seismic design: Application to a reinforced concrete structure, M.Sc. Thesis presented to IST-UTL, Lisbon

Falcão, S., Bento, R., 2002 – Analysis Procedures for Performance-based Seismic Design, Proceedings of the 12th European Conference on Earthquake Engineering, EAEE, Elsevier, London

Fédération Internationale du Beton (FIB), 2003 – Displacement-based seismic design of reinforced concrete buildings, Lausanne, Switzerland

Freeman, S.A., 1978 – Prediction of response of concrete buildings to severe earthquake motion, Douglas McHenry Symposium on Concrete and Concrete Structures, pp. 589-605, American Concrete Institute, ACI SP-55, Detroit, USA.

Freeman, S.A., 1998 – Developments and use of the capacity spectrum method, Proceedings of the 6th U.S. National Conf. Earthquake Engng., Seattle

Garstka, B, Krätzig, W.B. and Stangeberg, F., 1993 – Damage assessment in cyclically loaded reinforced concrete members, in Structural Dynamics: Eurodyn'93, Moan et al. (eds), Balkema, Rotterdam, V.1, pp. 121-128

Gutierrez, J. and Alpizar, M., 2004 – An effective method for displacement-based earthquake design of buildings, Proceedings of the 13th World Conf. Earthquake Engng., Vancouver, Paper no. 1512

Hibino, Y., Tozawa, T., N., Domingues Costa., J.L., Nielsen, M.P., Ichinose, T., 2005 – Dynamic response of the rigid-plastic model Part 2: Column collapse type model, Architectural Institute of Japan (AIJ), Summaries of Technical Papers of Annual Meeting AIJ;B-2, pp. 391-392

Hwang, T.H., and Scribner, C.F., 1984 – Reinforced concrete member cyclic response during various loadings. Journal of Struct. Div., ASCE, Vol. 110, ST3, pages: 477-489

Jirsa, J.O., Maruyama, K. and Ramirez, H., 1980 – The influence of load history on the shear behaviour of short RC columns. Proceedings of the 7th World Conference on Earthquake Engineering, Istanbul, Vol. 6, pages: 339-346

Karsan, I.D. and Jirsa, J.O., 1969 – Behaviour of concrete under compressive loadings. Journal of the Struct. Div. ASCE, Vol. 95 (ST12), pages : 2543-63

Kobayashi, K., Kokusho, S., Takiguchi, K. and Boo, C., 1984 – Study on the restoring force characteristics of RC columns to bi-directional deflection history, Proceedings of the 8th World Conference on Earthquake Engineering, San Francisco, Vol. 6, pages: 537-544

Krawinkler, H. and Seneviratna, G.D.P.K., 1998 – Pros and cons of a pushover analysis for seismic performance evaluation, Engng. Struct., Elsevier, vol. 20, 452-64

Krawinkler, H., 1994 – New trends in seismic design methodology, Proc. 10th European Conference on Earthquake Engineering, Vienna, Austria, Aug. 28 to Sept. 3, Vol. 2, pp. 821-830, Balkema, Rotterdam, The Netherlands.

Li, K-N., Aoyama, H. and Otani, S., 1987 – Reinforced concrete columns under varying axial load and bi-directional horizontal axial load reversals. Proceedings of the Pacific Conference on Earthquake Engineering, New-Zealand, Vol. 1, pages: 141-152

Marubashi, N., Domingues Costa, J.L., Nielsen, M.P., Ichinose, T., 2005 - A basic study on asymmetry of seismic response using the rigid-plastic model, Journal of Structural and construction Engineering, Transaction of AIJ (598), pp. 75-80 (2005).Architectural Institute of Japan (AIJ) , in Japanese

Marubashi, N., Domingues Costa, J.L., Nielsen, M.P., Umemura, H., Ichinose, T., 2006 - A basic study on asymmetry of seismic response using the rigid-plastic model, Proceedings of the 100th anniversary earthquake conference commemorating the 1906 San Francisco Earthquake, San Francisco, USA

Maruyama, K., Ramirez, H. and Jirsa, J.O., 1984 – Short RC columns under bidirectional laod histories, Journal of Struct. Div. ASCE, Vol. 110, pages: 120-137

Menjivar, M.A.L., 2004 – A review of existing pushover methods for 2-D reinforced concrete buildings, Ph.D Thesis, ROSE School, Istituto Universitario di Studi Superiori, Università degli Studi di Pavia.

Ministry of Construction, 2000 – Ministry order No. 1457, Japan.

Miranda, E. and Bertero, V.V., 1994 – Evaluation of strength reduction factors for earthquake resistant design, Earthquake Spectra, Earthquake Engineering Research Institute, vol. 10, 357-79

Neal, B.G., 1963 – The Plastic Methods of Structural Analysis, 2nd Edition, Chapman and Hall

Newmark N.M., 1959 – A method of computation for structural dynamics, Journal of the Engineering Mechanics Division, ASCE, Vol. 85, No. EM3, pp. 67-94.

Newmark, N.M. and Hall, W.J., 1982 – Earthquake spectra and design, Earthquake Engineering Research Institute, California, U.S.A

Nielsen, M.P. and Pilegaard Hansen, L., 1973 – Mekanik 3.2, Søjler og bjælkesøjler, Den private Ingeniørfond

Nielsen, M.P., 1998 – Limit Analysis and Concrete Plasticity, 2nd Edition, CRC Press, Boca Raton, USA.

Nielsen, M.P., 2000 – Beton 2, del 1, Bjælke- og rammekonstruktioner, Skæv bøjning, 1. udgave, Lyngby

Nonaka, T., 1977 – Shear and bending response of a rigid-plastic beam to blast type loading, Ingenieur Archiv, Band 46, Heft 1.

Otani, S. Cheung, V.W.T. and Lai, S.S., 1980 – Reinforced concrete columns subjected to biaxial lateral load reversals. Proceedings of the 7th World Conference on Earthquake Engineering, Istambul, V. 6, pages: 525-532

Ozecebe, G. and Saatciouglu, M., 1987 – Confinement of concrete for seismic loading. Structural Journal of the ACI, Vol. 84 (Jul-Aug), pages: 308-315

Paglietti, A., Porcu, M.C., 2001 – Rigid-plastic approximation to predict plastic motion under strong earthquakes, Earthquake Engineering and Structural Dynamics, Vol. 30, pp. 115-126.

Park, R. and Paulay, T., 1975 – Reinforced concrete structures, J. Wiley & Sons, New York

Park, R., Priestley M.J.N. and Gill, W.D., 1982 – Ductility of square confined concrete columns. Journal of Struct. Div., ASCE, Vol. 108, ST4, pages: 929-950.

Paulay, T. and Priestley, M.J.N., 1992 – Seismic design of reinforced concrete and masonry buidings, John Wiley&Sons, New York.

Paz, M., 1991 – Structural Dynamics: Theory and Computation, 3rd Edition, Van Nostrand Reinhold

Penelis, G.G. and Kappos, A.J., 1997 – Earthquake-Resistant concrete structures, E&FN Spon.

Pipa, M. and Vercesi, A., 1998 – Cyclic tests of grade B400 and B500 Tempcore Bars in Ductility of reinforced concrete structures, CEB bulletin nr.242, Lausanne, Switzerland, pp.183-196

Priestley, M.J.N and Park, R., 1987 – Strength and ductility of concrete bridge columns under seismic loadings, Structural Journal of the ACI, Vol. 84 (Jan-Fev), Pages 61-76

Priestley, M.J.N., 2003 – Myths and fallacies in Earthquake Engineering, Revisited, IUSS Press, Pavia

Priestley, M.J.N., Seible, F., Calvi, G.M., 1996 – Seismic design and retrofit of bridges, John Wiley&Sons, New York.

Rabat, B., Daniel, J.I., Weinmann, T.L. and Hanson, N.W., 1986 – Seismic behaviour of light – weight and normal –weight concrete columns. Structural Journal of the ACI, vol. 83 (Jan-Feb), pages: 69-78

Reinhorn, A. M., 1997 – Inelastic analysis techniques in seismic evaluations, in Seismic design methodologies for the next generation of codes, Balkema, Rotterdam, pp. 277-287

Sawyer, H.A., 1964 – Design of concrete frames for two failure states, Proceedings of the International Symposium on the Flexural Mechanics of Reinforced Concrete, ASCE-ACI, Miami, pp. 405-431

Scott, B.D., Park, R and Priestley, M.J.N., 1982 – Stress-Strain Behaviour of Concrete Confined by overlapping hoops at low and high strain rates. Structural Journal of the ACI, Vol.79 (1), pages:13-27

Scribner, C.F. and Wight, J.K., 1978 – Delaying shear strength decay in reinforced concrete flexural members under large load reversals, Dep. Of Civil Engineer, Univ. of Michigan, Ann Arbor, Mich

SeismoSoft, 2003 – SeismoStruct: A computer program for static and dynamic nonlinear analysis of framed structures. Available from URL: http://www.seismosoft.com

Antoniou S. and Pinho R., 2004 – Advantages and Limitations of Force-based Adaptive and Non-Adaptive Pushover Procedures, Journal of Earthquake Engineering, Vol. 8, No. 4, pp. 497-522.

Staaciouglu, M. and Ozcebe, G., 1989 – Response of reinforced concrete columns to simulated seismic loading. Structural Journal of the ACI, Vol. 86 (Jan-Fev), pages: 3-12

Staaciouglu, M., 1984 – Reinforced concrete columns subjected to uniaxial and biaxial laod reversals. Proceedings of the 8th World Conference on Earthquake Engineering, San Francisco, Ca Vol. 6, pages: 585-592

Takahashi, N., Marunashi, N., Domingues Costa., J.L., Nielsen, M.P., Ichinose, T., 2005 – Dynamic response of the rigid-plastic model Part 1: SDOF model, Architectural Institute of Japan (AIJ), Summaries of Technical Papers of Annual Meeting AIJ;B-2, pp. 389-390

Takeda, T., Sozen, M.A., Nielsen, N.N., 1970 – Reinforced concrete response to simulated earthquakes, Journal of Structural Division, ASCE, 96, No. ST12.

Takiguchi, K., Kokusho, S., Kobayashi and Kimura, M., 1980 – Response of RC Column to horizontal bi-directional deflection history, Proceedings of the 7th World Conference on Earthquake Engineering, Istanbul, Vol. 6, pages: 403-410

Timoshenko, S. P. and Gere, J. M., 1961 – Theory of elastic stability, 2nd ed., McGrawHill

Tozawa, T., Hibino, Y., N., Domingues Costa., J.L., Nielsen, M.P., Ichinose, T., 2005 – Dynamic response of the rigid-plastic model Part 3: Beam collapse type model, Architectural Institute of Japan (AIJ), Summaries of Technical Papers of Annual Meeting AIJ;B-2, pp. 393-394

Umehara, H. and Jirsa, J.O., 1982 – The shear strength of short RC columns. Proceedings of the 7th European Conference on Earthquake Engineering, Athens, Vol. 4, pages: 197-207

Umehara, H. and Jirsa, J.O., 1984 – Behaviour and design of short RC columns. Proceedings of the 8th World Conference on Earthquake Engineering, San Francisco, Vol. 5, pages: 877-884

Umehara, H. and Jirsa, J.O., 1984 – Short rectangular reinforced concrete columns under bi-directional loadings, Journal of Struct. Div. ASCE, Vol.110, 3, pages: 605-618

Wight, J.K. and Sozen, M.A., 1973 – Shear strength decay in reinforced concrete columns subjected to large deflections reversals, Civil Engineer Studies, Structures Research Series, N°403, Univ. of Illinois, Urbana I11.

Woodward, K.A. and Jirsa, J.O., 1984 – Influence of reinforcement on RC short columns resistance, Journal of Struct. Div. ASCE, Vol.110, 1, pages: 90-104.

List of symbols

A = Absolute acceleration

A_0 = Mass matrix coefficient for proportional damping

A_1 = Stiffness matrix coefficient for proportional damping

$a_g(t)$ = Ground acceleration

$a_r(t)$ = Relative acceleration

A_s = Longitudinal reinforcement area

a_y = F_y/m for the case of rigid-plastic oscillators or $F_y^*/\kappa m^*$ for the case of rigid-plastic structures; physically a_y, means the ground acceleration at the onset of plastic behaviour of a rigid-plastic system starting from rest

b = Cross-section width

$\mathbf{C}$ = Damping matrix

c = Viscous damping coefficient

d = Lateral displacement;
Effective cross-section depth

d_{max} = Peak relative displacement read from a rigid-plastic spectrum

$d_r(t)$ = Relative displacement

F = Force in general

$f_{c,dyn}$ = Concrete compressive strength under dynamic loading

f_c = Concrete compressive cylinder strength

$f(t)$ = Strength demand at the plastic hinge

f_P = Yield strength of a plastic hinge

F_y = Lateral strength of a rigid-plastic oscillator

F_y^* = Generalised yield strength of a rigid-plastic structure designed to develop a collapse mechanism

f_y = Reinforcement steel yield stress

GRPS = General rigid-plastic spectrum

h = Cross-section height

H = Height of a structure

h_i = Height of the floor i relative to the ground level

k = Stiffness coefficient

$\mathbf{K}$ = Stiffness matrix

$\bar{k}_i$ = Effective stiffness for time interval i

L = Length of a column rigid-plastic oscillator

l = Length of the structural member

m = Mass

m^* = Generalised mass of a rigid-plastic structure designed to develop a collapse mechanism

M = Bending moment

$\mathbf{M}$ = Mass matrix

m_i = Mass of floor i
M_P = Flexural capacity
N = Axial force
PGA = Peak ground acceleration
R = Force reduction factor
r = Post yield stiffness parameter for Modified Takeda model
R_{max} = Maximum dynamic response parameter read from a rigid-plastic spectrum
SRPS = Specific rigid-plastic spectrum
t = Time
T = Fundamental period of vibration
V = Shear force
$v_r(t)$ = Relative velocity
W = Virtual work

α = Unloading stiffness parameter for Modified Takeda model;
Primary pivot point parameter for the Pivot hysteresis model, span ratio
β = Numerical parameter for Newmark step-by-step integration procedure (equations 1.25 and 1.26);
Reloading stiffness parameter for Modified Takeda model;
Pinching pivot point parameter for the Pivot hysteresis model;
Width to height ratio of the cross-section according to example in section 2.3
Δ = Overall displacement;
Specimen deflection (Chapter 2)
Δa_g = Incremental ground acceleration
Δa_r = Incremental relative acceleration
Δd_r = Incremental relative displacement
ΔF_i = Effective incremental force
Δl = Plastic hinge length according to section 2.3
Δt = Time step
Δv_r = Incremental relative velocity
δ = Displacement, virtual displacement
ε = Strain
ε_c = Concrete compressive strain
ε_{cu} = Ultimate concrete compressive strain
ε_s = Reinforcement steel strain
$\dot{\varepsilon}$ = Strain rate
ϕ = Curvature
ϕ_i = Displacement coordinate of floor i
ϕ_u = Ultimate curvature

ϕ_y = Yield curvature

γ = Numerical parameter for Newmark step-by-step integration procedure (equations 1.25 and 1.26)

η = Material coefficient for calculation of available rotation capacity according to section 2.3

κ = Ground motion magnification factor of a rigid-plastic structure designed to develop a collapse mechanism

λ = Load parameter

μ = Ductility factor

μ_θ = Rotation ductility capacity according to section 2.3

$\mu_{\theta,exp}$ = Expected rotation ductility demand as defined in equation 3.33

ν = Normalized axial force

ρ_t = Tensile reinforcement ratio

ρ_w = Volume ratio of transverse steel

θ = Plastic hinge rotation

θ_P = Plastic hinge rotation capacity according to section 2.3

θ_y = Plastic hinge yield rotation according to section 2.3

σ = Stress

σ_c = Concrete compressive stess

σ_s = Reinforcement steel stress

τ = Bond stress

ω = Angular frequency

ξ = Damping ratio

ψ = Relative deflection increment

Appendix

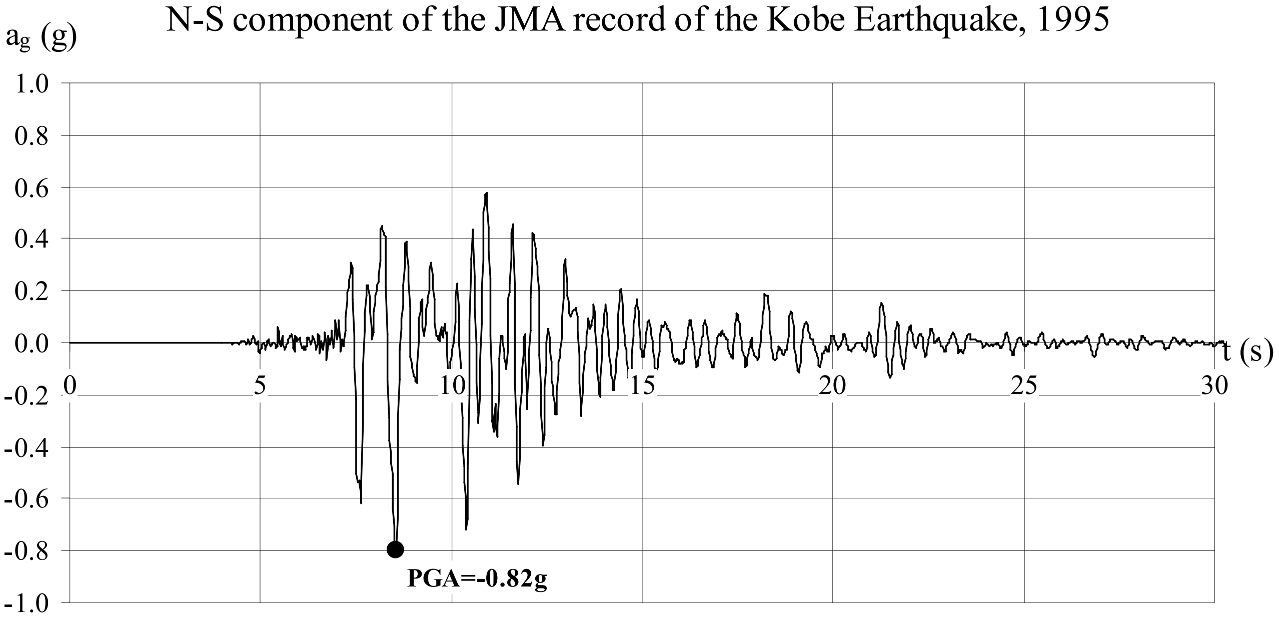
N-S component of the JMA record of the Kobe Earthquake, 1995

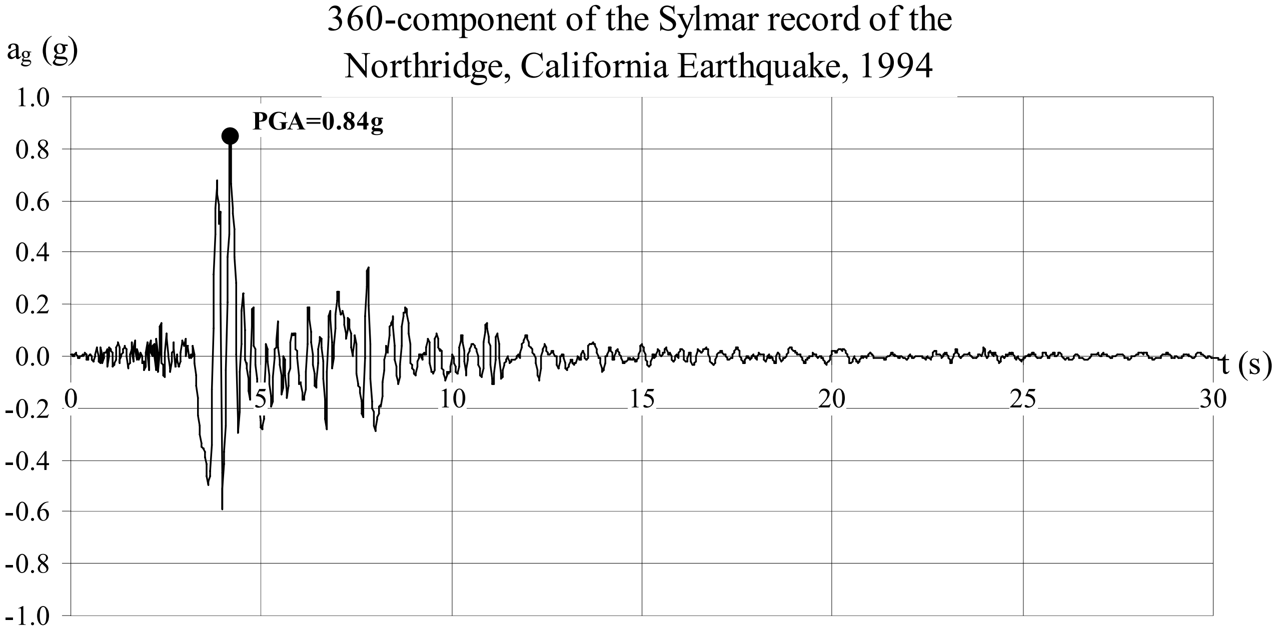
360-component of the Sylmar record of the Northridge, California Earthquake, 1994

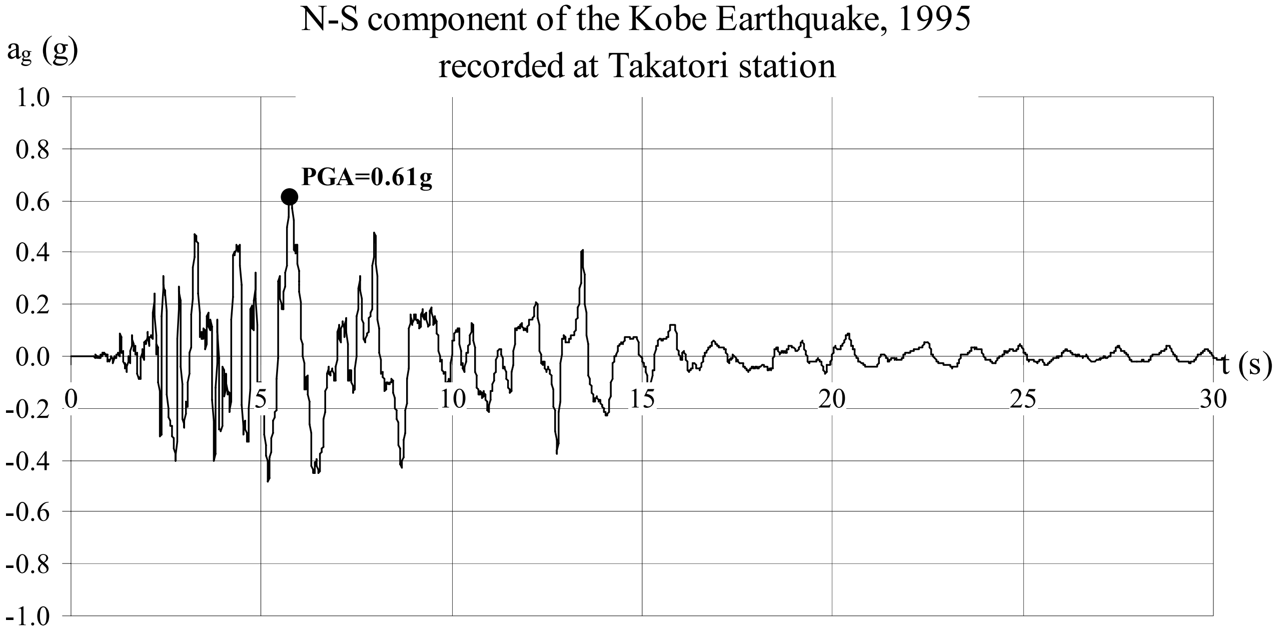
N-S component of the Kobe Earthquake, 1995 recorded at Takatori station

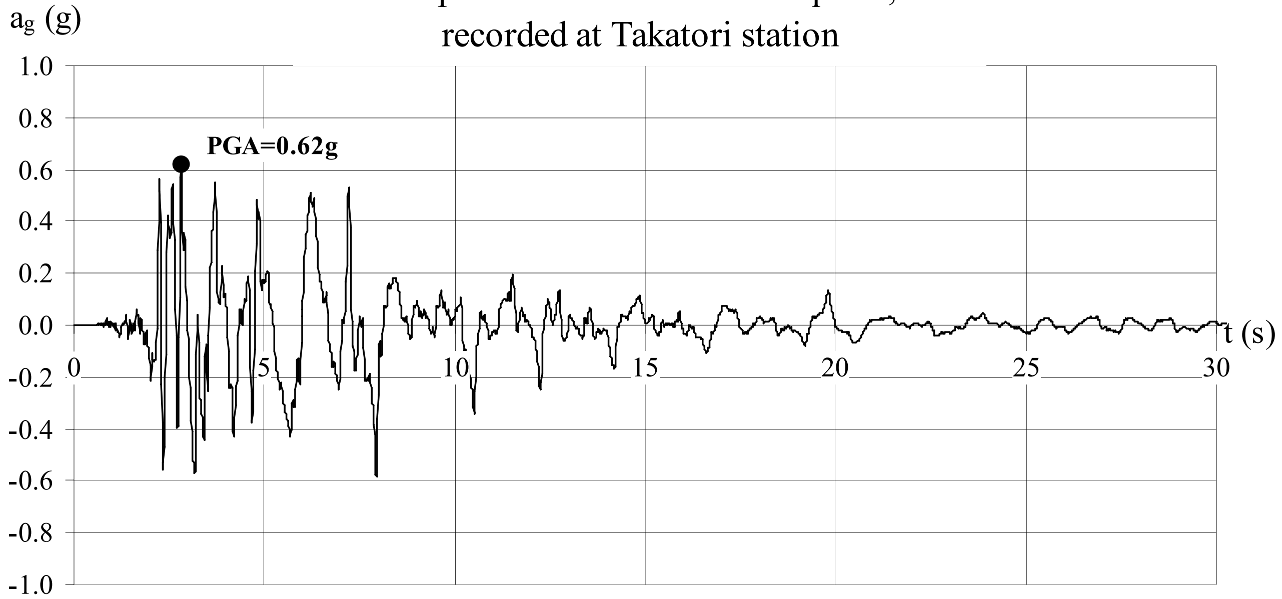

E-W component of the Kobe Earthquake, 1995
recorded at Takatori station

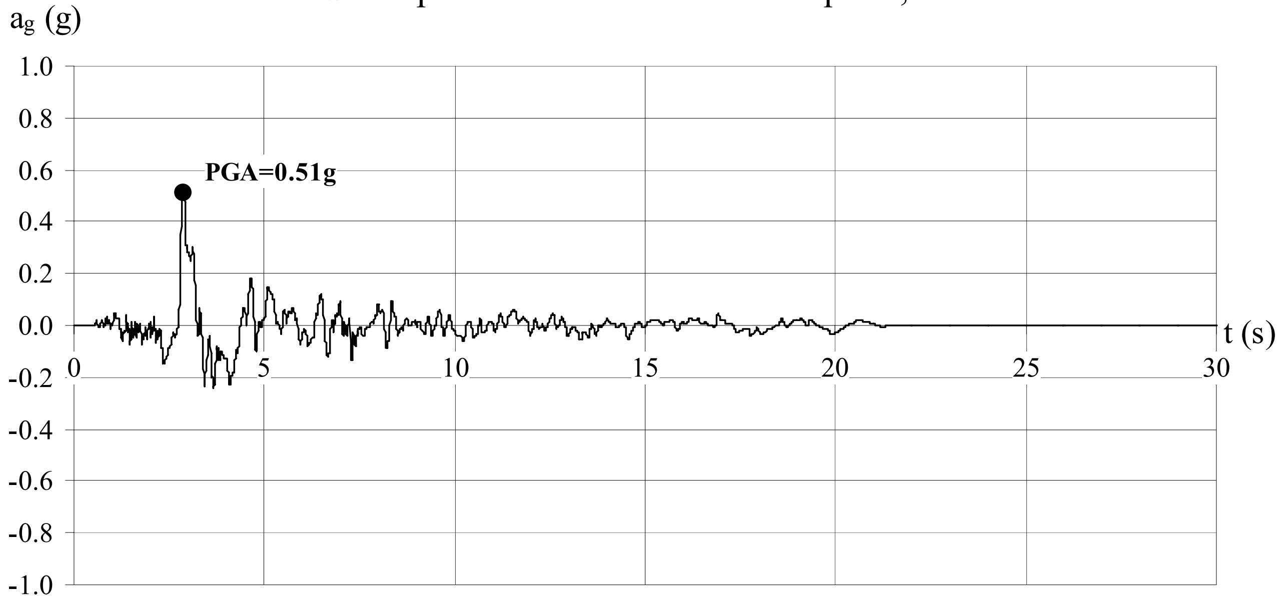

N-S component of the Erzikan Earthquake, 1992

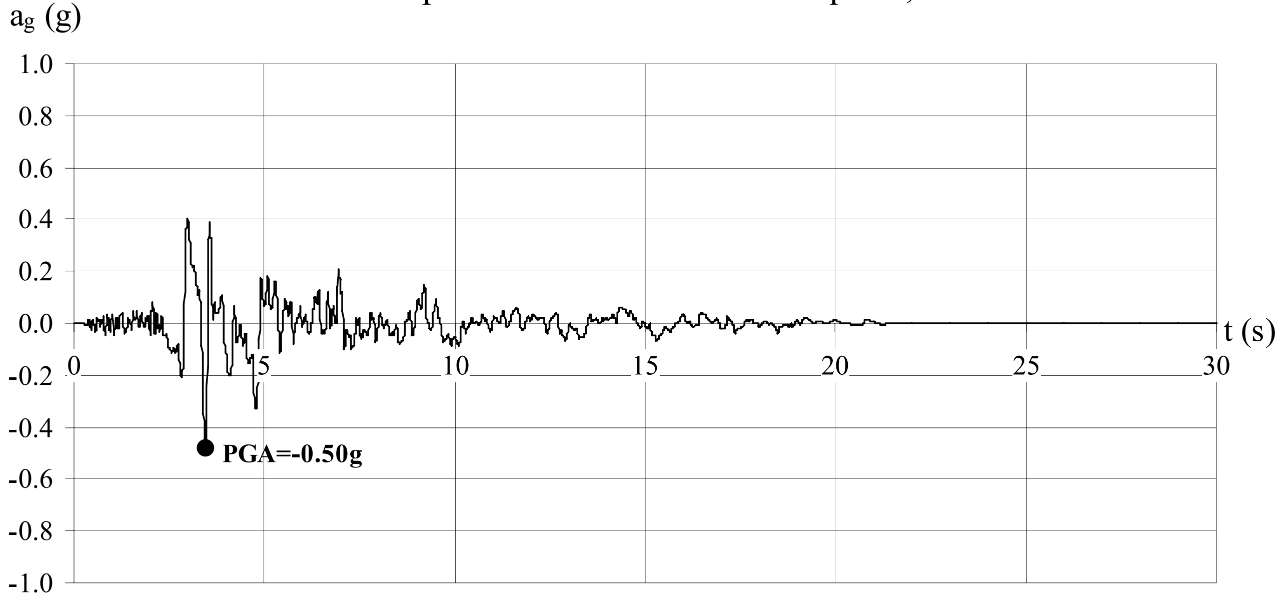

E-W component of the Erzikan Earthquake, 1992

Records artificially generated from the Friuli Earthquake, 1976 (Falcão, 2002)

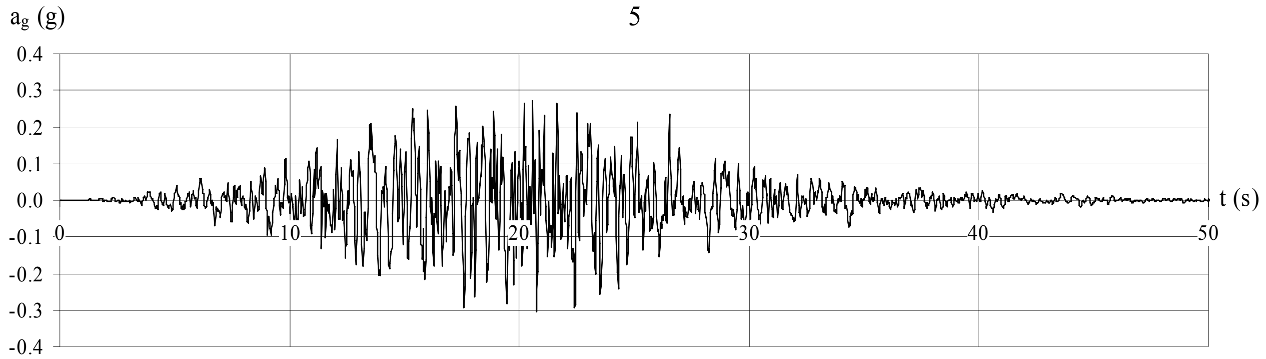

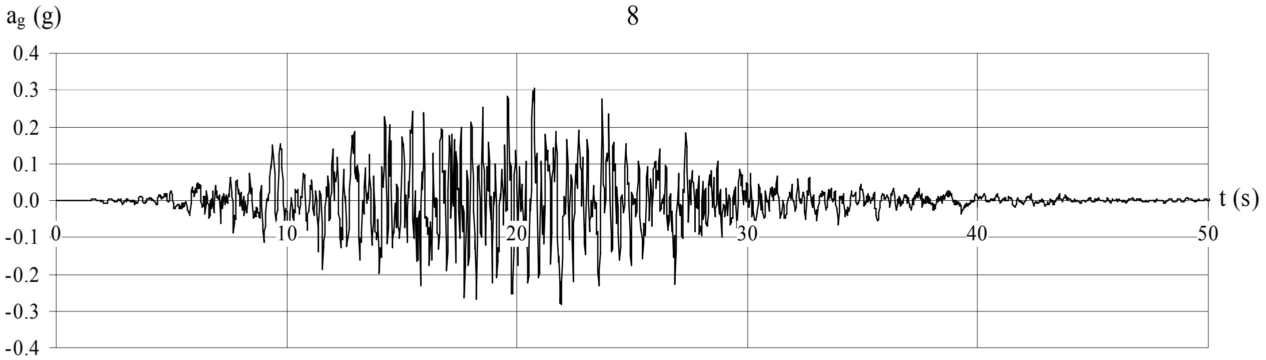

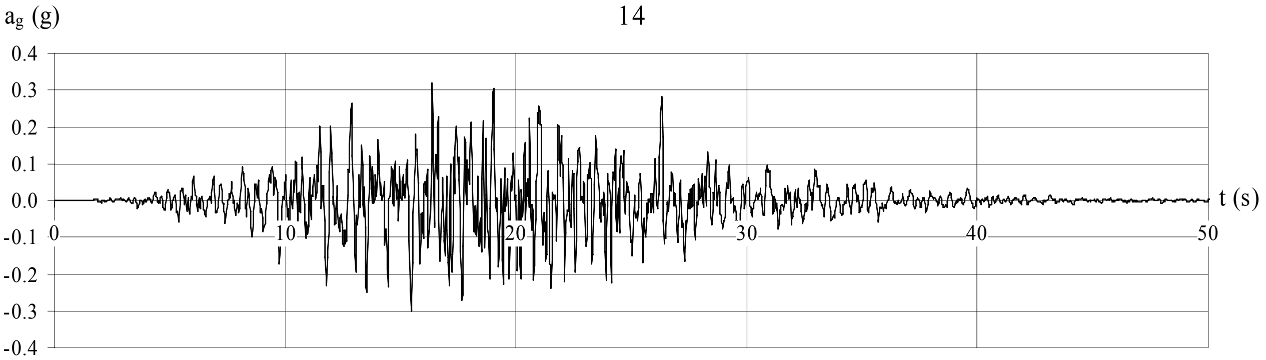

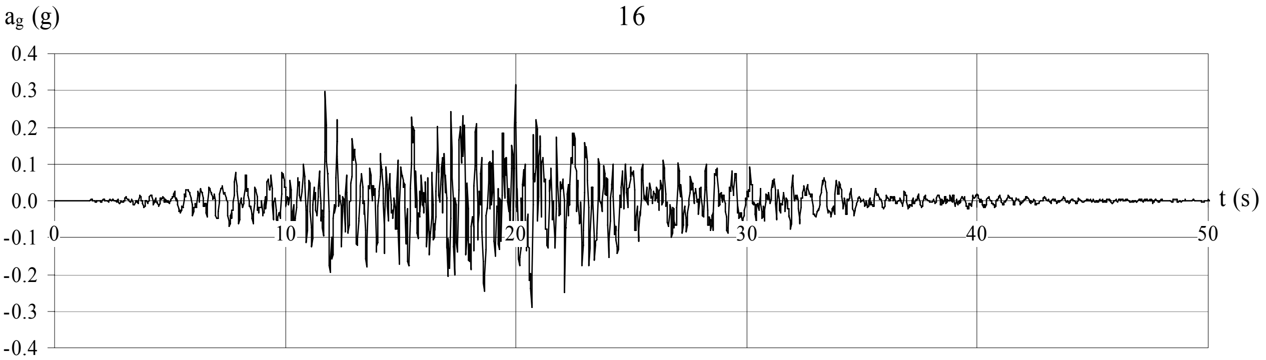

Records artificially generated from the Friuli Earthquake, 1976 (Falcão, 2002), *cont.*

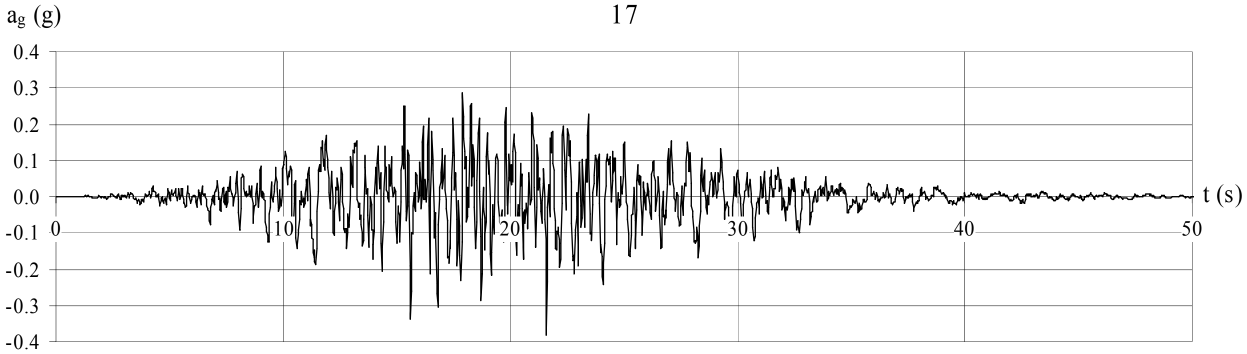

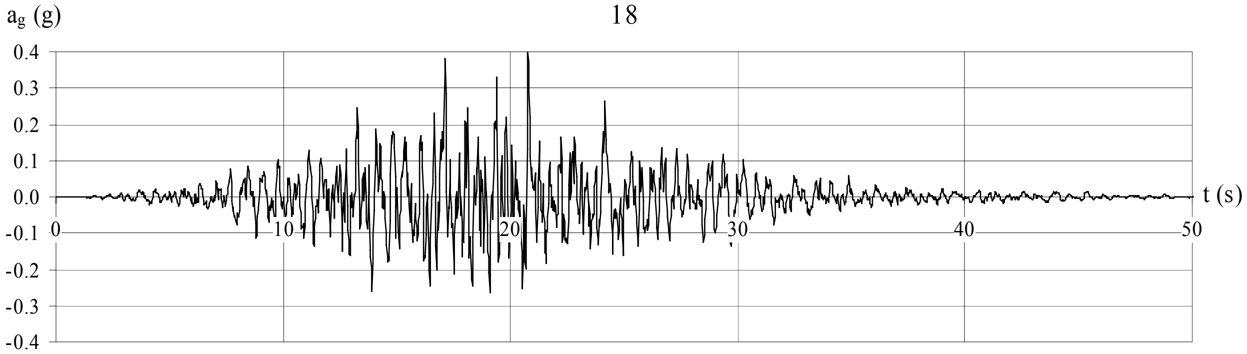

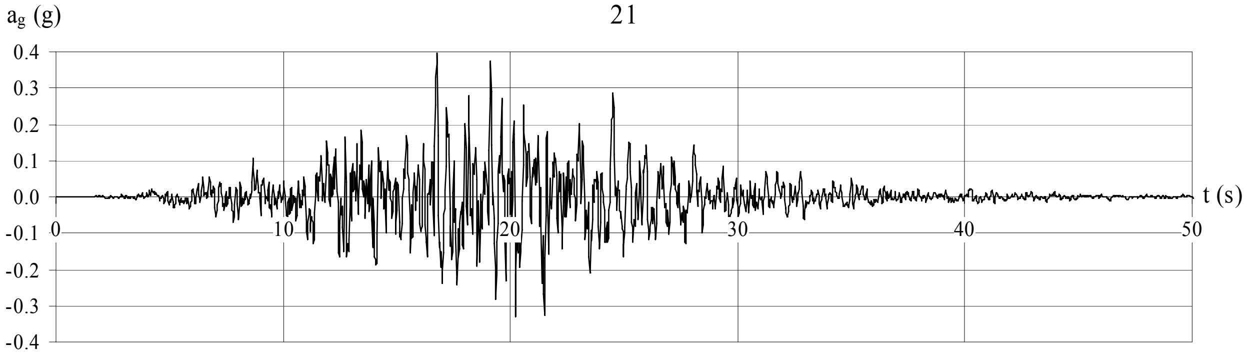

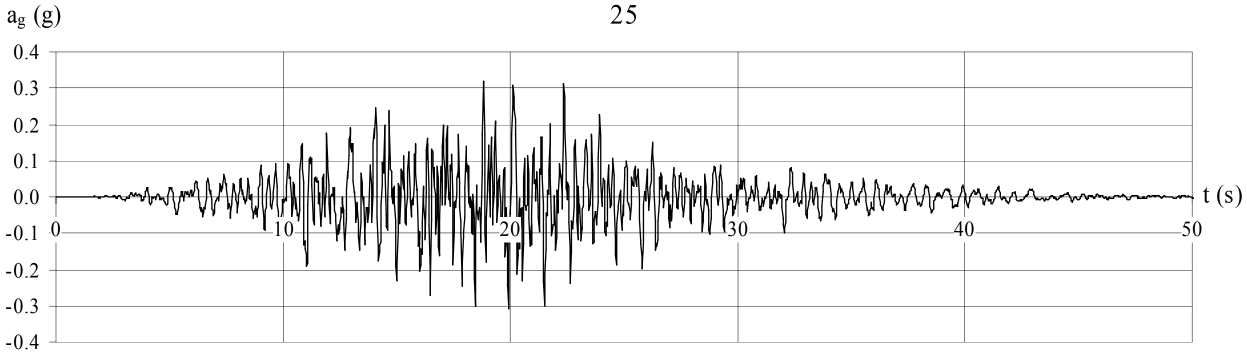

Records artificially generated from the Friuli Earthquake, 1976 (Falcão, 2002), *cont.*

29

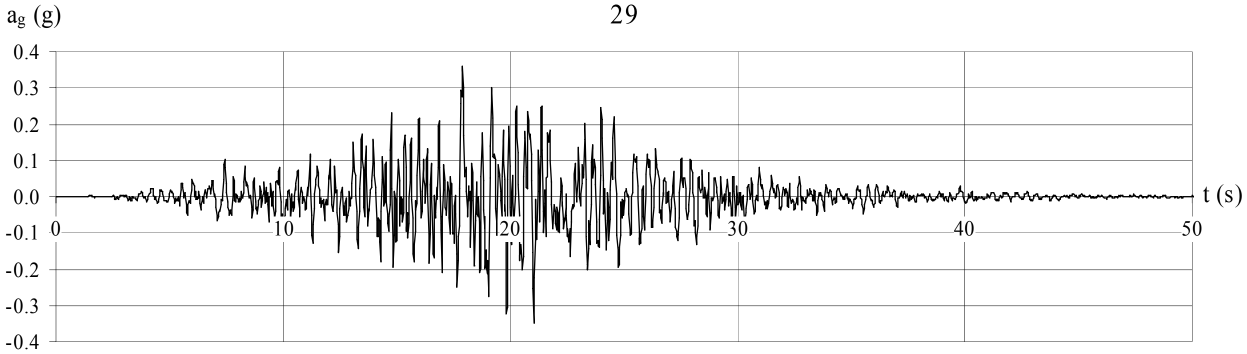

31

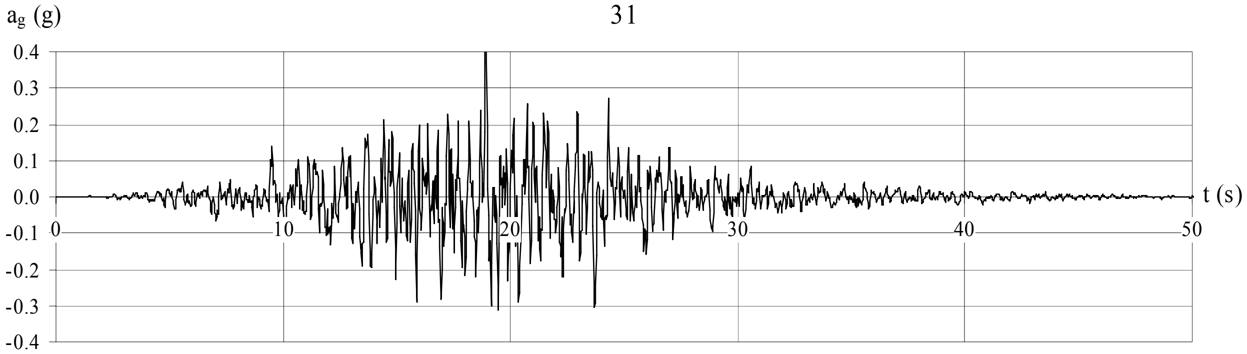

33

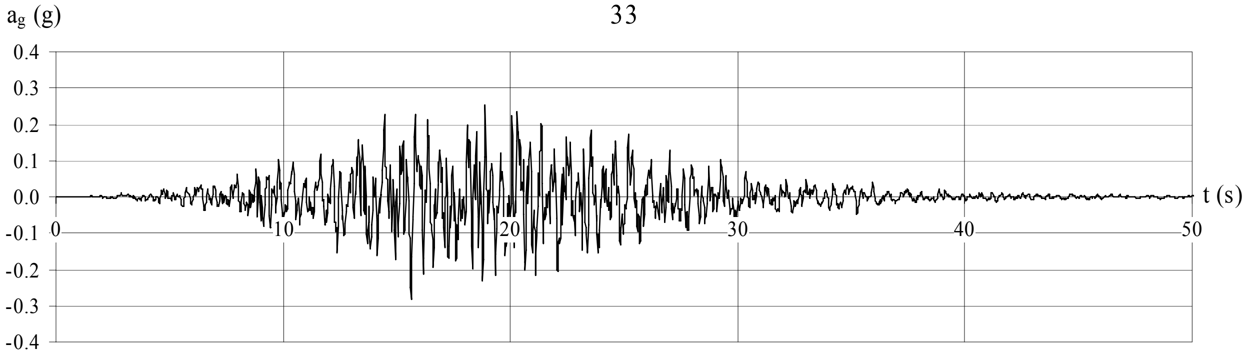

37

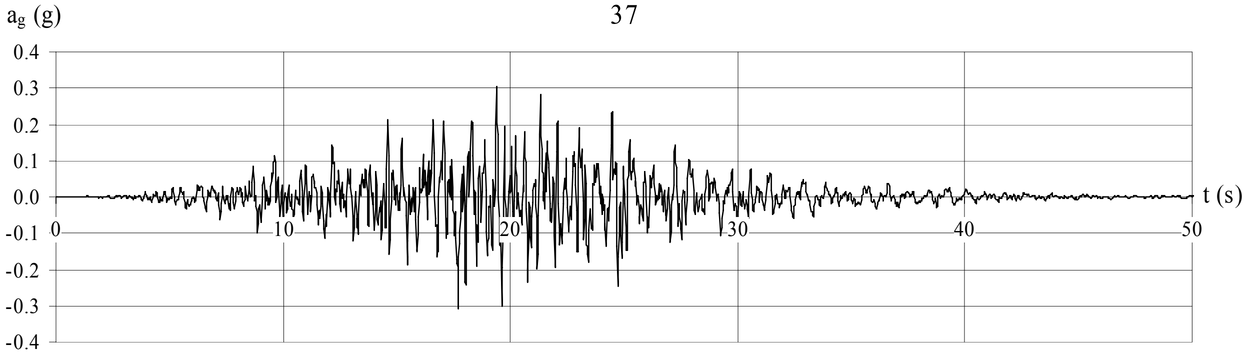

Records artificially generated from the Friuli Earthquake, 1976 (Falcão, 2002), *cont.*

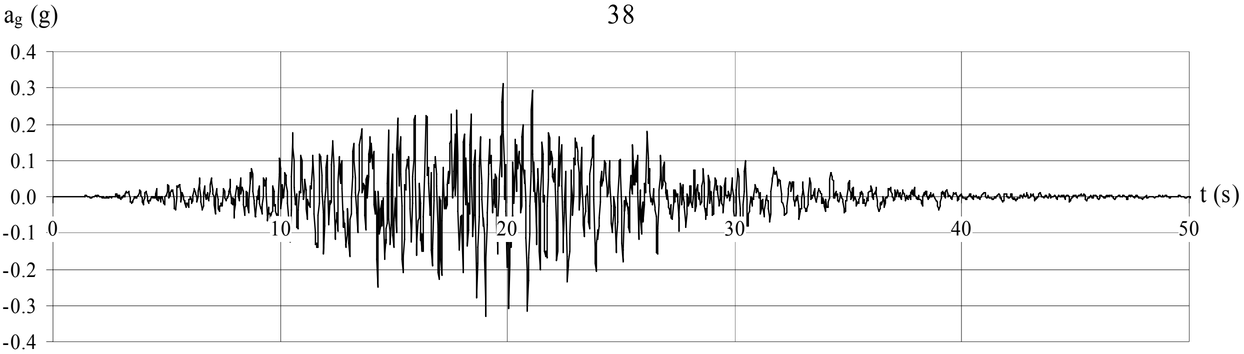

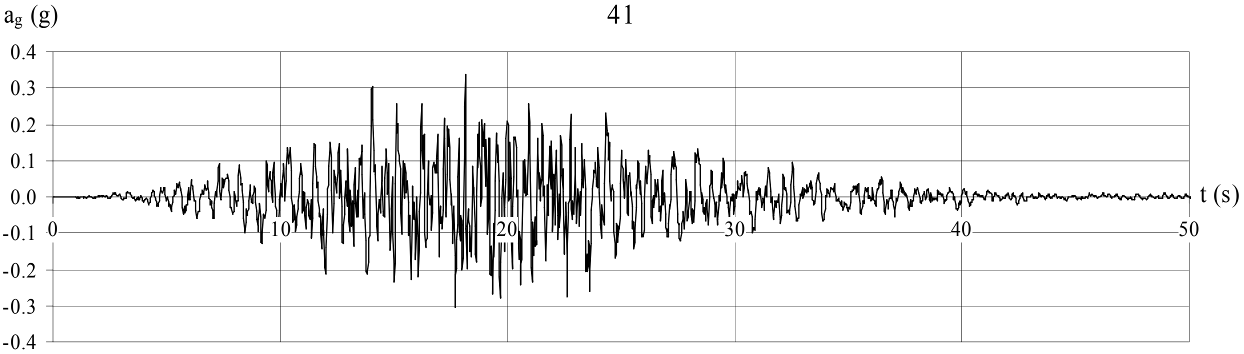

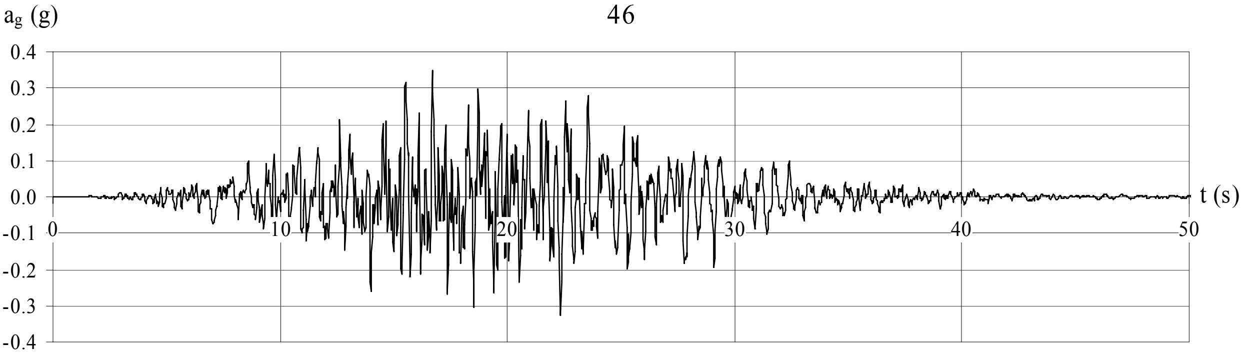

Report no R-149
ISSN 1601-2917
ISBN 87-7877-221-4